Principles for Aircraft Exergy Mapping

Berg, Frederick

Award date:
2013

Awarding institution:
University of Bath

Principles for Aircraft Exergy Mapping

submitted by

Frederick Timothy Neil Berg

for the degree of Doctor of Philosophy

University of Bath
Departments of Mechanical and Electrical Engineering

May 2013

Signature of the author .....

Summary

An increasing emphasis on energy efficiency in aircraft systems has in recent years led to greater interest in integrated design and optimisation within the industry. New tools are needed to understand, compare and manage energy use of an aircraft throughout its design and operation. This thesis describes a new methodology to meet this need: aircraft exergy mapping.

The choice of exergy, a 2nd law metric, to describe the energy flows is fundamental to the methodology, providing numerous advantages over energy alone. The basis for time-variant exergy analysis, a necessity when analysing aircraft systems in detail, is established. A set of software tools were developed to enable the creation, storage and analysis of the exergy map data.

To study the efficacy of the method for analysing a time-variant system, a hydraulic wave power test rig was used as a case study. The system was equipped with sensors to provide pressure and flow readings at relevant locations. A model of the system was used to supplement the exergy map detail.

Since aircraft will experience a range of atmospheric conditions during a flight, the effects of this on exergy calculations must be considered. A turbojet simulation was used to show that a reference state other than the varying, immediately exterior atmospheric conditions leads to unacceptable inaccuracy.

To consider the process of exergy mapping a whole aircraft, a case study based on an Airbus A320 was created, including a performance and turbofan model. An air conditioning system model represented a lower energy subsystem. Further analysis of the exergy map included the establishment of a method for assigning mass-induced exergy destruction and the attribution of costs to the aircraft case study. A comparison between two exergy maps of the same aircraft over different missions is made.

Publications

F. Berg, M. Balchin and P. Keogh, "Elucidation of aircraft energy use through time-variant exergy analysis", SAE Aerotech Conference, 2011-01-2683, 10.18.2011

F. Berg, M. Balchin and P. Keogh, "Challenges in time-variant exergy analysis of aircraft", IEEES-5 Conference, Luxor, Egypt, December 12-15, 2011

F. Berg, M. Balchin and P. Keogh, "New Principles for Dynamic Aircraft Exergy Mapping", AIAA Journal of Aircraft (early access available online)

Further publications based on Chapters 6, 7 and 8 in progress.

Acknowledgements

First and foremost, I would like to sincerely thank my academic supervisors Prof. Patrick Keogh and Dr. Martin Balchin for all the guidance and encouragement (and coffee!) they gave over the course of my PhD, which were so essential to its success. Many thanks must also go to my industrial supervisors at EADS Innovation Works, Caroline Turner and Matt Maynard, whose support, as well as enthusiasm for the topic, were always useful and morale-boosting. Thanks to Tom Owen who filled Caroline's shoes while she was away: we'll always have Toulouse. Sarah Nash, who inspired the project description in the first place, John Price, Graham Dodds and Sven Weier at IW are all gratefully acknowledged for their various contributions and collegiality. My friends and colleagues in the department of mechanical engineering at Bath are too numerous to enumerate, but Chris Cargo, whose hydraulic rig I used, deserves particular thanks for helping me upgrade and study it, as well as his off-putting banter. Thanks also to Alan Jefferis and Vijay Rajput for their help in making the rig alterations. Many thanks to the NLR of the Netherlands for the provision of an academic licence for GSP.

Although I will look back at my time as a PhD student very fondly, there is no doubt it was hard work at times. Special thanks to Joanne Compson for her patience, love and understanding throughout: Ile-Leu-Gln-Val-Glu-Tyr-Gln-Sec.

Drs. David Betts, Neil Baker and Adrian "Taffy" Townsend, my housemates for these 3-and-a-bit years have my sincere appreciation. Their net contribution to my sanity has probably been positive, despite their best efforts.

Finally, thanks to my family, who have supported me during this time and throughout my life.

This project was funded by an EPSRC CASE Award in association with EADS Innovation Works UK and the University of Bath.

Contents

List of Figures **11**

List of Tables **14**

1 Introduction **15**
1.1 Aircraft energy systems 16
1.1.1 Passenger aircraft energy flow 16
1.1.2 Energy modelling of aircraft 18
1.2 Analysis of energy use 20
1.2.1 Choice of metric 20
1.2.2 Exergy analysis of thermal systems 21
1.3 Exergy metric applied to aircraft 23
1.4 Exergy applied to specific aircraft subsystems 31
1.4.1 Propulsion 31
1.4.2 Environmental control 32
1.4.3 Other systems 32
1.5 Definition of thesis 33
1.5.1 Recapitulation of the topic 33
1.5.2 Objectives 34
1.5.3 Thesis structure 36

2 Background **38**
2.1 Exergy fundamentals 38
2.1.1 Exergy destruction and loss 40
2.1.2 Reference (dead) state 41
2.2 Physical exergy 41
2.2.1 Thermal exergy 42
2.2.2 Pressure exergy 42
2.2.3 General equation 43
2.3 Chemical exergy 45
2.4 Other exergy forms 47
2.5 Application of the exergy metric 48
2.5.1 Comparison of systems 48
2.5.2 Clarification of causes of loss 48
2.5.3 Improvement limitations and error prevention 49
2.6 Exergy limitations 50

2.6.1 Exergy and energy equivalence . . . 50
2.6.2 Information provided . . . 50
2.7 Conclusions . . . 51

3 Time-variant exergy analysis 53
3.1 Exergy analysis principles . . . 54
3.2 Time-variance and exergy storage . . . 56
3.2.1 Grassmann diagrams of time-variant analysis . . . 57
3.2.2 Known and unknown destruction . . . 58
3.3 Foundations of aircraft analysis . . . 59
3.3.1 Basis in literature . . . 59
3.3.2 Unmanned aerial vehicle case study . . . 59
3.4 Conclusions . . . 67

4 Software tool prototype design 69
4.1 Requirements . . . 70
4.1.1 Database . . . 70
4.1.2 Input interface . . . 70
4.1.3 Exergy calculators . . . 70
4.2 Selection of programming environment . . . 71
4.2.1 Database . . . 71
4.2.2 Software tools . . . 71
4.3 Database design . . . 72
4.4 Database control interface . . . 74
4.4.1 General input . . . 74
4.4.2 Map creation . . . 74
4.4.3 Calculators . . . 75
4.4.4 Calculation procedures and validation . . . 75
4.5 Analysis GUI . . . 80
4.6 Grassmann diagram generation tool . . . 80
4.7 Exergy mapping process . . . 82
4.8 Future requirements . . . 83
4.9 Conclusions . . . 84

5 Analysis of highly dynamic systems 85
5.1 Hydraulic system description . . . 86
5.2 Exergy readings . . . 86
5.3 Implementation in database . . . 90
5.4 Rig test run . . . 93
5.5 Analysis of rig data . . . 93
5.6 Rig simulation . . . 97
5.7 Results and discussion . . . 103
5.7.1 Experimental results discussion . . . 103
5.7.2 Comparison of physical and simulated results . . . 108
5.7.3 Result interpretation from a design standpoint . . . 112
5.8 Discussion of exergy mapping process . . . 113

5.9 Conclusions 114

6 Variable reference states **116**
6.1 Problem definition 116
6.2 Physical exergy 118
6.2.1 Kinetic exergy of air flow through a jet engine 118
6.3 Chemical exergy 119
6.4 Exergy of jet fuel 120
6.5 Other exergy forms 124
6.5.1 Electrical exergy 124
6.5.2 Kinetic exergy 125
6.5.3 Gravitational potential 125
6.6 Gas turbine simulation 125
6.6.1 Simulation program 127
6.6.2 Mission analysed 127
6.6.3 Calculations 128
6.7 Reference state schemes 129
6.8 Reference scheme results 130
6.9 Change in stock exergy 134
6.10 Conclusions 135

7 Exergy mapping of complex aircraft **138**
7.1 Mission 138
7.2 System exergy flow 139
7.3 Aerodynamics and performance 141
7.3.1 Exergy calculations 141
7.4 Propulsion 143
7.4.1 Exergy calculations 145
7.5 Air conditioning system 146
7.5.1 Simulation 147
7.5.2 Exergy calculations 151
7.6 Results 153
7.7 Discussion 159
7.7.1 Airframe and engines 159
7.7.2 Air conditioning system 159
7.8 Conclusions 160

8 Further exergy map analysis **162**
8.1 Assignation due to mass 163
8.1.1 Component masses 163
8.1.2 Exergy of lift method 163
8.1.3 Lift-induced drag assignation 166
8.1.4 Application to aircraft components 167
8.1.5 Application to air conditioning system 168
8.1.6 Whole system comparison 170
8.1.7 Other drag attribution 171

8.2 Fuel and carbon costs 171
8.3 Comparison of exergy maps 174
8.3.1 Secondary mission profile 175
8.3.2 Results and comparison 176
8.4 Conclusions 178

9 Conclusions **185**
9.1 Further work 190

Bibliography **192**

A Software tool details and instructions **199**
A.1 General input 199
A.2 Map creation 200
A.3 Calculators 201
A.4 Analysis GUI 202
A.5 Grassmann diagram generation tool 203
A.6 Exergy mapping process 204

B Enlarged Grassmann diagrams **208**

Nomenclature

A_A	=	Area of annulus (m^2)
A_i	=	Area of inlet (m^2)
A_P	=	Area of piston (m^2)
a	=	Wing aspect ratio
$\dot{C}$	=	Capacity flow (J/K·s)
C_{D_I}	=	Induced drag coefficient
C_L	=	Lift coefficient
c	=	Molar concentration (mol/m^3)
c_p	=	Constant pressure specific heat capacity (J/K)
D	=	Pump displacement (m^3)
D_I	=	Induced drag force (N)
E	=	Exergy (J)
$\dot{E}_d$	=	Unaccounted exergy loss or destruction rate (J/s)
$\dot{E}_I$	=	Exergy destruction rate due to induced drag (J/s)
$\dot{E}_i$	=	Exergy flow into control volume (J/s)
$\dot{E}^{LI}$	=	Exergy destruction rate due to lift (J/s)
$\dot{E}_l$	=	Accounted exergy loss or destruction rate (J/s)
$\dot{E}_o$	=	Exergy flow out of control volume (J/s)
$\dot{E}_q$	=	Exergy flow due to heat transfer (J/s)
$\dot{E}_w$	=	Exergy flow due to work (J/s)
$\dot{E}_D$	=	Exergy destruction rate (J/s)
E_S	=	Exergy stock (J)
$\dot{E}^{ch}$	=	Chemical exergy flow (J/s)
$\dot{E}^{elec}$	=	Electrical exergy flow (J/s)
$\dot{E}^{KE}$	=	Kinetic exergy flow (J/s)
$\dot{E}^{PE}$	=	Gravitational potential exergy flow (J/s)
$\dot{E}^{ph}$	=	Physical exergy flow (J/s)
e	=	Specific exergy
F	=	Hydraulic flow rate (kg/s)
G	=	Gibbs free energy (J)
g	=	Gravitational constant
g_G	=	Specific Gibbs free energy (J/kg)
h	=	Enthalpy (J)
I	=	Electric current (A)
I_R	=	Radiative energy (W/m^2)

L	=	Lift force (N)
l_{pax}	=	Length of passenger cabin (m)
M	=	Mach number
M_{acs}	=	Mass of air conditioning system (kg)
M_m	=	Molar mass of gas mixture (kg/mol)
m	=	Mass (kg)
P	=	Pressure (Pa)
P	=	Electrical power (W)
Q	=	Heat transfer (J)
$\dot{Q}_1$	=	Flow rate at flow meter 1 (m^3/s)
$\dot{Q}_2$	=	Flow rate at flow meter 2 (m^3/s)
$\dot{Q}_B$	=	Boost pump flow (m^3/s)
q	=	Specific heat transfer (J/kg)
R	=	Universal gas constant (J/kg·K)
R_a	=	Individual gas constant of air (J/kg·K)
R	=	Electrical resistance (Ω)
S	=	Entropy (J/K)
s	=	Specific entropy (J/kg·K)
S^w	=	Area of aircraft wing (m^2)
T	=	Temperature (K)
t	=	Time (s)
U	=	Internal energy (J)
U_{avg}	=	Overall coefficient of heat transfer
u	=	Specific internal energy (J/kg)
V	=	Volume (m^3)
v	=	Specific volume (m^3/kg)
$\mathcal{V}$	=	Velocity (m/s)
$\mathcal{V}_{gs}$	=	Ground speed (m/s)
$\mathcal{V}_y$	=	Vertical velocity (m/s)
$\mathcal{V}_\infty$	=	Free-stream velocity (m/s)
V	=	Voltage (V)
V	=	Stoichiometric coefficient
W	=	Work (J)
W_{HE}	=	Work done by heat engine (J)
$W_{p,useful}$	=	Useful work done by pressure difference (J)
$W_{total,useful}$	=	Total useful work (J)
w	=	Specific work (J/kg)
x_k	=	Mass fraction of gas species k
$\bar{x}_k$	=	Mole fraction of gas species k
Z	=	Capacity rate ratio
z	=	Altitude (m)
γ	=	Ratio of specific heat capacities
ε	=	Heat transfer effectiveness
ϵ	=	Span efficiency factor
η	=	Isentropic or adiabatic efficiency

ϑ	=	Temperature in Celsius (°C)
ρ	=	Density (kg/m^3)
ω	=	Angular velocity (rad/s)

Subscripts

0	=	Property at reference state
a	=	Atmospheric property
c	=	Component
ac	=	Aircraft
cv	=	Control volume
s	=	Stagnation property

Superscripts

ref	=	Property at standard reference conditions

Acronyms

APU	=	Auxiliary Power Unit
ATA	=	Air Transport Association
GSP	=	Gas turbine simulation program
GUI	=	Graphical User Interface
$ODBC$	=	Open database connectivity
NLR	=	Netherlands aerospace laboratories
NTU	=	Number of heat exchanger transfer units
PEM	=	Polymer Electrolyte Membrane
UAV	=	Unmanned Aerial Vehicle
KE	=	Kinetic energy/exergy
PE	=	Gravitational potential energy/exergy
SQL	=	Structured Query Language
LHV	=	Lower Heating Value
$LVDT$	=	Linear Variable Differential Transformer

List of Figures

1.1 General aircraft energy flow layout 18
1.2 Comparison of results for heat transfer parameter effects on turbine efficiency. Source: [1] 25
1.3 Proportions of exergy destroyed during the cruise phase. Source: [2] 27
1.4 Example loss envelopes as described by Roth 30

2.1 Exergies derived from pressure differences 39
2.2 Heat transfer from a pipe to illustrate difference between exergy loss and destruction. 41
2.3 Example heat engine 42
2.4 Piston in compressed (left) and expanded (right) positions 43
2.5 Extracting thermal and pressure exergy 45
2.6 Example chemical reference environment proposed by Ahrendts . . 46
2.7 Energy and exergy diagrams of coal power plant 52

3.1 Basic component control volume and Grassmann diagram 55
3.2 Detailed component control volume for time-variant vehicle analysis 57
3.3 Representation of changes in exergy stock in a component Grassmann diagram 58
3.4 Aircraft exergy flow diagram given by Paulus and Gaggioli 60
3.5 UAV exergy flow diagram, option 1 61
3.6 UAV exergy flow diagram, option 2 61
3.7 UAV mission 62
3.8 Grassmann diagrams for the three UAV flight phases 68

4.1 Component and interface illustration 73
4.2 Database structure 74
4.3 Input GUI: General input tab 75
4.4 Input GUI: Links and components input tab 76
4.5 Input GUI: Calculators tab 77
4.6 Input GUI: Chemical exergy calculator gui 79
4.7 Exergy map input analysis GUI 81
4.8 Subsystem Grassmann creation GUI 82

5.1 Photo of hydraulic rig 88
5.2 Hydraulic rig layout 89

5.3 DC power generation circuit 90
5.4 Hydraulic rig exergy map configuration 91
5.5 Hydraulic rig test run 93
5.6 Simulated and transducer pressure readings for P_1 99
5.7 Simulated and transducer pressure readings for P_2 99
5.8 Simulated and transducer pressure readings for P_3 100
5.9 Simulated and transducer pressure readings for P_4 100
5.10 Simulated and transducer pressure readings for P_5 101
5.11 Simulated and transducer pressure readings for P_6 101
5.12 Simulated and measures flow readings for flow meter A 102
5.13 Simulated and measures flow readings for flow meter B 102
5.14 Grassmann of experimental results: entire run 105
5.15 Grassmann of simulation results: entire run 105
5.16 Grassmann of experimental results: up-stroke 106
5.17 Grassmann of simulation results: up-stroke 106
5.18 Grassmann of experimental results: down-stroke 107
5.19 Grassmann of simulation results: down-stroke 107
5.20 Accumulator 1 simulation results: exergy in and exergy out over one cycle 110
5.21 Accumulator 1 simulation results 111

6.1 Example exergy differences of a gas flow at sea level and 10,000 m altitude 117
6.2 Effects of ambient conditions on exergy of pure atmospheric gases . 121
6.3 Effects of ambient conditions on exergy of gaseous hydrocarbons . . 122
6.4 Variation of dodecane with ambient temperature at 1 atm pressure and relative humidity of 70% 124
6.5 Turbojet exergy flowchart 126
6.6 Turbojet mission 127
6.7 Turbojet results for 30s at sea level 133
6.8 Turbojet results for 30s at 10,000 m altitude, sea-level reference . . 133
6.9 Turbojet results for 30s at 10,000 m altitude, engine-fixed reference 133
6.10 Turbojet results for 30s at 10,000 m altitude, sea-level intake 133
6.11 Exergy stock in equivalent fuel mass over mission 134

7.1 Aircraft flight mission 139
7.2 Exergy flowchart for engine, mass and aerodynamic subsystems . . 140
7.3 Comparison of thrust produced by GSP and performance models . . 145
7.4 Comparison of fuel required by GSP and performance model engines 146
7.5 Exergy flowchart for environmental control system 147
7.6 Cross-flow heat exchanger stream identification 148
7.7 Simulink model of air conditioning system 152
7.8 Grassmann diagram of engines and airframe for entire mission . . . 154
7.9 Grassmann for air conditioning system over whole mission 156
7.10 Grassmann for air conditioning system over 0-200 seconds 157
7.11 Grassmann for air conditioning system over 2,200-2,400 seconds . . 157

7.12 Grassmann for air conditioning system over 3,500-3,700 seconds . . 158

8.1 Exergy destruction rate due to mass per major component 169
8.2 Aerodynamic component Grassmann diagram 170
8.3 Air conditioning component exergy destruction 171
8.4 Exergy in- and outputs, direct and induced destructions of all system components 172
8.5 Comparison of original and secondary mission profiles 175
8.6 Grassmann diagram of engines and aircraft performance for modified mission 180
8.7 Comparison of Combustion Chamber component over whole mission 181
8.8 Comparison of Combustion Chamber component over climb 182
8.9 Comparison of Combustion Chamber component over cruise 183
8.10 Comparison of Core Exhaust component over whole mission 184

B.1 Enlarged version of Fig. 7.8 208
B.2 Enlarged version of Fig. 8.6 208

List of Tables

2.1 Comparison of energy and exergy metrics 47

3.1 UAV mission: climb phase results 65
3.2 UAV mission: cruise phase results 65
3.3 UAV mission: descent phase results 66

4.1 Physical exergy calculator validation 78

5.1 Hydraulic rig main component parameters 87
5.2 Results for experimental and simulation runs of hydraulic rig 104

6.1 Turbojet simulation main parameters 126
6.2 Reference state scheme study results 132

7.1 Aircraft design parameters 142
7.2 Engine design parameters 144
7.3 Heat exchanger model parameters 149
7.4 Aircraft exergy flows 155

8.1 Airframe and payload masses 164
8.2 Component masses 165
8.3 Engine exergy destruction, costs and CO_2 produced 173
8.4 Air conditioning exergy destruction, costs and CO_2 produced 174
8.5 Engine exergy destruction costs for modified mission 176

Chapter 1

Introduction

The importance of energy efficiency in all areas of human endeavour has grown significantly in recent years. In part, this is due to the cost of fossil fuel, which is widely expected to rise in the long term due to the depletion of easily accessible resources. Our civilisation's reliance on the combustion of these fuels as a means of generating electrical power and heating puts upward pressure on all energy costs. In addition to this, the ever more urgent requirement to reduce greenhouse gas emissions to limit the effects of anthropogenic climate change, further emphasises the need for greater efficiency of resource use and a switch away to more sustainable energy sources [3].

Transportation, by its nature, is a highly visible form of energy use. Cultural, economic and political pressure makes it necessary for the manufacturers of vehicles to respond by improving the efficiency of their products in a way that addresses one or more of these considerations. These concerns are heightened in the case of civil passenger aircraft. Fuel costs make up a large part of operating costs of passenger aircraft, upwards of 28% at the time of writing [4], and are highly dependent on current oil prices. This compares with only around 10% in 1998, when fuel prices were at a relative low. The visible nature and growth of aircraft transport also makes it subject to significant scrutiny with regard to emissions. It is estimated that the aircraft transport sector is accountable for around 2% of human greenhouse gas emissions, leading to around 3% of human-induced radiative forcing, due to the high altitude at which the emissions are released. The consequences of these economic and political factors mean fuel efficiency is now one of the main design drivers in the aircraft industry.

Research with the aim of decreasing fuel costs are under way in most areas of aircraft design. The theme in the majority of cases can be classed either as a reduction of engine losses, aerodynamic improvements or the reduction of weight in the remaining aircraft, through novel material use, more electric systems, etc. These have been the most significant opportunities for savings in the past. The complexity of large passenger aircraft means design changes must be considered in terms of their direct energy requirements as well their impact on other systems, including through their weight. Changes can have undesirable consequences elsewhere in the system, neutralising the intended positive effects. As the limitations of current design and optimisation practice are approached, new tools will be required by engineers in the aircraft sector, which will facilitate a deeper understanding of the fuel use of an aircraft and its subsystems. This thesis presents a new tool, which can provide a novel perspective on an aircraft's energy use, elicit deeper understanding of the system as a whole, and may lead to novel ways of improving aircraft design.

1.1 Aircraft energy systems

1.1.1 Passenger aircraft energy flow

A passenger aircraft, such as an Airbus A320, has the following major energy-using subsystems, which, in the aerospace industry, are organised by means of ATA chapters, given in brackets. In this thesis, the terms given in bold text will be used to refer to the group of subsystems described, unless otherwise specified.

- **Pneumatics** (36), which provide air to the anti-ice systems (30) and the cabin for breathing and heating (21).
- **Hydraulics** (29), which power the flight control surfaces (27) and landing gear (32).
- **Electrics** (24), which power lighting (33), avionics (22,23,34,42 etc.), in-flight entertainment and galleys (25,44) as well as a number of other services performed by other systems in newer aircraft.

- **Fuel system** (28); storing, delivering to engines and moving the fuel around the aircraft for balance and trim.
- **Propulsion** (61 and up); combustion of fuel, providing thrust and powering other subsystems.
- **Auxiliary power unit (APU)** (49), which is an additional power plant, typically a small gas turbine, able to provide power to electrical systems during flight below a certain altitude, as well as compressed air for starting the engines.

A simplified energy flow through the systems is illustrated in Fig. 1.1. For a normal passenger aircraft, all but a very minor amount of the energy required for a mission, is carried in kerosene-based fuel. The fuel, stored in various tanks in the wings, body or trim tank, is moved around the aircraft by the fuel system and delivered to the engines. By means of combustion in the engines, the chemical energy of the fuel is converted to provide thrust. The aerodynamic form of the aircraft converts forward motion into lift. Compressed air bled from the engines is used to supply the cabin and anti-ice systems. Shaft power taken from the engines is used to run electrical generators and hydraulic pumps to power the various subsystems. Dashed lines indicate other energy transfer routes that are not used during flight in normal operation. For example, the APU may provide power to an engine for starting, or the hydraulic system may power an electrical generator in the case of generator failure.

Each of the mentioned subsystems is highly complex and requires significant expertise to understand and develop. Essential systems have backups in case of failure. For example, an Airbus A320 has three separate hydraulic systems, each of which can work alone to provide sufficient aircraft flight control. Although this is not an exhaustive description of the energy flows, the complexity of the aircraft's 'system of systems' is made clear. It is difficult for individuals to maintain oversight of the energy use of the entire aircraft and, indeed, analysing all energy flows for an aircraft would be a considerable undertaking in itself. However, a fuller and more accessible understanding of the energy flows within an aircraft, would offer a new perspective of the way in which the aircraft's fuel is used. Currently, there is no

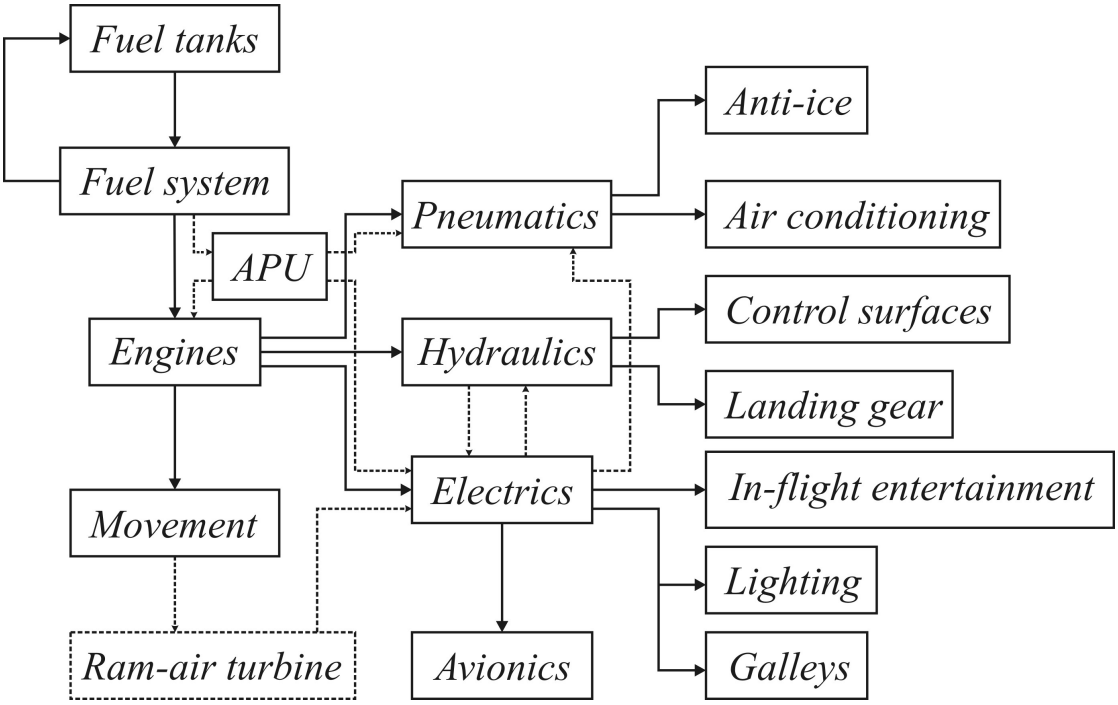

Figure 1.1: General aircraft energy flow layout

established method with which all aircraft energy use can be captured, compared and analysed in a clear and informed way.

1.1.2 Energy modelling of aircraft

Approached from numerous perspectives, a variety of research has taken place that seeks to generate more detailed understanding of energy use in aircraft by means of modelling the aircraft under a single methodology.

Lazarovich and Lee [5] approach the subject with the aim of understanding the electrical energy requirements of more-electric aircraft. By combining a number of system models in an integrated aircraft model and considering the power transfer between them, they propose to manage the varying levels of power requirements over a flight mission for the sake of safety and reliability. Owing to fact that modelling every system on an aircraft is difficult and time-consuming, they suggest the use of data from an aircraft load analysis to fill in unknown quantities. Their work focuses only on electrical power usage, given certain draws from electrically powered systems.

Liscouet-Hanke et al. [6–8] approach a similar subject with a broader scope.

The work focuses on developing a methodology for pre-designing aircraft power systems, coupling different models and using energy as a transfer metric. The reasons for the development of such a tool, such as the aim of integrating a large number of design disciplines involved in aircraft development and the need for a way of optimising systems with regard to all other aircraft systems, are echoed by other authors discussed in this section. The solution requires full, compatible models of each aircraft system to be developed in the early design stages of a new aircraft. Since this would require significant effort, only a small number of example systems are modelled in this work. The method would allow the coupling of subsystem models with aerodynamic and thermal models to provide a complete energy-based simulation model of the aircraft being designed. In principle, the methodology presented promises considerable benefit if it were adopted fully across an entire aircraft design organisation. The challenges of implementing unified techniques across divergent engineering disciplines cannot be underestimated.

The virtual iron bird initiative of Bals et al. [9] is another example of work aimed at this subject. In this case, the work focuses on the production of a Modelica [10] library of aircraft components to allow physical modelling of the entire aircraft under a single methodology with the aim of predicting electrical power demand over a given mission.

These examples are generally intended as methods for modelling during the design phase of the aircraft development. Providing cross-discipline understanding of energy use is not as much the aim as is the provision of a unified modelling technique for information exchange between disciplines. This is a highly worthwhile aim, but challenging to implement. Initial increases in workload and the potential loss of subject-specific functionality for some users would be of concern. When the aim is deeper understanding of energy use, as it is in this thesis, postulating a new modelling technique may be an excessively complex aim. It is likely that many of the benefits suggested by the previous authors can be achieved by integrating data that are already available from existing models. This project focuses on the possibility of analysing the systems in such a way, rather than on the modelling.

1.2 Analysis of energy use

Energy efficiency is a topic approached in many disciplines, which can have many different practical approaches and meanings depending on the context. In common parlance, it is normal to speak of energy as if it is something that is used up. This belies the first law of thermodynamics, which states that energy is a conserved property that can only change forms. Of course, what is normally meant is that it is the usefulness of the energy that is used up, which certainly is a non-conserved property. The usefulness of energy can be to produce heat or light, do mechanical work or, in a limited sense, facilitate the processing of information in electronics. What defines the usefulness is not the energy itself, but rather, a disequilibrium of states with the potential to be exploited. Because both the definition and magnitude of the usefulness of energy differ depending on context, the traditional approach to analysing energy efficiency of a system also varies depending on the system under examination.

1.2.1 Choice of metric

The value of energy in a system to an engineer depends on its form and intended use. Although the fuel energy available to the engine is, for example, also used to run electronics and heat the cabin air, the largest application of the energy in the fuel will be to produce mechanical work to move the aircraft. The ability of a system's energy to do work can be quantified by calculating its exergy.

Exergy can be defined as the maximum theoretical mechanical work that can be extracted when bringing into equilibrium an imbalance of state between a subject and a reference environment. Alternatively expressed, it is the amount of energy in a body or flow that can be theoretically converted into another form. Exergy allows the comparison of different energy types on a common basis. This is especially relevant when considering thermal, pressure and radiation-based energy flows compared with those that are mechanical and electrical. These advantages of the exergy metric make its use necessary for the comparison of different aircraft systems. More technical details on the exergy metric can be found in Chapter 2. Exergy's use in the literature is discussed in the following section.

1.2.2 Exergy analysis of thermal systems

The concept of available energy and available work was introduced by Gibbs in the late 19th century. Exergy has variously been known as 'availability', 'work potential' (also *'Arbeitsfähigkeit'*), 'potential entropy', 'useful energy' and 'essergy', although in some cases the latter has a subtly different definition. The term 'Exergy' itself was put forward as the standard word to replace these terms by Zoran Rant in 1953 from the Greek prefix *ex* (meaning 'out of' or 'from') and *ergon* meaning 'work' [11]. The topic was developed and matured over the following years, with publications on the topic and its application too numerous to fully survey in the context of this thesis. The literature survey here focuses on important recent work on the topic.

Exergy analysis as a tool for understanding the efficiency of industrial thermal processes has been commonplace for a number of decades and various methodologies are to be found in subject-specific textbooks (e.g. [12] and [13]). Its application is most widespread in thermodynamic processes that operate effectively in steady state for long periods, such as gas turbine power plants. The operating design point of the plant can be optimised without much notice being paid to transient phases such as start-up. A good example of such an analysis was performed by Rosen [14], a comprehensive exergy and energy analysis of similarly sized coal and nuclear power plants. The study is an example of good practice in exergy analysis of complex systems for the purpose of comparing losses in different components and processes. Some of the advantages of using the exergy metric are exemplified, such as being able to see the true location of losses in the system. This type of analysis is used in real-life applications to better understand power generation systems. Ameri et al. [15] also give details of an exergy analysis, performed on a combined cycle power plant. In each study, the largest exergy losses occur in the combustion process, something which is common to studies that include one.

Another area in which exergy analysis has gained some prominence in the last 5-10 years is in fuel cell systems. The nature of fuel cells, depending somewhat on the type and size, means they run best at a constant rate and have long start-up times [16], making them similar in those respects to larger thermal plants. This, and the novelty of the technology necessitating detailed analysis and optimisation

for design decisions, makes them ideal candidates for exergy analysis.

A good example of a straightforward fuel cell analysis is given by Cownden et al. [17] where the method is used to identify the main sources of inefficiency in a single system. The subject of the paper is the methodology of exergy analysis applied to fuel cells, rather than the thermodynamic optimisation of the fuel cell system operation and design. As with most published fuel cell exergy analyses, it uses data from a computational model of the plant rather than experimental. This is partly because of the difficulty in gathering such data from a physical system, as well as the aim of using the results to configure the system's design prior to assembly.

Fuel cell systems are of serious interest in transportation applications, including aircraft, and a large number of publications make use of exergy analysis to consider the suitability of systems to a role in a vehicle. Leo et al. [18] use the technique to compare two types of polymer electrolyte membrane (PEM) fuel cells for marine vehicle applications and consider the feasibility of their use. The data used in the analysis are taken from the optimal operating conditions of both fuel cell types. The study indicates that the main losses in the fuel cell systems occur in the fuel cell stack and burners. It is not explained that this result is symptomatic of the conversion of fuel energy into other forms, as with the previously mentioned studies. Although these are the main locations of exergy loss, they are caused firstly by the immaturity of the fuel cell technology and secondly by the aforementioned limit of converting heat to work. It is important to recognise that losses in other components, though relatively small compared to these examples, may not be negligible in terms of their potential for improving system efficiency. The paper concludes that the exergy analysis of these fuel cell systems cannot be used alone for distinguishing between the two system options, since the application on a marine vehicle, especially a submarine, is subject to other constraints such as weight and size. Vehicular analysis would therefore benefit from taking into account such connected factors. In the case of aircraft, weight is of particular importance, as will be discussed later.

Good use is made of exergy analysis in the optimisation of an ethanol fuelled PEM fuel cell system for automotive applications by Song et al. [19]. By con-

sidering the exergy destruction in the system components, design priorities are established to minimise the losses. Changes are made to a number of operating parameters (reforming factor, temperature parameters) to minimise the exergy destruction of the system. Such studies are more typical of exergy analysis publications, in which the exergy metric is used as an optimisation parameter and exergy destruction minimisation is the objective function. Understanding is gained of certain operating parameters, in this case the temperature range at which the fuel reformer should operate to maximise overall system efficiency.

1.3 Exergy metric applied to aircraft

While exergy analysis and accounting has become well-established in stationary, ground-based systems, it has been applied to aircraft systems in the literature only in the last 10-15 years, but has not been widely applied in real industrial practice [20]. Bejan and Siems [21] are among those calling for the use of the exergy metric in thermodynamic optimisation in aircraft systems. They provide a number of mathematical examples of exergy-based system optimisation: an environmental control system, the extraction of exergy from a hot stream of gas and flight itself. The examples are somewhat theoretical in nature but provide a starting point for initial aircraft and component design based on optimal exergy efficiency.

Another introduction to the use of exergy in the design of aircraft flight systems is given by Dincer and Rosen [22] within their informative book on exergy. A basic analysis of a turbojet engine is presented along with a brief explanation of the problem of reference state selection when analysing aircraft, a topic that is also discussed in Chapter 6 of this thesis.

Moorhouse [23] discusses the need for new design methods to bring about revolutionary design changes in passenger aircraft. A general exergy-based optimisation methodology is proposed, which allows the entire aircraft to be optimised in terms of minimal exergy destruction from the start. The analysis of different subsystems is discussed and the consideration is made that, while all systems add weight and direct or indirect exergy use, their function is not necessarily exergy-related. For example, the aircraft structure consumes exergy due to its weight,

but its function cannot be defined in terms of an energy effect. The flight control system, however, uses power, has weight and also affects exergy consumption of the aircraft due to the effects its use has on the aerodynamics. How to book-keep the exergy use of aircraft systems is a topic discussed in detail in this thesis.

Doty et al. [1] aim to prove the benefits of using an exergy-based approach when designing components for aerospace applications. Impenetrable terminology and unsuitable choices of examples are blamed for the lack of uptake in the aerospace sector. The paper uses a simplified gas turbine model with one degree of freedom, a duct heat loss parameter before the turbine, as an example system. The first conclusion reached is that the use of a 2nd thermodynamic law analysis alongside a 1st law analysis during a preliminary design investigation will inherently prevent design decisions that would theoretically improve a component's efficiency but break the 2nd law of thermodynamics. In this case, a reduced heat loss from the duct in question improves the component's energy efficiency, Fig. 1.2(a). A heat transfer into the duct, while improving energy efficiency, would not break the 1st law of thermodynamics but is shown to be physically infeasible when exergy is considered, Fig. 1.2(b), because it results in negative exergy destruction. It is argued that this alone makes exergy (or some other 2nd law metric) a requirement for preliminary design applications. It is also argued that using exergy as a metric for system analysis allows clear accounting of all losses in the system in equal terms, regardless of how they are caused. This allows studies on different components to be directly compared and interpreted.

Pellegrini et al. [24] attempt to show the advantages of exergy analysis applied to aircraft design using a comparison between an electric and an engine-powered bleed air environmental control system as a case study. Major simplifications, such as assuming equal system weight and only cruise conditions, limits its validity for the purpose of an actual technological comparison, but shows how the methodology can be applied to such systems, especially for the purpose of encouraging the use of the exergy metric to better understand and optimise aircraft energy use.

Paulus and Gaggioli [25] also discuss the use of exergy destruction minimisation as an objective function for the design of aircraft (and vehicles in general). Importantly, they include their interpretation of the exergy of lift, as in [26], which

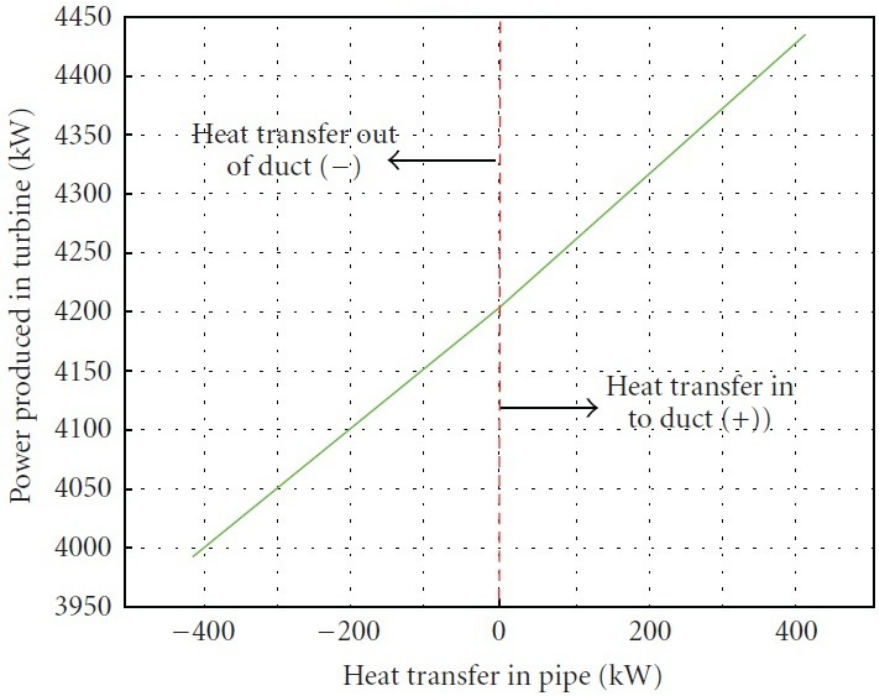

(a) Influence of heat transfer in pipe on turbine power, 1st law analysis

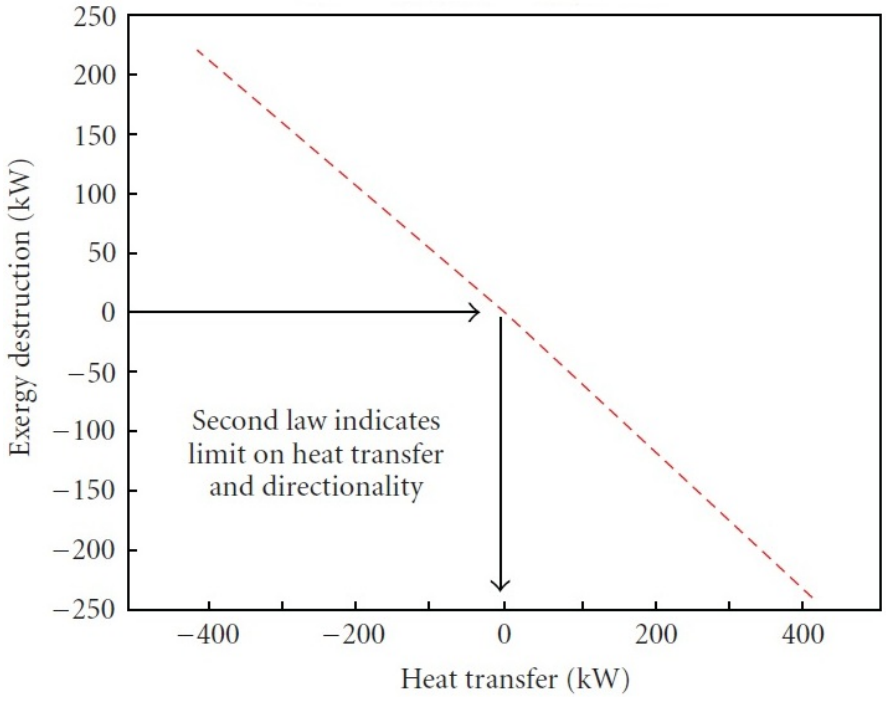

(b) Heat transfer and exergy destruction in pipe, 2nd law analysis

Figure 1.2: Comparison of results for heat transfer parameter effects on turbine efficiency. Source: [1]

provides a way of evaluating the exergy destruction caused by the aircraft's mass, alongside the exergy-consuming subsystems. Exergy flow diagrams are used to display the exergy use of a general aviation aircraft at a number of cruise and climb conditions. Further discussion of their approach can be found in Chapter 8.

Periannan et al. [27], again, compare the optimisation of aircraft systems when using energy and exergy as objective functions. They use environmental control and propulsion systems along with simple airframe flight models of a fighter aircraft. A typical combat mission is used, for which five different design optimisation problems are considered. They conclude that exergy is a better metric to use when comparing different system types because the 'common currency' provided by the metric allows the different energy forms to be directly compared, something that is not possible using energy alone.

Bejan and Siems [21] use exergy as a figure of merit to apply a new kind of design theory based on Bejan's constructal law. Although the highly theoretical nature of the research presented is far from being usable in real design work, some interesting concepts arise from the discussion within. The authors argue that efforts to optimise a complex system of systems such as an aircraft are subject to limitations because of the currently available methods. The complexity of such systems means the resources to specify the large number of possible configurations do not exist in industry, making true optimisation impossible. One can only choose the best of the limited number of designs one can specify. It is also argued that exergy analysis in its traditional form can only be used to identify the location and magnitude of losses and therefore provides only information on where, but not how, to improve the design. It is suggested that the only way one could achieve a true thermodynamically optimum design would be to adopt a new methodology for "synthesising the thermodynamic optimum system configuration directly from the physical laws".

Gandolfi et al. [28] perform an exergy analysis of a simplified aircraft over a flight mission. The aim of the paper is to show the comparative magnitudes of exergy destruction in each subsystem over a typical flight. A similar paper is presented by the same authors in [2] in which a more electric architecture is studied using the same method. Simple models are used to provide data for the

analyses over a flight mission represented by six operating conditions (take-off, climb, cruise, descent, holding and landing) active for relevant periods of time.

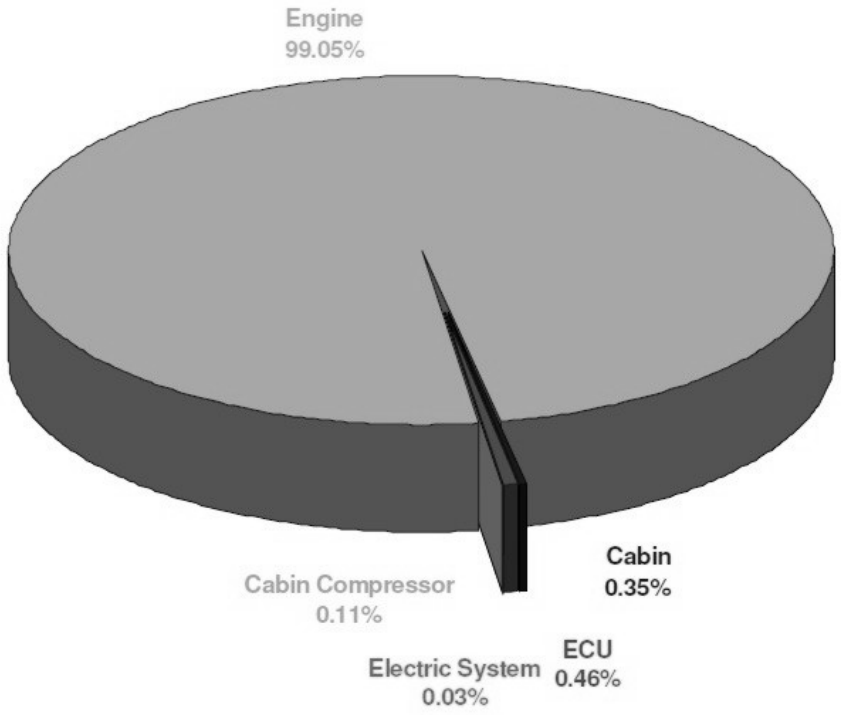

Figure 1.3: Proportions of exergy destroyed during the cruise phase. Source: [2]

Figure 1.3 shows one of the resulting breakdowns of exergy destruction, in this case for the cruise segment of the mission. The results show that the vast majority of the losses occur within the engine, dwarfing all other sources of exergy destruction. In [28], the second largest source of exergy destruction is the environmental control system, which is reduced in the more electric aircraft studied in [2].

The results of [2] confirm what has been shown in above examples: that the process of converting fuel energy into other forms tends to destroy a large amount of the original exergy. We know this to be inevitable with combustion technology. In the context of trying to optimise the aircraft's systems with an objective function of minimal net fuel use of the aircraft, the results tell us that the solution is likely to be one that also minimises the engine's exergy destruction. On modern civil airliners, the engine is also the primary power source for all aircraft subsystems. That means a minimisation of exergy use, and/or exergy destruction in any of

the subsystems will feed back and reduce the load on the engines. Again, the large proportion of exergy destruction in the engine does not rule out the value of reducing exergy destruction in other systems. The choice of a pie chart to compare the systems may be unhelpful for this reason. The work presented by these authors is important, however, for being the first published attempt at an exergy analysis of an entire aircraft over a mission.

A final noteworthy application of exergy to aircraft was performed by Roth [29]. The subject is approached from the perspective of analysing the risk involved in aircraft design, rather than from the more typical standpoint of direct thermodynamic optimisation. It is suggested that understanding the risks involved in today's ever more expensive aircraft development programmes is the only way to prevent the industry from being stifled in the near future due to prohibitively large development costs. A thermodynamic work potential similar to exergy - thrust potential - is used as metrics for the analysis of a Northrop F-5E aircraft, especially concentrating on the propulsion system. The concept of the loss management model is described, which forms part of the risk analysis method being described.

Roth argues that to understand the risk of a design, one must be able to understand and compare the constituent subsystems of an aircraft design according to a single figure of merit, so that the divergent disciplines involved in its development can be considered in a coherent way. This echoes the other authors highlighted previously. His hypotheses are quoted as follows:

1: *It is possible to quantify losses in aerothermodynamic performance of aerospace vehicle systems and sub-systems in terms of chargeable fuel weight (or mass).*

2: *It is possible to quantify the system-level impact of technologies in terms of: a) chargeable empty weight and b) aerothermodynamic performance losses integrated over a design mission* $\Rightarrow$ *chargeable fuel weight (by hypothesis 1).*

3: *It is possible to obtain a probabilistic description for the impact of technological uncertainty in terms of distributions on chargeable weight by using hypothesis 1 and 2 in conjunction with probabilistic analysis techniques.*

The work of Roth to answer the first two of these is directly relevant to the subject being considered in this thesis. A selection of publications arose from Roth's

work [30–32]. Exergy itself, however, is not the chosen metric for the analysis. Rather, another 2nd law metric, thrust potential, is chosen, allowing the interaction between aircraft mass, aerodynamics and propulsion to be more pertinently analysed, with the aim of avoiding the problem of the exergy destruction in the engine being overbearingly large. Roth establishes the concept of a 'loss deck' as part of his loss management model technique, which is made up of a comprehensive collection of loss envelopes, examples of which are given in Fig. 1.4). In principle, a loss envelope can be created for any component or loss aspect of a vehicle and shows the losses associated with that component for the velocity and altitude at which the vehicle is travelling. The data are created using models run over a range of possible conditions, but the loss deck allows the separation of the different types of model from the analysis and lets different mission profiles be analysed more quickly. Roth applies loss decks when establishing a method for aerodynamic chargeability in [32] and for engine components in [30]. What may be less convincing is the applicability of the loss deck method to internal aircraft subsystems. The product of Roth's method is a type of look-up table model of the aircraft, which would be capable of providing a lot of useful information to the users, but might be too complex to produce if considering detailed subsystem exergy use. The use of thrust potential as the analysis metric would also become less pertinent when comparing internal subsystems, as well as when considering the aircraft system in the context of broader economic analysis, compared to using exergy.

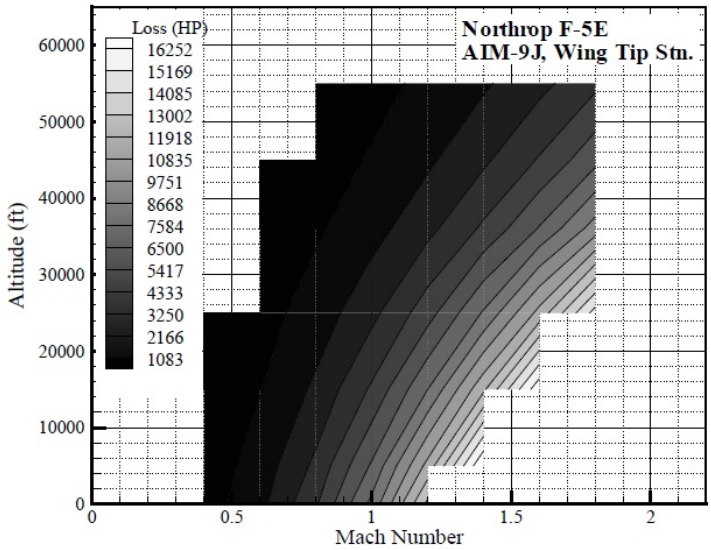

(a) Loss envelope of skin friction drag on Northrop F-5E. Source: [32]

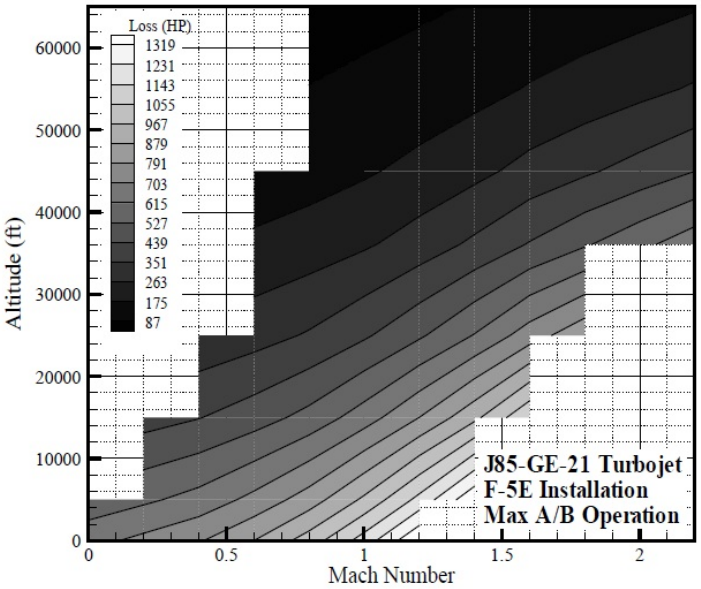

(b) Loss envelope of compressor in F-5E engine. Source: [30]

Figure 1.4: Example loss envelopes as described by Roth

1.4 Exergy applied to specific aircraft subsystems

Individual subsystems have been a more common subject of exergy analysis, generally for the optimisation of individual design parameters. Mostly, the systems under review have been for propulsion and environmental control, although there have been noteworthy exceptions considering other aspects.

1.4.1 Propulsion

Aside from the previously mentioned work of Bejan and Siems [21], Dincer and Rosen [22] and Doty et al. [1], which use simple analyses of turbojet engines to discuss the application of exergy to aircraft systems in general, a number of further publications concentrate more on the analysis and optimisation of aircraft propulsion for the sake of the improvement of the system itself. Engines are the most common individually analysed subsystem thus far. An early piece of work on the topic was given by Clarke and Horlock [33]. The fundamental thermodynamics of flow-based propulsion in terms of exergy are presented, although the old-fashioned expression 'essergy' is used in its place. Turgut et at. [34] provide an example of an exergy analysis of a turbofan engine with afterburner at sea level and 11,000 m, showing differences in efficiency between the two at component level detail.

Tona et al. [35] consider an entire flight profile including thermoeconomic analysis. The flight profile is simplified, using six steady operating conditions to represent take-off, climb, cruise, descent, holding and landing. The thermoeconomic analysis uses the exergy results to compare component costs to the cost of running them. This type of component-level analysis would not be possible to perform using energy as the metric, since energy losses do not coincide with the losses in energy value. The thermoeconomic analysis is, however, somewhat limited by the isolation of the engine from the aircraft mass and aerodynamics.

Amati et al. [36] perform an analysis of two scramjet configurations at cruise conditions. The comparison is between one that is directly fuelled with hydrogen and another that uses on-board kerosene reforming.

Hutchings and Metghalchi [37] study the pulse detonation engine using exergy

and energy analysis. They compare the Humphrey cycle's efficiency to the Brayton cycle, which is used in normal turbojet engines, at different compression ratios and using two types of fuel.

1.4.2 Environmental control

In traditional aircraft designs, the environmental control system (ECS) accounts for the next largest direct destroyer of exergy after the propulsion system [28]. This is because the air used in the cabin is extracted from the engines after compression at a far higher temperature and pressure than required and is then cooled and decompressed in the conditioning process.

Pérez-Grande and Leo [38, 39] perform an optimisation of an ECS using entropy generation minimisation as an objective function. They follow this with a thermoeconomic analysis of the same subsystem, showing the benefit of exergy as a metric that can easily be used to calculate the financial cost of economic losses.

Figliola et al. [40] consider the optimisation of an aircraft ECS using energy and exergy methods. Pellegrini et al. analyse an aircraft ECS as a case study for the application of exergy analysis to aircraft system design.

1.4.3 Other systems

Effort has been made by a number of parties to apply second law methods (exergy or entropy analysis) to aid the design of aircraft aerodynamics. Alabi et al. [41] present a set of modelling methods for the analysis of entropy generation by an airframe aerodynamics subsystem. Roth [32] presents a method of assigning drag loss to different aspects of the airframe using the aforementioned 'loss envelopes' that form part of an overall aircraft loss management model. Riggins et al. [20] present analytical methods for combining the equations of motion with aerospace vehicle energy availability, attempting to combine the analysis of propulsive and airframe systems.

1.5 Definition of thesis

1.5.1 Recapitulation of the topic

The focus of the literature review is on the application of the exergy metric to aircraft. A large number of published works have been for the purpose of encouraging the use of exergy in the context of optimisation of aircraft systems. These provide useful examples, most often propulsion and environmental control systems, within which certain parameters are optimised. Without exception, and generally by necessity, the studies are theoretical and exemplify work that might be undertaken as part of a preliminary design study to establish dimensions and operating points. In most papers, the advantages of exergy as a metric over energy are repeated, especially its potential as a 'common currency' to compare systems carrying divergent energy types on an 'apples to apples' basis. In the context of comparing energy use of different subsystems, the use of the exergy metric is essential, since using energy alone would lead to false comparisons, arbitrary reference conditions and many opportunities for misunderstanding.

There is a drive within the passenger aircraft industry to use simulations and calculations when designing new aircraft systems in order to mitigate the risks involved. The future aim of joining the system simulations together in order to optimise the aircraft globally (as a system of systems), rather than each subsystem individually, is cited often. The challenges inherent in such a task are significant, not least in the task of producing detailed, interacting and compatible models for an entire aircraft. Truly optimising a system with so many variables may also require currently unavailable levels of computational power. Of course, pursuing more optimal designs with a universal simulation and a limited number of variables remains a valid pursuit, which will gain in importance as the simulations are refined and available computing power increases. Using exergy, or more specifically, exergy destruction minimisation as the objective function may prove highly important in this approach.

More specific studies have concentrated on individual subsystems. To a large extent, these are optimisation studies, but do not include a study of the effects of the mass on the overall aircraft fuel consumption. It is very likely that the

subsystems on-board an aircraft can be designed to use less energy directly, but this will often be at a cost of increased weight. Understanding the connection between the two is vital.

Research published, which considers the application of exergy analysis to civil aircraft and makes direct reference to the current issues facing the sector, is deficient in a number of ways. In all publications other than those of Roth, there is a lack of a clear methodology for dealing with the variable and transient nature of a vehicle mission. Roth's approach in its current form is unsuitable for internal subsystem analysis.

There have been no studies of the exergy use of subsystems other than those of the propulsion, environmental control and the airframe. In part, this is because the values of energy and exergy are equal in electrical systems. It is already normal to speak of available energy, which is equivalent to exergy, in the context of hydraulic systems. Electrical systems have been the subject of optimisation studies, such as in the power optimised aircraft project [42]. These will gain in importance in the future because of the increasing reliance on more electric technology, gradually replacing the traditional subsystems.

An area that has had limited attention is the possibility of gaining better understanding of the complexity of aircraft energy use using information and models that already exist. The complexity of aircraft and the nature of the design processes used, including splitting design along ATA chapter boundaries, makes oversight of energy use difficult. A firm basis and method for analysing and understanding the energy use of aircraft in detail, giving a 'big picture' view and allowing direct comparison between all subsystems, does not exist. It is the aim of this thesis to introduce such a method, named the aircraft exergy map.

1.5.2 Objectives

An exergy map, building on some of the exergy analysis methods in the literature and some newly developed ideas, has the potential to provide an aircraft designer with a number of benefits. Firstly, it would provide detailed understanding of the way in which the fuel energy is used over a flight cycle. Using exergy as a metric would allow use, loss and destruction to be assigned to individual subsystems and

components and compared on the same terms. Insight into where to make design optimisations, what the theoretical limit of the improvements might be, or simply which aspects of the design are worthy of closer analysis and understanding would arise from this. The ability to convert exergy values directly into equivalent fuel allows straightforward economic analysis of the system.

The aim of the method will be to allow the capture and analysis of detailed information. It is important, therefore, that the detail that can be captured is unrestricted, both in terms of the component-level detail as well as the number of time periods a flight analysis is split into. High levels of detail require large amounts of data to be produced, stored and managed, which will lead to the need for some new software tools. A robust analysis of how to approach truly time-variant exergy analysis is also required, since this has not yet been approached in the literature. The comparison between analysing real-life systems and simulations as might be found in early design is an important one, since there would be potential for a method of analysis to be used from the early stages of development through to operation. Finally, the concept of weight-related loss assignment, as well as further use of the exergy map data, must be applied to the methodology to ensure the interpretation of the results are balanced.

The objectives for this thesis are therefore:

1. Develop a methodology for creating an account of exergy flow, loss and destruction for an aircraft:
   (a) Without limiting the component-level detail in which the system is analysed.
   (b) Allowing the direct comparison between systems of a different energy type.
   (c) Without necessitating a specific data source or the development of new models.
   (d) Without imposing time-based limits on analysis detail.
2. Research and expand exergy analysis theory as necessary to permit time-variant analysis, addressing item 1(d).

3. Design a software tool prototype to facilitate the creation and management of the exergy map:

   (a) Producing tools required for calculating relevant exergy values as far as is practical.

   (b) Allowing the capture of detailed system and exergy information while retaining accessibility and oversight.

   (c) Providing useful ways of visualising and interpreting the captured data in order to gain clearer understanding than was available before.

4. Consider the application of the methodology to an existing, physical, non-steady-state system in order to consider the feasibility of exergy mapping a real aircraft over a flight.

5. Apply the methodology to a case study of a real aircraft with an emphasis on high system detail, validating the software tool prototype and the visualisation and interpretation method available.

6. Establish a method for attributing exergy destruction due to mass and highlight further ways of interpreting the data.

1.5.3 Thesis structure

The thesis has been structured to reflect the objectives established above.

Chapter 2 provides background information on the exergy metric and exergy analysis in more detail.

Chapter 3 establishes the theoretical basis for time-variant exergy analysis. An unmanned aerial vehicle (UAV) is used as a case study to discuss its application. The UAV does not have thermal or pressure-based energy systems, so more advanced difficulties associated with exergy analysis of vehicles can be avoided.

Chapter 4 gives details of the software tools developed to allow the time-variant analysis of complex systems to take place. The software tools were used to produce all case studies in this thesis, having been developed in parallel.

Chapter 5 presents a detailed case study of a real system, a hydraulic wave power extraction device, the data for which was produced using sensors. Simu-

lations of the same system are used to complement the results. Consideration is made to the possibility of performing live flight exergy mapping.

Chapter 6 considers the correct reference states to use to calculate exergy in vehicular analysis. Exergy is a function of the deviation of a system from a reference state. When the atmosphere around the aircraft changes, however, the choice of which values to use is important in order to produce sensible results. A turbojet simulation is used to provide the relevant data.

In **Chapter 7**, an aircraft exergy map case study is created using data from various simulations, applying the techniques established in the previous chapters.

Chapter 8 is concerned with the assignment of exergy destruction due to mass, as well as discussing further uses for the tool and exergy map data. The case study produced in Chapter 7 is used as the example system. Two exergy maps of the same aircraft over different missions are compared.

Chapter 9 contains the concluding remarks and suggested future work.

Chapter 2

Background

In non-technical conversation it is usual to speak of energy as if it can be used up. This is despite the widely understood first law of thermodynamics, a form of which states that energy can never be destroyed - only change form. An aspect of energy that can be lost, however, is its quality. This chapter provides background on exergy, which is a metric that clarifies the usefulness of energy in a system.

2.1 Exergy fundamentals

The second law of thermodynamics states that any real process leads to a net increase in the entropy of the universe. Entropy, which can be imagined as a measure of disorder, is generated by any real process and can be used as a metric to calculate how irreversible a process is. Although very important to the understanding of a system, entropy is not an intuitive concept to use for the sake of system analysis, since it is a measure of what value has already been lost, rather than what is remaining.

One answer to this problem, and the most established among a number of similar concepts, is exergy. This is a measure of the potential of a system to do work. Work for the purposes of driving any other arbitrary, desired process, can theoretically be extracted when an imbalance of state exists between two bodies or regions. During a process in which the two bodies exchange energy or some other property to become balanced, work can be extracted. The maximum theoretical amount of work that can be extracted from one body when compared with another body representing the environmental conditions, is the exergy of the first body.

The formal definition and use of a reference state that is relevant to the system under study is a fundamental aspect of exergy, which entropy, energy and some availability metrics lack, and is what makes exergy highly relevant in an engineering context.

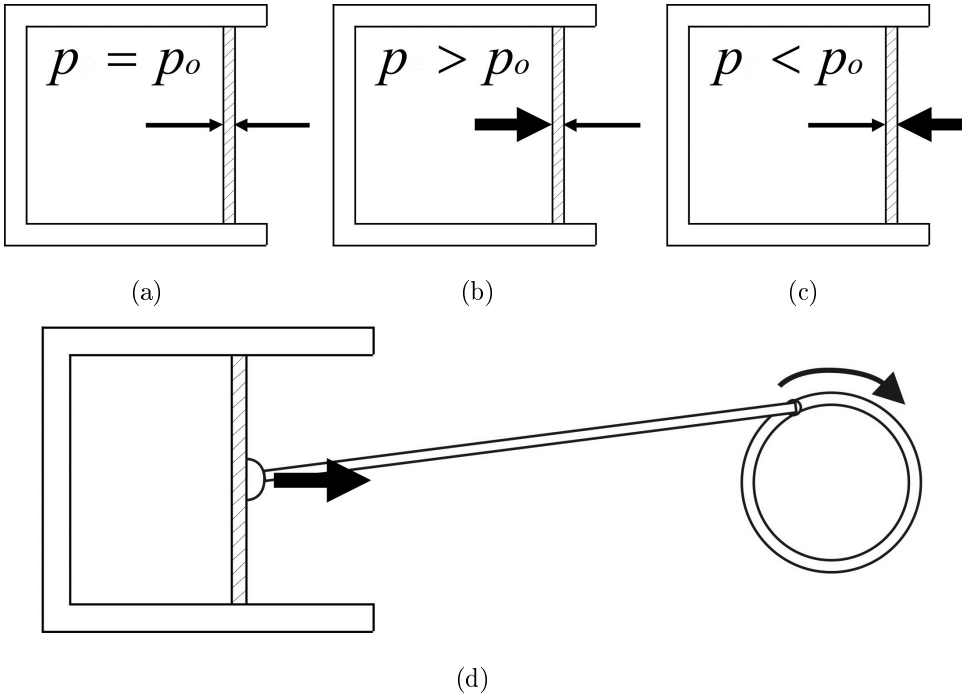

Figure 2.1: Exergies derived from pressure differences

Figure 2.1 illustrates in the simplest way how exergy is derived from a pressure difference. Cylinder (a) is filled with air at the same pressure as the outside atmosphere. Cylinder (b) has air at a pressure higher than the atmosphere and cylinder (c) has air at a lower pressure than the atmosphere. Assuming the temperature in each cylinder is the same as the outside atmosphere and that the chemical composition is equal, both cylinders (b) and (c) have exergy because work could be extracted by the mechanism shown in (d) by allowing the piston to move until the pressures inside and outside are equal. It is noted that, in the truest sense, there is no such thing as negative exergy. Cylinder (c) has the same work potential as (b) even though the piston would move inwards rather than outwards, assuming the pressure difference is the same. There are, however, situations in which neg-

ative exergy values are a useful concept when accounting the exergy in a system that diverges from the reference state in both directions. This is also discussed in Chapter 6.

The amount of exergy in the pistons to begin with is the work that could be done if the system were able to move without irreversibilities, such as friction, heat transfer, etc. In reality, once the pistons have moved, the work performed by the mechanism would be less than the exergy calculated at the start. This reduction is due to the destruction of exergy by the irreversibilities in the process. The exergy destroyed is proportional to the entropy generated and is irrecoverable.

2.1.1 Exergy destruction and loss

A subtlety in terminology that is not always observed in the literature is the difference between the terms 'loss' and 'destruction' of exergy. Exergy that is 'lost,' is defined as having left the system, but not having been destroyed; still existing exterior to the system being analysed. A hot fluid flow transferring heat through a pipe wall will be losing exergy, some of which is still theoretically recoverable at the pipe's exterior because the surface remains hotter than the reference conditions (Fig. 2.2). Moving away from the hot surface, the air temperature will gradually fall until it reaches the reference temperature. If the component is studied considering control volume B, it would be said that the control volume is losing exergy. If considering control volume A, the exergy within has already been destroyed because the volume contains the process of heat transfer over a temperature difference, which is irreversible. For the sake of a system's analysis, it is worthwhile making the distinction where possible because a loss of exergy indicates the possibility for recovery or harvesting. In most cases, however, a loss of exergy will indicate its imminent destruction. This concept is closely related to situations in which there is exergy in a system in a form that is not accessible to the system in question. For example, the exergy due to heat in a gas turbine is not directly available to the Brayton cycle and some other mechanism would be required to exploit it. Exergy such as this should not be considered lost or destroyed, but its inaccessibility must be appreciated to fully understand the system.

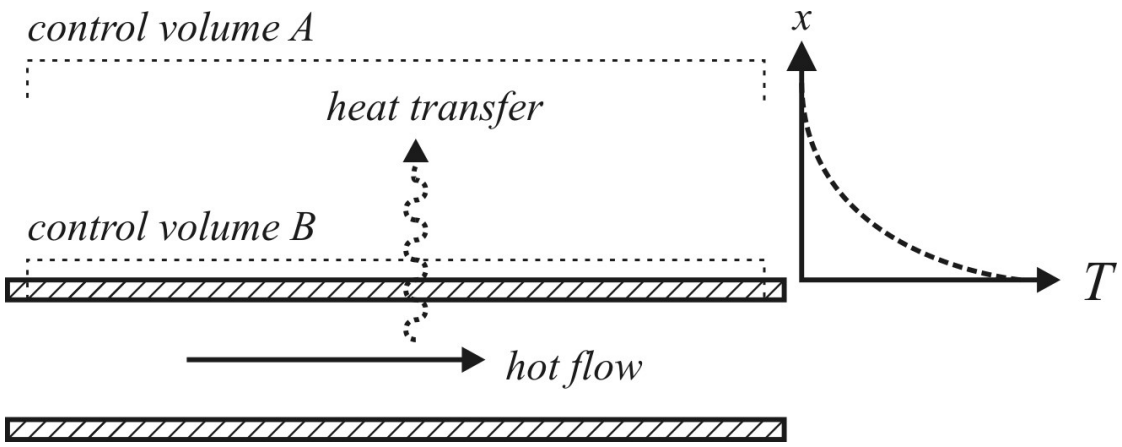

Figure 2.2: Heat transfer from a pipe to illustrate difference between exergy loss and destruction.

2.1.2 Reference (dead) state

The reference state, sometimes referred to as the dead state, is defined as the set of conditions considered to have no exergy, with which the system in question is compared. Normally this would be chosen as the atmospheric conditions surrounding the considered system. The reference state must be a body large enough to absorb the energy in the system without an appreciable change in its own conditions.

The restricted reference state is the set of conditions in which there is no physical exergy, but chemical exergy may remain, for example if a container of hydrogen gas is at atmospheric temperature and pressure. Chemical reference states are discussed in Section 2.3.

Kinetic and gravitational potential exergies require a position and velocity from which the system in question deviates.

The consideration of which reference state to use is an important one, which is of particular relevance in the context of aircraft system analysis. This topic is discussed in detail in Chapter 6.

2.2 Physical exergy

For the sake of completeness, the derivation of the general equation for calculating the physical exergy of a body or flow of a liquid or gas will now be given. Note that physical exergy is normally defined as that which arises from temperature, pres-

sure, kinetic or potential energy differences. The following explanation is adapted from that found in reference [43].

2.2.1 Thermal exergy

The work that can be extracted from a temperature difference is given by the theoretical efficiency limits of the Carnot heat engine.

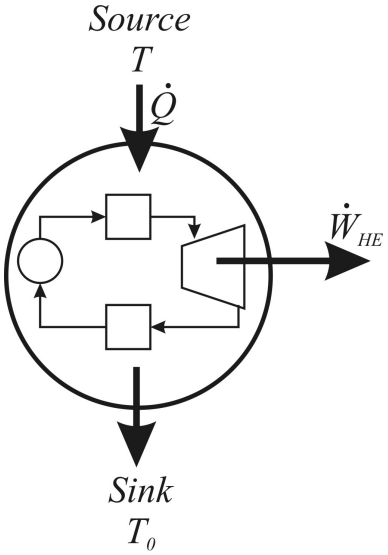

Figure 2.3: Example heat engine

The work potential of the heat transfer in Fig. 2.3 depends on the temperature difference between the source and the sink. In a reversible system, heat transfer must pass through a heat engine, since a transfer of heat over a finite temperature difference will destroy exergy. The work that can be extracted is given by:

$$\delta W_{HE} = \left(1 - \frac{T_0}{T}\right) \delta Q \tag{2.1}$$

where δQ is the heat transfer rate, δW_{HE} is the rate of work done by the process, T_0 is the reference temperature and T is the temperature of the system.

2.2.2 Pressure exergy

The work that can be extracted from a pressure difference is derived by imagining a perfectly insulated cylinder of compressed air that can only exchange energy

with its surroundings by pushing out a piston (boundary work), as shown in Fig. 2.4.

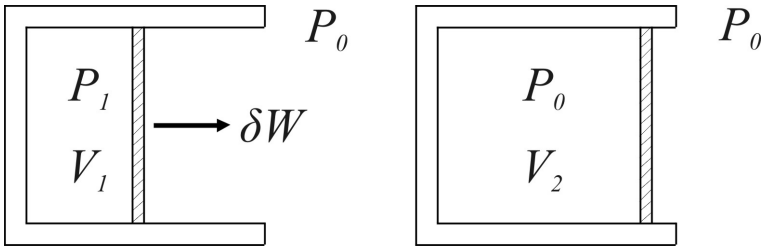

Figure 2.4: Piston in compressed (left) and expanded (right) positions

When a pressurised cylinder is allowed to expand by the differential distance dx in a quasi-equilibrium manner, the work done is given by

$$\delta W = Fdx = PA_p dx = PdV \tag{2.2}$$

where A_p is the area of the piston. Note that, by convention, δ denotes small transfers of a property into or out of the system while d denotes small changes to the internal system properties. The useful work done by the piston is only due to the pressure in the cylinder above that of the atmosphere. The useful work can therefore be separated from the non-useful work with

$$\delta W = PdV = (P_1 - P_0)dV + P_0 dV = \delta W_{p,useful} + P_0 dV \tag{2.3}$$

Kinetic and potential Since there is no physical efficiency limit for the transfer of kinetic energy from one body to another, the kinetic energy and exergy of a body are equivalent. Similarly, gravitational potential energy and similar lossless stores (ideal springs, etc.) can be considered equal in magnitude to their exergy.

2.2.3 General equation

Figure 2.5 shows a cylinder of hot, compressed air at temperature T and pressure P, where work, W, can be extracted from the pressure difference by a reversible piston and a heat engine extracts work as the temperature drops to atmospheric levels, P_0, T_0. Since a reversible process is considered, the only heat exchange can be through a heat engine and the only mechanical work done is by boundary

work. The energy in the control volume is the internal energy, U of the air. For the control volume inside the cylinder then, the following is true:

$$dU = -\delta Q - \delta W \tag{2.4}$$

Rearranging equation (2.1) and noting that for a reversible system where S is entropy, by definition $dS = \delta Q/T$:

$$\delta W_{HE} = \left(1 - \frac{T_0}{T}\right)\delta Q = \delta Q - \frac{T_0}{T}\delta Q = \delta Q - (-T_0 dS) \tag{2.5}$$

leads to

$$\delta Q = \delta W_{HE} - T_0 dS \tag{2.6}$$

Combining equations (2.3) and (2.6) into (2.4) gives

$$-(\delta W_{HE} + T_0 dS) - (\delta W_{p,useful} + P_0 dV) = dU \tag{2.7}$$

which may be rearranged to give

$$\delta W_{total,useful} = \delta W_{HE} + \delta W_{p,useful} = T_0 dS - P_0 dV - dU \tag{2.8}$$

Then, integrating between the starting state of the control volume and the dead state gives

$$W_{total,useful} = T_0(S - S_0) - P_0(V - V_0) - (U - U_0) \tag{2.9}$$

where the 0 subscript describes the properties of the control volume when it has reached the dead state. Adding the kinetic and potential exergies gives a general equation for the exergy of a closed control volume

$$E = (U - U_0) + P_0(V - V_0) - T_0(S - S_0) + \frac{m\mathcal{V}^2}{2} + mgz \tag{2.10}$$

where m is the mass of the gas in the control volume, z is its elevation above sea level and $\mathcal{V}$ is its velocity. or, per unit mass

$$e = (u - u_0) + P_0(v - v_0) - T_0(s - s_0) + \frac{\mathcal{V}^2}{2} + gz \tag{2.11}$$

where lower case letters represent the intensive $(1/m)$ values of the variables.

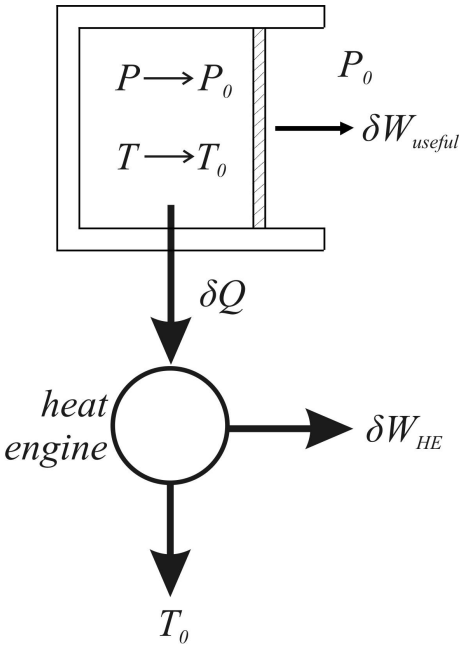

Figure 2.5: Extracting thermal and pressure exergy

Flow exergy To find the equation for the exergy of a flow medium, a further term accounting for the flow energy of the fluid is needed. The flow energy can be shown to be given by $w_{flow} = Pv$. The exergy, analogous to the static pressure scenario, is the work done by the pressure above that of the atmosphere. The flow exergy is therefore given by

$$e_{flow} = Pv - P_0 v = (P - P_0)v \tag{2.12}$$

This term is added to equation (2.11), and knowing that $h = u + Pv$, where h is the specific enthalpy, may be rearranged to give to the general equation for the exergy of a flow, which is used throughout this thesis:

$$e = (h - h_0) - T_0(s - s_0) + \frac{\mathcal{V}^2}{2} + gz \tag{2.13}$$

2.3 Chemical exergy

The theoretical work that can be extracted from a chemical imbalance is called the chemical exergy. To define it, one must first establish a reference environment with which to compare the chemical medium under consideration. The reference

environment is chosen to reflect the lowest energy form of each element as found in an accessible sample of earth's atmosphere, seas and crust. There are a number of publications discussing the best choice of chemical reference states for each element, and these vary depending on a number of factors, such as the depth of the Earth's crust to include and whether to choose a lower energy reference substance or one that is more likely to be formed given the availability of the reactants [44]. The differences between them are, however, unlikely to affect overall results in a typical engineering system study as long as one is chosen and used consistently [45]. This is especially true when considering substances with fairly common elements, which holds true in the case of analysing aircraft systems. A visualisation of the reference state proposed by Ahrendts in [46] is shown in Fig. 2.6. This contains the low-energy forms of a number of common substances in the air (top left), dissolved substances found in the sea (bottom left) and in the Earth's crust (bottom right).

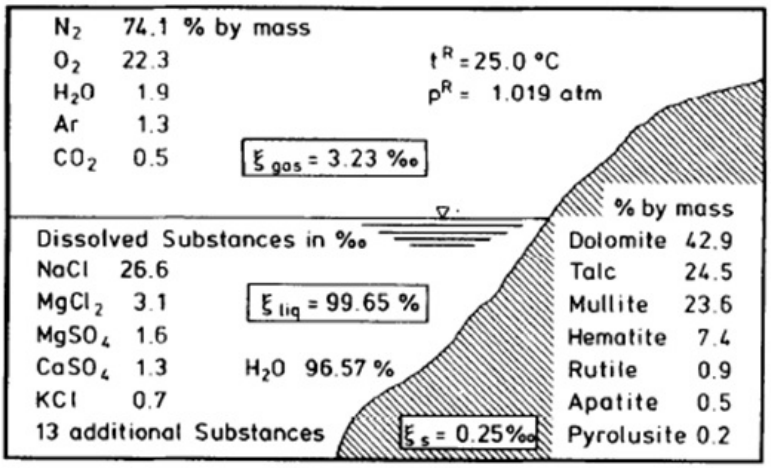

Figure 2.6: Example chemical reference environment proposed by Ahrendts. Source: [46]

Chemical exergy is made up of two types of chemical imbalance. The first is a difference in concentration of a substance that already exists in the chosen chemical reference state, for example CO_2 which exists freely in the atmosphere. Given a cylinder that is at the restricted dead state, but is filled with pure CO_2, which only makes up around 0.05% by mass of the Earth's atmosphere, the cylinder has chemical exergy. This is because work can theoretically be extracted as the concentrated CO_2 expands to its partial pressure in the reference environment.

The second component of chemical exergy is the work that can be extracted as a substance that is not present in the reference state undergoes a chemical reaction and turns into one or more of those substances. This is also known as the Gibbs free energy. The most basic example of this would be the oxidation of pure hydrogen. When combusted, hydrogen combines with oxygen to form water, which is present in the reference state, and releases energy. Many common substances have standard exergies that can be looked up in textbooks. Fuel exergies can be difficult to calculate directly, but equations are available in the literature to make accurate estimations. These are based on the regression analysis of known fuels, and require only the quantities of various elements in their composition.

The topic of chemical exergy is also discussed in Chapter 6. Further information can be found in references [45] and [43].

2.4 Other exergy forms

A summary of the different energy and exergy forms is given in Table 2.1. The differences between energy and exergy arise in thermal, chemical and also radiative energy forms, whereas kinetic, potential, mechanical and electrical are equivalent.

Table 2.1: Comparison of energy and exergy metrics. Based on: [11]

Type of energy flow	Specific energy	Specific exergy	Notes
Kinetic	$0.5\mathcal{V}^2$	$0.5\mathcal{V}^2$	J/kg
Potential	$g(z-z_0)$	$g(z-z_0)$	J/kg
Thermal	q	$q(1-\frac{T_0}{T})$	J/kg
Mechanical	w	w	J/kg
Electrical	$It\Delta$V	$It\Delta$V	J
Chemical (pure)	Δg_G	$\Delta g_G + RT_0 \ln(\frac{c}{c_0})$	c = molar conc.
Radiative	I_R	See [47]	W/m^2

2.5 Application of the exergy metric

The usefulness of exergy as a metric for the analysis of complex systems has been well established in the literature (see Chapter 1). This section provides a detailed explanation of the benefits exergy offers in the context of the work in this thesis as well as the limitations and potential drawbacks.

2.5.1 Comparison of systems

Exergy is a second-law metric, which provides a means of evaluating the quality of the energy in a system, regardless of its form. The opportunity this provides lies both in the possibility of comparing systems and their energy use directly, but also the simplicity of converting every exergy destruction and loss into equivalent fuel costs.

2.5.2 Clarification of causes of loss

The nature of exergy being a 2nd law metric clarifies the energy use of a system much better than energy would alone. This is illustrated well by Rosen [14] in the energy and exergy analysis of a coal power plant. It is shown, significantly, that energy and exergy efficiencies of the overall plants are similar, but the energy losses in the plants are associated with their emissions, whereas the exergy destruction actually identifies the location and hence, to an extent, the cause of inefficiencies in the system. This is illustrated best by the process diagrams in Fig. 2.7. The diagrams (in the case of energy, called Sankey diagrams and for exergy, called Grassman diagrams) represent the magnitude of energy and exergy flow in the system to scale by means of the width of the arrows at each point. When considering the exergy, the majority of the destruction occurs in the steam generation and power production sections of the plant. Considering only the energy, however, would suggest that the major losses are occurring because heat is being ejected from the plant (flow labelled Q_r). The exergy of the rejected heat, however, is comparatively insignificant. This makes it clear that recovering work from the rejected heat would be unproductive. To improve the efficiency of the plant, efforts should be concentrated on the design of the two aforementioned subsystems. The largest

exergy destruction occurs in the conversion of the fuel's chemical energy to thermal energy. As mentioned, energy in the form of heat cannot be fully converted to work because of the Carnot heat engine efficiency limit. This leads to large exergy losses inevitably occurring in combustion chambers. Care must be taken to acknowledge this effect in the analysis and not be misled into concentrating solely on the reduction of this destruction.

2.5.3 Improvement limitations and error prevention

Another benefit of using the exergy metric is the clarification of the limits of improvement of the efficiency of a component. For example, in the conversion of chemical to thermal energy, a certain amount of exergy destruction is unavoidable. It is possible to distinguish between the unavoidable exergy destruction and what could be avoided in theory, providing an upper limit to the improvement of a component.

Another viewpoint for this was discussed by Doty [1]. The optimisation of a system without reference to a 2nd law metric - either exergy or entropy - has the potential to lead to solutions that break the laws of thermodynamics. A somewhat simplistic example is illustrated in Fig. 1.2, wherein the work produced by a turbine is studied while changing the heat transferred into or out of a pipe supplying the input gas. Figure 1.2(a), relying only on 1st law analysis results, shows only that the best results are given when the maximum heat is transferred into the duct. Using only energy, the first law metric, a number of solutions are given that provide better turbine efficiency, but are actually physically impossible. Figure 1.2(b) provides results of the exergy analysis, stating in clear terms that the results transferring heat into the pipe result in the creation of exergy, thus breaking the 2nd law. Although the example is somewhat trivial, the argument that such preliminary design analysis requires both the 1st and 2nd law to be taken into account is valid. The aim is to immediately be aware of physically impossible designs and avoid wasting time in pursuing these further.

2.6 Exergy limitations

The merits of using exergy in optimisation studies and systems analysis are often strongly highlighted in the literature, making its use appear at first glance to be some kind of panacea for all engineering problems. Clearly this is not true, and for this reason a short discussion of the limitations of the metric is required.

2.6.1 Exergy and energy equivalence

As seen in Table 2.1, the usual energy metrics only differ from exergy in thermal, chemical and radiative forms. This means that many isolated studies of individual systems on an aircraft will not be improved by using exergy. This applies to any purely mechanical, aerodynamic, electrical or electronic system. Although using the term exergy instead of energy can be equally valid when designing such systems, the confusion caused by the less-known term will normally outweigh the benefits. In the case of systems where exergy analysis could prove beneficial, such as in gas turbine engines, isolated engineering fields have their own metrics for efficiency, e.g. specific fuel consumption. Exergy cannot replace such metrics directly, and when considering only fuel in versus thrust out, speaking in terms of exergy rather than energy will provide little benefit. The qualities of exergy are seen when studying systems that involve a number of energy forms, especially if they include thermal and chemical systems. An exergy analysis would, for existing engineering groups, generally be in addition to currently used techniques to provide a different perspective, more precise information and all the other potential benefits discussed.

2.6.2 Information provided

The analysis of a system in terms of exergy will indicate the locations at which the energy value is lost, but does not indicate in itself a means of improving the situation. A comparison between two system configurations is the minimum when trying to improve a design using exergy analysis.

In addition to this, it must be noted that exergy only indicates the work potential of the energy in the system. The usefulness of a stream of hot gas for heating is not immediately clear from only its exergy, although considering the 2nd law

in heating system analysis is important. When calculating the heating potential of a stream of hot gas, its ability to run an ideal heat pump in reverse should be considered.

2.7 Conclusions

This chapter provides the basic introduction to exergy that is necessary for this thesis to be self-contained. The derivation of the equation to calculate the physical exergy of a stream of gas is presented, which is the most important in the context of aircraft systems. Other forms of exergy are discussed and it is noted that energy and exergy are equivalent in a number of cases.

For the sake of tracing and mapping the energy in an aircraft in detail, the advantages offered by the exergy metric make its use essential. The aim of the project is to allow the direct comparison of the systems in terms of their energy use, but using energy as the metric in itself would obscure the results and limit the potential benefits. Exergy is a measure of the true value of the energy in the system and its use as a common currency throughout will allow all energy streams to be compared directly. The non-conserved nature of exergy means a clear limit is placed on the detail of the analysis and streams of low-grade energy can be interpreted correctly. Results will be clearer in meaning with its use.

The drawbacks of exergy do not invalidate its use within the context of this project, but do indicate its limits. Exergy analysis does not indicate how to improve a system, only where exergy destruction is occurring. Optimisation studies that use exergy destruction minimisation as the objective function must be limited in scope in order to limit the number of variables. The method proposed in this thesis leads to a highly detailed analysis of a system with limitless complexity for the sake of providing understanding and overview of energy use. The more detailed the analysis, the harder it is to produce an analysis of another system for comparison.

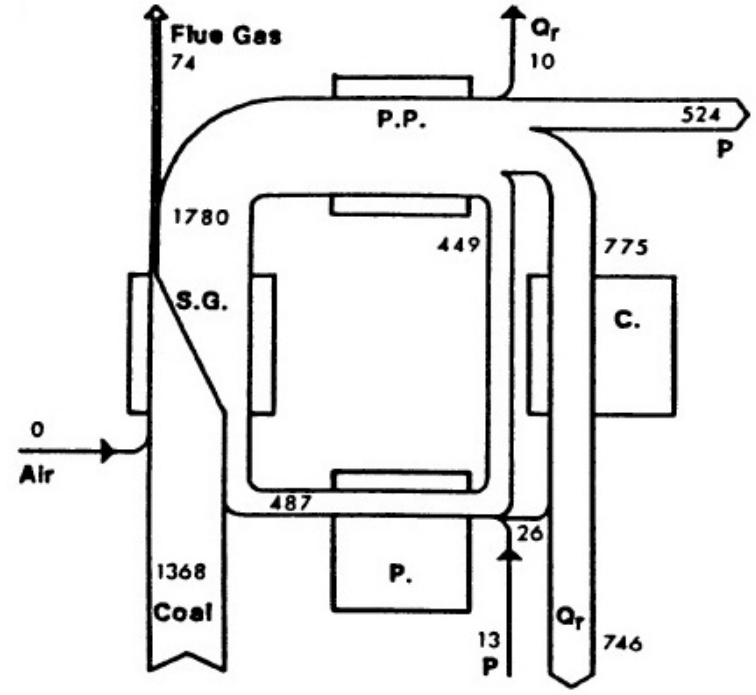

(a) Sankey diagram

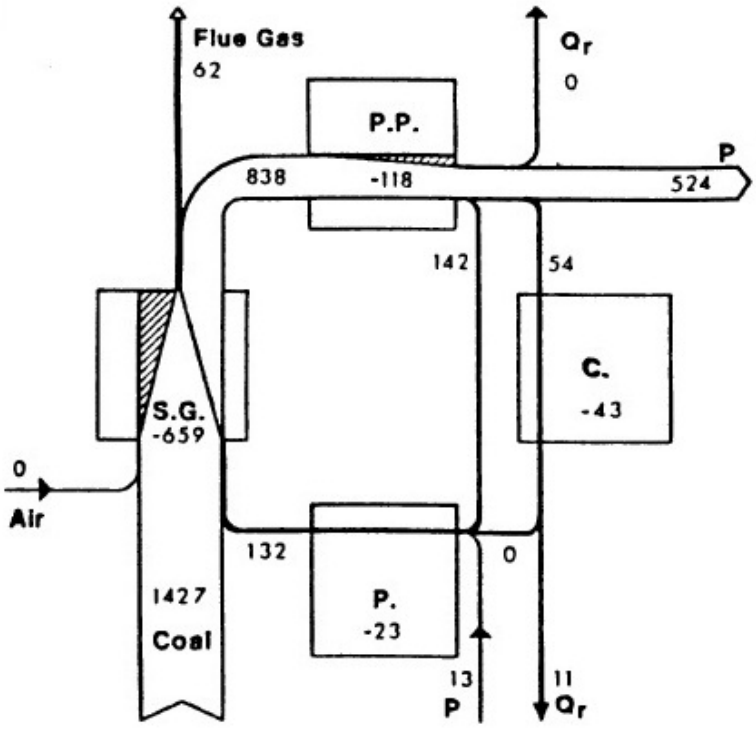

(b) Grassmann diagram

Figure 2.7: Process diagrams of energy (a) and exergy (b) flow rates for a coal-fired power plant. Steam generation (S.G.), power production (P.P.), condensation (C.), preheating (P.), electrical power (P) and heat rejected (Q_r) are labelled. Source: [14]

Chapter 3

Time-variant exergy analysis

The longest standing area of application of exergy analysis has been ground-based thermal plants that operate under effectively steady-state conditions at or near a single design point. Analyses of such systems will only consider that steady operating point and will neglect transient behaviour, including start-up and shut-down periods because they make up an insignificant portion of operating time. Although there has been significant previous work in the application of exergy analysis to individual aircraft subsystems for the purpose of optimisation, it almost invariably makes the assumption of steady operation. Most often, this is a point during the cruise phase that is suitably representative. The aim of this thesis, however, is not the specific optimisation of an individual system. Rather, the aim is to gain a better understanding of the exergy use of an aircraft in detail, to produce a reference tool for comparing systems and identifying potential for design improvements. It is therefore necessary to be able to compare an aircraft's systems without presumption of steady operation. Certain aircraft subsystems, such as hydraulics, do not have a steady operating point. Their use is determined by the demands of the mission and will vary with every flight. Even more significant is the consideration that the largest exergy user, the propulsion system, can only be assumed to operate steadily in very limited circumstances. A real mission, even during cruise, will involve regular changes of the engines' operation.

For the purpose of this work, there must be a clear intention not to limit the fidelity of the information captured, since the aim is to create a tool that is as broadly useful as possible. The assumption of steady operation when analysing an aircraft must therefore be rejected. The intrinsic complications of applying

time-variant exergy analysis are broached in this chapter. A simple case study of an electrically powered UAV is presented, which does not contain thermal or pressure based systems. This isolates the vehicle from the complication of variable reference states, which is a topic addressed in Chapter 6.

3.1 Exergy analysis principles

This section introduces the basics of exergy analysis as defined in the literature. The term 'exergy analysis' is sometimes considered to inherently include the optimisation of a system, but in this context will be thought of only as the process of close study using the exergy metric. In the scope of this thesis, the term 'analysis' refers simply to the act of gathering and understanding of data, without implying the optimisation of the system with regard to variables.

An analysis of a system will involve an exergy balance on at least one control volume, into and out of which exergy can flow. Such a balance is illustrated with Fig. 3.1.

The control volume balance is most often written as

$$0 = \dot{E}_i - \dot{E}_o - \dot{E}_q - \dot{E}_w - \dot{E}_D \tag{3.1}$$

where $\dot{E}_i$ and $\dot{E}_o$ are the total exergy input and output flow rates to the control volume, respectively. $\dot{E}_D$ is the exergy destruction rate in the control volume by irreversibilities. Also,

$$\dot{E}_q = \sum_k \left(1 - \frac{T_0}{T_k}\right) Q_k \tag{3.2}$$

the rate of exergy of heat transferred out of the component, usually a form of exergy loss, which could be lumped with the exergy destruction, $\dot{E}_D$, if the control volume is drawn large enough (see section 2.1.1). Also,

$$\dot{E}_w = \dot{W}_{cv} - p_0 \left(\frac{dV_{cv}}{dt}\right) \tag{3.3}$$

the rate of exergy transferred out of the control volume by means of mechanical work. The Grassmann diagram in Fig. 3.1 represents the exergy flows proportionally by means of the width of the arrows. The exergy destroyed in the control

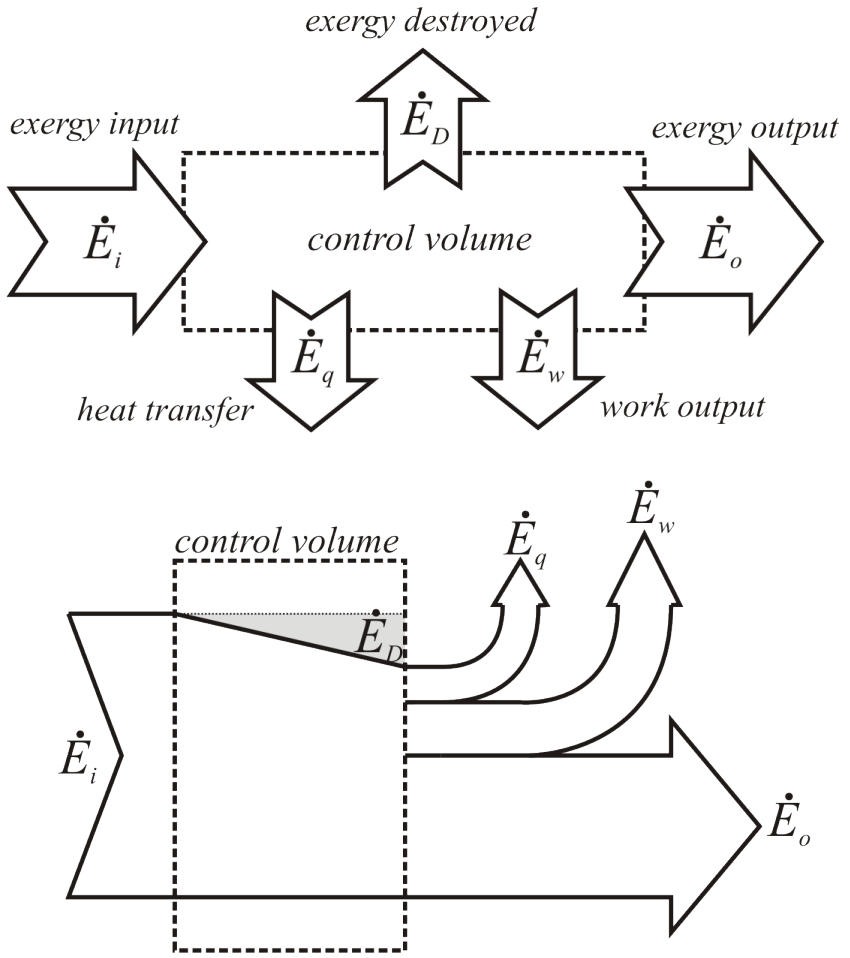

Figure 3.1: Basic component control volume and Grassmann diagram. First published in [48].

volume is shown as a reduction in the width of the arrow within the control volume, whereas the outputs $\dot{E}_o$, $\dot{E}_w$ and $\dot{E}_q$ are shown as exergy leaving with the potential to perform work elsewhere.

When considering components that do not carry exclusively thermal energy, in general terms, the exergy balance on a control volume can be written most simply as

$$\sum \dot{E}_i = \sum \dot{E}_o - \sum \dot{E}_D \tag{3.4}$$

where $\dot{E}_i$ and $\dot{E}_o$ may have a number of different forms:

$$\dot{E}_{i,o} = \dot{E}^{ph}_{i,o} + \dot{E}^{ch}_{i,o} + \dot{E}^{elec}_{i,o} \tag{3.5}$$

where

$$E^{ph} = (H - H_0) - T_0(S - S_0) + \frac{1}{2}m\mathcal{V}^2 + mgz, \tag{3.6}$$

$\dot{E}_{i,o}^{ch}$ is the chemical exergy flow rate and $\dot{E}_{i,o}^{elec}$ is the electrical exergy flow rate. This is applicable to a stationary component. The kinetic and gravitational potential exergy included in the physical exergy term, $\dot{E}_{i,o}^{ph}$, is that of the working fluid rather than the component itself. In the case of an analysis of a vehicle, the component's mass will also lead to exergy input and output in connection with the vehicle's movement and change in altitude. Equation (3.5) then becomes,

$$\dot{E}_{i,o} = \dot{E}_{i,o}^{ph} + \dot{E}_{i,o}^{ch} + \dot{E}_{i,o}^{elec} + \dot{E}_{i,o}^{KE} + \dot{E}_{i,o}^{PE} \tag{3.7}$$

where $\dot{E}_{i,o}^{KE}$ and $\dot{E}_{i,o}^{PE}$ are the component's kinetic and gravitational potential exergy due to its embodied mass, not including the mass of any working fluid that carries exergy in or out of the control volume.

3.2 Time-variance and exergy storage

The primary difference when the assumption of steady operation is no longer applicable is that an exergy balance across the component is no longer certain. To an extent, all components will store and release exergy temporarily, especially when including their mass-related kinetic and potential exergies. Equation (3.1) becomes

$$\dot{E}_s = \dot{E}_i - \dot{E}_o - \dot{E}_q - \dot{E}_w - \dot{E}_D \tag{3.8}$$

where $\dot{E}_s$ is the rate of change of storage within the control volume, which, like the previous exergy flows, is made up of the different exergy forms:

$$\dot{E}_s = \dot{E}_s^{ph} + \dot{E}_s^{ch} + \dot{E}_s^{elec} + \dot{E}_s^{KE} + \dot{E}_s^{PE} \tag{3.9}$$

The entire component control volume scheme that these equations describe is illustrated in Fig. 3.2.

For a fixed time period, T, the exergy balance over a component control volume is given by integrating,

$$\int_0^T \dot{E}_i(t)\,\mathrm{d}t = \int_0^T \Big(\dot{E}_o(t) + \dot{E}_D(t) + \dot{E}_s(t)\Big)\,\mathrm{d}t \tag{3.10}$$

This will, in a real analysis, be calculated using instantaneous values at regular time intervals. Equation (3.10) applies as long as the change in stored exergy,

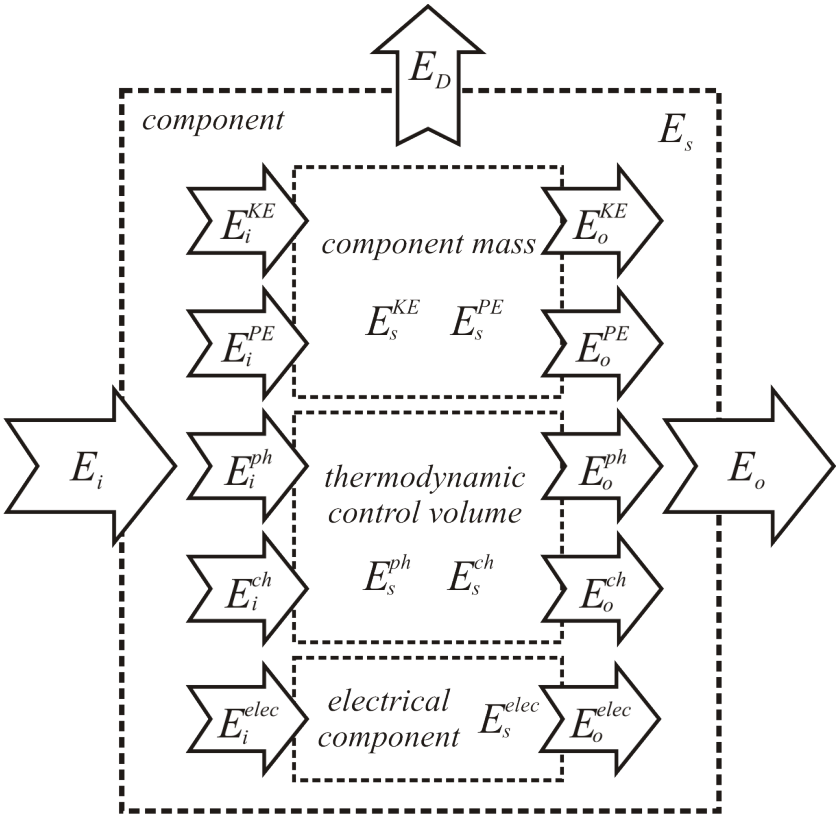

Figure 3.2: Detailed component control volume for time-variant vehicle analysis. First published in [48].

ΔE_s, is zero over the time period in question. This will rarely be the case when applied to an aircraft's mission, so a method of analysis must allow for this. A limited storage of fuel provided to the aircraft at the beginning of a mission must also be accountable. This means any exergy storage must be accounted in terms of stock, the total quantity at any given time, rather than flow. Equation (3.10) must therefore become

$$\int_0^T \dot{E}_i(t)\,\mathrm{d}t = \int_0^T \left(\dot{E}_o(t) + \dot{E}_D(t)\right)\mathrm{d}t + \Delta E_s \tag{3.11}$$

3.2.1 Grassmann diagrams of time-variant analysis

Leading on from the implications of Eq. (3.11), the commonly used Grassmann diagram has been adapted to deal with the storage term. However, the instantaneous stock of exergy in a component cannot be drawn to scale with the flows, because it will often be orders of magnitude larger. Rather, the change in storage

must be drawn. Figure 3.3 shows example diagrams for positive change in exergy stock (a) and negative change (b). Note that the storage arrows remain within the control volume, differentiating them from exergy inputs or outputs.

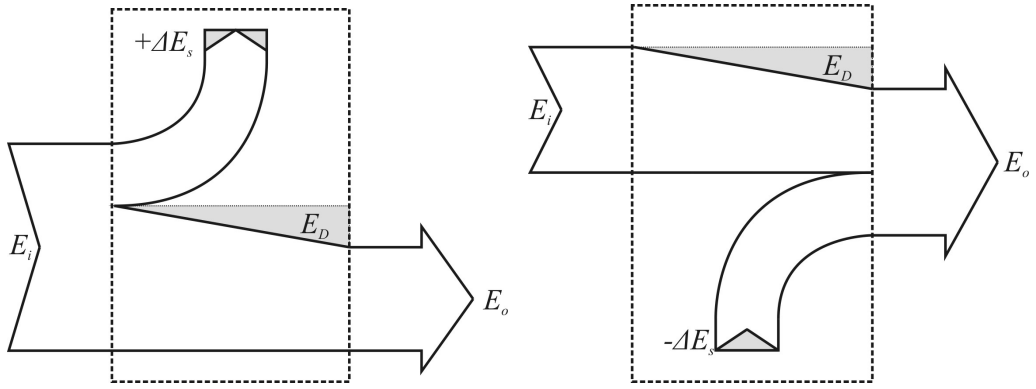

(a) Increase in exergy stock (b) Decrease in exergy stock

Figure 3.3: Representation of changes in exergy stock in a component Grassmann diagram

3.2.2 Known and unknown destruction

In a typical analysis of a complex system, such as an aircraft, the models or sensors providing the data are unlikely to give a comprehensive exergy balance on each component. Certainly, most losses and destruction mechanisms will be lumped together because only the exergy input and output are measured, implying the destruction of exergy by their difference. In cases where more detail of a component becomes known, the lumped exergy destruction term, $\dot{E}_D$, will be split:

$$\dot{E}_D = \sum_c \dot{E}_{l,c} + \dot{E}_d \tag{3.12}$$

where $\dot{E}_l$ is a known exergy destruction or loss that can be accounted separately for the sake of higher fidelity. $\dot{E}_d$ represents the remainder of exergy destruction that is only accounted for by the difference in inputs and outputs. The $\dot{E}_l$ terms will be important in cases where losses are significant, so that they can be distinguished from exergy destruction. $\dot{E}_d$ will remain large where higher energy forms (chemical, electrical) are being converted to heat. A negative value for $\dot{E}_d$ is indicative of an error.

3.3 Foundations of aircraft analysis

Having established the concept of exergy mapping for a time-variant system, this section considers its application to aircraft with the use of an electrically-powered unmanned aerial vehicle (UAV).

3.3.1 Basis in literature

The work by Paulus and Gaggioli [25, 26] serves as a starting point. The analyses presented in these papers are the only ones that combine the exergy of lifting and propelling the aircraft's mass with that running the subsystems. The example presented within is of a simple aircraft and the analysis takes place at a small number of operating points under the assumption of steady state. Figure 3.4 is an example of the exergy flow diagrams produced as a final visualisation of the results. The example is for cruise at 8,000 ft. The fuel's chemical exergy is transferred from the fuel stock to the engine, where the largest portion of exergy is destroyed, denoted by a negative number in the component. The propeller, powered by the engine, passes exergy to the wing and fuselage. The wing produces lift, which is distributed among the components according to their mass. This distribution is discussed in detail in Chapter 8.

The limitations of analysing and visualising an aircraft in the manner presented are relevant here. While the techniques presented in references [25, 26] are an important step, their application to a more complex system would soon become difficult to oversee. The only other application of exergy analysis to an entire aircraft was performed by Gandolfi et al. [2], but on a one-time basis at a limited number of steady-state flight times without discussing methodology.

3.3.2 Unmanned aerial vehicle case study

To provide an aid to discussion and establish the first procedures for creating an exergy map, a hand-launched, electrically powered, unmanned aerial vehicle (UAV) weighing 9 kg is used as a case study. The basis for this study is a real, commercially available aircraft for which data from a test flight was made available.

The use of an electrically powered UAV allows the analysis of an aircraft in

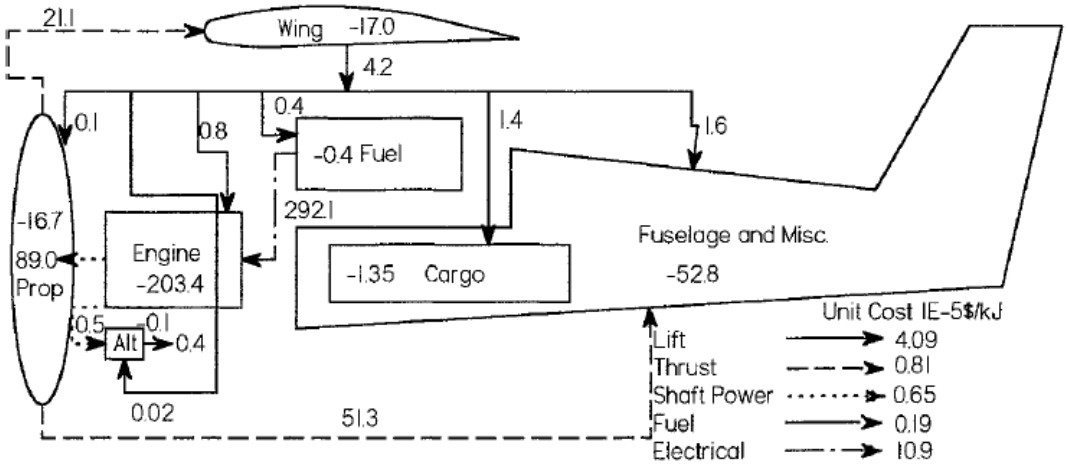

Figure 3.4: Aircraft exergy flow diagram given by Paulus and Gaggioli. Source: [25]

isolation from the consideration of variable thermodynamic reference states. This topic is addressed in detail in Chapter 6. This case study uses the software tool described in Chapter 4.

Exergy flow logic

The aircraft itself is powered by a pair of 9.6 Ah lithium polymer batteries, running two Orbit 25/18 brushless DC motors made by Plettenberg Electromotoren. These, in turn, run propellers produced by the aircraft manufacturer. The thrust provided by the propellers is transmitted to the various aircraft components in the form of kinetic exergy. The kinetic exergy is converted, through lift, into gravitational potential exergy, as well as being destroyed by various drag mechanisms. The gravitational potential increases as the aircraft climbs and decreases as it descends, being converted first into kinetic exergy and then being destroyed by drag.

Splitting the major components into control volumes and following the example set by Paulus and Gaggioli [25, 26], one might arrive at an exergy flow diagram as shown in Fig. 3.5. The exergy flows due to kinetic and potential exergy are accounted for each component, including those that have mass but do not perform active, exergy-consuming functions.

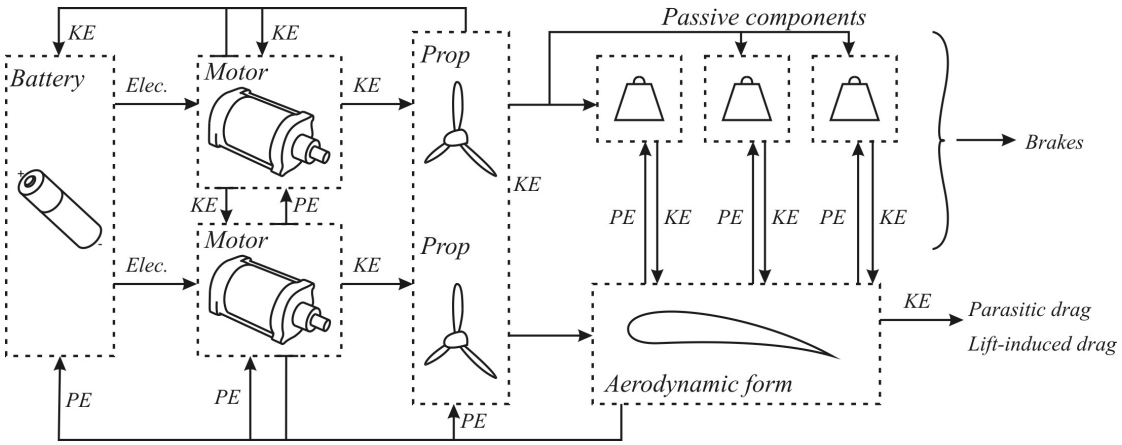

Figure 3.5: UAV exergy flow diagram, option 1

Analysis of the system in these terms would be complex due to the large number of exergy flows between components due to their mass. The outcome is not strictly the physical truth, because the destruction of exergy due to mass does not occur in the components themselves, but in the aerodynamics, especially due to increased lift-induced drag. The interpretation of how the wing's drag losses are assigned to the aircraft's mass is also made somewhat inflexible. A system much more complex than the one in question would become difficult to oversee and manage. It is more suitable, for the sake of allowing the analysis of larger aircraft, to strictly represent all exergy destruction where it occurs physically and to maintain simplicity by keeping the number of exergy transfers to be analysed at a minimum. For these reasons, the analysis of the UAV is undertaken using the exergy flow scheme shown in Fig. 3.6.

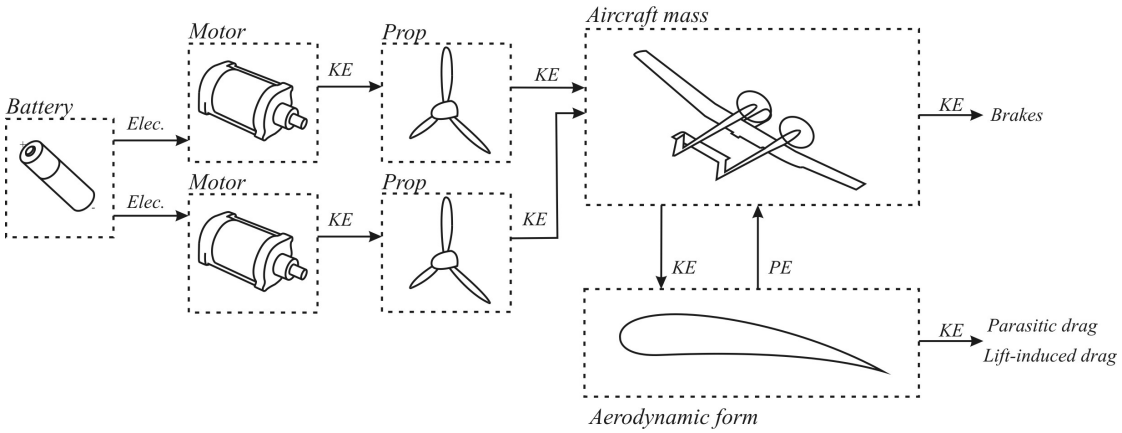

Figure 3.6: UAV exergy flow diagram, option 2

In this case, the exergy used by the propulsion system components to perform their active roles is accounted as before, but the entire aircraft's mass, including that of the active components, is lumped together under the 'mass' component. There may be value in considering the aircraft's fuel mass as a separate component to improve the fidelity of the accounted exergy flows, although this is not implemented in this thesis. The aircraft's interaction with the air is considered as one component, named 'aerodynamics,' which includes the wing and is the physical location for all drag mechanisms. This method of accounting exergy destruction precisely where it occurs physically is important to allow highly complex systems to be analysed, but will require another step to fully understand the exergy costs incurred by the mass of the aircraft. This topic is discussed in detail in Chapter 8.

Mission description

Figure 3.7 shows the variation of altitude and airspeed as recorded for the test flight being analysed. These data were provided by EADS Innovation Works.

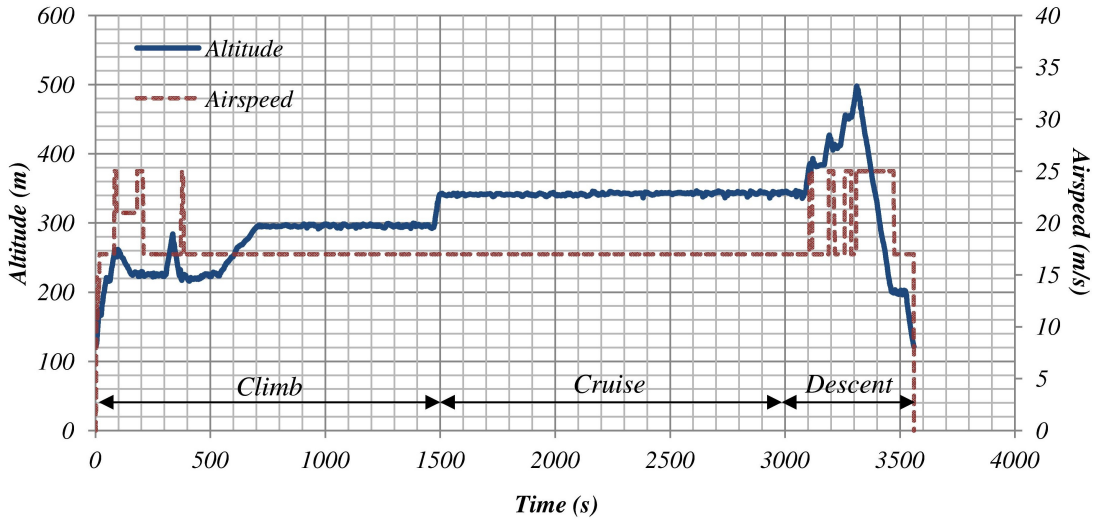

Figure 3.7: UAV mission

Calculations

The airspeed, in the case of the UAV, was not measured, so the line shown represents the requested speed. For this simplified analysis, the requested airspeed was

smoothed, so the transitions between 17 and 25 m/s were not instantaneous. To calculate the kinetic exergy of the aircraft, it may normally be desirable to use the ground speed, although this is not available in this study. Using the airspeed of the aircraft is equivalent to using an instantaneous local reference state for the exergy calculation. The effects of this in are discussed in Chapter 6. For now, this choice also reduces the effects of unknown wind speed and direction, which would cause unaccountable increases and decreases in the aircraft's kinetic exergy throughout the mission. The altitude readings were smoothed with a moving average to reduce non-physical fluctuations. A typical propeller efficiency of 0.8 was used throughout the mission as suggested by the manufacturer. A conservative estimate of 0.85 was used for the electric motor efficiency based on the motor manufacturer's efficiency tests during climb conditions (14.8 V, 20 A/motor) [49]. These efficiencies would, in reality, fluctuate depending on conditions. Greater accuracy could be achieved with a detailed model of the components. To calculate gravitational potential, the take-off altitude is used as the reference point. This is equal to the landing altitude, so exergy stock at the beginning or end of the mission is zero. The study uses data points taken at a sampling frequency of 5 Hz.

For the purpose of creating the exergy map, the following items were therefore known:

- Airspeed
- Altitude
- Motor electrical power inputs
- Aircraft mass
- Motor efficiency
- Propeller efficiency

The values for the various stages of the exergy flow map were calculated with the following equations:

$$\dot{E}_{out}^{battery} = \dot{E}_{in}^{motor1} + \dot{E}_{in}^{motor2} \tag{3.13}$$

$$\dot{E}_{out}^{motor} = 0.85\dot{E}_{in}^{motor} \tag{3.14}$$

$$\dot{E}_{out}^{propeller} = 0.8\dot{E}_{in}^{propeller} \tag{3.15}$$

$$\dot{E}_{in}^{mass} = \dot{E}_{out}^{propeller} + \dot{E}_{out}^{aerodynamics} \tag{3.16}$$

$$E_{store,KE}^{mass} = \frac{1}{2} m_{ac} \mathcal{V}^2 \tag{3.17}$$

$$E_{store,PE}^{mass} = m_{ac} g z \tag{3.18}$$

$$E_{store}^{mass} = E_{store,KE}^{mass} + E_{store,PE}^{mass} \tag{3.19}$$

$$\dot{E}_{out}^{mass} = \begin{cases} \dot{E}_{in}^{mass} - \dot{E}_{store,KE}^{mass} & \text{if } \frac{\mathrm{d}z}{\mathrm{d}t} \geq 0 \\ \dot{E}_{in}^{mass} - \dot{E}_{store,KE}^{mass} - \dot{E}_{store,PE}^{mass} & \text{if } \frac{\mathrm{d}z}{\mathrm{d}t} < 0 \end{cases} \tag{3.20}$$

$$\dot{E}_{out}^{aero} = \begin{cases} mg\frac{\mathrm{d}z}{\mathrm{d}t} & \text{if } \frac{\mathrm{d}z}{\mathrm{d}t} > 0 \\ 0 & \text{if } \frac{\mathrm{d}z}{\mathrm{d}t} \leq 0 \end{cases} \tag{3.21}$$

Results

The exergy data for the mission was calculated using Eqs. (3.13) - (3.20). The data were then inserted into the database structure according to the layout shown in Fig. 3.6 using the software tool developed for the task, which is described in Chapter 4. The results, integrated over the three mission segments identified in Fig. 3.7 are given for each component in Tables 3.1 - 3.3. Grassmann diagrams to visualise the results are given in Fig. 3.8.

The Grassmann diagrams in Fig. 3.8 are to scale. Exergy is stored in the mass component during the climb phase. The net storage change in the descent phase represents the release of that exergy again. The exergy coming from the Battery component is represented as being released from storage. The exergy destruction in the motor and propeller components remain proportionally constant and their

Table 3.1: UAV mission: climb phase results

Component	Input exergy (kJ)	Output exergy (kJ)	Destr. exergy (kJ)	Storage exergy (kJ)
Battery	0	245.5	0	-245.5
Motor 1	122.4	104.04	18.36	0
Motor 2	123.1	104.63	18.46	0
Propeller 1	104.04	83.23	20.81	0
Propeller 2	104.63	83.71	20.93	0
Mass	232.02	207.17	0	24.85
Aerodynamics	207.17	65.08	142.1	0

Table 3.2: UAV mission: cruise phase results

Component	Input exergy (kJ)	Output exergy (kJ)	Destr. exergy (kJ)	Storage exergy (kJ)
Battery	0	252.34	0	-252.34
Motor 1	125.41	106.6	18.81	0
Motor 2	126.93	107.89	19.04	0
Propeller 1	106.6	85.28	21.32	0
Propeller 2	107.89	86.31	21.58	0
Mass	201.65	199.77	0	1.88
Aerodynamics	199.77	30.06	169.17	0

total is similar in magnitude to the aerodynamic exergy destruction (drag). The exergy converted by the wing into lift is represented by the loop returning to the mass component.

The descent phase diagram is smaller, mainly due to the shorter time period being analysed. The total exergy flowing through the components is less. Counter to intuition, the exergy consumed by the aircraft during climb and cruise is similar. While the aircraft requires a significant amount of extra power to accelerate at launch and exergy is stored as gravitational potential during climb, other effects during cruise compensate for this. For example, the aircraft maintains altitude

Table 3.3: UAV mission: descent phase results

Component	Input exergy (kJ)	Output exergy (kJ)	Destr. exergy (kJ)	Storage exergy (kJ)
Battery	0	95.49	0	-95.49
Motor 1	48.53	41.25	7.28	0
Motor 2	46.96	39.92	7.04	0
Propeller 1	41.25	33	8.25	0
Propeller 2	39.92	31.94	7.98	0
Mass	92.84	109.62	0	-16.78
Aerodynamics	109.62	27.9	81.7	0

by switching off its motors when it has climbed too high, leading to the need to accelerate to resume the requested airspeed. Higher wind speeds at altitude are likely also to have an influence.

During each time period being analysed, all the exergy provided by the battery is either destroyed or stored. This is shown in each diagram, where the widths of the ramps representing exergy destruction and the storage arrows add up to the width of the original input arrow. The diagrams and numerical results show the gross inputs and outputs of each component and how they are linked over the time period in question. The mass component, for example, receives some of the 'same' exergy twice during each phase, once from the propellers and once, in the form of lift, from the wings. For this reason, the exergy shown in the loop back from the aerodynamic to the mass component does not have a visible destruction. This type of duplication of exergy can cause confusion if the data are viewed primarily in numerical form, but can be more easily seen when graphically represented. It is an inevitability in many types of systems where exergy travels circularly, including in internal combustion engines where exergy extracted from the fuel is required to self-perpetuate the engine.

Difficulty in this particular analysis arises due to uncertainty in the motor and propeller efficiencies, both of which would in reality fluctuate somewhat depending on operating conditions. There is therefore a discontinuity between the known power data from battery to mass. The kinetic and potential exergies of the mass

component were calculated from known velocity and altitude data while the values in the electrical components were calculated from electrical instrument readings. This means that some losses that should be occurring in the propeller component are being accounted for in the aerodynamic component or vice-versa. Such discontinuities will be unavoidable in many such analyses and should be taken into consideration in any conclusions drawn. In analyses where the results will have a bearing on design decisions, data should be validated and uncertainty properly taken into account.

3.4 Conclusions

This chapter forms the theoretical basis of time-variant exergy analysis of aircraft. This provides the initial requirements for the software tool developed, as described in Chapter 4. A method of accounting for temporary storage is identified as a necessity to allow for time-variant analysis. The principles for dividing a system into control volumes are established and the exergy balance equations across the components are written down. As an example, an electrically powered UAV, for which flight data were available, was used as a case study. A method for accounting the exergy flow associated with mass and movement was established, which relies on the consistent accounting of exergy destruction in the physical location in which it takes place. This simplification will allow the analysis of highly complex systems, but means a further layer of analysis is required to allow the allocation of exergy destruction due to lift-induced drag to the aircraft components' individual masses. This topic is addressed in Chapter 8.

The UAV is analysed and results for three distinct flight phases are presented, including Grassmann diagram visualisations. Although it is clear that quality of data used in the case study means the results are of limited use to the aircraft's engineers, the study does provide preliminary confirmation of the technique of analysis and the software tool used to implement it. The diagrams provide excellent visualisation of the results and show potential to be useful in understanding complex data sets in combination with the exergy flow tables. The basis for exergy mapping has been established and the more complex aspects of its implementation are dealt with in the remainder of the thesis.

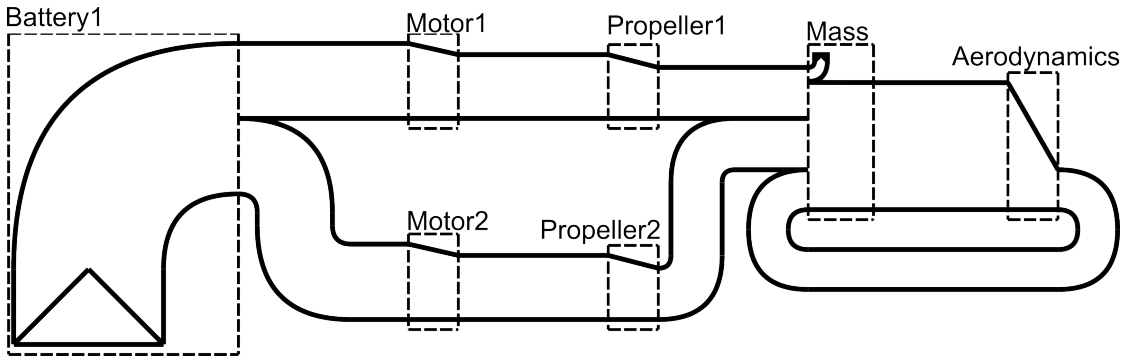

(a) Climb phase

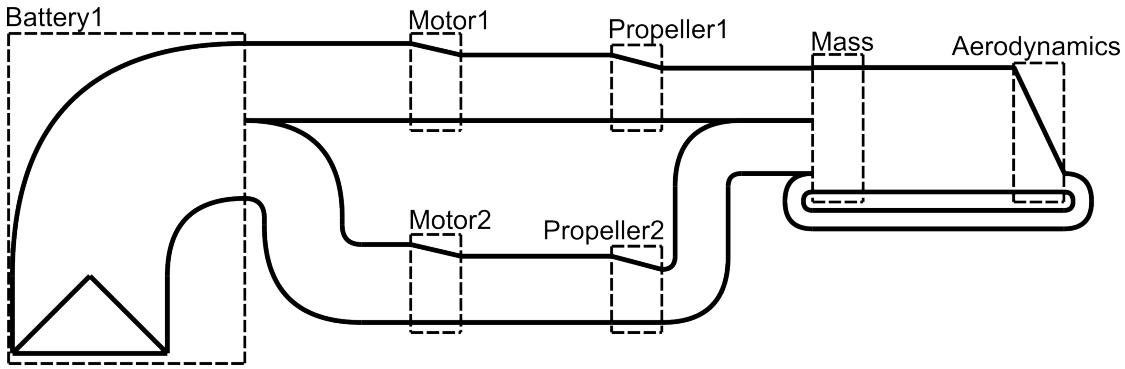

(b) Cruise phase

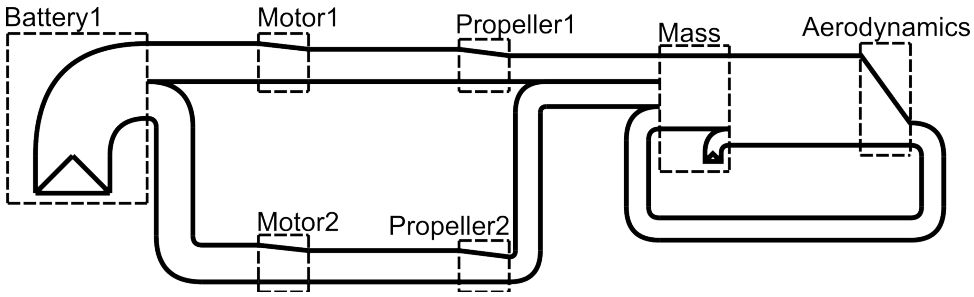

(c) Descent phase

Figure 3.8: Grassmann diagrams for the three UAV flight phases. First published in [48].

Chapter 4

Software tool prototype design

It is the aim of this thesis to present a method by which an aircraft can be analysed in terms of exergy in unrestricted detail. The basics of time-variant exergy mapping have been established in the previous chapter, but to be able to create an exergy map of a complex aircraft, a software tool is required that allows oversight to be maintained. The inclusion of time-variance means data must be stored at a certain frequency at every instrumented or simulated control volume boundary for the entire mission. This frequency should be sufficient to provide reasonable accuracy when numerical integration is applied to the data and show enough detail when analysing only short time periods.

The calculations required to produce exergy data for such an analysis also become complex and time-consuming. A set of tools to automate certain calculations are required, which must be suitably validated against known results. The requirements to produce a software tool prototype exist because the limits of off-the-shelf software, such as spreadsheets, would be too prohibitive when trying to map complex aircraft. Maintaining oversight, memory limitations and accessing portions of the data as required would prove problematic. Developing the software tool as part of the research project is important for creating the case studies that validate the approach being considered, but is also necessary in itself to prove its feasibility.

4.1 Requirements

The software tool's required functions are described here. These constitute the software prototype developed over the course of this project.

4.1.1 Database

A relational database is typically used in large data applications of this nature. The aircraft's components must be stored in a systematic way, without imposing limits on the size and complexity of the system being analysed. Alongside, the exergy flow and stock data must be maintained and associated with the relevant system location. In order to interpret the system and exergy data, the flow sequence and direction through the system must also be captured.

Relational databases are useful for such tasks because they can prevent data duplication and certain types of input error. Specific data points can be accessed easily and quickly with the correct query – a task that can be problematic with any other kind of data storage. The possibility of concurrent access to the database could be useful if two or more users wish to access and edit it at the same time, something that may be relevant in the future if a truly complex system is being mapped in an industrial setting.

4.1.2 Input interface

The database must be populated by the user with the data that makes up the exergy map. To do so, a suitable interface is required that will make straightforward the transition from a written-down system layout and an associated exergy data set to a completed exergy map database.

4.1.3 Exergy calculators

A set of calculators are required that allow large sets of thermal data (temperature, pressure and mass flow rate) and chemical data (composition, mass flow rate) to be processed into exergy. Calculations of this nature are somewhat complex and rely on tabulated data for the materials involved. In order to process large data sets, these calculations must be automated.

4.2 Selection of programming environment

This section describes the reasoning behind the choice of software and programming environment used to produce the exergy mapping tools.

4.2.1 Database

The choice of database software is not one of lasting importance. For the purpose of the software tool prototype, Microsoft Access, being a constituent of MS Office, was chosen as the database software because it is generally available to the majority of potential users. The databases produced can be accessed and edited from external software using ODBC (Open Database Connectivity) drivers using SQL (Structured Query Language) commands. Provided the database structure and naming are exactly the same, any other SQL database format should be accessible from the software tools, provided the relevant ODBC drivers are available.

4.2.2 Software tools

The uncertain nature of what, precisely, would be required in terms of calculation and data manipulation, both for the purposes of the project and by any later user, makes the choice of a typical compiled programming language (C++, Java etc.) unwise at this stage. For the purpose of developing a software prototype in a research context and allowing direct manipulation of large datasets in previously unforeseen ways, Matlab [50] will prove a more flexible environment. This software is widely available in engineering facilities. Should a set of tools for the purpose of exergy mapping become complete in the future and widely required, it would be feasible to translate the software to a compiled language to produce a distributable executable file. This would ultimately be useful for the purpose of improving accessibility to the tools (removing requirement for a Matlab licence) and for computer resource efficiency.

In order to make use of the ODBC drivers that allow interaction with the database, Matlab's database toolbox is required. It is important to note that one must use the 32-bit or 64-bit versions of MS Access and Matlab together, since the ODBC drivers will not be compatible otherwise and the connection between the

two will not work.

Matlab has many inbuilt mathematical functions that would not be immediately available using other programming environments. It provides a working data manipulation environment that would not be feasible to replicate externally and as such is highly useful for the work in question. It also provides functions for the creation of graphical user interfaces (GUIs), which are important to enable the use of the software tools. GUIs can be created graphically, using the GUIDE tool, or programmatically, especially in conjunction with the freely available GUILayout toolbox. The interfaces for the software tools were produced with the latter method (except for the analysis GUI), because the final product can have a more efficient and professional design, can be resized and can include tabs and other, more complex features.

4.3 Database design

As discussed in Chapter 3, the exergy mapping method is based on splitting the system under analysis into component control volumes ('components'). These components have inputs, outputs, storage, loss and known destruction mechanisms, collectively to be known as 'interfaces', at which data is stored, Fig. 4.1. Components are part of a subsystem, such as the hydraulics or propulsion.

The database layout settled upon is shown in Fig. 4.2. Each box represents a database table with the table name at the top and respective field names listed underneath. The relational structure of the database is represented by the connecting lines. Relationships are one-to-many, indicating, for example, that a subsystem can contain many components, but each component can only be a member of one subsystem. The key symbols indicate key fields, which by themselves or in combination (composite key) create a unique identifier for each record.

The Links table (Fig. 4.2) contains the data required to represent the exergy flow layout of the system. It simply contains the identifier for the interfaces downstream of each interface – the next interface to which the exergy flows.

The Datapoints table serves as a junction between the Interfaces and Data tables. For the sake of consistent accounting, exergy should only be lost or destroyed

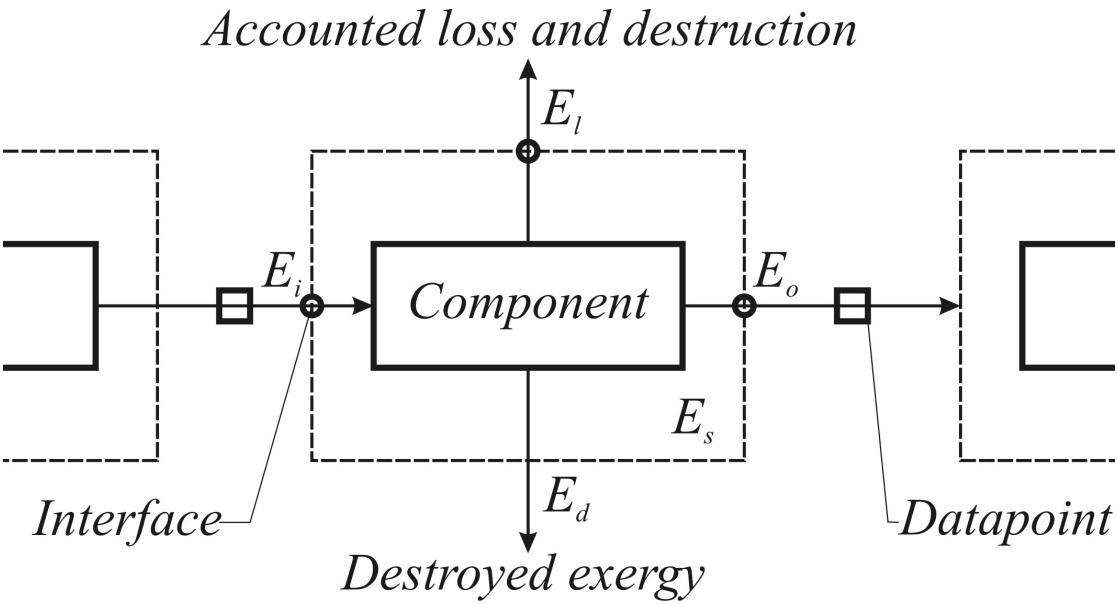

Figure 4.1: Component and interface illustration

across a component control volume. Therefore, if an interface links with a single interface downstream, the exergy leaving the first must equal the input to the next. Using a junction table allows the data to be re-used, rather than duplicated at each interface.

The Data table contains the exergy flow and stock data for each data point at each time step. The different possible exergy types are kept in separate fields to allow the distinct representation of mixed exergy flows. An example of this might be a hot fuel flow, where the distinction between the chemical exergy and thermal exergy would be important, if both are included in the analysis. This table will normally constitute the majority of the database's file size. The use of a composite key reduces the number of fields required by one, and implicitly prevents duplicate records. The time points, however, must be stored as integers in order to be used as key fields since floating point numbers (single or double precision) are not accurate enough to be directly referenced. This means the software tool interface requires an input from the user to define the time step size.

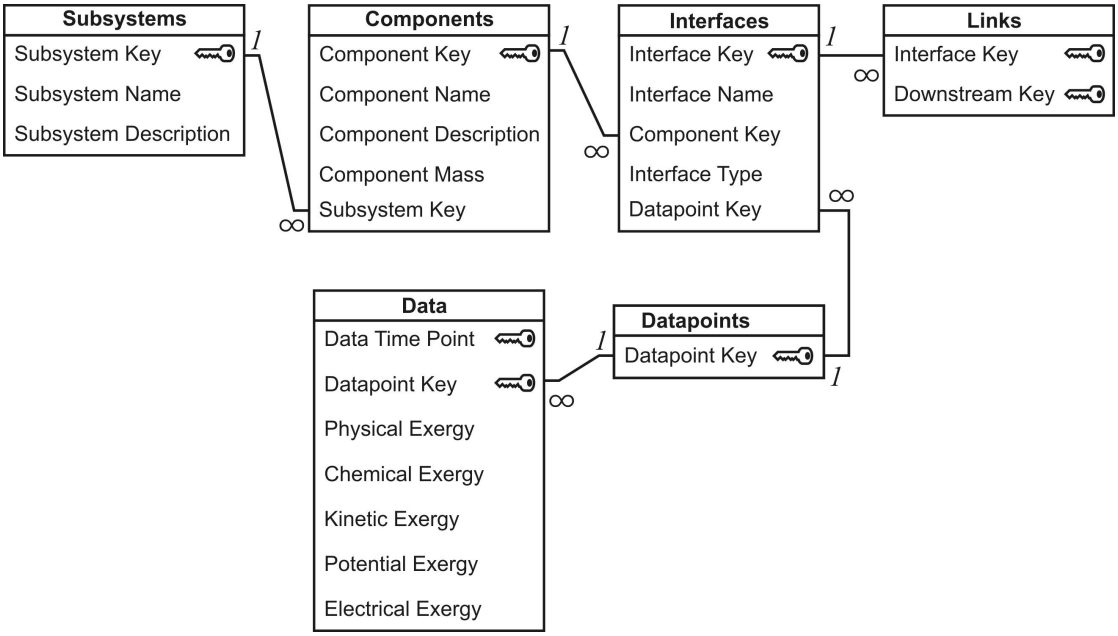

Figure 4.2: Database structure

4.4 Database control interface

This GUI is for the purpose of creating the exergy map in the database. It includes tools for calculating exergy from raw data, tools for creating the layout of the system and tools for inserting the exergy data into the relevant locations.

4.4.1 General input

Figure 4.3 shows the input GUI layout with the general input tab open. The list boxes on the left show the names of the subsystems, components and interfaces in the database being edited. All the subsystems are displayed at all times, but the components and interfaces are accessed by selecting the subsystem or component they are located in. The detailed description of functions is given in Appendix A.

4.4.2 Map creation

Figure 4.4 shows the Links tab, which contains tools for the direct manipulation of the system structure in the database. The subsystem/component/interface navigation on the left remains the same as before. Further details on the functions and use can be found in Appendix A.

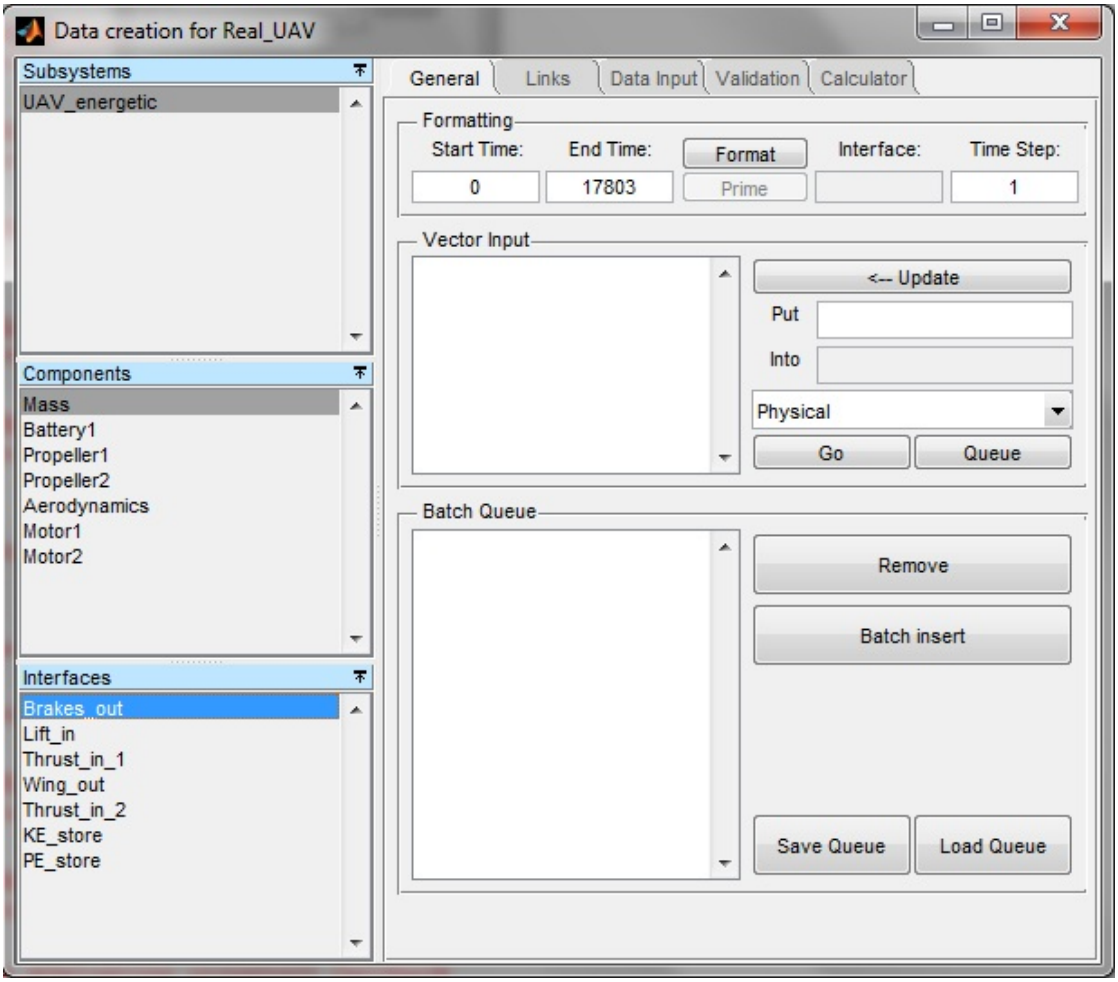

Figure 4.3: Input GUI: General input tab

4.4.3 Calculators

Figure 4.5 shows the calculator tab with the physical exergy calculator open. Figure 4.6 shows the chemical exergy calculator, which can be accessed by minimising the physical exergy calculator. The methods used for the calculations and validation of the results are given in Subsection 4.4.4. Details on the interface can be found in Appendix A.

4.4.4 Calculation procedures and validation

Physical exergy calculator

The physical exergy calculator is limited to calculating the exergy of gas mixtures that can be assumed ideal. The calculator uses the HOT thermodynamic tool

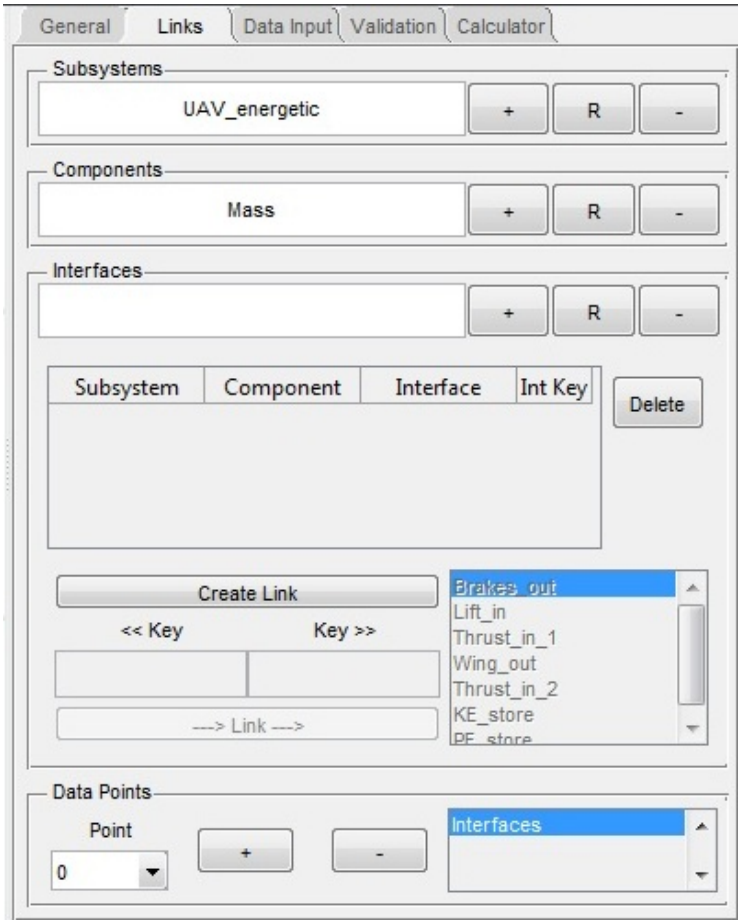

Figure 4.4: Input GUI: Links and components input tab

release 2.6 made available under the Academic Free Licence v3.0 [51] to look up entropy and enthalpy data for gas mixtures. The data used by the HOT tool are derived from NASA and Stanjan data. The tool was checked for consistency with tabulated textbook [43] data before its integration with the software being developed.

The specific physical exergy of an ideal gas mixture is found using

$$e^{ph} = \sum_k x_k \left(h_k - h_{k,0} - T_0 \left(s_k - s_{k,0} \right) \right) \tag{4.1}$$

where x represents the mass fraction of gas species k. The enthalpy and entropy at the system's temperature and pressure, as well as the reference state's temperature and pressure are found. Multiplying the results of Eq. (4.1) by the mass flow rate yields the exergy flow rate.

To validate the results of the calculator, a worked example of a cogeneration

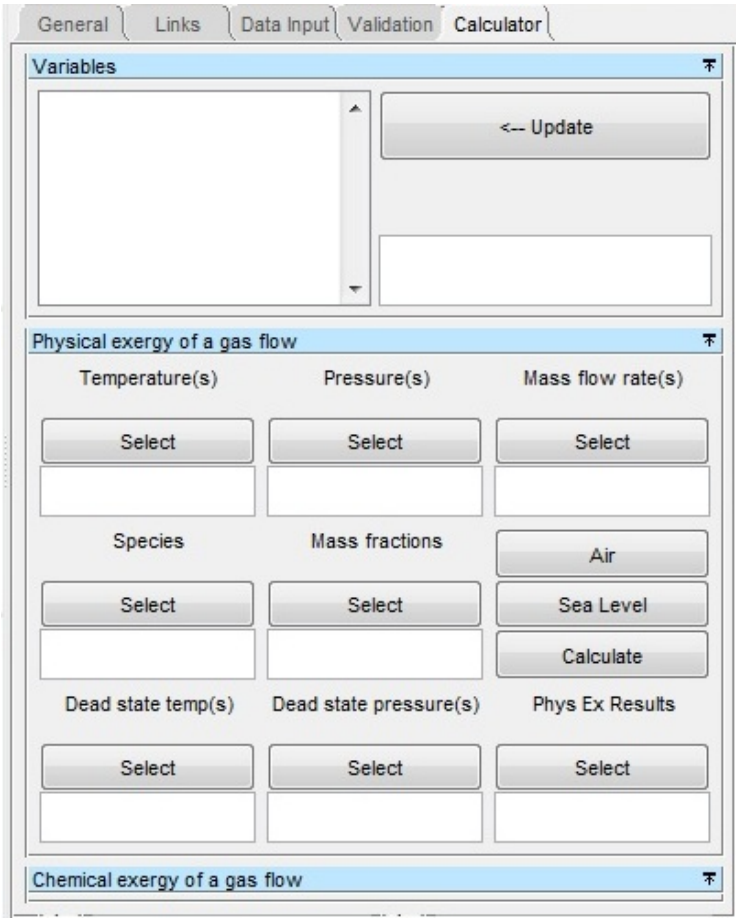

Figure 4.5: Input GUI: Calculators tab

power plant in Bejan et al. [45] (p.127) was used. A reference environment of $T_0 = 298.15$ K and $p_0 = 1.013$ bar applied. Results are compared in Table 4.1.

The accuracy of all results except Point 9 are acceptable for most purposes, although Points 3 and 4 diverge somewhat. The errors are primarily due to the incomplete handling of the water vapour species using the HOT thermodynamic tool alone. The addition of complete steam table look-up functions to the calculator have slowed down the calculation process excessively. For now, the results for gas streams composed of large amounts of water vapour cannot be calculated. Other gas streams with only small fractions will be sufficiently accurate but effort should be made to allow for water vapour if the tool is used in an analysis in which accuracy is of greater importance.

Table 4.1: Physical exergy calculator validation

Point	T (K)	P (bar)	Mass flow rate (kg/s)	Gas species	Mass fractions	Bejan (MW)	Calculator (MW)	Error (%)
1	298.15	1.013	91.2757	$N_2, O_2, CO_2, H_2O(g)$	0.758, 0.230, 0.000461, 0.0119	0	0	0
3	850	9.623	91.2757	$N_2, O_2, CO_2, H_2O(g)$	0.758, 0.230, 0.000461, 0.0119	41.94	41.38	1.35
4	1520	9.142	92.9176	$N_2, O_2, CO_2, H_2O(g)$	0.744, 0.155, 0.0489, 0.0516	101.1	100.7	0.4
9	485.57	20	14	$H_2O(g)$	1	12.79	6.871	86.15
10	298.15	12	1.6419	CH_4	1	0.627	0.627	0

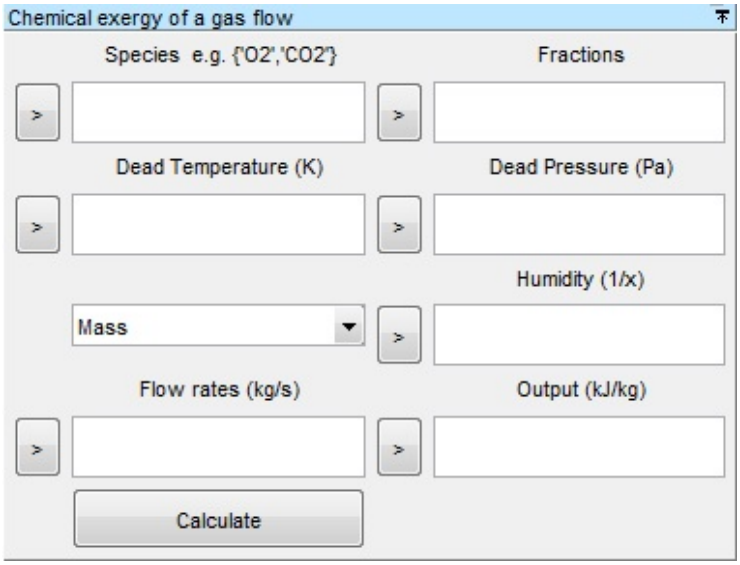

Figure 4.6: Input GUI: Chemical exergy calculator gui

Chemical exergy calculator

This tool was primarily developed to assist in the study presented in Chapter 6. The most likely situations in which the chemical exergy is going to be required in an aircraft analysis will be the fuel flow and the combustion products of an engine. This tool is only intended for gas flow calculations, so will only be useful for the latter. The chemical exergy of a gas mixture can be found using [45]

$$\bar{e}^{ch} = \sum_k \bar{x}_k \bar{e}_k^{ch} + \bar{R}T_0 \sum_k \bar{x}_k \ln \bar{x}_k \tag{4.2}$$

where $\bar{R}$ is the molar gas constant (8.314 J/K$\cdot$ mol) and bars represent molar quantities. The standard chemical exergy, $\bar{e}^{ch}$, of a particular species can be looked up or calculated using

$$\bar{e}_k^{ch} = -\bar{R}T_0 \ln \bar{x}_k^e \tag{4.3}$$

if the gas is present in the reference environment, where $\bar{x}_k^e$ is its mole fraction therein. Ertesvåg [52] provides a method of calculating the effect of a change in reference state on the chemical exergy of a gaseous fuel. The full equations are

$$\bar{e}_k^{ch} = \bar{e}_k^{ch,ref} \frac{T_0}{T^{ref}} + \frac{T^{ref} - T_0}{T^{ref}} \left(-\Delta H^{ref}\right) - W_1 - W_2 + T_0 \bar{R} \sum_{j \neq k} \mathsf{V}_j \ln \frac{x_j^{ref}}{x_j^e} \tag{4.4}$$

where

$$W_1 = \sum_j \mathsf{V}_j \int_{T^{ref}}^{T_0} c_{p,j}(T) \left(1 - \frac{T_0}{T}\right) \mathrm{d}T \tag{4.5}$$

and

$$W_2 = T_0 \bar{R} \sum_j \mathsf{V}_j \ln \frac{p_0}{p^{ref}} \tag{4.6}$$

Usually, W_1 and W_2 can be neglected because their contribution is small [52]. The superscript ref refers to the standard reference conditions, at which standard chemical exergy of species k, $\bar{e}_k^{ch,ref}$, was calculated. The 0 subscript refers to the new reference state. V_j is the stoichiometric coefficient of co-reactant or product j. For fuels, $-\Delta H$ is the negative of the lower heating value (LHV).

Equations (4.2) and (4.4) were used, along with a look-up table for a set of substances likely to be found in an aircraft, to create the chemical exergy calculator. To validate, the results provided by the calculator were compared to those published in [52] and found to precisely match the results. Ertesvåg's results only span temperatures between 50°C and -30°C, so the validity of calculations outside that range may require further investigation in future if precision in these calculations is critical. It is not possible to validate the calculator's results against a separate source, since Estesvåg's is the only currently available work on this topic.

4.5 Analysis GUI

The analysis GUI, shown in Fig. 4.7, is for the viewing, interpretation and visualisation of the data entered in the aircraft exergy map database. It is intended to enable understanding the physical location of exergy destruction, the relative magnitude of exergy flows and for checking the validity of the entered data. More details on this interface can be found in Appendix A.

4.6 Grassmann diagram generation tool

A tool was created to allow the automated drawing of a Grassmann diagram for subsystems. Although the diagrams are useful for understanding and communicating exergy flow data, their manual creation requires some skill with drawing software and a large amount of time. In order to allow the relatively quick comparison of exergy data using these diagrams, this tool was developed.

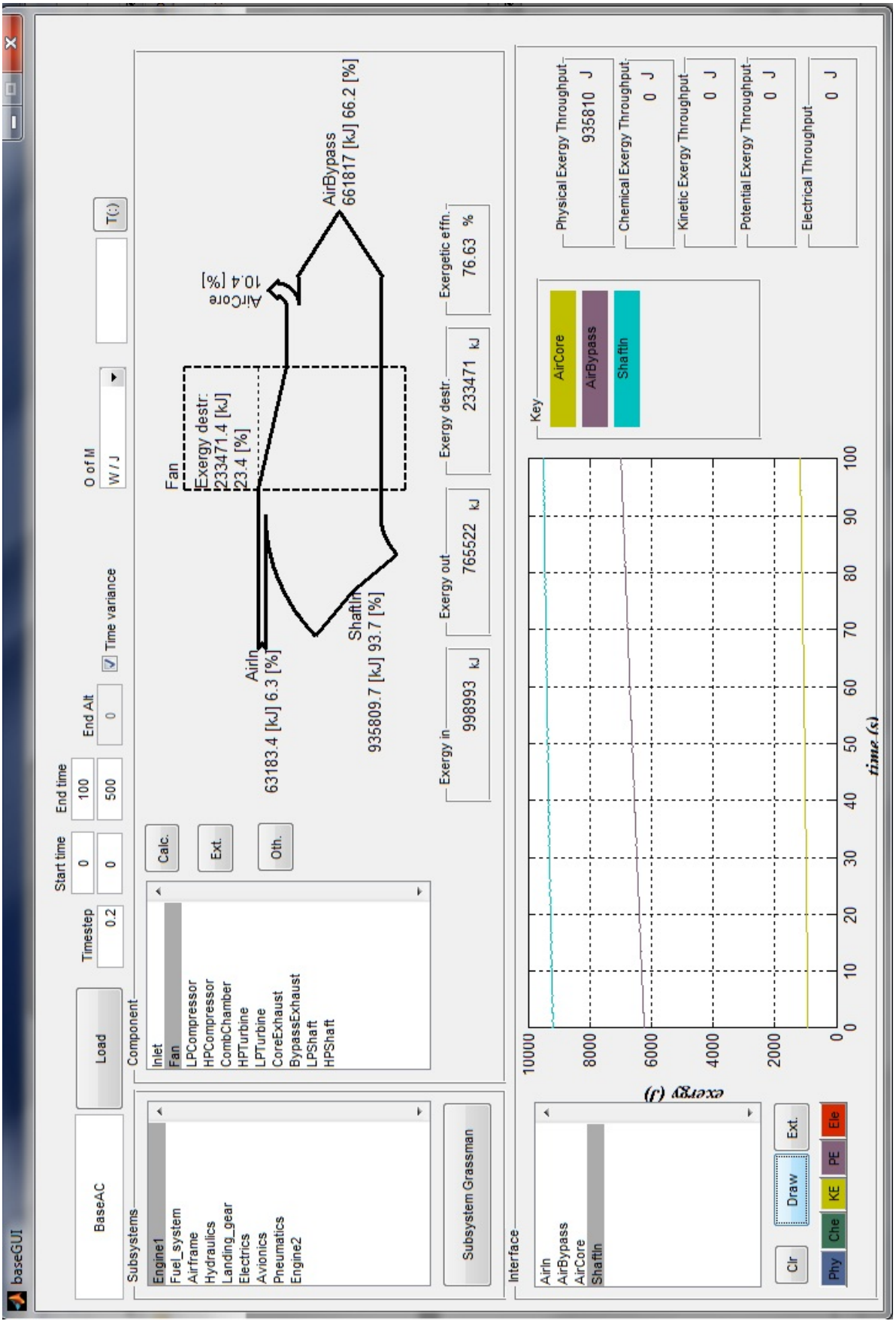

Figure 4.7: Exergy map input analysis GUI

When opened, the calculations for the time period chosen in the Analysis interface are performed for every component in the selected subsystem. A GUI, shown in Fig. 4.8 opens, which allows the layout of the diagram to be established. More than one subsystem can be selected to be drawn together. Details on this interface can be found in Appendix A.

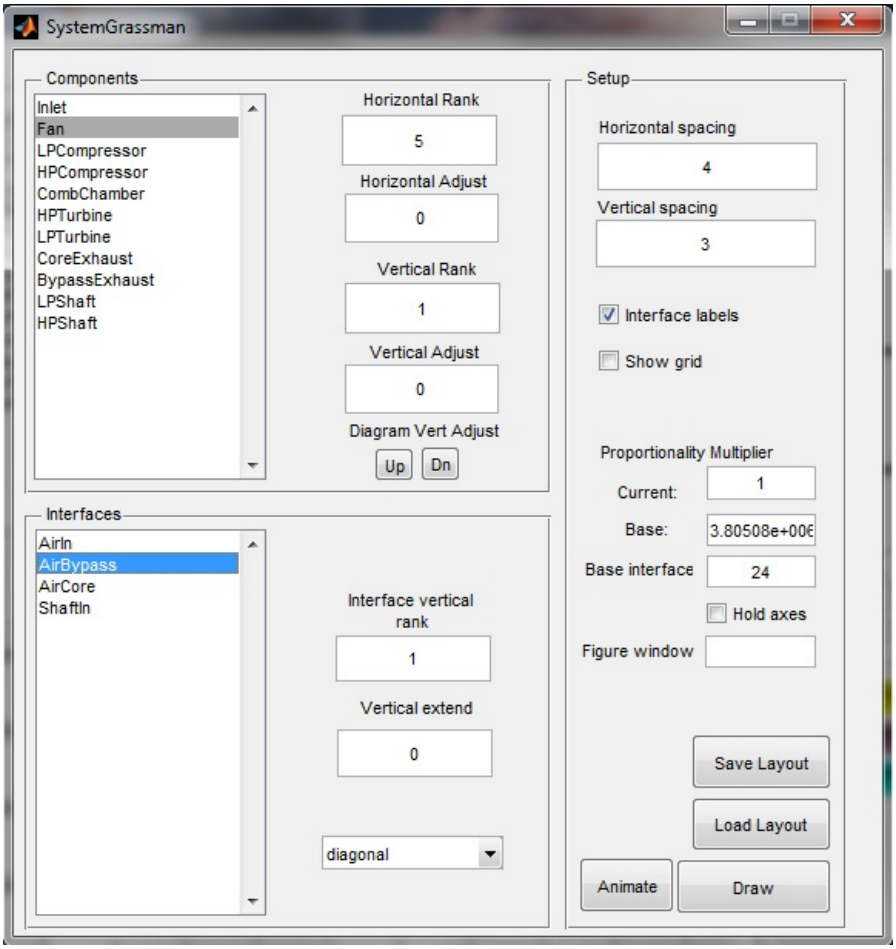

Figure 4.8: Subsystem Grassmann creation GUI

4.7 Exergy mapping process

The process of using the software to create a new exergy map is described in detail in Appendix A.

4.8 Future requirements

The software tools presented fulfil a number of tasks that are essential in the performance of an exergy mapping process of a complex, time-variant system. The tools themselves have been created to allow the creation of an exergy map without direct interface to modelling software. This provides flexibility with regard to the data source used, but it is likely that exergy mapping will find a place alongside system-wide modelling implementations, such as those presented by Hanke et al. [7] if the methodology is applied in a design, rather than research, setting in the future. As a stand-alone set of tools, there remain a number of improvements that would improve the usefulness significantly.

Integrated flow chart A GUI that allows the graphical 'drag and drop' manipulation of the system layout would improve the user-friendliness of the database creation and analysis tools immeasurably. This would replace most of the functions of the Data Creation 'General' tab. It would be difficult, but most likely possible to implement in Matlab, although it would be significantly easier in a compiled language (C++, Java etc.) in which the graphical tools required are already available.

Speed of data processing The use of an external database is a sensible choice for the management of the system layout data (subsystems, components, interfaces, links). However, when managing a complex system, the exergy flow and stock data becomes cumbersome when kept in the Data table in the database file. This is because of the need to import and export the data. The number of data points required is inevitably large for a complex system analysed at frequent intervals over an extended period. An improvement that may be required when the tools are applied to a more complex system than the case studies lies in either optimising the data accessing code or allowing the data to be stored permanently as an array in Matlab. The latter would significantly improve the speed of calculations and access but would reduce the reliability of the data stored and the potential for remote or concurrent access.

Exergy calculators Although already useful for the majority of cases likely to be found in an aircraft analysis, there are a number of possible ways in which the exergy calculators could be improved. The handling of gaseous water in the physical exergy calculator would be of primary importance. This would require access to steam tables in the calculation process. Although attempts were made to use freely available tools to include this, the calculation speeds were too slow to be acceptable. A faster steam table look-up tool would need to be developed for this to be implemented.

The chemical exergy calculator is only able to handle a limited number of gas species. Although these do include all of those most commonly found in an aircraft system, the data source table could be appended with further species if required, and if the relevant data can be found.

4.9 Conclusions

This chapter describes the software tools created alongside, and as part of, the research in this project. The exergy mapping analysis being described in this thesis is only possible using specifically designed tools, because the detail and data intensity involved would be prohibitive when using off-the-shelf software. The development of a package of prototype software tools was therefore an essential enabler for the research that took place. It is, however, also a valid aspect of the research in itself, to serve as evidence of the feasibility of the intended methodology. This feasibility has been proven with the software created, although the opportunity for improvement undoubtedly remains. The software tools were developed in Matlab in order to make use of the excellent data manipulation functions and the simplicity of the developing environment. However, the limitations in the graphical interface development mean the tools themselves are not as user-friendly or quick as they could have been, if developed in another environment. Although the tools developed have proven powerful and useful in a research setting, any wider use, such as in the aircraft design process, would necessitate the features discussed in Section 4.8.

Chapter 5

Analysis of highly dynamic systems

As has been established previously, the detailed exergy mapping of a moving vehicle must take into account the dynamic nature of such a system. The fundamental considerations of time-variant exergy analysis were established in Chapter 3. In this chapter, a case study is performed on a hydraulic system that does not perform in steady state during normal operation, but in which there are no exergy exchanges associated with the system's mass. This allows the study of a system similar in nature to an aircraft's internal subsystems such as the hydraulics and fuel system. The software tools described in Chapter 4 are employed in the analysis.

For the purposes of this case study, an existing experimental hydraulic rig originally built by Cargo [53] was adapted with pressure transducers and flow meters to be analysed. A simulation in Simulink/Simscape [50] was also adapted to provide exergy information at the same points in the rig, as well as more detailed data not available from the rig's sensors.

The present chapter contains the first example of an exergy/available energy analysis of a system of this type, so the main aim is to provide an introduction to the process and the new perspective it provides to the analyst. The comparison of simulation with real sensor data also provides an opportunity to validate the software tool and method. Finally, it allows the first discussion of the use of sensors to provide exergy data during operation as well as the consideration of exergy imbalances that may arise from real system analysis.

5.1 Hydraulic system description

The hydraulic rig being analysed, (Figs. 5.1 and 5.2, Table 5.1), is a laboratory-based wave power off-take system designed to convert an input emulating sea waves, first into steady hydraulic flow, and then into electric current. The wave input is provided by a linear actuator powered by an external hydraulic circuit that is not included in the analysis. The movement of the linear actuator powers a double-acting hydraulic cylinder with unequal piston/annulus areas. The flow from the annulus and piston sides of the cylinder passes through a rectifying system of one-way valves. A 4-litre accumulator (A) 'smooths' the flow before it passes through an external gear motor, which turns a shaft connected to a DC generator. The DC generator is connected in series with a resistance representing a useful load. The hydraulic flow, once past the motor, reaches the low pressure side of the system, which is kept above tank pressure by an external gear pump powered by a 3-phase AC motor. This is a necessity to ensure the oil on the piston side does not cavitate during the cylinder down-stroke, when flow is required from the low pressure side. A 1-litre accumulator (B) on the low pressure side allows some of the available energy to be stored during the cylinder up-stroke, during which no flow can enter the high-pressure side. Pressure relief valves prevent overpressure at 90 bars gauge on the high pressure side and 7 bars gauge on the low pressure side.

5.2 Exergy readings

The exergy of a hydraulic flow is equivalent to the generally used hydraulic available energy. This is given by

$$\dot{E}_{hydr} = \dot{F}(P - P_0) \tag{5.1}$$

where $\dot{F}$ is the flow rate and $P - P_0$ is the gauge pressure in the system if the atmospheric pressure is used for the reference state.

Pressure transducers with a $0 - 100$ bar range were installed in the system at six points. Flow meters before and after the large accumulator provide direct readings. Flow leaving the piston/annulus is calculated from the cylinder velocity

Table 5.1: Hydraulic rig main component parameters

Component	Parameter	Value
System	Maximum pressure (gauge)	100 bar
Power take-off cylinder	Bore diameter	40 mm
	Rod diameter	28 mm
	Stroke	±150 mm
Gas accumulator A	Pre-charge pressure	10 bar
	Volume	3.8 l
Gas accumulator B	Pre-charge pressure	2 bar
	Volume	1.0 l
External gear motor	Displacement	4.0 cm^3 / rev
DC generator	Rated power	90 W
	Rated speed	3,000 rpm
	Internal resistance	0.6 Ω
External gear boost pump	Displacement	4.0 cm^3 / rev
	Rated flow	6 l / min
High pressure relief valve	Relief pressure (gauge)	90 bar
Low pressure relief valve	Relief pressure (gauge)	7 bar
Driving (wave input) cylinder	Maximum force	20 kN
	Maximum velocity	0.35 m/s
	Stroke length	±125 mm

Figure 5.1: Photo of hydraulic rig

and the respective areas.

A load cell affixed at the top of the cylinder provides continuous force readings. A linear variable differential transformer (LVDT) provides cylinder to piston relative velocity. These readings can be validated against pressure/velocity readings and requested input values, respectively.

Electrical exergy input at the AC motor is difficult to measure due to the 3-phase power supply. Power input was therefore calculated by means of

$$\dot{E}_{mech} = D\omega(P - P_0) \tag{5.2}$$

where D is the pump displacement and ω is the angular velocity of the shaft input. This gives a value for the exergy that has reached the gear pump, but not how

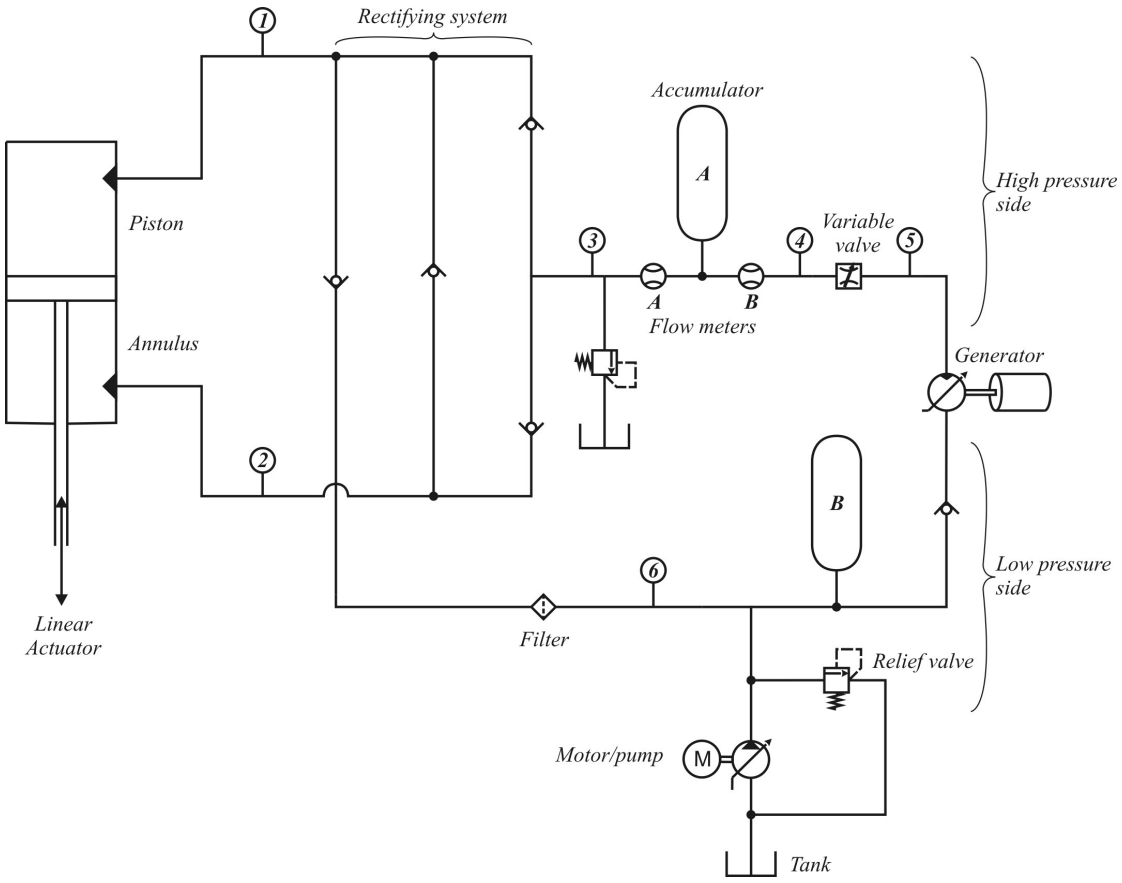

Figure 5.2: Hydraulic rig layout

much was provided upstream to that.

The electrical output from the DC generator is dependent on the load attached across the terminals. A resistor is used to equal the generator's internal resistance of 0.6 Ω. The circuit is shown in Fig. 5.3. The voltage across the resistor is read via the same analogue box as the other signals.

Given that the hydraulic flow rate is inherent in the rig design and the wave input, and the hydraulic motor displacement is fixed, the angular velocity of the shaft input to the DC generator cannot be directly influenced for the purpose of maximising electrical power output. The maximum power extraction from the hydraulic fluid is therefore gained by matching the internal, R_I, and external, R_E, resistances.

To increase the power produced and efficiency of the DC generator, it would be necessary to increase the input shaft speed to increase the voltage given the same hydraulic flow rate. The electrical power output of the generator is then

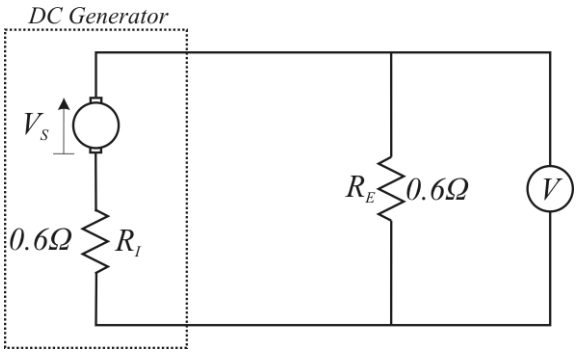

Figure 5.3: DC power generation circuit

calculated using $P_E = V_E^2/R_E$ where the subscript E relates to the external work done across the resistor that would be convertible to other work, were the resistors replaced with a useful load.

5.3 Implementation in database

For the purpose of mapping the exergy flow over a given time period, the hydraulic system was split into 10 components (numbered in corners), with 21 data points (squares) and 35 interfaces (circles), Fig. 5.4. Arrows indicate the direction of the exergy flow.

For completeness, the entire system is represented in the database as shown in Fig. 5.4. Although it was not possible to take readings to calculate exergy values at every data point for the real rig, the same system representation was re-used to contain the simulation data in which more readings were available.

The design of the layout is an important initial consideration when creating an exergy map and the result is not always immediately intuitive. The following points provide explanation of specific aspects with reference to their component and data point numbers in Fig. 5.4.

Cylinder The cylinder is split into three components: the linear actuator (Component 1), piston (C 2) and annulus (C 3). The linear actuator receives exergy from the exterior hydraulics (Data Point 1). The piston, above the cylinder head, and the annulus, below, receive the exergy via mechanical work and transfer it to the hydraulic working fluid via data points 4 and 5. It was necessary to split

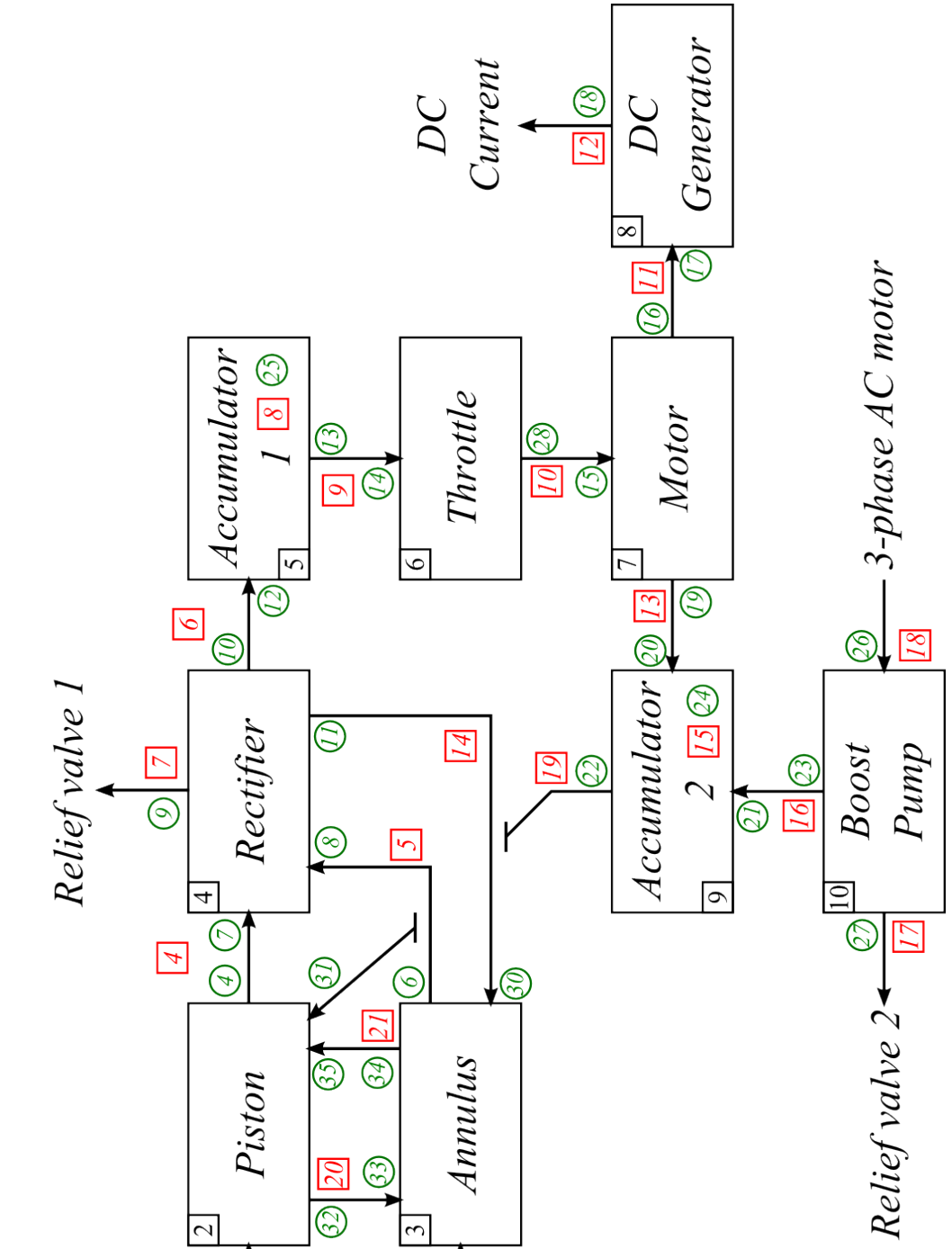

Figure 5.4: Hydraulic rig exergy map configuration

the cylinder assembly in this way in order to properly represent the complexity of the exergy flow. During the cylinder up-stroke, work is done by the actuator to pressurise the piston component and is assisted by pressure on the annulus side, recorded in DP 21. The reverse happens during the down-stroke where the movement is assisted by pressure in the piston side, recorded in DP 20. This is also clarified in Section 5.5.

Rectifier This component (C 4) receives the exergy from the cylinder components (via DPs 4 and 5). Some exergy returns to the annulus (via DP 14) during the piston up-stroke and the remainder continues to the main circuit (via DP 6). The exergy lost via the relief valve is also assigned to this component as an accountable loss although this could also be attributed to the Accumulator 1 component. Including the relief valve as a separate component would not be useful, since the exergy destroyed across it is expected to be complete.

Accumulator 1 The first component (C 5) with an exergy storage interface (DP 8), this is mapped as being in-line with the hydraulic exergy flow.

Motor The exergy is split between that going to the DC generator via mechanical shaft (DP 11) and that remaining in the hydraulic fluid afterwards (at DP 13).

Accumulator 2 This component acts as the low pressure reservoir, essentially the whole of what is marked as the low pressure side in Fig. 5.2, receiving exergy from the motor (DP 13) and the boost pump (DP 16) and releasing it to the piston component (DP 19).

Boost pump The shaft input from the 3-phase AC motor is received here (via DP 18), being converted to hydraulic exergy and output to DP 16. The second relief valve is an accounted loss in this component.

5.4 Rig test run

The hydraulic rig was run over a pre-defined period of 300 seconds (Fig. 5.5). In order to see the effects of the different exergy inputs, values were first recorded for 30 seconds with both the actuator and the boost pump switched off. After this time, the boost pump was turned on. After 90 seconds, the actuator was started, the input demand being a sine wave of frequency $2\pi/3$ rad/s. This was allowed to run until 210 seconds had elapsed and the boost pump was switched off at 220 seconds. A throttle valve near the main accumulator was then opened, allowing the system to return to tank pressure with the intention of preventing residual exergy from remaining in the system, especially the accumulators, in the form of above-atmospheric pressure.

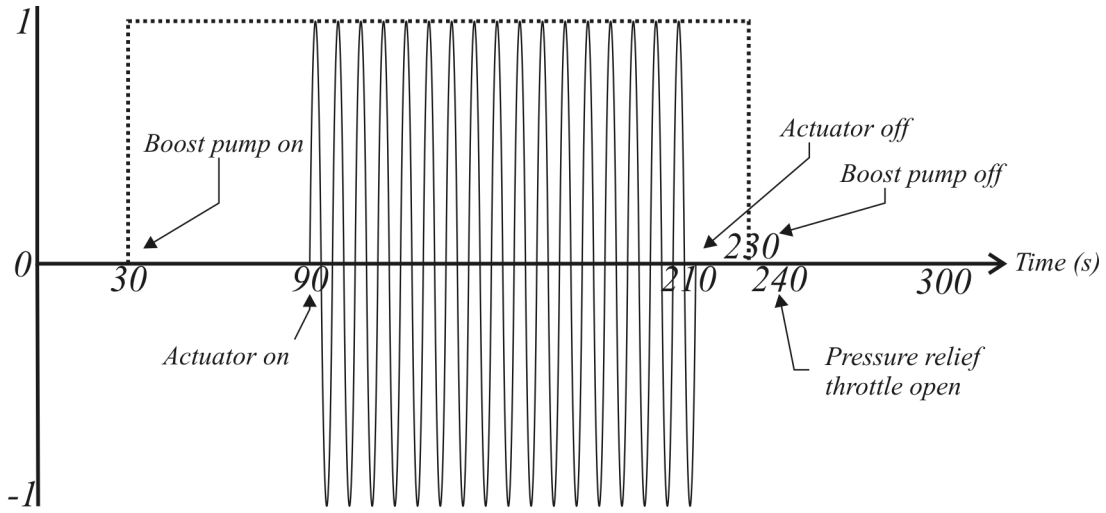

Figure 5.5: Hydraulic rig test run. Dotted line represents boost pump status, solid line represents actuator position. Note: frequency of sine wave not drawn to scale.

5.5 Analysis of rig data

The exergy calculations were performed using the following equations, where the subscripts for the exergy flow rates $\dot{E}$ correspond to the data points (squares) in Fig. 5.4. A script was written in Matlab to perform these calculations directly on the rig output data so that different test runs could be processed quickly. The

equations used in this section make use of modulus brackets to ensure the exergy flow at each data point only travels in one direction, which is necessary for the exergy mapping method being presented. The intended direction of exergy flow is given by the arrow directions in Fig. 5.4.

Actuator

The actuator rod input exergy

$$\dot{E}_1 = |(A_P P_1 - A_A P_2)\mathcal{V}_c| \tag{5.3}$$

where A_P and A_A are the piston (1256 mm^2) and annulus (641 mm^2) areas and P_1 and P_2 are the measured pressures at the corresponding data points. $\mathcal{V}_c$ is the velocity of the piston, which is measured by the LVDT. The output exergy is split between the pistons and annulus sides of the cylinder:

$$\dot{E}_2 = \frac{1}{2}|\mathcal{V}_c|\left((A_P P_1 - A_A P_2) + |A_P P_1 - A_A P_2|\right) \tag{5.4}$$

$$\dot{E}_3 = \frac{1}{2}|\mathcal{V}_c|\left((A_P P_1 - A_A P_2) - |A_P P_1 - A_A P_2|\right) \tag{5.5}$$

Piston

The piston hydraulic flow output exergy is calculated using the measured pressure during the down-stroke period:

$$\dot{E}_4 = \frac{1}{2}P_1\left(A_P\mathcal{V}_c + |A_P\mathcal{V}_c|\right) \tag{5.6}$$

whereas the exergy provided to the annulus side during the down-stroke is given by

$$\dot{E}_{20} = \left|\frac{1}{2}P_1\left(A_P\mathcal{V}_c - |A_P\mathcal{V}_c|\right)\right| \tag{5.7}$$

Annulus

The annulus hydraulic flow output exergy is calculated using the measured pressure during the down-stroke period:

$$\dot{E}_5 = \left|\frac{1}{2}P_2\left(A_A\mathcal{V}_c - |A_A\mathcal{V}_c|\right)\right| \tag{5.8}$$

$$\dot{E}_{21} = \frac{1}{2}P_2\left(A_A\mathcal{V}_c + |A_A\mathcal{V}_c|\right) \tag{5.9}$$

Rectifier

It is not possible to measure the exergy lost to the relief valve, but it is assumed to be negligible because the relief pressure is much higher than normal operation pressure.

The rectifier's flow exergy output is given by

$$\dot{E}_6 = P_3 \dot{Q}_1 \tag{5.10}$$

where $\dot{Q}_1$ is the flow rate measured by the first flow meter. The flow values were multiplied with a constant of 1.25 to compensate for what was adjudged to be an inaccurate reading. With this compensation, the total flow over the test run equals that expected from calculations using the cylinder velocity and areas. It is noted that the reading offset is unlikely to be linear, since the flow meters will become more accurate with higher flow rates.

The return flow to the annulus is given by

$$\dot{E}_{14} = \frac{1}{2} P_2 \left(A_A \mathcal{V}_c + |A_A \mathcal{V}_c| \right) = \dot{E}_{21} \tag{5.11}$$

as there is no way of distinguishing between the values $\dot{E}_{14}$ and $\dot{E}_{21}$ using the sensors available.

Accumulator 1

The exergy stored at any given time cannot be measured directly using the available equipment, so an assumption is made that the accumulator is 100% efficient. Any exergy entering is considered stored until it is recorded leaving the component again.

$$\Delta \dot{E}_8 = \int_{t1}^{t2} \left(\dot{E}_6 - \dot{E}_9 \right) \, \mathrm{dt} \tag{5.12}$$

The exergy of the hydraulic output flow is given by

$$\dot{E}_9 = P_4 \dot{Q}_2 \tag{5.13}$$

where the second flow meter reading, $\dot{Q}_2$, is multiplied by 0.95 to balance with the calculated total flow. Since pressure readings at this point are lower than those closer to the cylinder, the signal noise becomes more significant. To counteract

this, the pressure signals are passed through a 6th order low-pass Butterworth filter. This filter type was chosen to minimise the phase shift of the output, which could cause incorrect exergy balances in components over short time periods.

Throttle

The exergy of the hydraulic output flow is given by

$$\dot{E}_{10} = P_5 \dot{Q}_2 \tag{5.14}$$

Motor and DC Generator

The shaft power provided by the motor is not measurable using the available equipment. The power produced by the DC generator is given by

$$\dot{E}_{12} = \frac{\mathrm{V}^2}{R_{load}} \tag{5.15}$$

which is the exergy being converted to heat in the external load resistors, where R_{load} is the external resistance of 0.6 Ω and V is the voltage measured across it. Because the internal resistance of the DC generator is equal to the resistance across its terminals, the exergy destroyed within the windings is approximately equal. As an estimate, the motor shaft input exergy is therefore given by

$$\dot{E}_{11} = 2\dot{E}_{12} \tag{5.16}$$

which ignores the other, less significant motor losses. The hydraulic exergy remaining in the working fluid is given by

$$\dot{E}_{13} = P_6 \dot{Q}_2 \tag{5.17}$$

Accumulator 2 and Boost Pump

Because there is insufficient equipment to distinguish between the exergy lost through the relief valve and the exergy stored and released again, it is not possible to measure the stored exergy at the accumulator. The storage term, $\dot{E}_{13}$ is therefore set to 0 and any exergy not passed to the piston is assumed destroyed.

Similarly, the exergy input to the system via the 3-phase AC power supply that powers the boost pump is complex to measure. The power provided by the boost

pump to the fluid is given by

$$\dot{E}_{16} = \dot{Q}_B P_6 \tag{5.18}$$

where $\dot{Q}_B$, the boost pump flow, is calculated from the known AC power frequency, the known frequency response of the AC motor and the gear pump displacement. The input power to the system is set to equal $\dot{E}_{16}$.

The exergy provided to the piston during the down-stroke is given by

$$\dot{E}_{19} = \frac{1}{2} P_6 \left| (A_P \mathcal{V}_c - |A_P \mathcal{V}_c|) \right| \tag{5.19}$$

5.6 Rig simulation

An existing Simulink/Simhydraulics model of the hydraulic rig was adapted to provide the same readings as the real rig sensors, with some additions to show more detail in areas that were insufficiently instrumented. The test run used on the real rig was applied to the simulation and variables in the simulation were adjusted so that pressure and flow readings were as close as possible. In particular, these variables were the rotor damping of the electric motor and the throttle valve orifice and discharge coefficient, as well as the check valve passage areas. A comparison between pressure readings from the rig and simulation can be seen in Figs. 5.6 – 5.11. Results are considered to be sufficiently similar to draw comparison in the remainder of this chapter, as discussed next. Instantaneous drops in pressure in the simulated results (especially at P_2, Fig. 5.7) can be attributed to a lack of elasticity in the simulated model and a faster sensor response time.

Although best effort was made to calibrate the pressure transducers during installation, some uncertainty always exists that must be taken into account when drawing conclusions on the work. For the purposes of this study, however, it will be assumed that pressure readings from the real rig are accurate and can be relied upon to tune the simulation. Due to the difficulty of measuring the flow rates in the system accurately, however, the calculated simulation flow rates are taken to be accurate.

When comparing the flow readings with simulated values (Figs. 5.12 and 5.13), flow meter A agrees well with simulated results, with the latter varying between a larger range. This is attributed to the inertia of the flow meters. The flow spike

near the end of the run is due to the opening of the manual valve to tank allowing accumulator B to empty via flow meter A. This behaviour is not observed at all in the experimental results, which may be an indication of the flow meter not responding fast enough or the accumulator not charging as expected.

Flow meter B shows the effect of the accumulator in preventing the spikes and drop-off in flow rate. The physical flow meter is clearly overestimating the flow at all times, however, which is accounted for in the exergy calculations as discussed previously. The simulated flow rates display a similar pattern but the flow is smoother, suggesting the simulated accumulator to be more effective than the real one.

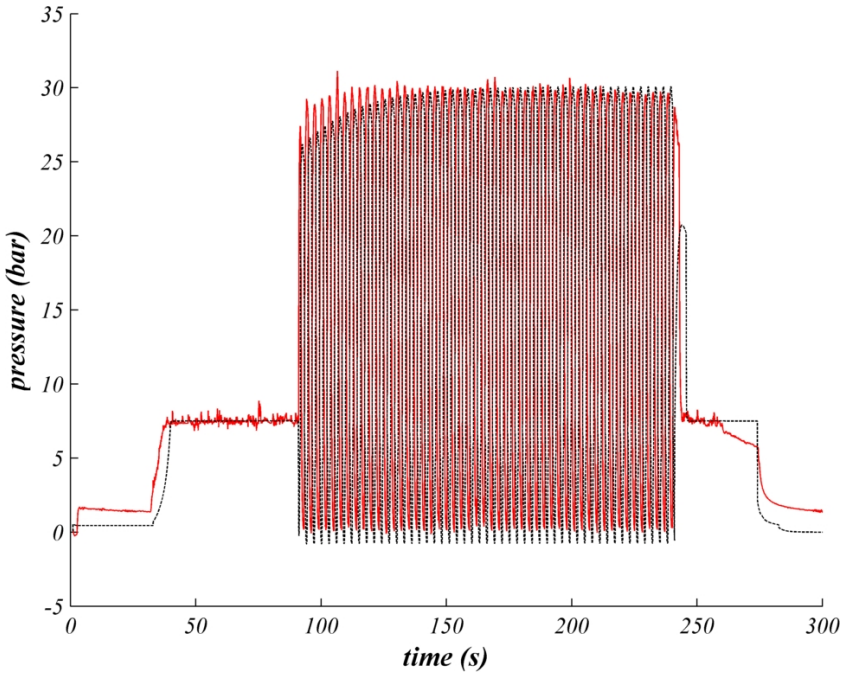

Figure 5.6: Simulated (black, dashed) and transducer (red, solid) pressure readings for P_1

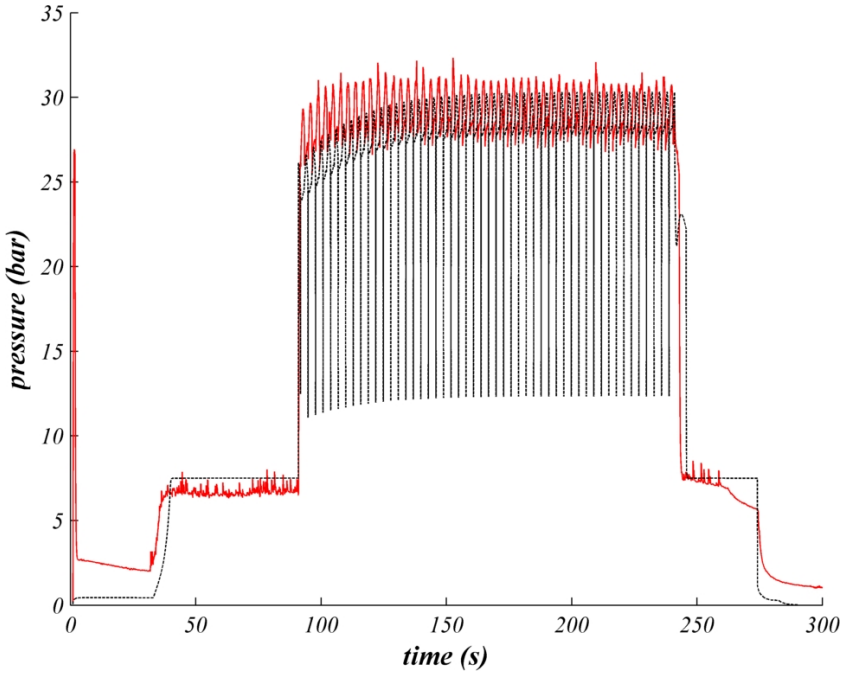

Figure 5.7: Simulated (black, dashed) and transducer (red, solid) pressure readings for P_2

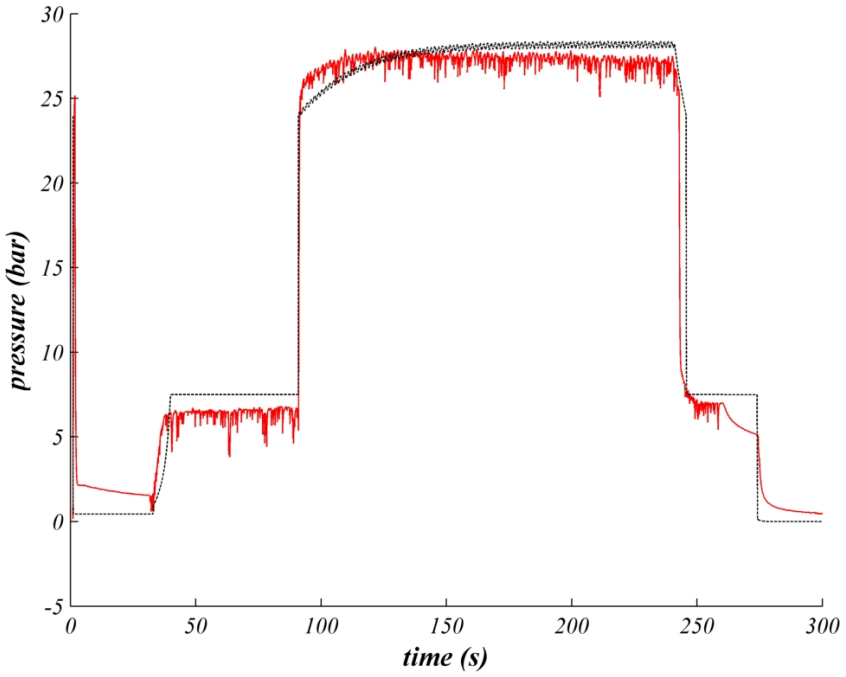

Figure 5.8: Simulated (black, dashed) and transducer (red, solid) pressure readings for P_3

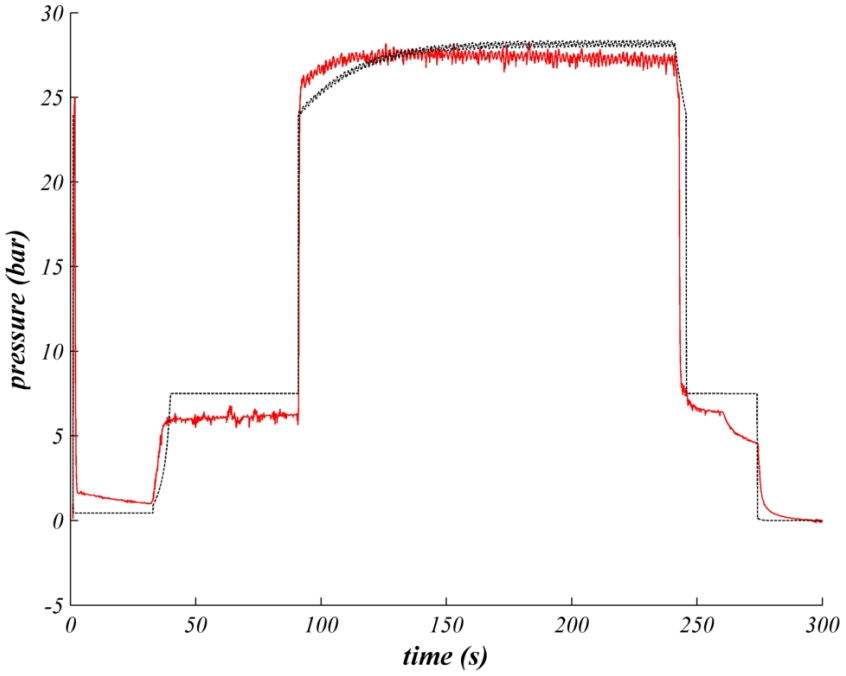

Figure 5.9: Simulated (black, dashed) and transducer (red, solid) pressure readings for P_4

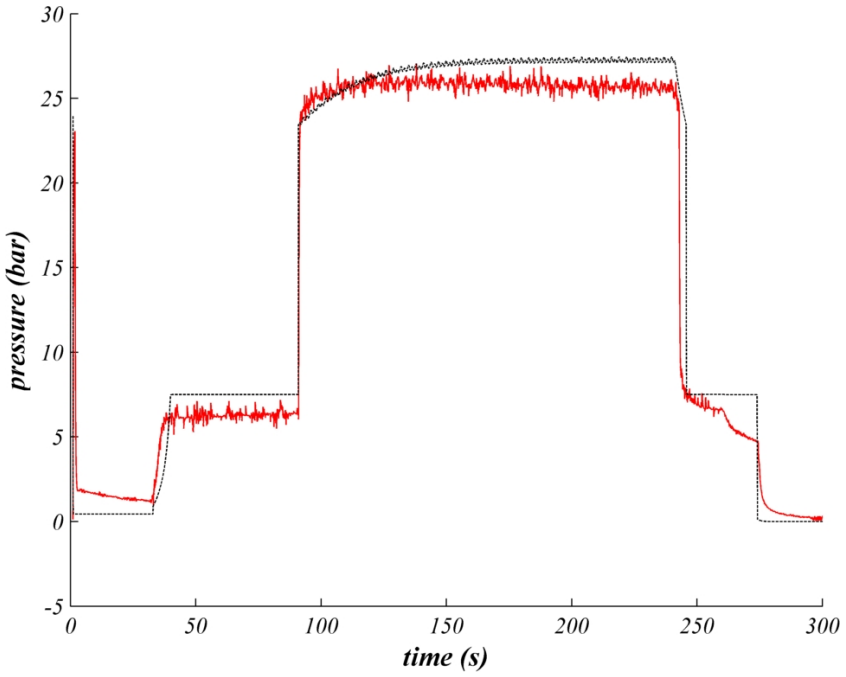

Figure 5.10: Simulated (black, dashed) and transducer (red, solid) pressure readings for P_5

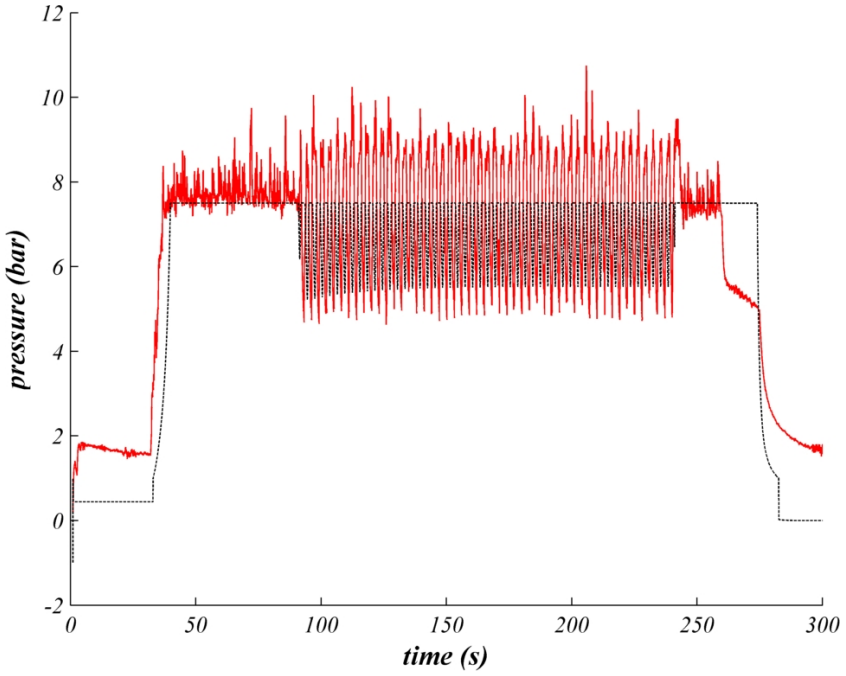

Figure 5.11: Simulated (black, dashed) and transducer (red, solid) pressure readings for P_6

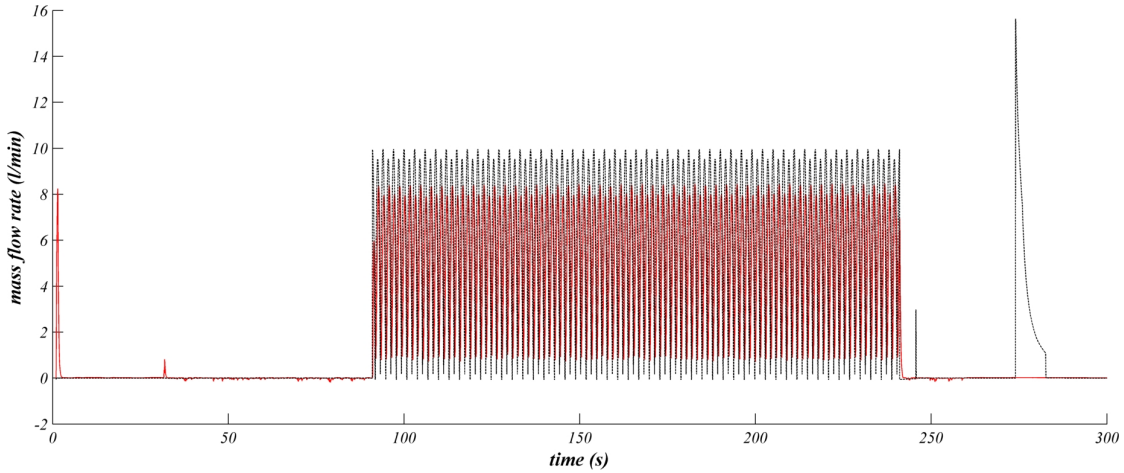

Figure 5.12: Simulated (black, dashed) and measured (red, solid) flow readings for flow meter A

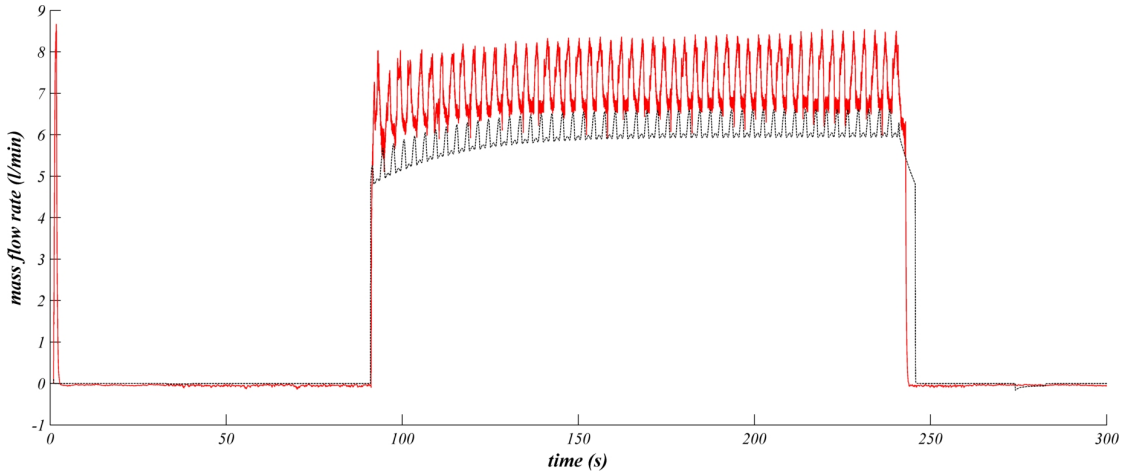

Figure 5.13: Simulated (black, dashed) and measured (red, solid) flow readings for flow meter B

5.7 Results and discussion

Numerical results for the experimental and simulated test runs are given in Table 5.2. Results given are for the exergy passing through the system during a single down-stroke, single up-stroke and over the entire 300 second run.

5.7.1 Experimental results discussion

A Grassmann diagram of the entire test run is shown in Fig. 5.14. This is a representation of the total exergy that has passed through the system. Figures 5.16 and 5.18 show an isolated up-stroke (200.3-201.8 seconds) and down-stroke (201.8 - 203.3 seconds) respectively, which help to clarify the exergy flows. The following notes on individual aspects of the results are made:

Actuator

The exergy provided by the wave input actuator is close to being equal in the up-stroke and down-stroke directions despite the piston and annulus areas not being equal. This is due to the rig design, which allows half the piston flow to return to the annulus, halving the work required to push upwards. This also doubles the observed exergy output from the piston. Note that the annulus is shown above the piston for the Grassmann diagrams' organisation.

Piston

This component has a greater observed loss than the annulus, which comes about during the down-stroke, when flow from the low pressure side is assisting the downward motion of the hydraulic cylinder. The exergy provided from the low pressure side is inefficiently passed on to the annulus. This can be seen in Fig. 5.18.

Accumulator 2

Owing to the difficulty of measuring exergy losses when the relief valve operates, these losses are accounted in the 'Accumulator2' component for the sake of this analysis. Figure 5.16 suggests that all exergy provided by the boost pump is lost during the upstroke. It is not possible, however, to fully resolve the exergy flow in

Table 5.2: Numerical results for experimental and simulation runs of hydraulic rig, with single up-stroke, single down-stroke and entire run results given. All numbers in MJ.

	Experimental exergy (MJ)			Simulation exergy (MJ)		
Data point	Up	Down	All	Up	Down	All
1	0.412	0.388	40.8	0.477	0.441	45.0
2	0.408	0.008	21.1	0.477	0.000	23.4
3	0.004	0.380	19.3	0.000	0.440	21.6
4	0.858	0.002	43.0	0.917	0.000	44.9
5	0.001	0.481	24.3	0.001	0.474	23.3
6	0.423	0.445	43.3	0.423	0.443	42.4
7	0	0	0	0	0	0
8	0.001	0.025	2.2	0.000	0.001	0.0
9	0.419	0.431	42.1	0.423	0.442	42.3
10	0.395	0.405	39.7	0.394	0.412	39.7
11	0.095	0.103	9.7	0.108	0.118	11.1
12	0.047	0.051	4.8	0.054	0.059	5.5
13	0.148	0.117	13.1	0.112	0.102	10.7
14	0.453	0.001	22.4	0.446	0.000	21.9
15	0.001	0.000	0.0	0.088	-0.088	0.0
16	0.115	0.090	17.6	0.104	0.091	14.9
17	0	0	0	0	0	0
18	0.115	0.090	17.6	0.104	0.091	14.9
19	0.001	0.192	9.7	0.000	0.203	10.1
20	0.000	0.108	5.5	0.000	0.203	10.1
21	0.453	0.001	22.4	0.446	0.000	21.9

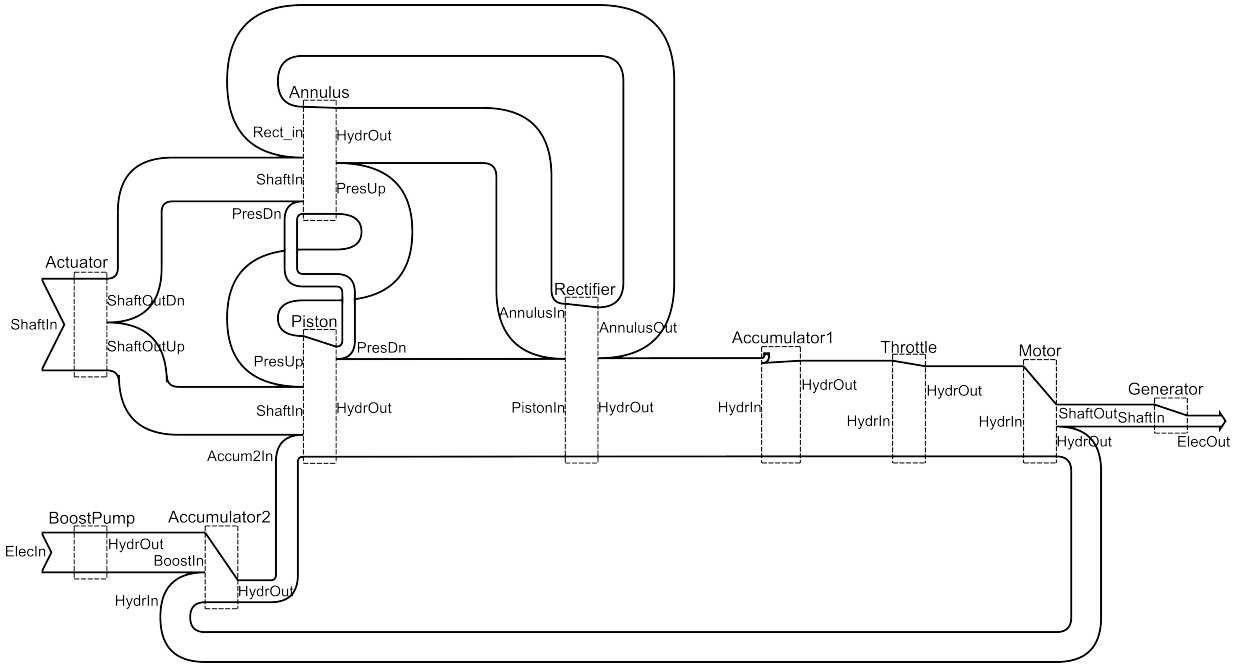

Figure 5.14: Grassmann of experimental results: entire run

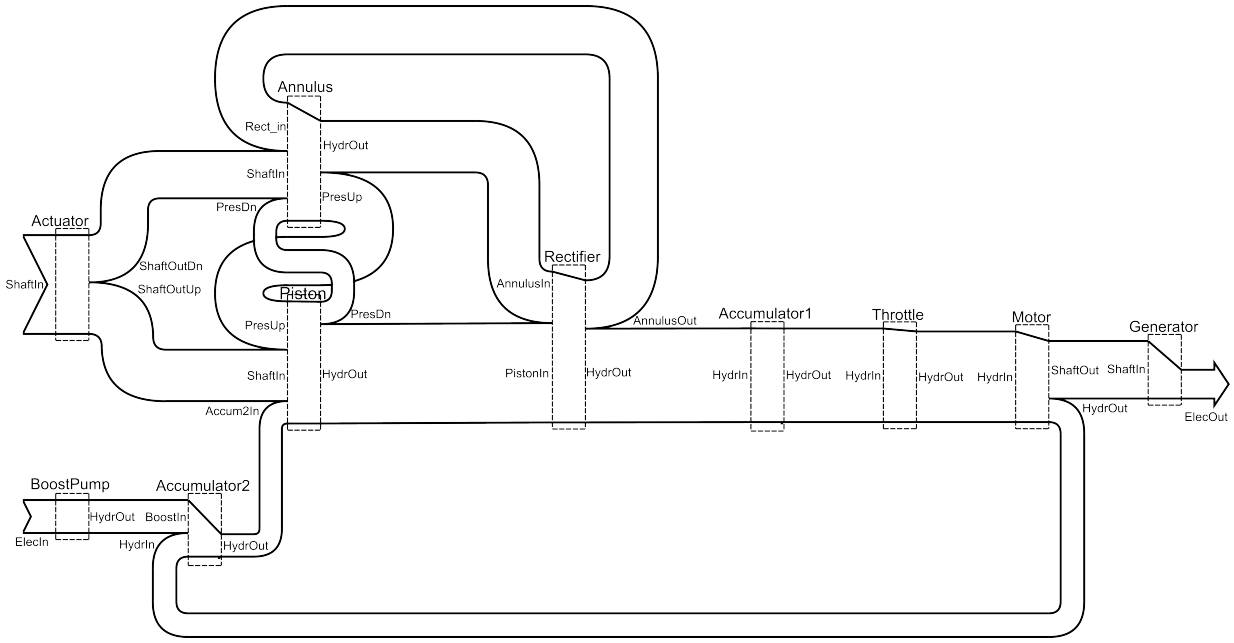

Figure 5.15: Grassmann of simulation results: entire run

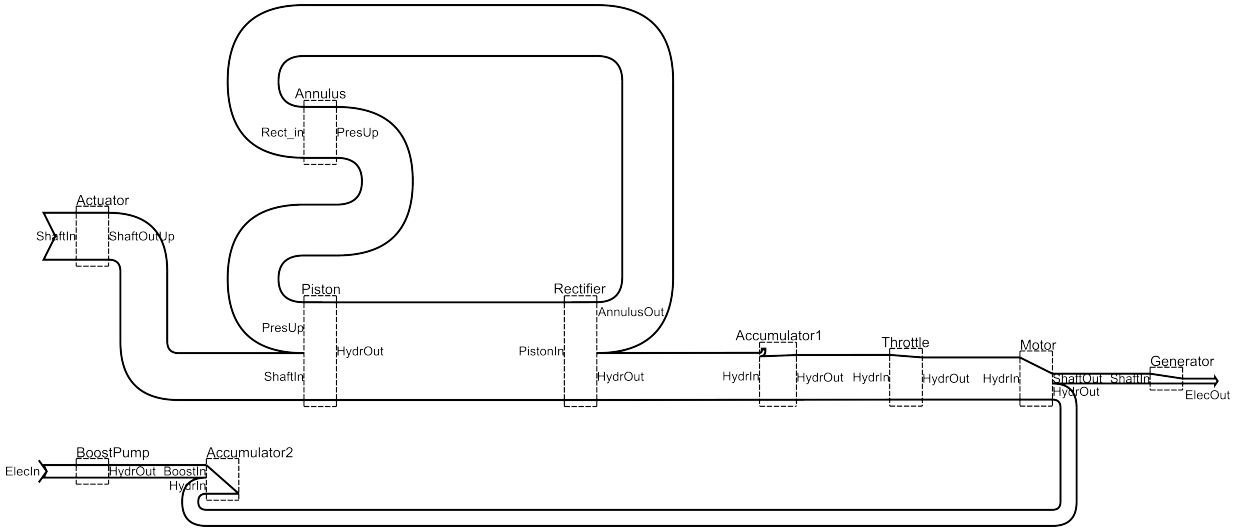

Figure 5.16: Grassmann of experimental results: up-stroke

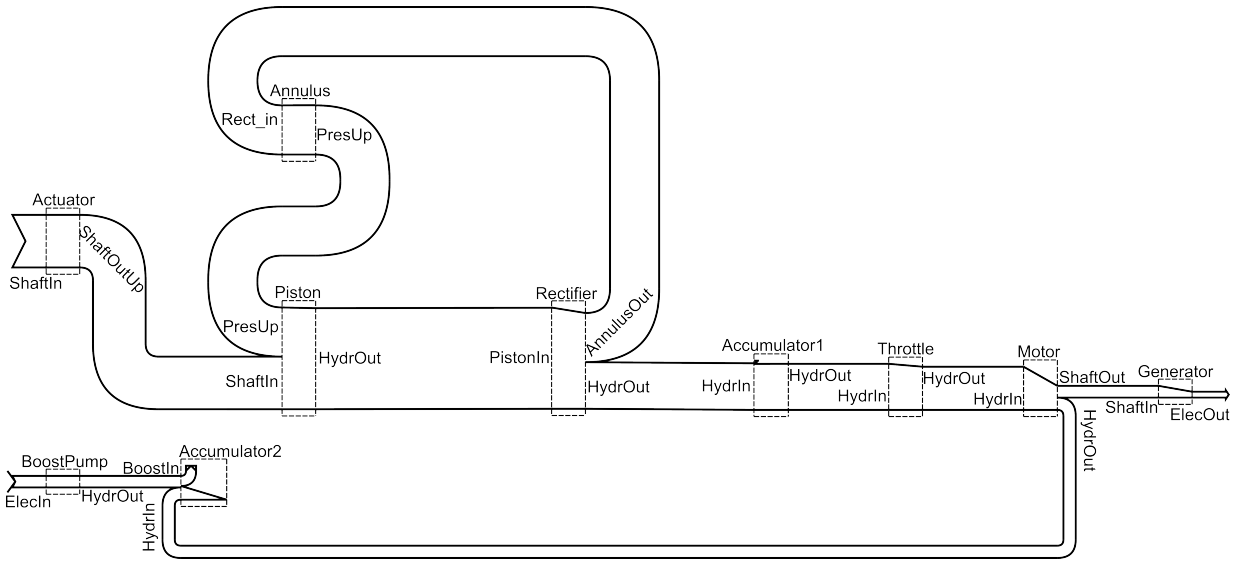

Figure 5.17: Grassmann of simulation results: up-stroke

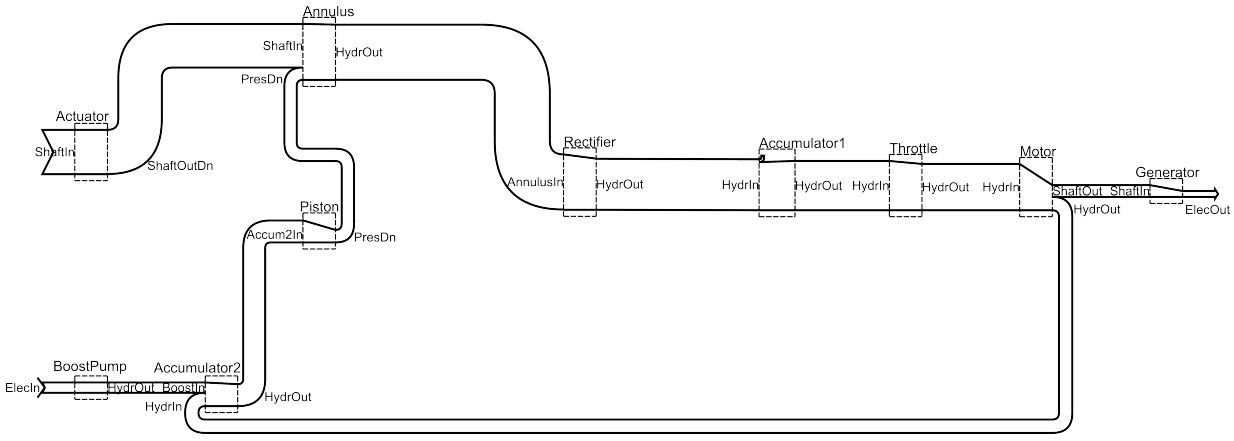

Figure 5.18: Grassmann of experimental results: down-stroke

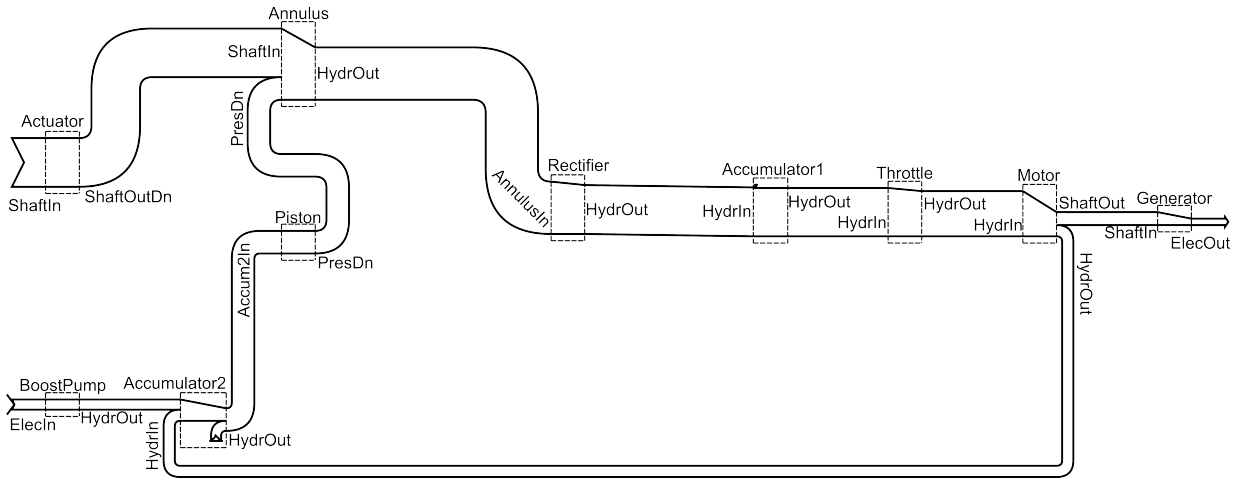

Figure 5.19: Grassmann of simulation results: down-stroke

this section of the system because of the difficulty of knowing the exergy stored in an accumulator at any given time. The exergy stored in the accumulator or lost through the relief valve cannot be distinguished. However, none is provided to the piston during the upstroke.

Accumulator 1

This component is shown as violating the 2nd law, seen by an increase in exergy across the component. This is likely due to the difficulty in establishing exactly how much exergy is being stored in the accumulator at any given time using the equipment available. The difficulty in accurately measuring the slow flow rates in the system are also a contributory factor.

Throttle

The exact loss seen in the throttle may be influenced by the exergy reading at the previous data point. However, since the same flow-meter reading is used, the exergy efficiency of the component is expected to be accurate. In this test run, the throttle was fully open, but the temporary narrowing of the flow would still cause some exergy destruction.

Motor and Generator

The hydraulic motor component causes the largest exergy destruction in the system by a significant margin. The exact proportion of exergy destroyed in the motor and generator is not certain because of the difficulty in accurately measuring the shaft power transfer. It could be argued that these two components should be represented as one because of this, but keeping them separate allows for better comparison with the simulation data later and the re-use of the exergy map database structure.

5.7.2 Comparison of physical and simulated results

The following is a comparison between results derived from measured data and those derived from the simulation.

Actuator

Since no efficiency information is available for the actuator, this remains a lossless component. It is likely to be good practice to leave components for which sufficient information is unavailable as 100% efficient so that these can be recognised later, rather than using over-simplistic estimates that could be confused as genuine results. Since the supply side of the actuator is not part of the analysis, knowledge of the component's efficiency would not be useful.

Annulus and Piston

In the experimental results, a transfer of exergy from the low pressure side of the system to the high pressure side was observed during the down-stroke (Fig. 5.18), which occurs because of the boost pump assisting the downward motion of the piston. This effect is shown as far less significant in the simulation, with most of the exergy available on the low-pressure side during the down-stroke not reaching the high-pressure side of the system. Some confusion arises because exergy is accounted as being destroyed primarily in the piston component in the experimental results, but in the annulus component in the simulated results. The location of the exergy destruction being in the piston or annulus component is physically unimportant since the distinction between the two is abstract. The difference between the two sets of results is due to calculation methods.

Rectifier

The rectifier shows a more reasonable destruction during both the up-stroke and down-stroke in the simulation. The losses caused by the check valves that make up the rectifier are not expected to be insignificant. The more reliable flow results in the simulation are responsible for this improvement.

Accumulator 1

Principally, the same method for calculating the stored exergy in the accumulator is used for the simulation results, but the more reliable flow readings mean there is no net exergy gain across the component. Accumulator net output occurs around

the top and bottom of each stroke when the flow is slower.

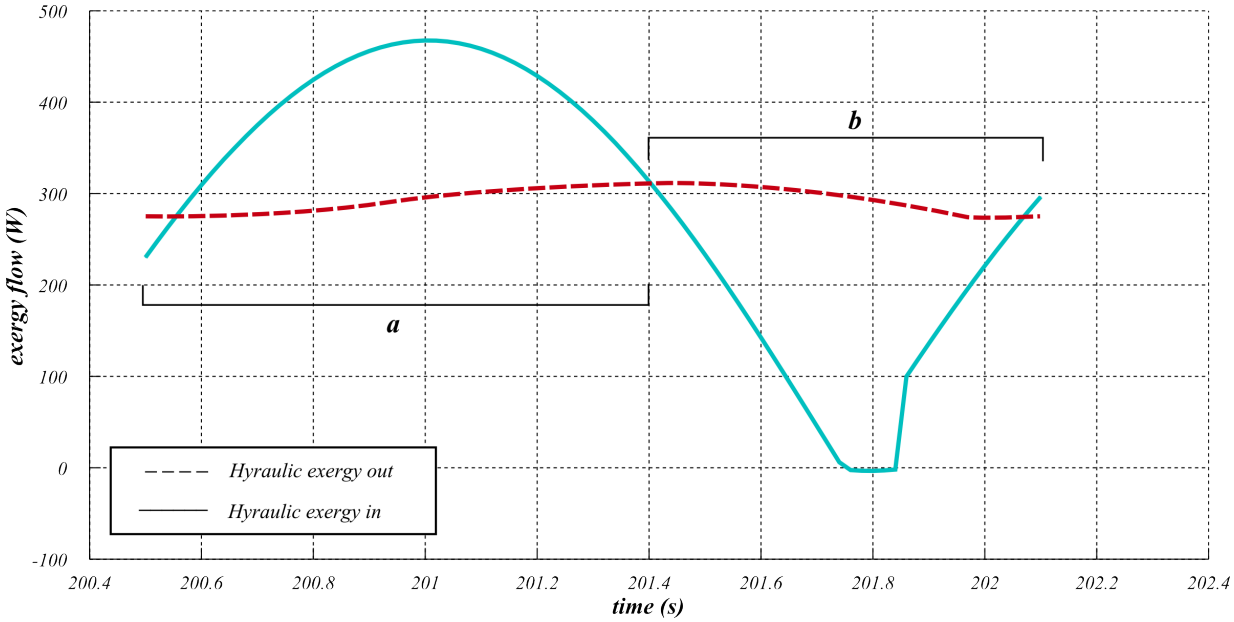

Figure 5.20: Accumulator 1 simulation results: exergy in and exergy out over one cycle

Figures 5.20 and 5.21 give an example of the flexibility of the software tool to analyse very short periods of time in the exergy map. In this case, individual storage and release phases of the accumulator are shown. Limitations of the simulation data or the calculation method are likely to become visible at these levels of detail. For example, the accumulator's storage and release are here found not to be perfectly synchronised with the input and output of exergy, leading to the perceived generation and loss of exergy over these periods even though the component is not modelled with irreversibilities. Viewed on a larger timescale, these inaccuracies balance out. Understanding of this type of inaccuracy is important when using the exergy map to avoid confusion or incorrect conclusions. It is highly likely that these types of inaccuracy will be unavoidable in large systems, especially when using real sensor data or data from different sources.

Throttle

Throttle losses are expected to be similar to those recorded on the physical rig, because the pressure values either side were used to adjust the simulation and the

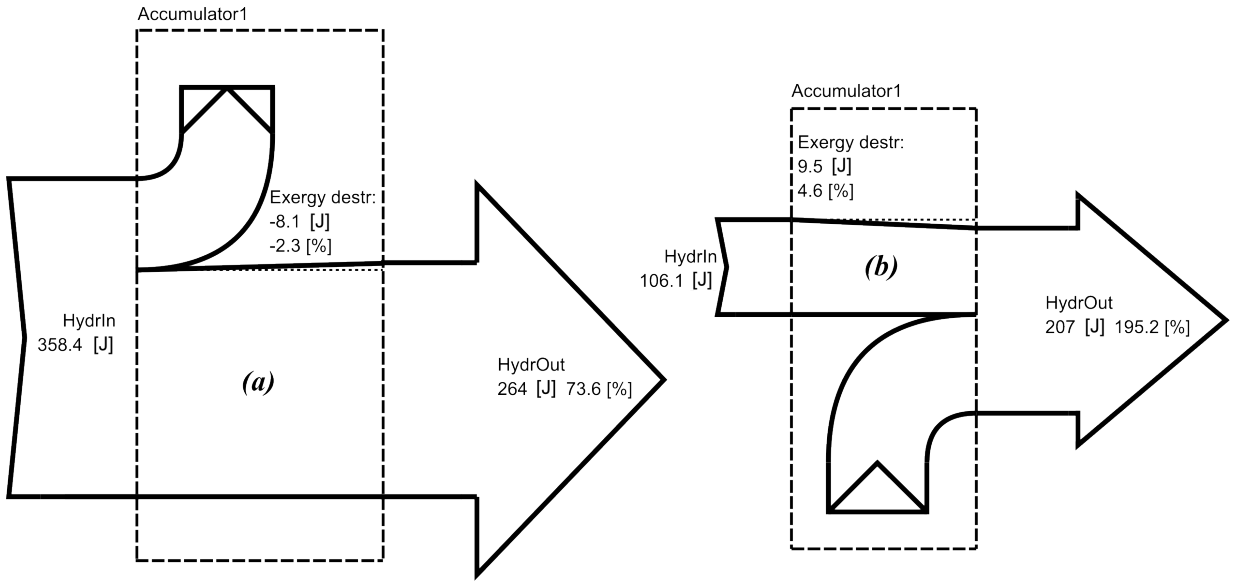

Figure 5.21: Accumulator 1 simulation results: Grassmann diagrams of a) storage and b) release phases

flow data used are the same on either side.

Motor and Generator

The generator's internal resistance and the external load resistance across the terminals known from the physical rig were used in the model, while the simulated generator's mechanical inertia and damping were adjusted so that the simulation's pressure readings matched those from the rig. The outcome is that the electrical power generation is shown as similarly inefficient in the simulation as in the measured results.

Boost pump and Accumulator 2

The difficulty of gaining results from the real rig in this section means the simulation can provide more sensible results, showing the losses and periodic storage of exergy in the accumulator. Exergy is stored when the check valve to the high pressure side is closed and is released again when it is open. In theory, this allows the boost pump to run at a slower speed while still preventing the piston from cavitating. The losses shown in the accumulator component are due to the pressure relief valve opening, as in the real rig, when pressure exceeds 7 bar. The negative

value at data point 15 in Table 5.2 represents the release of exergy from the storage in Accumulator 2. This release is not visible in the experimental results.

5.7.3 Result interpretation from a design standpoint

If using these results to consider improving the system's efficiency, there are three major areas for design and operation changes.

Power off-take

Despite the throttle being wide open, a significant loss is visible across the component (Fig. 5.14). Its removal would be the first step to improve efficiency. Currently, the system produces a lower exergy output than is put in at the boost pump. Clearly, this is an unacceptable outcome which stems from the inefficiency of the power off-take system, comprising the external gear motor and DC generator. The system used is not what would be used in a real wave power system and the reason for this is apparent in the resulting inefficiency. Using an external gear motor with its displacement of 4 cm^3 has the limitation of moving too slowly to work at a reasonable efficiency in conjunction with the DC generator it is connected to. A variable speed hydraulic motor to drive the DC generator would be the next step in improving efficiency.

Boost pump and accumulator

If it could be done efficiently, it would be preferable to run the boost pump intermittently, preventing most of the exergy added to the system from being destroyed by the pressure relief valve. It would still be required to keep the low pressure side at sufficient pressure to prevent cavitation in the piston during down-stroke. Certainly, it should not be run when there is no wave input. A larger accumulator would be required in order to permit an increase in the pressure relief valve setting. This would lead to more exergy being stored during the up-stroke and hence released during the down-stroke. The extent of the transfer of exergy during the down-stroke from the low pressure to the high pressure side via the piston is not entirely clear, since the simulation does not show as much exergy transfer as the real results. Allowing the residual exergy in the hydraulic fluid and the exergy

provided by the boost pump to remain in the system and be partly converted to electricity would be beneficial to the overall efficiency of the system. Even better still would be finding a way of removing the boost pump altogether.

Rectifier

The check valves in the rectifier destroy a significant amount of exergy. An improvement may be achievable by using higher quality valves. A more efficient rectifying method may also exist.

5.8 Discussion of exergy mapping process

This is the first application of the exergy mapping method being developed to a system that was not fully understood in advance. The exergy map of a system is intended to be a means of analysis of a system's energy use, a reference tool to be consulted and referred to when making design decisions and a means of communicating between disparate design groups. It becomes clear when analysing a comparatively simple system such as this, that the process of producing the data reliably and mapping the exergy flow is a complex task. The data required are not necessarily naturally produced by engineers developing the system, although a physical model, such as the one produced in Simscape in this case will generally be easy to adapt to provide suitable output.

The process of producing the exergy map necessitates an alternative understanding and perspective of the system in question from that which an engineer would gain in traditional circumstances. The insight the analyst gains when producing an exergy map must be transferable to others by means of the GUI that interprets the exergy map and the visualisations and reports generated by the software tool. The initial process of splitting the system into components may often require some explanatory notes, to elucidate the exergy flow in the system and how it is interpreted. The best way of dividing a system may not always be intuitive, as with the annulus and piston components in this case. There will always be a number of ways of dividing a system that are physically correct but don't provide the same information, are impractical to produce data for or do not show enough

detail. In this case, several iterations of the layout were required until a suitable one was chosen. This had to be settled upon before the pressure transducers were added to the system in the appropriate locations for producing the component input/output data.

The perfect synchronisation of all the data in the exergy map may be difficult even with pure simulation data. Discontinuities are more likely to exist when there is an interface between data sources and best efforts should be made to prevent this affecting the integrity of the exergy map. As discussed above, when the time span being analysed is sufficiently small, some discontinuity will become apparent and will place a lower limit on the time-frame over which the system can be sensibly analysed.

The results from the physical rig were produced under a limited budget, so the detailed exergy flow on the low pressure side was difficult to capture, as was the storage of exergy in the accumulators. Flow readings were of limited accuracy because the flow meters were operating at or below the lower bounds of their design flow rates. In a normal situation, a simulation such as the one used may not require as many sensor locations to validate the model. However, part of the aim of the real rig analysis was to gain a better understanding of the validity of using sensors to produce exergy map data. A vehicle, especially an aircraft that operates at varying conditions over ever-changing cycles, is a system that would benefit most from being analysed constantly, since results would vary significantly from flight to flight. However, the weight and complexity of equipping an aircraft with sensors to provide detailed exergy mapping data could be prohibitive except in unique cases, such as within the scope of instrumented test flights. A small selection of sensors, in addition to the existing ones aboard an aircraft, could be used to maintain the accuracy of a live simulation, allowing more detail to be produced without excessive numbers of sensors.

5.9 Conclusions

This chapter presents the first example of a time-variant exergy or available energy analysis of a hydraulic system known to the author. Using the exergy mapping

techniques established, it was possible to show the feasibility of including a system such as this in an exergy map, which is an advance on the most closely related literature. Results show the process of exergy destruction in the system clearly, and simulation data clarifies and corrects some aspects of the sensor data. The combination of both data sources makes the final results reliable and usable to support design decisions. This chapter can be used as a reference for future analyses of this type.

Fundamentally, this chapter must be seen as the establishment of the method of exergy mapping of a highly time-variant electro-hydraulic system, which is suitably representative of many aircraft subsystems. However, there is no example in the literature of a sensor-based exergy analysis, so this study is an important first step for discussing the feasibility of live exergy mapping. It is concluded that such an analysis will most likely be undertaken with a combination of sensor and simulation data in order to preserve accuracy but minimise the need for expensive instrumentation. The use of a highly dynamic system such as this is equally valid as a form of validation for the methodology when applied to a more steadily operating system. However, the data point frequency used in this analysis may be excessive for slower systems.

For the purpose of this thesis, this topic of live exergy mapping of aircraft must be left as future work because of the difficulty of accessing real aircraft sensor data, which is of a sensitive nature. Live analysis of the hydraulic system, rather than processing the data afterwards, would be highly feasible, although would have required a prohibitive amount of further programming and improved lab equipment for little immediate gain above that already shown. The topic of live exergy analysis of aircraft for the provision of greater information to the operator may be best addressed in an industrial setting.

Chapter 6

Variable reference states

An important consideration in any exergy analysis is the choice of reference state. In traditional exergy applications, such as thermal plants, typical outdoor temperatures can be chosen, which can often be assumed constant. The application of time-variant exergy analysis to aircraft raises the difficulty of a constantly and quickly changing outside atmosphere, making the choice of reference environment far more contentious. This chapter aims to establish a normal procedure for reference environment choices when creating an aircraft exergy map.

6.1 Problem definition

Figure 6.1 shows the results of basic exergy calculations on a stream of gas similar to that exiting a turbojet combustion chamber ($T = 1,230$ K, $P = 6.73$ bar) with a typical composition assuming full combustion. The physical exergy makes up around 95% of the total when considering a sea level reference state. For comparison of the effects of reference conditions, the standard atmosphere values at sea level and 10,000 m and an assumed constant 70% humidity are used to calculate exergy values for the gas flow. The physical exergy is affected far more by the changing conditions than the chemical.

Etele and Rosen [54] (presented also in Dincer and Rosen [22]) were the first to consider the effect of the varying reference state on the analysis of aircraft systems. The effect of the reference state on the rational efficiency of a simple turbojet was analysed over a mission. Fixed reference states at sea level and cruise altitude were compared with an engine-fixed reference state which varies with the current

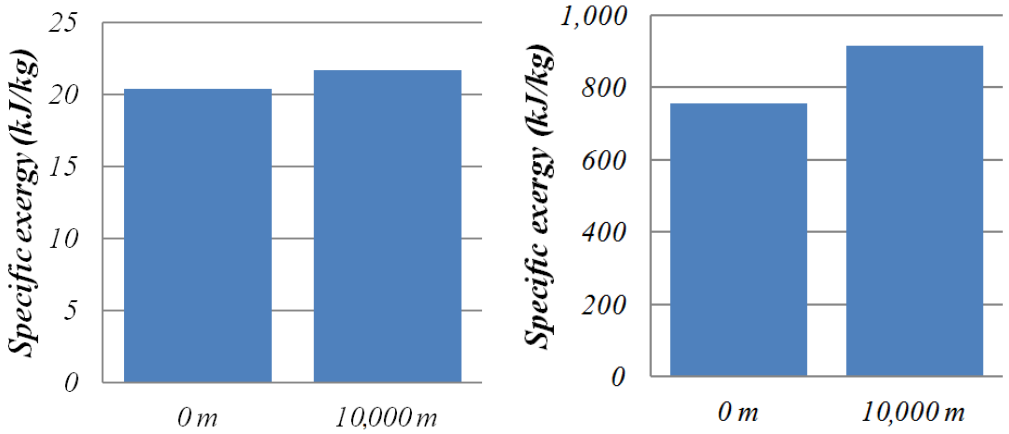

(a) Chemical exergy variation

(b) Physical exergy variation

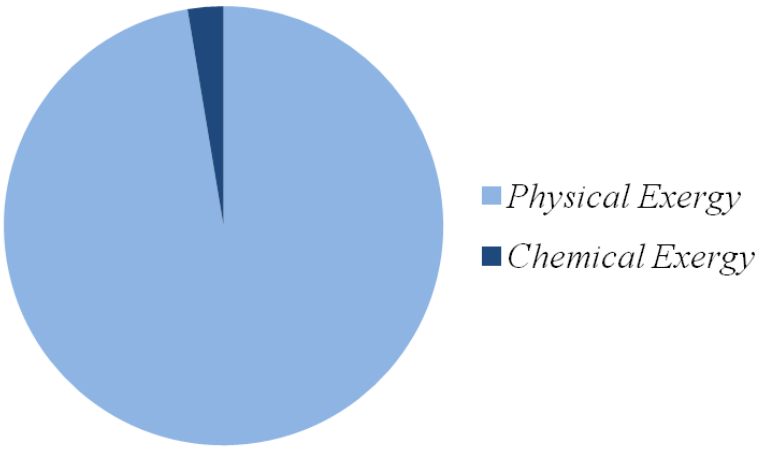

(c) Exergy form comparison

Figure 6.1: Example exergy differences of a gas flow at sea level and 10,000 m altitude

altitude. It is shown that despite the exergy values being affected by the choice of reference state, the rational efficiency of the engine only varies by up to 3% in the most extreme cases. In some situations, the choice of reference condition would not affect the qualitative outcome of a study.

Rosen and Dincer [55] also consider the effects of changing reference states, but in this case only with regard to ground-based systems. A coal power plant is analysed to study the subject and it is shown that in such situations, the effect of varying reference states will have little to no impact on conclusions or recommendations arising from an exergy analysis.

These studies, while certainly reaching valid conclusions, do not answer the same question as what is being posed in this thesis. The intent of the exergy map is to provide a tool that can be used in a large variety of situations. The aim is to avoid making presumptions and hence, the effect of a varying reference state needs to be studied in the context of exergy mapping. For example, when considering the availability of energy for harvesting or recovery, the accuracy could be far more important than some optimisation study where relative changes in parameters are being compared to each other.

Some consideration must also be given to reference points used for calculating kinetic and potential exergy to ensure the subject is fully understood.

6.2 Physical exergy

Physical exergy of an ideal gas flow is calculated using

$$e = (h - h_0) - T_0(s - s_0) + \frac{\mathcal{V}^2}{2} + gz \tag{2.13}$$

It is clear from this equation that the reference properties h_0 and T_0 will have as much bearing on the result as the conditions being analysed. The velocity, $\mathcal{V}$ and height z are written alone by convention, but more precisely should be written as $\mathcal{V} - \mathcal{V}_0$ and $z - z_0$. In the case of exergy mapping a vehicle, these terms should normally be calculated using a local frame of reference, i.e. movement relative to the system in question. For fluid flows internal to the aircraft, the gravitational potential and kinetic energy of the static fluid should be included in the calculations for the mass component of the aircraft (Chapter 3). Only the values associated with its relative movement to the aircraft should be accounted for as a property of the fluid flow. Since these components will often be small, it is likely that they will be neglected in many cases.

6.2.1 Kinetic exergy of air flow through a jet engine

There are two possible interpretations of the kinetic exergy as it passes through the engine.

Kinetic exergy relative to engine The kinetic energy of the flow through a gas turbine can be significant. The air entering the engines will have high speeds relative to the aircraft which will lead to increased pressure and temperature when slowed down. Including the kinetic exergy of the air flow through the engine can be done by using the stagnation values of temperature and pressure, or the kinetic term can be added to the static exergy values. The exergy of the still air must equal zero, assuming the local reference state is used. Its kinetic term due to the relative velocity of the aircraft, which is an exergy input to the engine, equals the difference between the gross and net thrust values, so must originate from the engine exhaust component.

Kinetic exergy relative to ground The intake air's kinetic exergy is calculated relative to its ground speed. The air taken into the engine core will be accelerated relative to the ground in the direction of travel. Any air velocity in the direction of aircraft travel must be considered negative exergy in order to avoid 2nd law violation. The bypass air and core exhaust is accelerated against the direction of travel, leading to only the net thrust and the air's physical exergy leaving the exhaust component. Any exergy observed at the exit of the inlet component must originate from the aerodynamic component.

6.3 Chemical exergy

The chemical exergy reference environment is not standardised, although that proposed by Szargut [44] is probably the most commonly chosen. The environment consists of the lowest energy, commonly found molecules in the atmosphere, sea and Earth's crust. For aircraft, a basic reference environment such as Szargut's will not change. For spacecraft or other devices and vehicles operating outside reach of the Earth's atmosphere a new reference environment would need to be established. This is, however, beyond the scope of this thesis.

Ertesvåg [52] presents a study of the effects of varying physical conditions on chemical exergy calculations. For gases that exist in the reference environment, such as CO_2 or N_2, the chemical exergy is a function of the difference in partial pressure of the species. The molar chemical exergy of an atmospheric gas i is given

by

$$\bar{e}_i^{ch} = -\bar{R}T_0 \ln \bar{x}_i^e \tag{6.1}$$

where $\bar{R}$ is the universal (molar) gas constant and $\bar{x}_i^e$ is the mole fraction of species i in the reference environment. $\bar{x}_i^e$ is affected by the water content of the air through following equation:

$$\bar{x}_i^e = (1 - \bar{x}_{H_2O}^e)\, \bar{x}_i^{dry} \tag{6.2}$$

where $\bar{x}_i^{dry}$ is the mole fraction of species i in dry air and $\bar{X}_{H_2O}^e$ is the mole fraction of water vapour. The chemical exergy variation with reference environment can be compensated for with Eqs (4.4) – (4.6) [52].

Some pertinent results from Ertesvåg's work are reproduced using the chemical exergy calculator described in Chapter 4. These are displayed in Figs 6.2 and 6.3. In Fig. 6.2(a) it is shown that the exergy of atmospheric gases is affected strongly by the ambient temperature, which changes the water fraction in the air. This effect becomes smaller at lower temperatures because the maximum dilution of water in the air reduces. Figure 6.2(b) shows the effect the relative humidity has on atmospheric gases and H_2 at 25°C. Water is affected most strongly as might be expected.

Figure 6.3 shows the variation of the exergy of simple gaseous hydrocarbon fuels and carbon monoxide with ambient temperature. The variation is considerably less than for atmospheric gases and decreases with increasing hydrocarbon complexity. Figure 6.3(b) shows the effect of relative humidity on the exergy of the hydrocarbons. The variation is small, even negligible for carbon monoxide (CO).

6.4 Exergy of jet fuel

Jet fuel, such as Jet-A1, is a kerosene-based liquid that consists of a mixture of long hydrocarbon chains. The ratio of types of hydrocarbons is not prescribed directly, although the fuel must behave within certain parameters to meet specifications. It is typical in chemical analyses to use 'surrogate mixtures' of fewer, known hydrocarbon ratios that would behave chemically and physically similarly as the more complex fuel [56]. The accuracy required of these surrogate mixtures in such research contexts is, however, likely to be larger than for the purpose of

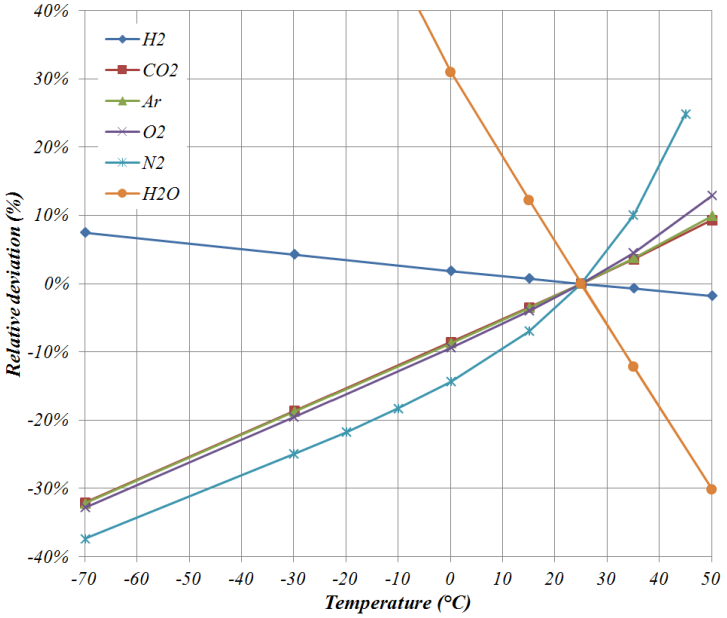

(a) Chemical exergy deviation of pure atmospheric gases with ambient temperature at constant 70% relative humidity and 1 atm pressure

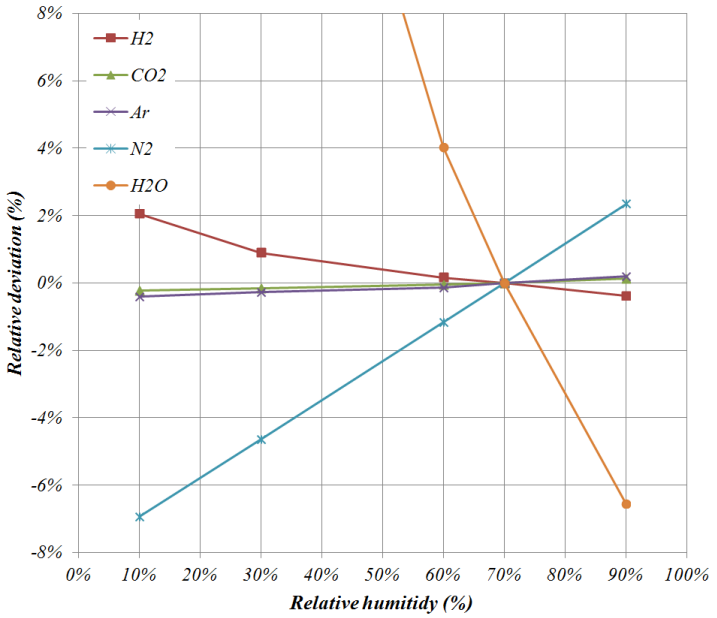

(b) Chemical exergy deviation of pure atmospheric gases with relative humidity at 25°C and 1 atm pressure

Figure 6.2: Effects of ambient conditions on exergy of pure atmospheric gases. Based on: [52]

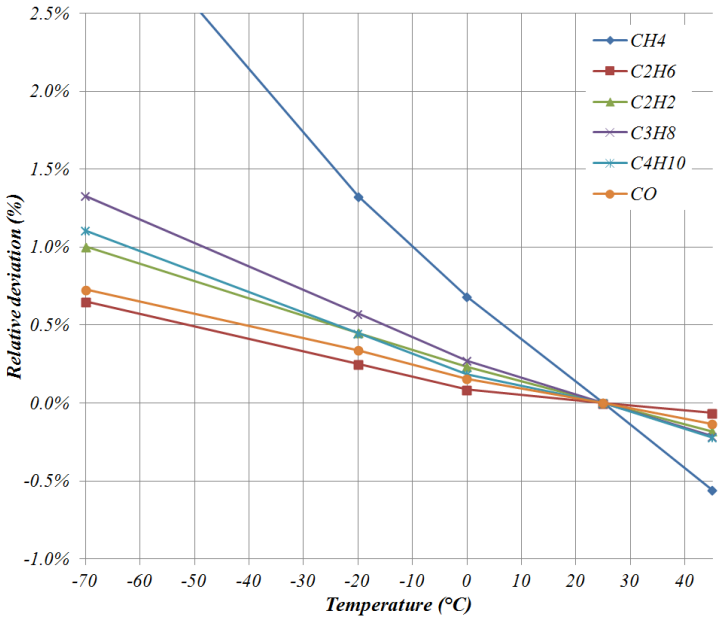

(a) Chemical exergy deviation of gaseous hydrocarbons with ambient temperature at constant 70% relative humidity and 1 atm pressure

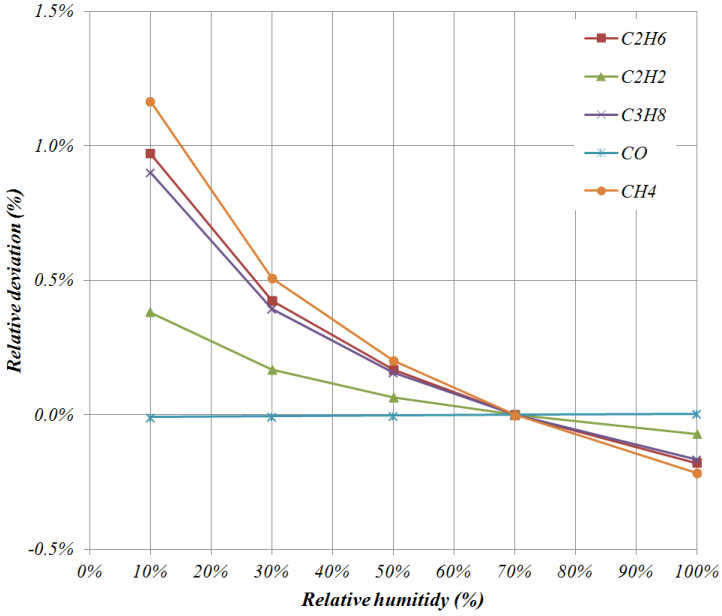

(b) Chemical exergy deviation of gaseous hydrocarbons gases with relative humidity at 25 °C and 1 atm pressure

Figure 6.3: Effects of ambient conditions on exergy of gaseous hydrocarbons. Based on: [52]

exergy mapping where a consistently applied value is more important. The selection of the surrogate model will also depend on the aspect of the fuel being researched [57] and is a complex area of research.

Kotas [12] presents a formula connecting the lower heating value (LHV) of a fuel, which is often known, to its exergy via the following ratio:

$$\phi = \frac{e}{LHV} \tag{6.3}$$

where ϕ is calculated using an equation derived using regression analysis of various hydrocarbon fuels:

$$\phi = 1.0401 + 0.1728\frac{\mathrm{h}}{\mathrm{c}} + 0.0432\frac{\mathrm{o}}{\mathrm{c}} + 0.2169\frac{\mathrm{s}}{\mathrm{c}}\left(1 - 2.0628\frac{\mathrm{h}}{\mathrm{c}}\right) \tag{6.4}$$

Here h, c, o and s are the hydrogen, carbon, oxygen and sulphur fractions respectively. The accuracy of this equation is estimated as $\pm 0.38\%$ [12]. A very simple surrogate for Jet-A1 is pure dodecane ($C_{12}H_{26}$) [58]. For the purpose of using the above equations, this will provide a proportion of carbon to hydrogen similar to the mean values one might expect in kerosene. This has a LHV of 44,109 kJ/kg as a liquid fuel and 44,467 kJ/kg as a gaseous fuel [59] at 25° C. Using Eqs (6.3) and (6.4), and $c = 0.847$, $h = 0.153$, the chemical exergy is calculated to be 47,255 kJ/kg at 25° C.

For comparison, using the method given by Ertesvåg to calculate the exergy of a gaseous fuel, and assuming the dodecane to be in gas form, the exergy was calculated to be 46,926 kJ/kg. Its variation with ambient temperature, according to the method discussed previously, is shown in Fig. 6.4.

Although the representation of jet fuel as dodecane is not completely accurate, a more complex analysis of this topic is beyond the scope of this thesis, since any more precision would only be of limited use. A certain level of uncertainty will always exist in the estimation of the fuel exergy, partly dependent on the choice of reference environment. The exergy of the fuel would be used in an exergy map to calculate the stock of exergy in the fuel tanks at any time, and as an input to the engine exergy balance. Variations in the accuracy of the fuel's chemical exergy will only have an impact on the exergy efficiency of the engines, something that will vary far more due to external factors. The additional time required to account for chemical exergy variation of the fuel due to ambient conditions would also be

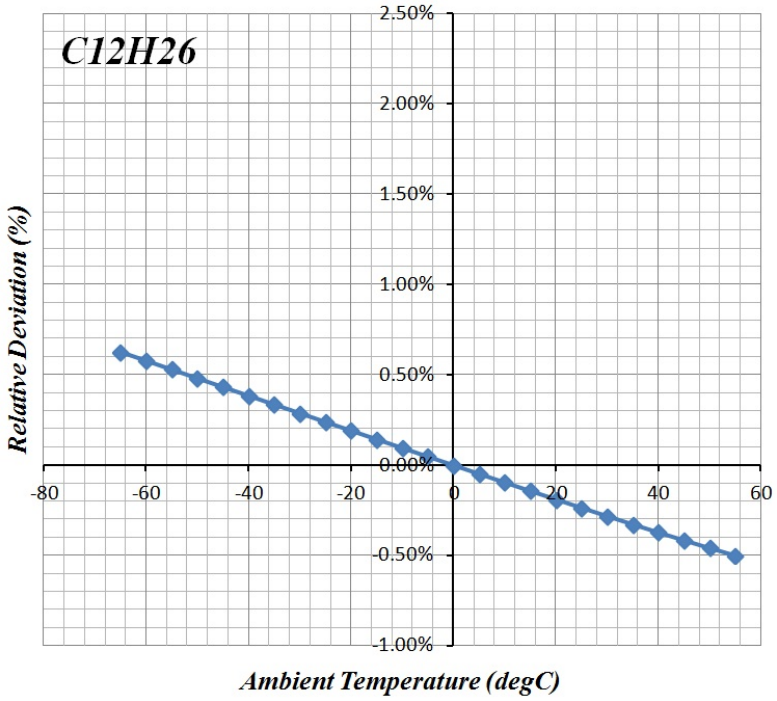

Figure 6.4: Variation of dodecane with ambient temperature at 1 atm pressure and relative humidity of 70%

considerable. The advantages of assuming a constant exergy value for the fuel for the sake of thermoeconomic analysis is therefore likely outweigh any benefits that would be seen. Fuel can be regarded as a fixed exergy stock when the remaining energy carriers fluctuate throughout the mission.

6.5 Other exergy forms

6.5.1 Electrical exergy

The energy and exergy of electricity are equivalent, since the transformation of electrical power to another form is not limited by the 2nd law. Electrical energy or power reference states are therefore the same as those used to calculate exergy. Voltages throughout the aircraft should be measured relative to the same zero-voltage reference for consistency.

6.5.2 Kinetic exergy

The kinetic exergy of the aircraft's mass requires some consideration when performing an exergy analysis of an aircraft. The question to be answered would generally be whether to use the velocity of the outside air as the reference state or the ground. This is the same as using either the true airspeed or the ground speed to calculate the kinetic energy. Arguments can be made for either option, depending on the application. The aircraft's air speed will determine the availability for any system harvesting exergy from the relative movement of air, such as the ram-air turbine (RAT). An exergy analysis that studies only an aerodynamic subsystem may consider the aircraft's position to be the reference state and the air to carry exergy.

For the purpose of developing an exergy map, however, the ground speed must be used. Gusts of wind will have an effect on the drag of the aircraft, indirectly affecting the kinetic exergy of the mass. Using the air speed would lead to direct reductions and increases in calculated kinetic exergy, which is certainly to be avoided.

6.5.3 Gravitational potential

For the calculation of gravitational potential of the aircraft's mass, it is simplest to use the lowest point of the aircraft's mission as the reference altitude. If the landing altitude is lower than that at take-off, the aircraft will begin with some potential exergy stock in its mass, which will be expended at the end of the flight. This will avoid negative exergy accounting problems, which should not exist with the correct selection of reference state. Using sea level as the reference state would work in most situations, except in the rare cases of flights to or from airports below sea level (Amsterdam Schiphol being a notable example!).

6.6 Gas turbine simulation

The effects of a varying reference state on a thermal system are considered in more detail in this section. Following the example of Etele and Rosen [54], a simple turbojet was chosen as the subject of study. The exergy map layout is given in

Fig. 6.5. Since the variation of chemical exergy will be more pronounced for simpler

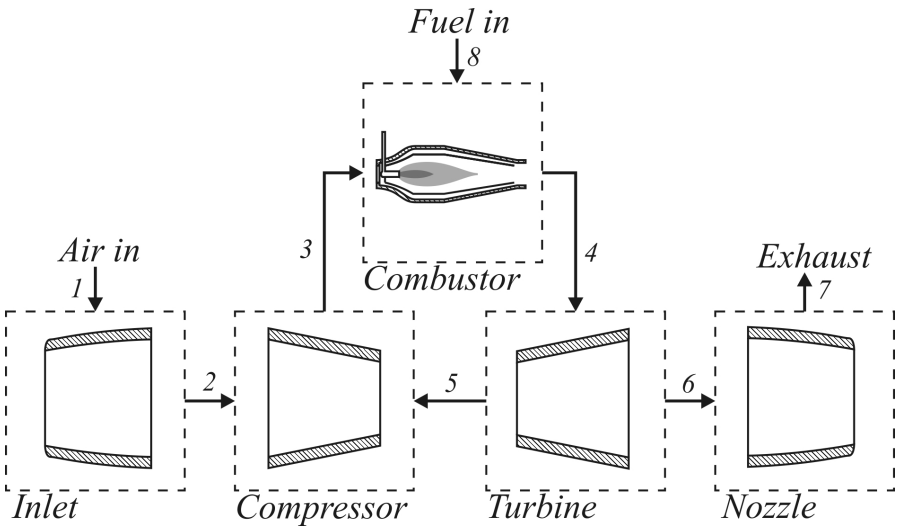

Figure 6.5: Turbojet exergy flowchart. First published in [48].

hydrocarbons, methane was used as the fuel in the simulation, being provided at a constant rate of 0.2 kg/s. The remaining major component parameters are given in Table 6.1.

Table 6.1: Turbojet simulation main parameters

Component	Parameter	Value	Units
Inlet	Design mass flow	19.9	kg/s
	Design pressure ratio	1	-
Compressor	Design rotor speed	16540	rpm
	Design pressure ratio	6.92	-
	Design efficiency	0.825	-
Turbine	Design rotor speed	16540	rpm
	Design efficiency	0.880	-
	Spool mechanical design efficiency	0.990	-
	Spool inertial moment	0.758	kg m^2

6.6.1 Simulation program

The gas turbine model was created using GSP (Gas turbine simulation program) [60], developed by the Dutch National Aerospace Laboratory (NLR). The software allows gas turbine components to be stacked as required to produce a complete model. Simulations can be performed for time-variant missions. The software uses one-dimensional models of the individual components, combined with component maps. Non-linear differential equations are solved to determine the off-design behaviour, including time derivatives for transient simulations. A multi-variable Newton-Raphson method is used to solve the equations [61].

6.6.2 Mission analysed

The mission used for the analysis is illustrated in Fig. 6.6. To avoid the complication of kinetic exergy transfer to intake air, the simulation assumes zero horizontal velocity and zero airspeed. The turbojet is raised steadily from sea level to 10,000 m altitude and back to sea level over 1,000 seconds.

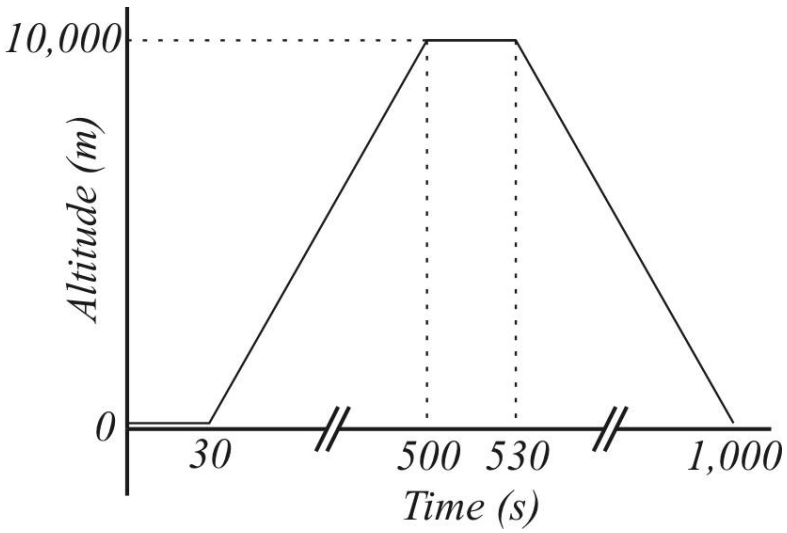

Figure 6.6: Turbojet mission. First published in [48].

6.6.3 Calculations

The physical exergy of the air from intake to combustion chamber (Points 1, 2 and 3, Fig. 6.5) are calculated using

$$\dot{E}^{ph}_{1,2,3} = \dot{m}\left(h_{air} - h_{air,0} - T_0(s_{air} - s_{air,0})\right) \tag{6.5}$$

For the gas flows after the combustion chamber, in which the gas concentrations will deviate from those of the atmosphere, the physical exergy is given by

$$\begin{aligned}\dot{E}^{ph}_{4,6,7} = \dot{m}\big[&x_{N_2}\left(h_{N_2} - h_{N_2,0} - T_0\left(s_{N_2} - s_{N_2,0}\right)\right)\\ &+ x_{O_2}\left(h_{O_2} - h_{O_2,0} - T_0\left(s_{O_2} - s_{O_2,0}\right)\right)\\ &+ x_{H_2O(g)}\left(h_{H_2O(g)} - h_{H_2O(g),0} - T_0\left(s_{H_2O(g)} - s_{H_2O(g),0}\right)\right)\\ &+ x_{CO_2}\left(h_{CO_2} - h_{CO_2,0} - T_0\left(s_{CO_2} - s_{CO_2,0}\right)\right)\\ &+ x_{Ar}\left(h_{Ar} - h_{Ar,0} - T_0\left(s_{Ar} - s_{Ar,0}\right)\right)\big]\end{aligned} \tag{6.6}$$

where x_i is the mass fraction of species i, provided complete combustion has occurred. Insignificant species and condensation are neglected.

The chemical exergy of combustion products is in part due to the Gibbs energy of gases that do not exist in the reference environment, which are very limited after complete combustion. Mainly, the chemical exergy exists because of a difference in concentration of atmospheric gases. For a mixture of gases, the standard molar chemical exergy can be found using

$$\bar{e}^{ch} = \sum \bar{x}_k \bar{e}^{ch}_k + \bar{R}T_0 \sum \bar{x}_k \ln \bar{x}_k \tag{4.2}$$

where the standard molar chemical exergy $\bar{e}^{ch}_k$ of species k can be either found in the literature, e.g. [12, 45] or is calculated using Eq. (6.1) if the species is present in the reference environment.

To account for the variation of the fuel and combustion gas chemical exergy, the method described in Subsection 6.3 is used. The specific exergy for the fuel becomes

$$\begin{aligned}\bar{e}^{ch}_{CH_4} = \bar{e}^{ch,ref}_{CH_4}\frac{T_0}{T^{ref}} + \frac{T^{ref} - T_0}{T^{ref}}(LHV_{CH_4})&\\ + T_0\bar{R}\left(\ln\frac{x^{ref}_{CO_2}}{x^{e}_{CO_2}} + 2\ln\frac{x^{ref}_{H_2O}}{x^{e}_{H_2O}} - 2\ln\frac{x^{ref}_{O_2}}{x^{e}_{O_2}}\right)&\end{aligned} \tag{6.7}$$

and the equation used for the combustion gases, but which would equally apply to any of the engine's gas flows, is

$$\begin{aligned}\dot{E}^{ch}_{1,2,3,4,6,7} = \frac{\dot{m}}{M_m}\big[&\bar{x}_{N_2}\bar{e}^{ch}_{N_2} + \bar{R}T_0\bar{x}_{N_2}\ln\bar{x}_{N_2} \\ &+ \bar{x}_{O_2}\bar{e}^{ch}_{O_2} + \bar{R}T_0\bar{x}_{O_2}\ln\bar{x}_{O_2} \\ &+ \bar{x}_{CO_2}\bar{e}^{ch}_{CO_2} + \bar{R}T_0\bar{x}_{CO_2}\ln\bar{x}_{CO_2} \\ &+ \bar{x}_{Ar}\bar{e}^{ch}_{Ar} + \bar{R}T_0\bar{x}_{Ar}\ln\bar{x}_{Ar}\big] \end{aligned} \tag{6.8}$$

noting that the equation would have to be extended to include other species present in the flow if combustion were incomplete. These equations were used to calculate the exergy flows through the turbojet at each time point over the mission. To do so, the physical and chemical exergy calculators described in Chapter 4 were used. Time points for the entire analysis were at regular intervals of 0.2 seconds.

6.7 Reference state schemes

To clearly identify the effect of a varying reference state, the following reference state schemes were used in the calculations for comparison.

Scheme 1: Reference state fixed at ground level The simulation is run over the mission depicted in Fig. 6.6. The exergy at each interface is calculated using standard atmosphere sea level conditions ($T_0 = 288.15$ K and $P_0 = 101,325$ Pa) as the fixed reference state. This scheme is chosen to represent any fixed reference point analysis. There would be a temptation to use a fixed reference point when comparing two flight phases in order to allow two flows of the same temperature and pressure to have the same exergy. This might be seems as a way to maintain a fixed link between the common currency of exergy and the thermal properties.

Scheme 2: Reference state moving with engine The standard atmosphere conditions at the current altitude at each time step are used to calculate the exergy. This scheme represents the most physically accurate exergy calculations at any given time.

Scheme 3: Constant inlet conditions, changing reference state For comparison, it is assumed that the turbojet can be provided with air at sea level conditions and exhausts to sea level conditions while following the same reference state conditions as in Scheme 2. This is to counter the problem that the atmospheric conditions also have a significant effect on the efficiency of the engine components. The effect of the changing dead state alone can be better considered in isolation by using this scheme and the true magnitude of the distortion caused by the choice of an incorrect reference state can be examined.

6.8 Reference scheme results

The results for the reference state schemes are given in Table 6.2. Figures 6.7 - 6.10 show Grassmann diagrams for these results in the same order. The first 30 seconds, during which the engine is at sea-level are equal for all three schemes, hence this section is only depicted once in Fig. 6.7. Figures 6.8 – 6.10 show the results over a 30-second time period at 10,000 m altitude for the different reference schemes. The diagrams are to scale with each other, allowing for clear comparison. Figure 6.8 shows that using a ground-based reference state at high altitude leads to the air being drawn in with a positive exergy value. Although exergy cannot in itself have a negative value, the calculated exergy in this case arises because the conditions deviate from the reference state in the opposite direction to that of the air after the compressor, being colder rather than hotter than the reference state. This leads to the compressor component displaying a large, artificial inefficiency (Fig. 6.8 point (a)) as the exergy values cancel each other out.

Figure 6.9 shows the results when using a reference environment corresponding to the atmosphere directly outside the turbojet. This, by definition, leads to the inlet air having zero exergy. The compressor efficiency is therefore represented truthfully. The non-fuel gas flows in the system are larger than their equivalents in Fig. 6.8 because the reference state (being at lower temperature and pressure) deviates further from the internal values. The shaft work passing from the turbine to the compressor remains the same, since this is mechanical work and therefore unaffected by reference states. The chemical exergy of the methane fuel, meanwhile,

increases only by about 1.3% due to the changes in reference conditions.

Figure 6.10 shows a hypothetical case of a reference state equivalent to 10,000 m standard atmosphere, but with sea-level inlet and outlet conditions. In effect, this shows what the thermodynamic values used to produce Fig. 6.7 become when using a high altitude reference state. The inlet air flow has a large exergy value, but the direction of deviation from the reference state is the same as that of the remaining non-fuel gas flows (unlike in Fig. 6.8), since all temperatures and pressures are higher than the reference values. This causes the compressor's efficiency to be unnaturally high because the magnitude of exergy destruction remains the same, but the total exergy throughput is higher. The high exergy value of the gas flows leads to more exergy being present after the combustion chamber than is entering via fuel. These diagrams show the various problems that can be brought about by using a fixed reference state. Figure 6.10 illustrates the problem more clearly than Fig. 6.8 because the effects of the reference state are not hidden by the changes in gas turbine performance.

Table 6.2: Reference state scheme study results

Scheme	Component	In (kJ)	Out (kJ)	Destr. (kJ)
Sea-level	Inlet	0.00	0.00	0.00
(Sea-level reference)	Compressor	108.23	96.28	11.95
	Combustion Ch.	407.49	279.60	127.90
	Turbine	279.60	274.16	5.40
	Exhaust	166.72	166.72	0.00
10,000 m	Inlet	19.26	19.26	0.00
(Sea-level reference)	Compressor	87.46	32.47	54.99
	Combustion Ch.	343.67	256.12	87.55
	Turbine	256.10	253.56	2.54
	Exhaust	185.36	185.36	0.00
10,000 m	Inlet	0.00	0.00	0.00
(Aircraft-fixed reference)	Compressor	68.22	54.91	13.31
	Combustion Ch.	370.20	300.17	70.03
	Turbine	300.17	298.14	2.03
	Exhaust	229.94	229.94	0.00
Sea-level	Inlet	47.28	47.28	0.00
(10,000m reference)	Compressor	153.79	145.29	8.50
	Combustion Ch.	460.58	359.74	100.84
	Turbine	359.74	354.57	5.17
	Exhaust	248.06	248.06	0.00

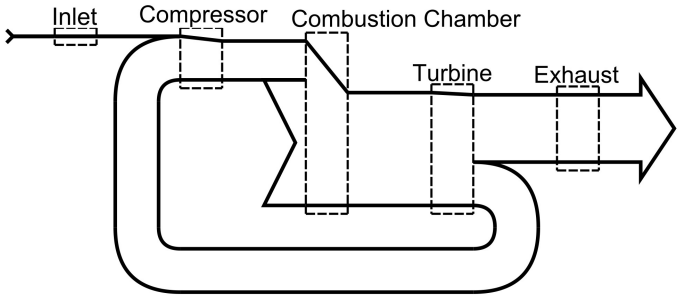

Figure 6.7: Turbojet results for 30s at sea level. First published in [48].

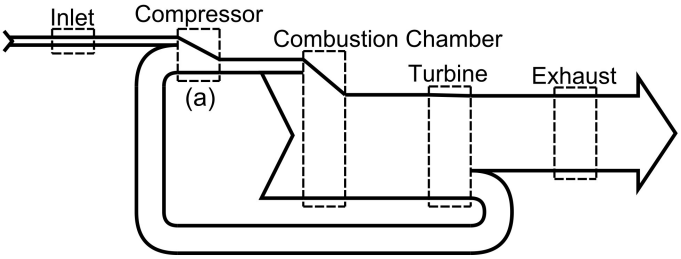

Figure 6.8: Turbojet results for 30s at altitude, sea-level reference. First published in [48].

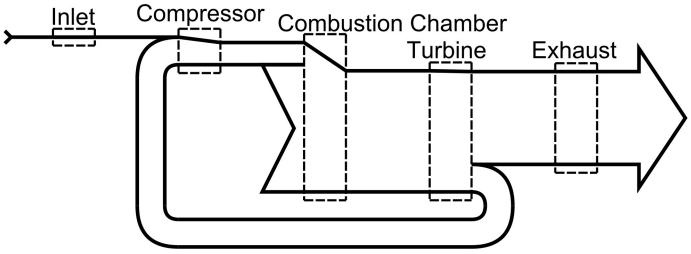

Figure 6.9: Turbojet results for 30s at altitude, engine-fixed reference. First published in [48].

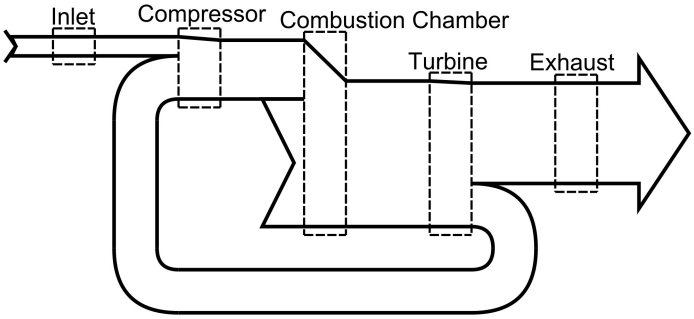

Figure 6.10: Turbojet results for 30s at altitude, sea-level intake. First published in [48].

6.9 Change in stock exergy

It is evident that using the varying reference state to calculate the instantaneous exergy values at each time point provides the most sensible results. The data required to do so can either be based on standard atmosphere models in the case of simulations or could use temperature and pressure data that are typically recorded by an aircraft in operation if the analysis in question were of a real mission and aircraft. It may, however, lead to another difficulty. To illustrate this, another theoretical situation is considered in which the same simulation data are used. For the first 30 seconds, however, it is assumed that the exhaust gas can be stored losslessly and isentropically instead of being expelled. Thereafter, the exhaust is released into the atmosphere as before.

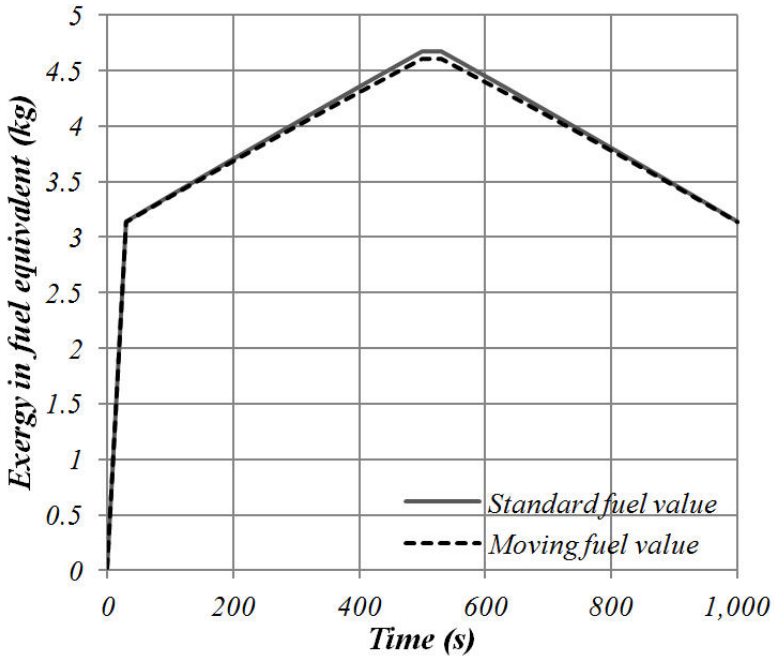

Figure 6.11: Exergy stock in equivalent fuel mass over mission. First published in [48].

Figure 6.11 shows the exergy stock in the exhaust storage component over the mission. The exergy values are converted to the mass of methane with the equivalent amount of chemical exergy. The first 30 seconds of the mission, while the engine is on the ground, is the period over which the storage is filled, shown by a quick increase. After this, the engine gains in altitude and the effect of the

changing reference state increases the exergy of the storage despite no further gas being added. The exergetic value of the stored gas is increased by around 49%. The effect of the reference state on the exergy value of the fuel and therefore the equivalent value of the stored gas can be seen by comparing the two plotted data sets. The solid line represents the variation in equivalent fuel value if the fuel's standard (room temperature, pressure) chemical exergy is used, while the dashed line shows that of the chemical exergy of the fuel adjusted for the local reference state. Clearly, the difference between the two cases is small, showing, again, that the effects of the local atmosphere on chemical exergy are far less than the effects on the physical exergy.

Although the effect of the reference state causes a change in stored exergy, this change does represent a real physical effect. For example, if a perfectly insulated box of hot gas is able to exchange heat with a colder body than the local atmosphere, the work that can be produced is higher. The difficulty produced by this effect in the context of a vehicle exergy mapping tool is that the relationship between the cost of producing the stored gas to begin with cannot be easily interpreted if the stored gas is utilised at different environmental conditions. A change in reference conditions will also lead to the storage gaining exergy despite there being no input of mass, heat or work to the control volume, which will confuse the accounting method.

6.10 Conclusions

This chapter discusses the choice of reference conditions when producing an exergy map of an aircraft. Although the topic of varying reference conditions has been approached in the literature before, the conclusions drawn are not necessarily relevant to the exergy mapping process. This chapter builds on the subject with a more detailed analysis and some new aspects.

Kinetic and potential exergy reference states for the aircraft's motion are established. Generally, the ground speed must be used to calculate the aircraft's kinetic exergy, since the airspeed, when considering a real flight, would vary constantly due to wind gusts. Using ground speed means wind will affect drag exergy

destruction. The gravitational potential of the aircraft should be calculated relative to the lowest point on an aircraft's mission. The aircraft will tend to start or end with a stock of exergy due to this. Internal system flows will normally neglect kinetic and potential components, but these will be calculated with reference to the system's position. An exception is made for gas turbine flows, where the air speed should be calculated relative to the ground.

Chemical exergy reference environments will not affect the validity of an exergy map, although a single environment should be chosen and used throughout. The variation of chemical exergy with atmospheric conditions is small, although not insignificant. However, the chemical exergy component of gas flows found in aircraft is also likely to be small in most cases, provided combustion in the engine is near complete. In most studies involving normal aircraft over typical missions, including the variation of chemical exergy due to environmental conditions would not be of interest. This may change, however, if the systems under consideration involve unusual gas flow composition, such as those involving fuel cells might. The exergy of jet fuel is shown only to be affected by around 1.1% over the whole range of operating temperatures that a passenger aircraft is likely to be exposed to. Since the accuracy of the exergy estimations are not entirely precise (the two estimates given being 0.7% apart), the exergy of jet fuel can generally be considered constant.

A study of the physical exergy effects on the analysis of a simple jet engine allowed the clear visualisation of the effects that a varying reference state has. Using a consistent reference state for exergy calculations can be superficially tempting, perhaps because the 'currency' role that exergy is meant to fulfil would appear more stable. However, the case study used makes it clear that for exergy mapping, there is no alternative to an aircraft-fixed reference state. It is shown that an inaccurate reference state will lead to engine intake air being shown as having significant exergy, but due to deviation from the reference environment in the opposite direction to the remaining system. It is also shown that the changes in the performance of the engine due to different air intake conditions go some way toward hiding the true magnitude of the effects of incorrect reference state selection.

The variation of the reference environment will have a significant effect on any

physical exergy stock maintained over a long period of time (e.g. greater than 1 minute) while the aircraft is in climb or descent. The link between the generation costs of that exergy stock and its current value will be skewed. This phenomenon is unlikely to be of major concern in normal exergy analyses, since storages of exergy, such as cabin air, accumulators, etc. are usually brief and continuously replenished.

Chapter 7

Exergy mapping of complex aircraft

With the basics of time-variant exergy mapping having been established in previous chapters, it is relevant to perform a case study of an aircraft more representative of the intended application. This serves as an example of the final use of the method for future reference, as well as an opportunity to highlight further difficulties that might arise when using the technique. In this chapter, an aircraft exergy map is created, based on an Airbus A320 over a short-haul flight. The two critical systems in terms of exergy use, the aerodynamic and propulsion systems, are included alongside a simplified air conditioning system. The latter is representative of an internal subsystem, which requires considerably less exergy than the others. In addition to the method of creating the exergy map, the results will be used in Chapter 8 to exemplify the further use and interpretation of the exergy map data.

7.1 Mission

The mission over which the aircraft is analysed is based on a short haul flight of 850 km, approximately the distance from London Heathrow to Zurich, which has been modified to satisfy the limitations of the performance model (Section 7.3). The velocity and altitude over the course of the mission are shown in Fig. 7.1. The analysed mission starts shortly after take-off and ends shortly before landing.

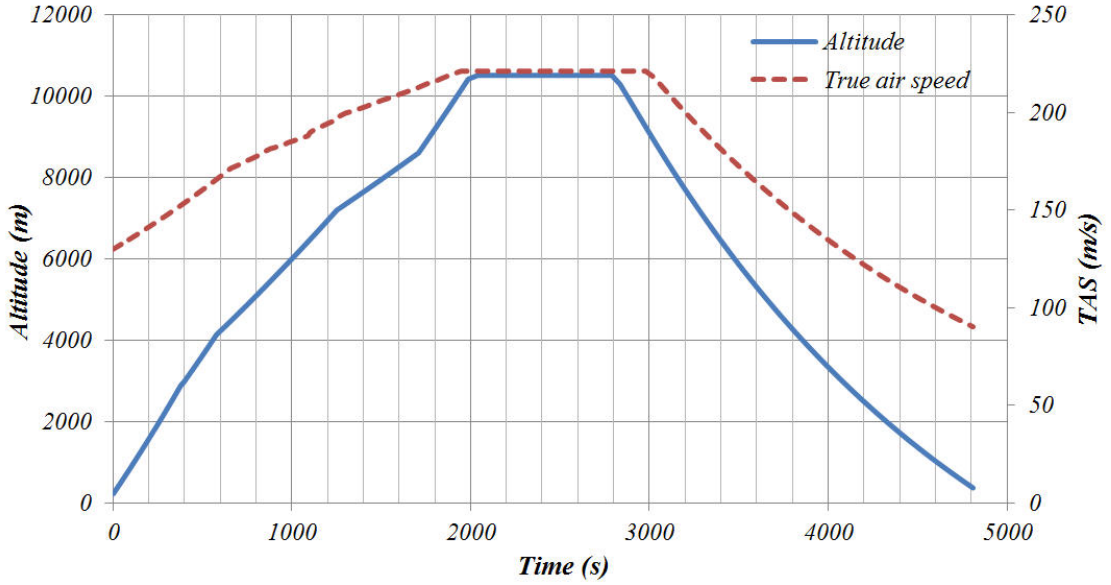

Figure 7.1: Aircraft flight mission

7.2 System exergy flow

The exergy flowchart for the system including the turbofan engine, aircraft mass, aerodynamics and air conditioning system is given in Fig. 7.2. The system is split into three subsystems, enclosed in boxes. Numbers given are the data points at which exergy flow and stock data are accounted. The only exergy source is from the fuel input at Point 19. Exergy is transferred from the bypass and core exhausts of the engine to the aircraft mass (Points 25 and 20), from the aerodynamics to air conditioning inlets due to ram effects (Point 34) and from the engine's high pressure compressor to the air conditioning precooler (Point 18). The exergy of the engine inlet's ram air originates from the bypass and core exhaust components (Points 38 and 39), so it is expected that the exergy of the atmospheric air (Point 1) would be zero at all times given an aircraft-fixed reference state.

The engine components are duplicated in the exergy map (not shown in Fig. 7.2) because the aircraft has two engines. The data points are re-used for the other engine, so exergy flow data need not be duplicated in the database. The air conditioning system, which in reality would also be duplicated, is only linked to one of the engines.

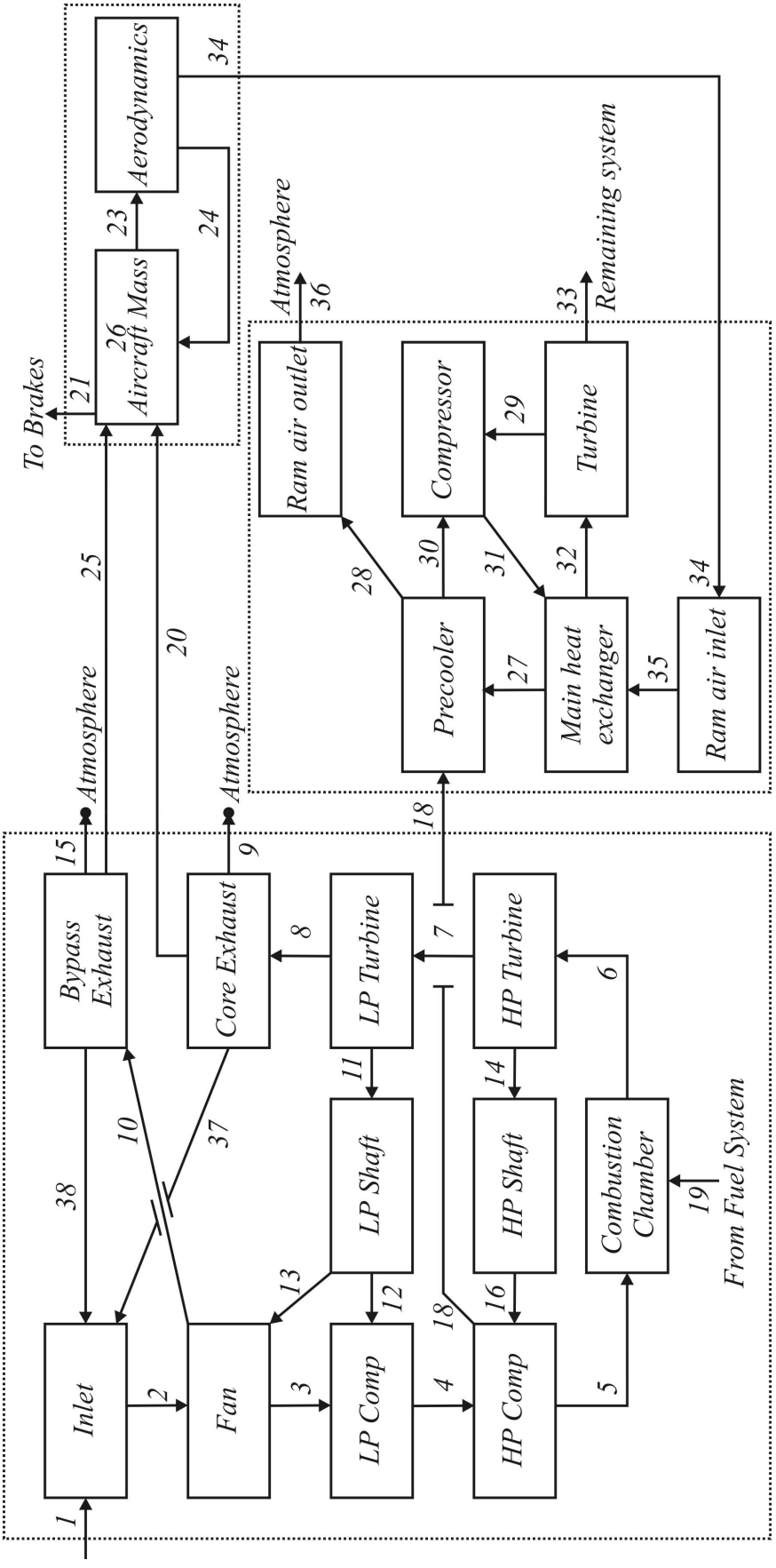

Figure 7.2: Exergy flowchart for engine, mass and aerodynamic subsystems

7.3 Aerodynamics and performance

This study uses a quasi-steady-state aircraft performance model provided by Airbus, which is representative of an A320-sized passenger aircraft. The model itself is a black box system that accepts a file with position, altitude and velocity data points along with basic aircraft parameters (Table 7.1) and calculates realistic acceleration, path, time, fuel consumption and thrust over the mission. As a results of its simplicity, the model is limited to certain trajectory constraints. The aircraft cannot exceed Mach 0.76, cannot accelerate faster than 0.1 m/s^2 and cannot climb at a rate greater than 0.05:1. Take-off and landing phases cannot be represented because of this. The aircraft starts its mission with 13,750 litres (11,041 kg) of fuel and at maximum take-off weight.

7.3.1 Exergy calculations

The aircraft performance model calculates the thrust, altitude and velocity at irregular intervals of approximately 1.2 seconds. The data were interpolated to provide readings at intervals of 0.5 seconds for the entire mission. Because of the slowly varying nature of the flight profile, this is not expected to significantly affect the accuracy of the results. With reference to the data point numbers in Fig. 7.2, the following equations were used to calculate the exergy flows for the aircraft performance, starting with E_{26}, the stock exergy in the mass component:

$$E_{26,KE} = \frac{1}{2} m \mathcal{V}_{gs}^2 \tag{7.1}$$

$$E_{26,PE} = mgz \tag{7.2}$$

$$E_{26} = E_{26,KE} + E_{26,PE} \tag{7.3}$$

where m is the current total mass of the aircraft, which varies with time due to fuel burn, $\mathcal{V}_{gs}$ is the ground speed and z is the altitude above the minimum mission altitude. This is 213.36 m in the case of this mission.

In steady, level flight, the thrust provided by the engines is equal to the drag-based exergy destruction in the engines. No net lift is accounted as being transferred to the mass, despite work being done to counteract gravity. During ascent

Table 7.1: Aircraft design parameters

Area	Parameter	Value	Units
Cabin	Passengers (Econ)	160	pax
Fuselage	Length	39.3	m
	Height	3.88	m
	Width	3.88	m
	Gross wetted area	377.6	m^2
Wing	Reference area	121.04	m^2
	Span	33.01	m
	Mean aerodynamic chord	4.4	m
	Aspect ratio	9	–
	Taper ratio	0.25	–
	Sweep	23.69	°
	Gross wetted area	194.4	m^2
Hor. Tailplane	Reference area	28.4	m^2
	Aspect ratio	5.1	–
	Taper ratio	0.35	–
	Sweep	28.04	°
	Lever arm	17.99	m
	Gross wetted area	50.10	m^2
Ver. Tailplane	Reference area	20.18	m^2
	Aspect ratio	1.7	–
	Taper ratio	0.4	–
	Sweep	34.95	°
	Lever arm	17.03	m
	Gross wetted area	39.55	m^2
Design	Range	5600	km
	Max. Take-off weight	73300	kg
	Operating weight empty	39700	kg

and acceleration, the thrust provided by the engines overcomes the drag and increases the exergy stock in the mass component due to kinetic energy. The wings provide lift, which is also stored in the mass. During descent, in extremis, the engines may produce no thrust. The drag that is overcome in the aerodynamic component is provided by a reduction in potential and kinetic exergy stock in the mass component. The exergy transferred from the mass to the aerodynamic component at any time is therefore:

$$\dot{E}_{23} = (\dot{E}_{20} + \dot{E}_{25}) - \dot{E}_{26,KE} + \frac{1}{2}(\dot{E}_{26,PE} - |\dot{E}_{26,PE}|) \tag{7.4}$$

The exergy converted to lift by the wing and transferred back to the mass is given by

$$\dot{E}_{24} = \frac{1}{2}(\dot{E}_{26,PE} + |\dot{E}_{26,PE}|) \tag{7.5}$$

which is simply the increase in the aircraft's potential exergy. The exergy provided to the ram air for the air conditioning system is calculated as part of the simulation in Section 7.5.

7.4 Propulsion

The engine used in this study is based on the International Aero Engines V2500-A1, which is a two-shaft, high-bypass turbofan commonly used on older A320 aircraft. The essential parameters used are given for reference in Table 7.2.

The engine model was created using GSP [60]. The engine's overall pressure ratio, design thrust and fuel consumption at sea level were made to match the V2500-A1 as closely as possible by altering unknown design parameters, such as the compressor pressure ratios, heat loss and design efficiencies. Areas are estimated from a cross-section drawing of the engine.

To match the engine's performance with that of the aircraft, its fuel input over time was adjusted so that the thrust produced matched that required by the aircraft model. The engine's altitude over time was also set to match that of the aircraft. The comparison of the final values is shown in Fig. 7.3, noting that the engine thrust has been doubled to account for there being two engines, which are assumed to be operating identically.

Table 7.2: Engine design parameters (* denotes values taken from reference [62]. Remaining parameters are estimates.)

	Parameter	Value	Units
Basic Parameters	Sea-level static thrust*	111.2	kN
	SLST specific fuel consumption*	0.0357	kg/N/h
	Bypass ratio*	5.4	–
	Design mass flow	354.3	kg/s
	Overall pressure ratio*	35.8:1	–
Inlet	Area in	1.88	m^2
	Area out	1.79	m^2
Fan	Area out core	0.25	m^2
	Area out duct	1.22	m^2
	Design pressure ratio*	1.6	–
LP compressor	Area out	0.22	m^2
	Design pressure ratio	2.08	–
HP compressor	Area out	0.0375	m^2
	Design pressure ratio	10.75	–
Comb. Chamber	Exit velocity	0.258	Mach
HP Turbine	Area out	0.138	m^2
LP Turbine	Area out	0.437	m^2
Cold exhaust	Throat area	1.91	m^2
Hot exhaust	Throat area	0.64	m^2

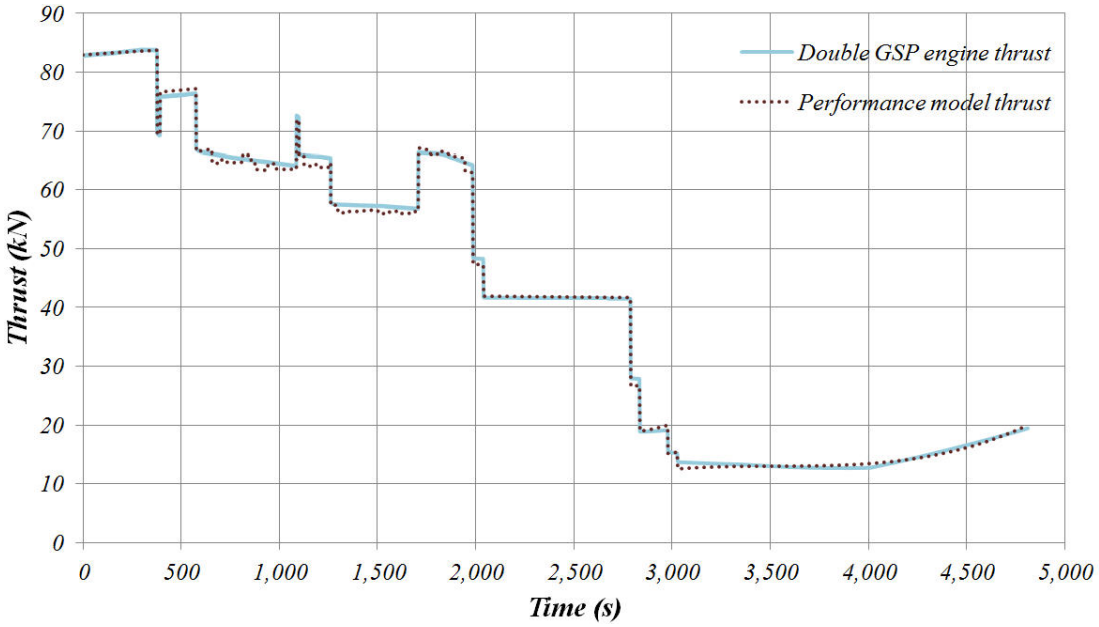

Figure 7.3: Comparison of thrust produced by GSP and performance models

The comparison of the fuel flow calculated over the mission by the GSP and performance models is shown in Fig. 7.4. The fuel input to the engine model differs significantly from that of the performance model. This is most likely due to a combination of a number of parameters and assumptions in the two models. When using two independent models as in this case, such discrepancies are likely to arise to some degree, but effort should be made to minimise them. In this study, the accuracy is not of paramount importance. For the exergy calculations, the fuel flow rate and thrust of the performance model will be used, since this will agree with the rate of change of the aircraft mass and velocity calculated by the same model. The remaining engine model readings will be used to calculate internal exergy values. The effect of this is an increase in the combustion chamber efficiency over what might be expected.

7.4.1 Exergy calculations

Results provided by the engine simulation software are sufficient to calculate the exergy at every point shown in Fig. 7.2. The gas composition after combustion is provided. Fuel chemical exergy and gas flow exergy are assumed to be unaffected by altitude, according to the conclusions reached in Chapter 6. Engine exergy

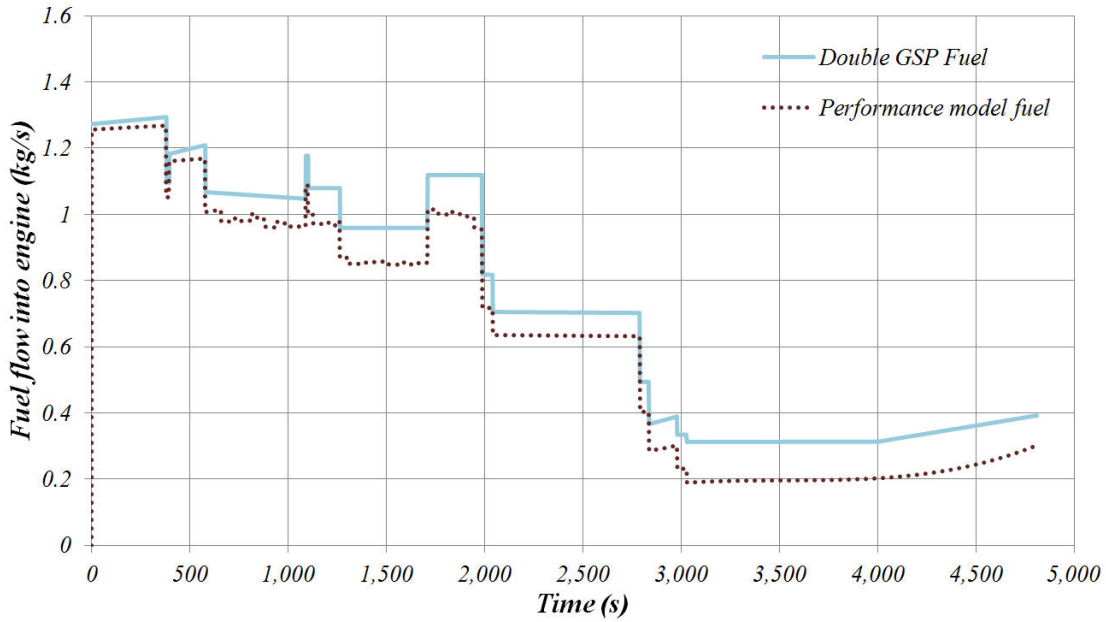

Figure 7.4: Comparison of fuel required by GSP and performance model engines

calculations were performed using the physical and chemical exergy calculators described in Chapter 4. Throughout the mission, simulation results indicated near-complete combustion, so the chemical exergy of the gas flow remained minimal. A fuel exergy of 47,255 kJ/kg, based on the exergy of liquid dodecane at 25°C (Chapter 6) was assumed. Equations (6.5), (6.6) and (6.8) are still applicable for the pre-combustion chamber, post-combustion chamber and chemical exergy flows, but the kinetic energy of the gas flow was included in the physical exergy calculations by using total (stagnation) temperature and pressure values (Subsection 6.2.1).

7.5 Air conditioning system

To provide an example subsystem to include in the aircraft exergy map, a Simulink model was created, based on the layout of the bootstrap air cycle system studied by Pérez-Grande and Leo [38]. The exergy flowchart is given separately in Fig. 7.5. The system conditions hot, pressurised air bled from the engines to provide the cabin with a comfortable atmosphere. For the purpose of this model, the hot

input air flow rate is a constant 0.62 kg/s, with temperature and pressure being determined by the engine model. To cool the air, ram air enters through an inlet on the underside of the aircraft. The cold air passes through the main heat exchanger first, cooling the hot air stream, then passes to the precooler and out of the ram air nozzle. The hot air is first cooled in the precooler and is then recompressed in the compressor component, the compression process also heats the air. The main heat exchanger cools the air further and the air is then allowed to expand through a turbine, which drives the compressor via a directly connected shaft. For this model, the air then exits the analysed system where, in reality, it would be dehumidified and mixed with unconditioned air from the engines to create a temperature that is comfortable for the cabin.

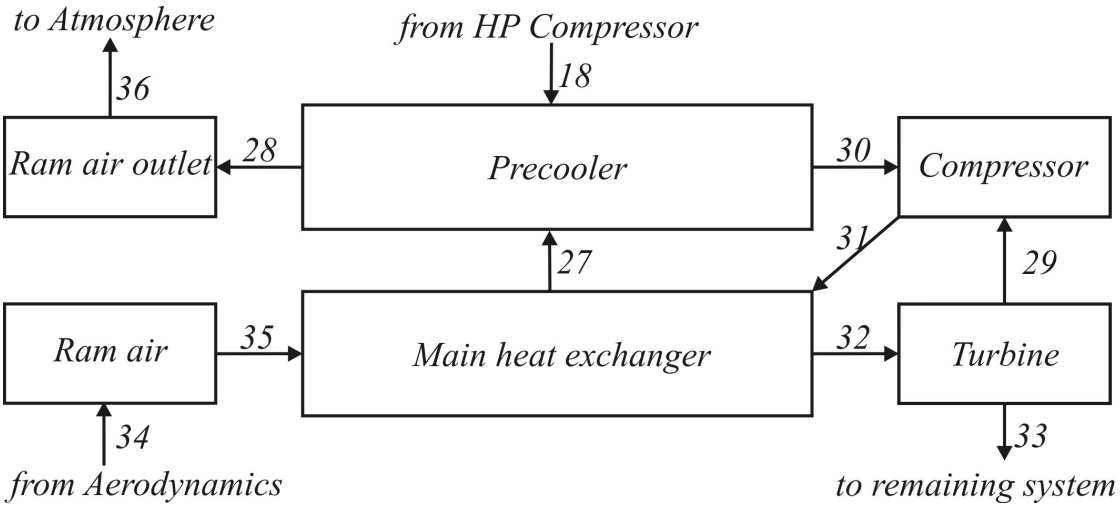

Figure 7.5: Exergy flowchart for environmental control system

7.5.1 Simulation

Heat exchangers The heat exchangers are modelled as air-to-air, flat-plate, cross-flow heat exchangers based on work by Wetter [63]. The model is intended for static behaviour without condensation, but its accuracy will suffice for the current purposes, since variation in the input parameters will be slow in this analysis. For clarification, Fig. 7.6 indicates the subscripts used to identify the flows into and out of the heat exchanger.

The model is initiated with nominal parameters, which are given in Table 7.3.

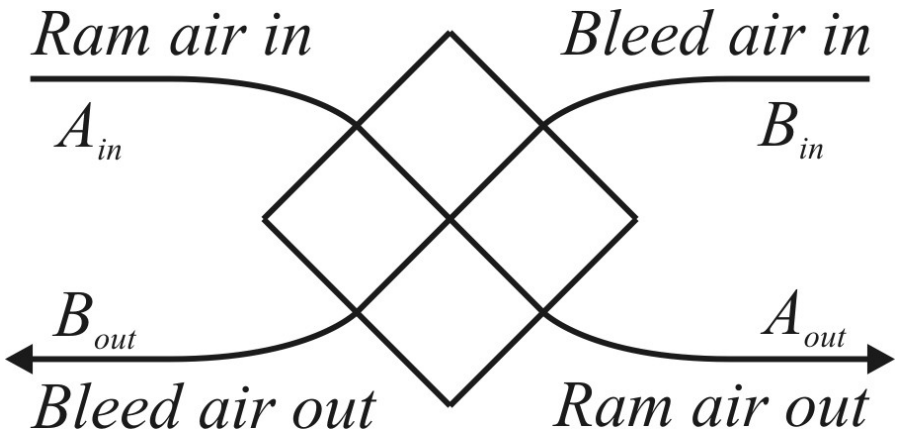

Figure 7.6: Cross-flow heat exchanger stream identification. Adapted from [63]

These were chosen so that the system's response at cruise conditions approximated example pressure and temperature values provided by Airbus for an A340-500 system.

The heat transfer effectiveness, ε, is calculated with

$$\varepsilon = \frac{\dot{C}_A(\vartheta_{A,in} - \vartheta_{A,out})}{\dot{C}_{min}(\vartheta_{A,in} - \vartheta_{B,in})} \tag{7.6}$$

where the $\dot{C}$ variables are the capacity flows given by $\dot{C} = \dot{m}c_p$, and $\dot{C}_{min}$ is the lower of the two streams. The ϑ variables are the nominal input and output temperatures in degrees Celsius. The number of exchanger heat transfer units, NTU, is a dimensionless value calculated with

$$1 - \exp\left(\frac{e^{-NTU^{0.78}Z} - 1}{Z\, NTU^{-0.22}}\right) - \varepsilon = 0 \tag{7.7}$$

which was solved using bisection. Here, Z is the capacity rate ratio $\dot{C}_{min}/\dot{C}_{max}$. Using this, the product of the heat transfer area A and the overall coefficient of heat transfer U_{avg} for the nominal conditions can be found using

$$(U_{avg}A)^N = NTU^N \dot{C}_{min,0} \tag{7.8}$$

While running the model, the following equations are solved continuously to provide the output temperatures given input temperatures that vary from the nominal values

$$(U_{avg}A) = \frac{(U_{avg}A)^N(1+r)}{\left(\left[\frac{(\dot{m}T)^N_{A,in}}{(\dot{m}T)_{A,in}}\right]^{0.78} + r\left[\frac{(\dot{m}T)^N_{B,in}}{(\dot{m}T)_{B,in}}\right]^{0.78}\right)} \tag{7.9}$$

Table 7.3: Heat exchanger model parameters

	Parameter	Value	Units
Precooler	$T^N_{A,in}$	473	K
	$T^N_{A,out}$	403	K
	$T^N_{B,in}$	246	K
	$\dot{m}^N_A$	0.52	kg/s
	$\dot{m}^N_B$	0.62	kg/s
	$(U_{avg}A)^N$	236	n/a
	Pressure ratio A	0.95	-
	Pressure ratio B	1.1	-
Main heat exchanger	$T^N_{A,in}$	453	K
	$T^N_{A,out}$	343	K
	$T^N_{B,in}$	251	K
	$\dot{m}^N_A$	0.52	kg/s
	$\dot{m}^N_B$	0.66	kg/s
	$(U_{avg}A)^N$	624	n/a
	Pressure ratio A	0.89	-
	Pressure ratio B	1.1	-
Compressor	Isentropic efficiency, η_c	0.75	-
	Pressure ratio	1.4	-
Turbine	Isentropic efficiency, η_t	0.8	-
Ram air inlet	Isentropic efficiency, η_d	0.9	-
Ram air outlet	Isentropic efficiency, η_n	0.95	-

where

$$r = \left(\frac{(\dot{m}T)_A^N}{(\dot{m}T)_B^N} \right)^{0.78}. \tag{7.10}$$

Then, the NTU can be found with

$$NTU = \frac{U_{avg} A}{\dot{C}_{min}} \tag{7.11}$$

and the current effectiveness with

$$\varepsilon = 1 - \exp\left(\frac{e^{-NTUZ\eta} - 1}{Z\eta} \right) \tag{7.12}$$

where $\eta = NTU^{-0.22}$. The outlet temperature in Celsius of flow A, $\vartheta_{A,out}$, is then given by

$$\vartheta_{A,out} = \vartheta_{A,in} + \varepsilon \frac{\dot{C}_{min}}{\dot{C}_1} (\vartheta_{B,in} - \vartheta_{A,in}) \tag{7.13}$$

The heat transfer rate, $\dot{Q}$ is then

$$\dot{Q} = \dot{C}_1 (\vartheta_{A,out} - \vartheta_{A,in}) \tag{7.14}$$

and the outlet temperature of flow B is

$$\vartheta_{B,out} = \vartheta_{B,in} - \frac{\dot{Q}}{\dot{C}_2} \tag{7.15}$$

Compressor and Turbine The temperatures and pressures at inlets and outlets are related through the adiabatic efficiency of the compressor,

$$\eta_c = \frac{(P_{31}/P_{30})^{(\gamma-1)/\gamma} - 1}{(T_{31}/T_{30}) - 1} \tag{7.16}$$

and the turbine,

$$\eta_t = \frac{1 - (T_{33}/T_{32})}{1 - (P_{33}/P_{32})^{(\gamma-1)/\gamma}} \tag{7.17}$$

where γ is the specific heat capacity ratio, $\gamma = c_P/c_V$. The compressor and turbine equations are coupled according to

$$T_{32} - T_{33} = T_{31} - T_{30} \tag{7.18}$$

Ram air inlet The ram air inlet mass flow rate is calculated using

$$\dot{m}_{34} = \rho \mathrm{V} A_i = \frac{p_a}{RT_a} M \sqrt{\gamma R_a T_a} A_i \tag{7.19}$$

where A_i is the cross-sectional area of the inlet. Stagnation temperature, $T_{s,34}$, and pressure, $p_{s,34}$ at the ram air inlet are calculated with

$$T_{s,34} = T_a \left(1 + \frac{\gamma - 1}{\gamma} M^2\right) \tag{7.20}$$

$$p_{s,34} = p_a \left(1 + \frac{\gamma - 1}{\gamma} M^2\right)^{\gamma/(\gamma-1)} \tag{7.21}$$

where the exergy gained due to the velocity of the air is taken as originating from the aircraft aerodynamic component. The diffuser is assumed to decelerate the flow in such a way that $T_{s,34} = T_{35}$ and kinetic energy is otherwise neglected in the analysis. The pressure after the diffuser can then be calculated via its isentropic efficiency, η_d:

$$p_{35} = p_a \left(\eta_d \left(\frac{T_{s,34}}{T_a} - 1\right) + 1\right)^{\gamma/(\gamma-1)} \tag{7.22}$$

Ram air outlet nozzle Given a low Mach number at the nozzle entrance (point 28), the nozzle's isentropic efficiency, η_n can written as

$$\eta_n = \frac{1 - (T_{28}/T_{36})}{1 - (p_a/p_{28})^{(\gamma-1/\gamma)}} \tag{7.23}$$

where $p_{36} = p_a$. The various efficiencies and variables used in the model are given in Table 7.3. The Simulink model is depicted in Fig. 7.7, with the components described above included in the respective subsystems. Initial conditions and transfer functions are present to permit the simulation to start.

7.5.2 Exergy calculations

The inlet air conditions are derived from the aircraft's current Mach number and the standard atmosphere conditions at the current altitude. A constant flow of 0.62 kg/s bleed air is taken from the engine's high pressure compressor. The temperature and pressure of this air varies depending on atmospheric conditions and is calculated as part of the GSP simulation. Exergy is calculated for all points using

$$\dot{E}^{ph} = \dot{m} \left(h_{air} - h_{air,0} - T_0(s_{air} - s_{air,0})\right) \tag{7.24}$$

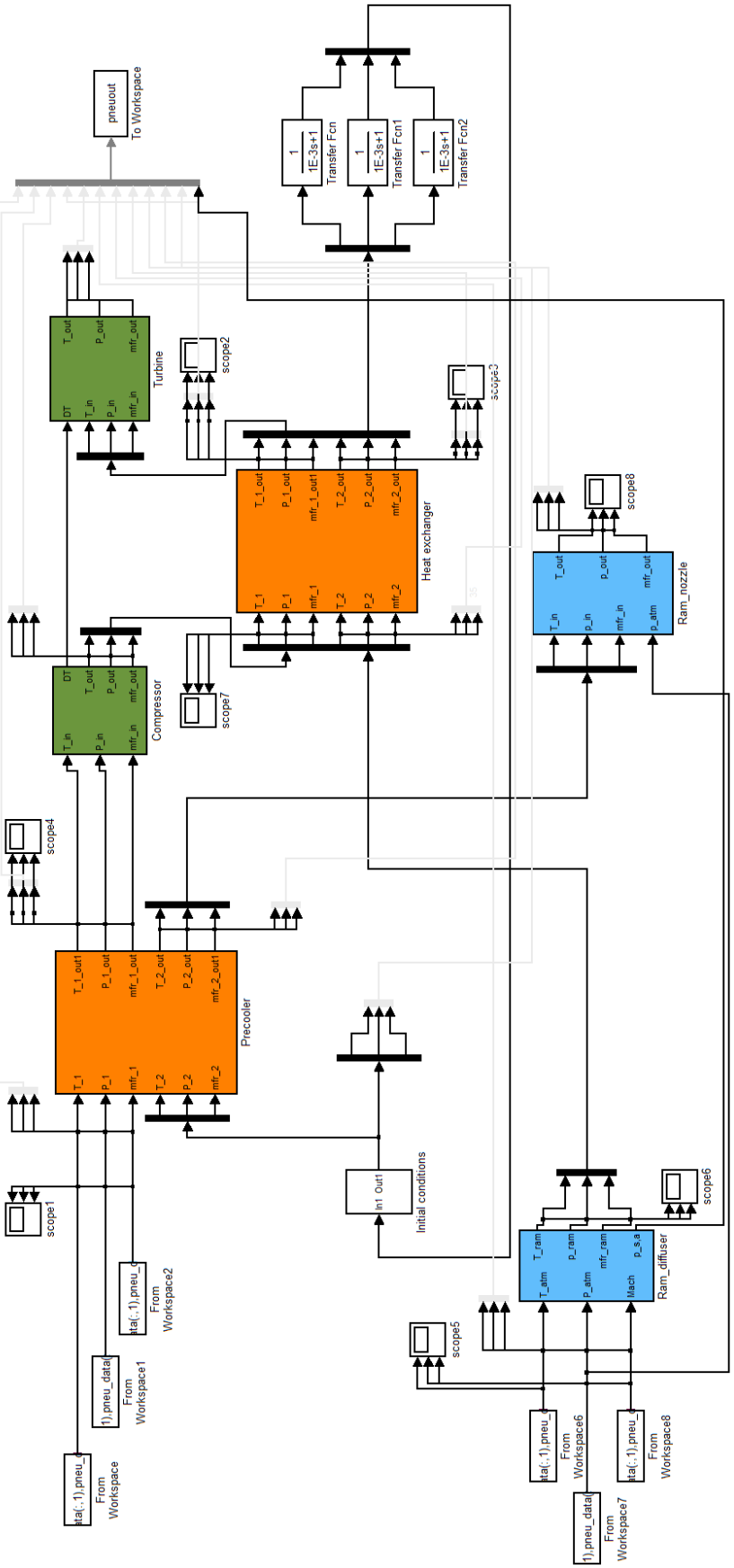

Figure 7.7: Simulink model of air conditioning system

with kinetic and gravitational potential components being neglected. Exergy was calculated at each point assuming dry air throughout. In a more precise analysis of a real system, the separate exergies of gaseous and liquid water due to condensation may be worth taking into account, especially for flight phases near the ground, where the specific humidity will be higher.

7.6 Results

Figure 7.8 shows a Grassmann diagram of the two engines and airframe for the entire mission. This was produced with the Grassmann diagram generation tool (Chapter 4) and edited for detail (label positioning, minor corrections) using vector graphics software. The air conditioning system is not represented in the diagram because, by comparison, the arrow widths for the system are negligible. The largest destruction of exergy occurs in the two combustion chambers and, due to drag, in the aerodynamic component. The exhaust gas leaving the core exhaust components has substantial exergy which is displayed as a system output, but can be considered destroyed. The exergy input at the engine inlet components is due to the incoming air's kinetic energy. This is shown as originating from the exhaust components, named 'Ram Thrust', to show the portion of the gross thrust that is not provided to the mass for acceleration. Table 7.4 gives numerical results of the entire system analysis for the whole flight. A small exergy generation across the aircraft mass component, which is not meant to display any net gain or loss of exergy, is indicative of a small cumulative error when performing numerical integration during exergy storage calculations. It is likely that this would be reduced to zero with a higher frequency of time steps in the analysis.

Figure 7.9 shows the exergy flow through the air conditioning system over the entire mission. The air at the Ram Air Inlet component has exergy supplied by the aircraft Aerodynamics component, while the input at the precooler originates from the engine's high pressure compressor. The greatest destruction of exergy occurs in the heat exchanger and through the release of compressed, heated air back to the atmosphere. The precooler, compressor and turbine also contribute significantly to the exergy destruction. The loop from the heat exchanger to the

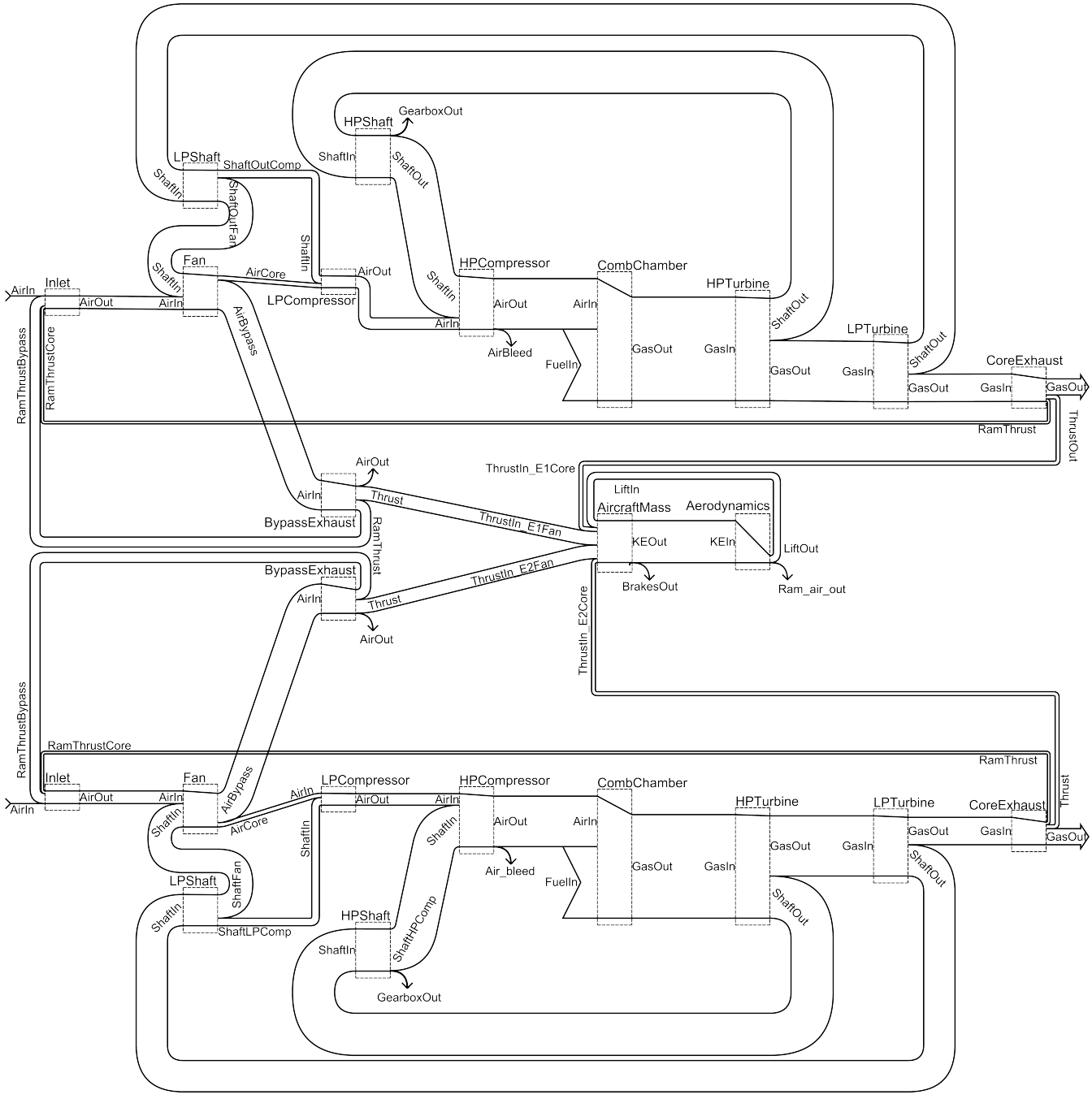

Figure 7.8: Grassmann diagram of engines and airframe for entire mission. Enlarged version provided in Appendix B Fig. B.1.

Table 7.4: Aircraft exergy flows

Subsystem	Component	Exergy in (MJ)	Exergy out (MJ)	Exergy des. (MJ)
Engine	Inlet	13,017	13,017	0
	Fan	37,287	34,844	2,443
	LP Compressor	12,237	11,919	318
	HP Compressor	55,140	52,582	2,558
	Comb. Chamber	126,475	107,257	19,218
	HP Turbine	107,257	106,040	1,217
	LP Turbine	62,381	60,872	1,509
	Core Exhaust	28,460	24,812	3,648
	Bypass Exhaust	30,416	26,035	4,381
	LP Shaft	32,412	32,078	334
	HP Shaft	43,658	43,637	21
Airframe	Aircraft Mass	43,379	43,612	-233
	Aerodynamics	43,612	7,293	36,319
Air Conditioning	Precooler	355	329	26
	Compressor	394	371	23
	Main Heat Exch.	467	408	59
	Turbine	337	314	23
	Ram air inlet	105	96	9
	Ram air outlet	71	27	44

precooler represents the cooling ram air flow. The other loop from the turbine to compressor represents the shaft work. Figures 7.10 - 7.12 show the air conditioning system over three short phases to scale, noting that they are not to scale with Fig. 7.9.

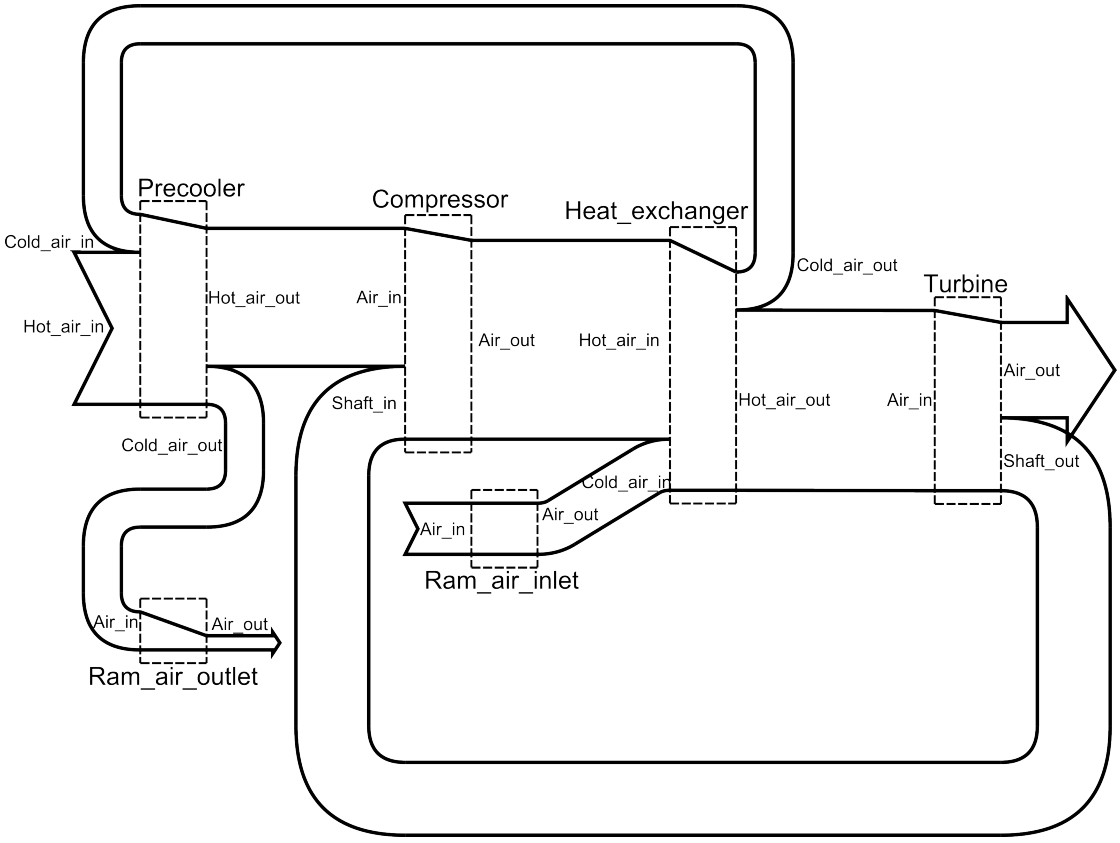

Figure 7.9: Grassmann for air conditioning system over whole mission

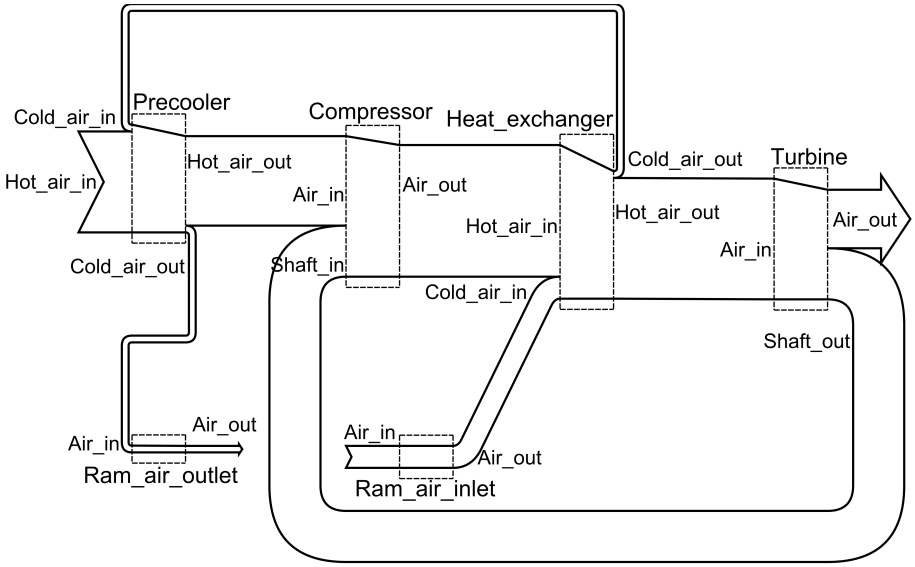

Figure 7.10: Grassmann for air conditioning system over 0-200 seconds

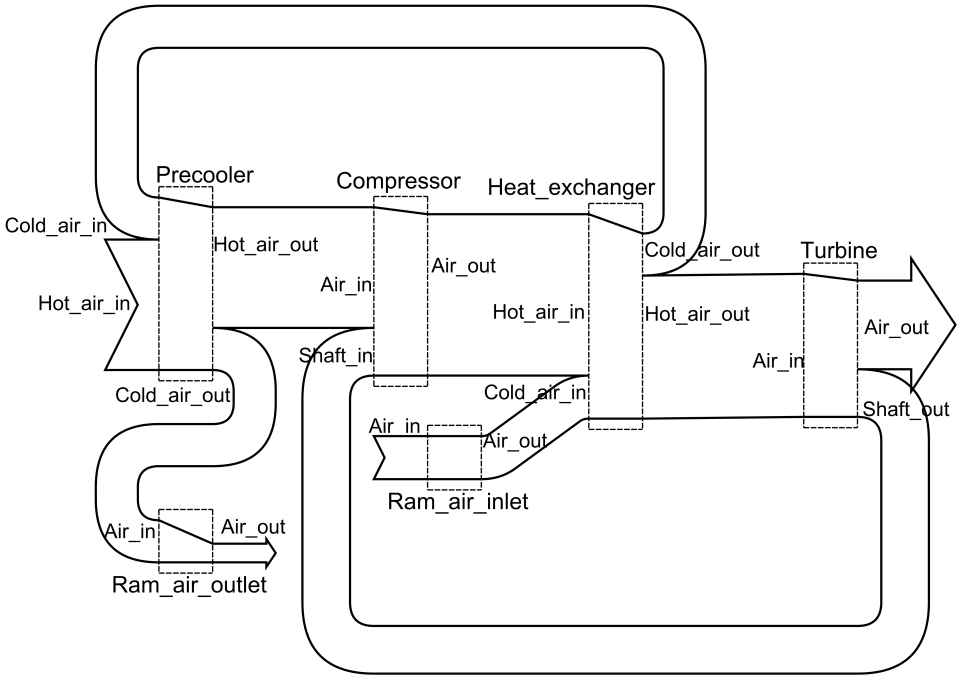

Figure 7.11: Grassmann for air conditioning system over 2,200-2,400 seconds

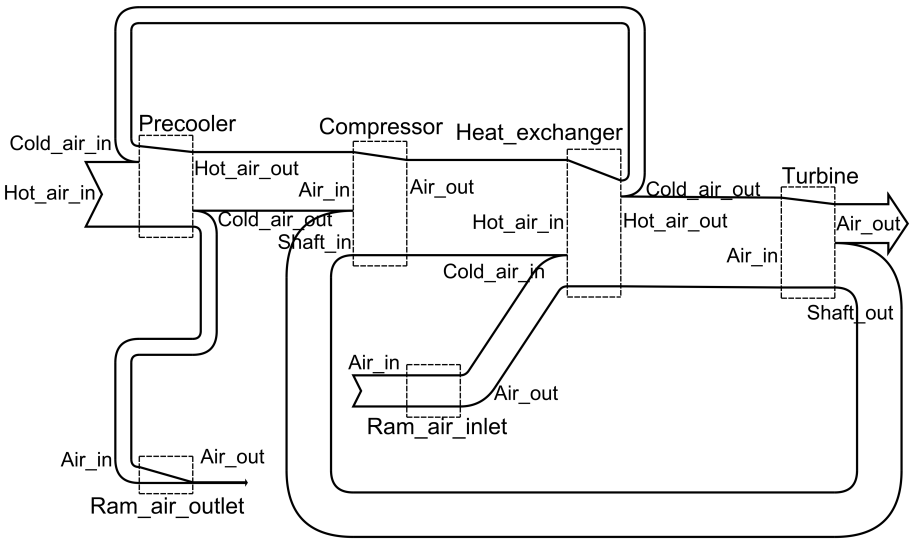

Figure 7.12: Grassmann for air conditioning system over 3,500-3,700 seconds

7.7 Discussion

7.7.1 Airframe and engines

The exergy analysis results for the engines and airframe are illustrated clearly by the Grassmann diagram (Fig. 7.8). The diagram, coupled with the basic numerical results in Table 7.4 allows the general pattern of exergy flow through these most exergy hungry systems to be understood and compared easily. The use of Grassmann diagrams reaches its limits when applied to systems that vary in flow exergy by orders of magnitude. Including the pneumatic system on the same figure as the engines and airframe, for example, would show only 1-dimensional lines. The same would be true of other proportional charts, such as bar charts, pie charts, etc. From numerical results, it can be seen that the exergy destroyed in the low pressure compressor is similar to the exergy bled from the engine for the purpose of air conditioning (Precooler input). Calculation or modelling uncertainty in the engines or aircraft performance may lead to errors larger than the total exergy flows through some subsystems. An example of this is seen in this case in the aircraft mass component, over which some exergy appears to be generated. It is clear that any improvements in efficiency in the engines, especially in the process of converting the chemical exergy of the fuel or making use of the core exhaust gas exergy, is likely to have a large effect on system efficiency. As future design improvements become ever more expensive and incremental in turbofan engines it may, however, be the case that improvements in subsystem efficiency will be more cost effective. A clear method of comparison using the exergy metric may be essential to future design decisions.

7.7.2 Air conditioning system

An aspect of the air conditioning system exergy results that must be considered is that the required outcome of the system is not mechanical work, but conditioned air, so the exergy output of the system can seem an abstract concept. Exergy is added to the system via hot, pressurised bleed air and ram compression. Air that is comfortable for passengers must carry exergy by virtue of being out of equilibrium with the atmosphere outside the aircraft. It must be noted that regardless of the

system providing it, the air output will always have the same exergy. The system's effectiveness must be judged by the exergy required at input to achieve the same output. The magnitude of exergy within the system at each point remains relevant from a broader perspective, showing the availability present in the flows that might be used for other purposes. The variation of this depending on altitude can be seen from the differences between Figs 7.10 - 7.12. The comparison between the three phases of operation allows for a number of qualitative observations that improve understanding of this particular system (although the simplifications involved in creating the model may limit the usefulness of the results in general). Ram air input is highest during cruise (Fig. 7.11), which is due to higher aircraft velocity and hence, higher air kinetic exergy. During the same phase, the hot air input has more exergy even though the input temperature and pressure are lower than during the other phases. This is because of an even larger reduction in reference state conditions. The higher exergy input is indicative of the higher cost associated with providing the air flow. In reality, the bleed location in the engine would vary, so this observation may not hold true for all such systems.

7.8 Conclusions

An aircraft performance model, bypass engine model and air conditioning system model have been set up and created to provide exergy data over a single, representative flight. The aircraft being mapped is similar in size and performance of an Airbus A320 with IAG-V2500 engines. The air conditioning system examined is based on a simple bootstrap air cycle machine with two cross-flow heat exchangers. The primary aim of the study was to create an example of a larger exergy map, more representative of a system the methodology is intended for. Since an exergy map of a full aircraft in all its system detail would be a prohibitively large task in the context of this project, a pneumatic system was chosen as a representative subsystem, in addition to the essential engine and flight performance/aerodynamic systems. The aircraft performance and engine models were created using 3rd party software, but the air conditioning system models used are described in detail.

The methodology and software tool as described in the previous chapters were

effective for the purposes of the analysis. The exergy results produced are informative and provide clarity of the relative sizes of energy flows through the modelled systems. The system map layout that has been established for the engine and aircraft flight systems can be re-used in future analyses involving similar engines and is logically sound. Exergy calculation equations given for the aircraft performance aspects of flight are also generally applicable.

It becomes clear from the error in the mass component accounting that model and calculation accuracy will need to be high for the engine and performance calculations to be reliably comparable to the lower exergy subsystems. An understanding of the uncertainty in results would help lend weight to any conclusions drawn.

Final consideration in this type of analysis must include the effects of the system's mass on the exergy consumption, without which it cannot be considered complete. Further use of the exergy map data is discussed in the next chapter.

Chapter 8

Further exergy map analysis

The work presented so far in this thesis has concentrated on the mapping of the physical location of exergy flows through an aircraft over a mission. The results of this, exemplified in Chapter 7, provide a clear basis for the understanding and comparison of those flows. In a stationary system, the results may provide sufficient new insight. However, an aircraft's complexity leads to the need for an additional consideration, namely the influence of mass on the system's exergy destruction. This is mainly due to the lift-induced drag, observed in the aerodynamic component, which is a function of the aircraft's mass. Each component's mass must be considered a destroyer of exergy. This topic was first raised by Paulus and Gaggioli [25, 26] and must be taken into account to gain a full appreciation of the exergy use of an aircraft. No object aboard an aircraft can be considered exergetically passive for this reason and the lift-induced drag must be assigned fairly to reflect this. It is arguable, once mass-related destruction is included, that the causes of exergy destruction for an entire aircraft can be pinpointed. Since there is only one significant source of exergy aboard the aircraft, all destruction can be directly converted to fuel costs. This process is discussed using the case study aircraft described in Chapter 7 as an example.

Finally, an additional step is taken to compare the exergy map of the mission from the previous chapter with an exergy map of a modified mission in order to allow discussion of the use of exergy maps in the aircraft design process.

8.1 Assignation due to mass

8.1.1 Component masses

For the purpose of this study, the mass breakdown of the aircraft under analysis was provided by Airbus, and is given in Table 8.1. Individual component masses from the subsystems in question are given in Table 8.2. Payload mass is based on a mean of 75 kg plus 18 kg baggage per passenger in accordance with Torenbeek [64]. The pneumatic system mass is also estimated using Torenbeek:

$$M_{acs} = 14.0 l_{pax}^{1.28} \tag{8.1}$$

where l_{pax} is the length of the passenger cabin, which is taken as $l_{pax} = 25.51$ m. Equation (8.1) gives $M_{acs} = 975$ kg, which is taken as an acceptable estimate for the air conditioning and anti-ice systems. The air conditioning alone typically makes up around 13% of the aircraft internal systems mass [65], which leads to an estimate of 552 kg for the entire air conditioning system. Assuming the duplicated system being analysed makes up around two thirds of that mass, with the remainder covering the dehumidifiers and mixer units, the the collection of components shown in Fig. 7.5 will add up to around 184 kg. The assumed subdivision between components is given in Table 8.2, which add up to the total of that mass. These are intended as examples in order to be able to discuss the allocation and are only required to be reasonable estimates for the purposes of this work. Masses for the engine components given are based purely on estimates.

8.1.2 Exergy of lift method

Paulus and Gaggioli [25, 26] present a proposal for the exergy required to maintain a component's mass at altitude, $\dot{E}_c^{LI}$, which is given by

$$\dot{E}_c^{LI} = m_c g \left(V_y + \frac{2 m_a g}{\pi a \rho S_w V_\infty} \right) \tag{8.2}$$

where m_c is the component mass, V_y is the vertical velocity of the aircraft, a is the wing aspect ratio, S_w the wing area and V_∞ the free-stream velocity. The second group of terms represent the 'dead-state velocity,' at which the aircraft would descend given an elliptical wing planform, leading to minimum induced drag, and

Table 8.1: Airframe and payload masses

Subject	Component	Mass (kg)
Airframe	Wing	7,768
	Fuselage	9,001
	Horizontal Tailplane	629
	Vertical Tailplane	588
	Landing Gear	2,751
	Pylons	836
	Engines	6,076
	Systems	4,251
	Furnishings	3,174
	Operational Items	4,622
Fuel	Starting fuel	18,282
Payload	Passengers	12,000
	Luggage	2,880
	Crew	450
Total	Take-off weight	73,308

Table 8.2: Component masses

System	Component	Mass (kg)
Engines	Inlet	62
	Fan	308
	LP Compressor	411
	HP Compressor	718
	Comb. Chamber	308
	HP Turbine	205
	LP Turbine	411
	HP Shaft	103
	LP Shaft	205
	Core Exhaust	205
	Bypass Exhaust	103
Air Conditioning	Ram Air Inlet	12
	Ram Air Outlet	12
	Precooler	65
	Main Heat Exchanger	75
	Compressor	10
	Turbine	10

no parasitic drag mechanisms and no thrust input. Essentially, the authors assert that the vertical velocity of the aircraft should not be calculated from a fixed position, but rather the descent velocity of a 'perfect' wing. This has the effect of increasing the supposed power required to hold a mass aloft.

In the context of the exergy mapping method established thus far, this technique cannot be applied directly, because it relies on the analysis of instantaneous mission segments in steady flight, assuming steady state operation. The exergy provided to the aircraft mass is considered destroyed, even though, over the whole flight, a significant portion will be released again during descent. Since the exergy map method already accounts for lift as as increase in stored exergy in the mass, this topic must be approached differently.

8.1.3 Lift-induced drag assignation

Lift-induced drag is unavoidably created when generating lift. In steady, level flight, the power required to overcome this force is the cost of keeping the aircraft vertically out of equilibrium with the environment. The total induced drag coefficient of an aircraft can be estimated with

$$C_{D_I} = \frac{C_L^2}{\pi \epsilon a} \tag{8.3}$$

where ϵ is the span efficiency factor, which is unity for elliptical wings and is otherwise given by

$$\epsilon = \frac{1}{1+\delta} \tag{8.4}$$

where δ is a function of aspect and taper ratios. In the case of the aircraft in question, it has been found to be $\delta = 0.013$. Also,

$$C_L = \frac{L}{\frac{1}{2}\rho V_\infty^2 S_w} \tag{8.5}$$

where L is the lift force being exerted by the wing, which is equal to the aircraft weight during level flight. Clearly, the induced drag of the aircraft is a strong function of the mass of the aircraft, but is also dependent on the design of the wing. In order to reduce induced drag, it is common design practice to maximise the wing's aspect ratio within structural constraints. The divergence of the wing

design from an elliptical planform also has an effect on the induced drag through the efficiency ratio.

The interpretation of whether the design of the wing should bear some 'responsibility' for the lift-induced drag it generates is a matter of perspective. For example, if the design of the wing has not yet been fixed, a comparison between wings of different aspect ratios will need to differentiate between the destruction due to mass and destruction due to wing design. For an exergy map of an existing aircraft, it is simpler and more pertinent to consider all induced drag to be caused by the aircraft's mass and distributed proportionally.

The lift-induced drag coefficient is related to the drag force, D_I, via

$$C_{D_I} = \frac{D_I}{\frac{1}{2}\rho V_\infty^2 S_w} \tag{8.6}$$

where ρ is the air density, V_∞ is the free stream velocity and S_w is the wing planform area. Equations (8.3) and (8.6) can be combined and rearranged to give

$$D_I = \frac{\frac{1}{2}\rho V_\infty^2 S_w C_L^2}{\pi e a} \tag{8.7}$$

giving the rate of exergy destroyed to overcome induced drag, $\dot{E}_I$ as a function of the lift coefficient as

$$\dot{E}_I = \frac{\frac{1}{2}\rho V_\infty^3 S_w C_L^2}{\pi \epsilon a}. \tag{8.8}$$

Since the current lift coefficient is a typical output of aircraft performance models, including the one used to produce the case study being considered, no further manipulation is required. The rate of exergy destroyed by each component is given simply as

$$\dot{E}_{I,c} = \frac{m_c}{m_{ac}} \dot{E}_I. \tag{8.9}$$

This equation neglects the effect of changes in parasite and wave drag due to variation in lift coefficient. If coefficients for these are known, they can be included as required, which would increase the drag attributed to the mass a little (although the latter only for supersonic flight).

8.1.4 Application to aircraft components

Equation (8.9) is first applied to the various major aircraft components of the case study according to the masses given in Table 8.1. Figure 8.1 shows the breakdown

of the lift-induced exergy destruction over the course of the mission. Although the total mass of the aircraft reduces by around 3,000 kg over the course of the flight due to fuel burn, other factors have a far larger effect on the induced drag. During climb, lift can be lower than in cruise because thrust is angled downward. The increase in lift toward the end of the mission is due to the slow airspeed (see Fig. 7.1).

A variation on a Grassmann diagram for the aerodynamic component is given in Fig. 8.2. This illustrates the exergy flow through the component over the entire flight, with the total exergy flow as lift being compared to the destruction due to parasitic drag and induced drag. The contributions of the various major aircraft components to the induced drag are shown as bars without arrowheads, indicating that the exergy does not physically leave the component.

8.1.5 Application to air conditioning system

Using the estimated component masses given in Table 8.2, the air conditioning components are attributed the exergy destruction due to induced drag and compared with their direct exergy destruction. The entire system, based on the total direct exergy destruction and total mass of 276 kg, including passive components, is also included. Figure 8.3 shows this comparison. Note that the ram air inlet component is mapped as isentropic in this analysis for the same reason as the engine inlets. Only the exergy transferred to the intake air is accounted as being transferred from the aircraft aerodynamic component, while the rest is accounted as drag and is not attributed to the inlet component. This could be rectified with more precise calculations. Additionally, the parasite drag associated with the inlet and outlet could be attributed to those components.

The contribution of the components' masses to their total exergy destruction when calculated in this way is small. This is exaggerated by the lack of a take-off and landing phase in the analysed mission, during which the lift produced would be very high. The lift-induced drag is also not the only means by which additional mass increases exergy destruction during a flight. Given a fixed aircraft design and varying payload, a number of small differences to the mission profile may contribute to a higher total fuel burn as well as the need to carry more fuel, which

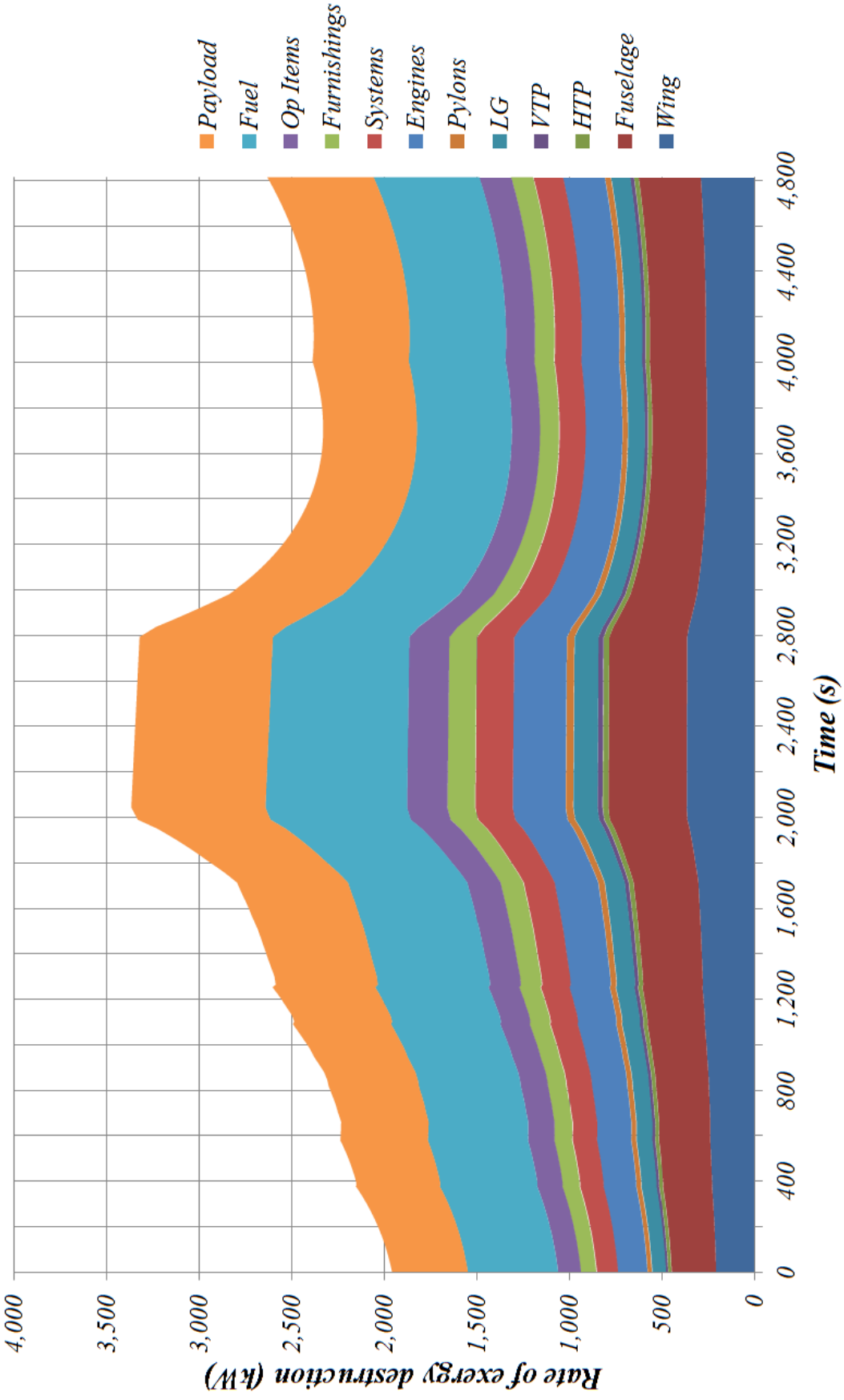

Figure 8.1: Exergy destruction rate due to mass per major component

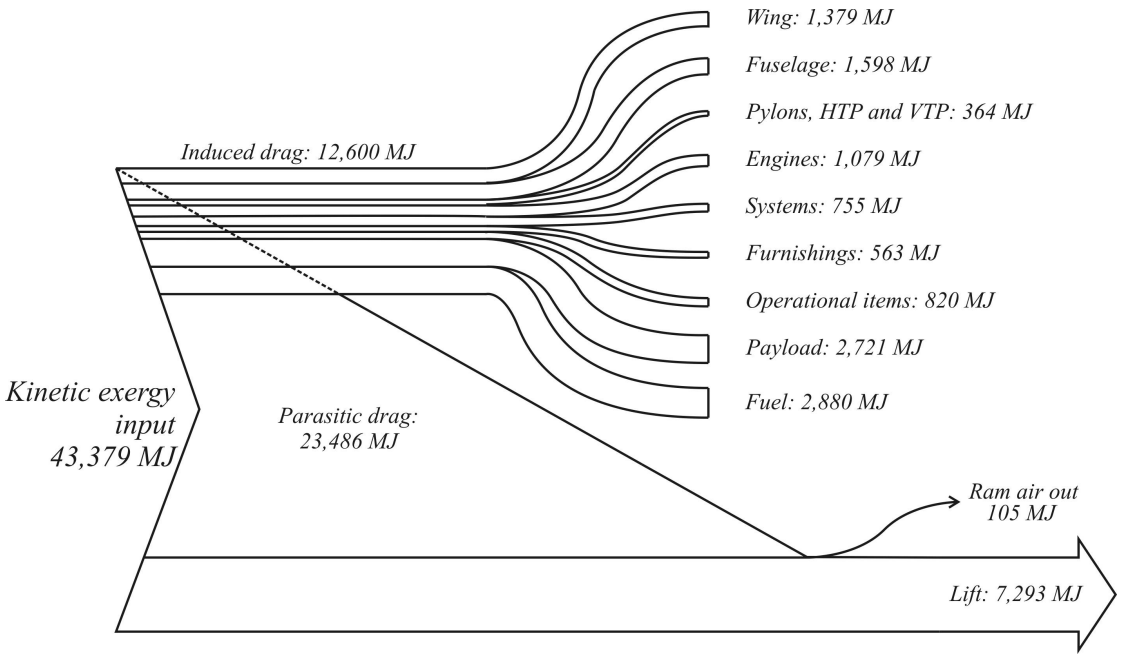

Figure 8.2: Aerodynamic component Grassmann diagram

adds further mass. Even more importantly, during preliminary design, an increased component mass given a fixed payload requirement can have a 'snowball' effect on the design's mass due to requirements for larger wings, more powerful engines and the stronger structures associated with carrying them. When considering a fixed aircraft design, however, induced drag allocation as presented here is the only straightforward method of assigning 'blame' for fuel burn to mass. The limitations of this approach must be borne in mind when drawing conclusions on the validity of reducing mass to improve aircraft efficiency. As part of a system analysis, the method is, however, valid.

8.1.6 Whole system comparison

Since Grassmann diagrams are unsuited to displaying data that differs in orders of magnitude, as the results for the engine and air conditioning system do, a logarithmic bar chart can be used to visualise the essential results. This allows the magnitudes of the exergy in and out flows to be placed on the same chart as the direct and mass-related destruction values. This can be consulted alongside results tables to assist interpretation. Figure 8.4 shows the results for the aircraft case study in such a chart.

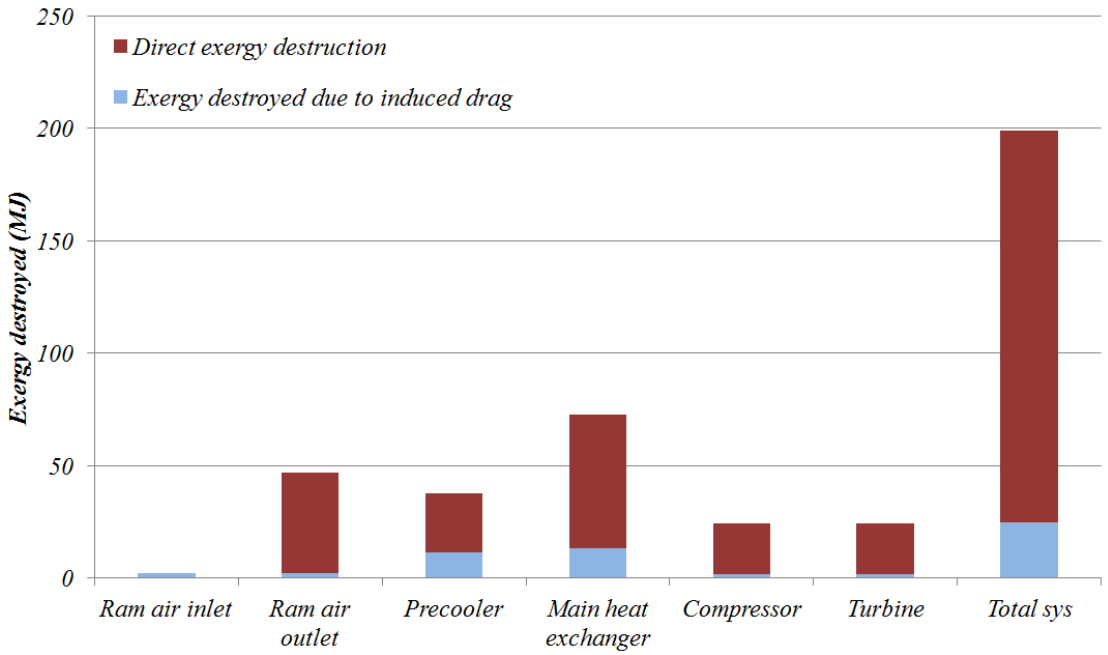

Figure 8.3: Air conditioning component exergy destruction

8.1.7 Other drag attribution

Further attribution of drag-related exergy destruction could take place by dividing the skin friction and form drag components proportionally to the wetted area of the aircraft. This would give an indication of the exergy costs of exterior components and may be of most interest with regard to protuberances such as pitot tubes, which could be attributed a cost. Similarly, the additional drag caused by the deflection of a flight control surface could be attributed to the hydraulic system and added to the exergy destroyed directly by the actuation, leading the way to assigning an exergy cost due to a flight manoeuvre. The basics of this topic were broached by Roth [32], but in the context of this work is left for future investigation.

8.2 Fuel and carbon costs

With a properly attributed exergy map, it is a small step to begin equating exergy destruction with fuel costs or even equivalent carbon dioxide emissions. The previously established value of the chemical exergy of jet fuel surrogate dodecane ($C_{12}H_{26}$) was 46,926 kJ/kg (Chapter 6). Knowing the atomic weight of Carbon

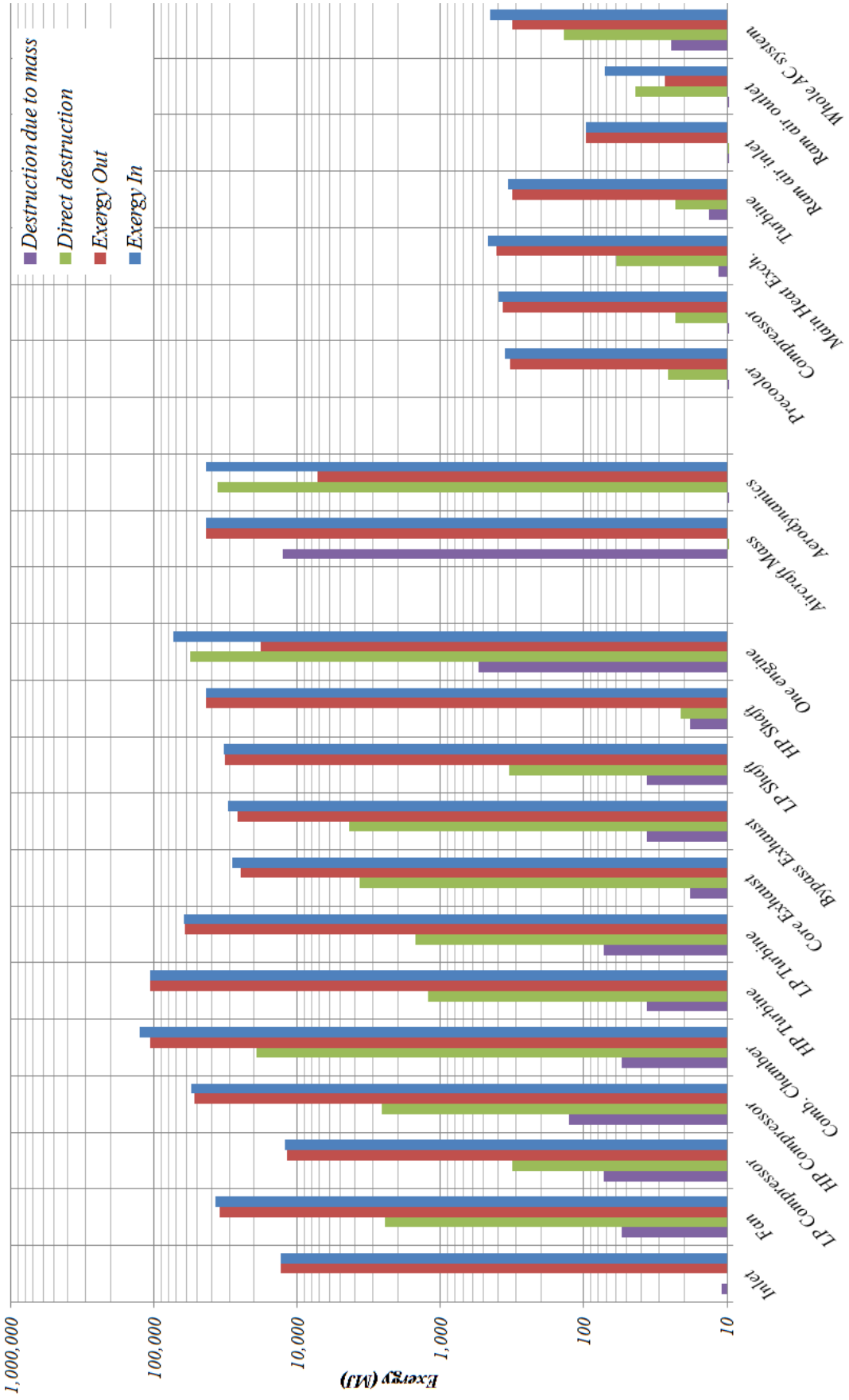

Figure 8.4: Exergy in- and outputs, direct and induced destructions of all system components

(12), Hydrogen (1) and Oxygen (16), 1 kg jet fuel can be estimated to contain 0.847 kg of carbon, which leads to emissions of 3.106 kg CO_2 per kg fuel burn or 0.0185 kg CO_2 per MJ fuel exergy.

An example fuel price of 2.88 \$/USgal is taken (based on International Air Transport Association data on the 5th April 2013 [66]). Assuming a constant density of 780.8 kg/m^3 (again, based on pure dodecane), this converts to a cost of 0.975 \$/kg fuel or 0.0208 \$/MJ exergy.

Table 8.3: Engine exergy destruction, costs and CO_2 produced

Component	Direct (MJ)	Induced (MJ)	Total (MJ)	Cost (US\$)	CO_2 (kg)
Inlet	0	11	11	0.23	0.2
Fan	2,443	55	2,498	51.95	46.21
LP Compressor	318	73	391	8.131	7.23
HP Compressor	2,558	128	2,686	55.86	49.68
Comb. Chamber	19,218	55	19,273	400.87	356.54
HP Turbine	1,217	36	1,253	26.07	23.19
LP Turbine	1,509	73	1,582	32.90	29.27
Core Exhaust	3,648	18	3,684	76.64	68.16
Bypass Exhaust	4,381	36	4,339	91.50	81.39
LP Shaft	334	36	370	7.71	6.85
HP Shaft	21	18	39	0.82	0.73
Engine	36,347	539	36,886	767.24	682.40
Exhaust loss	-	-	19,735	410.49	365.10

Tables 8.3 and 8.4 summarise the exergy destroyed directly and due to induced drag by the engine and air conditioner components, with costs and CO_2 emissions attributed proportionally to their total exergy destruction. For comparison, the total fuel burned over the flight is calculated as 3,012 kg, which converts to a cost of \$2,937 or 9,355 kg CO_2 released. The exergy still present, not including kinetic, in the core and bypass flows when expelled from the engine is included for comparison at the bottom of Table 8.3. The attribution of costs follows the established method of assigning 'blame' to the physical location of the exergy destruction, except for the induced drag, which is allocated proportionally to component mass. The

Table 8.4: Air conditioning exergy destruction, costs and CO_2 produced

Component	Direct (MJ)	Induced (MJ)	Total (MJ)	Cost (US$)	CO_2 (kg)
Ram air inlet	0	2.13	2.13	0.04	0.039
Ram air outlet	44.51	2.13	46.64	0.97	0.863
Precooler	26.19	11.54	37.73	0.79	0.698
Main heat exch.	59.17	13.32	72.49	1.51	1.341
Compressor	22.44	1.78	24.22	0.50	0.448
Turbine	22.32	1.78	24.10	0.50	0.446
Total	174.63	24.50	199.13	4.14	3.684

outcome can be argued to be a fair interpretation of the running costs of the various components in the system, which could be used in further economic analysis. The ease of this conversion of system losses to monetary costs is due to the use of exergy as a common currency.

The accuracy of the results given is affected by a number of simplifications made to the analysis. The mission does not include taxi, take-off or landing phases and the climb rate and maximum velocity are lower than a typical A320 aircraft would perform, leading to a shorter cruise phase. Correctly including the former considerations in the analysis would increase total fuel use somewhat, since these are inefficient flight phases, albeit short in duration. The climb rate and velocity limitations of the model have the effect of improving overall efficiency for the flight, especially since lower velocity will lead to lower drag, or may extend the flight time, thus increasing total fuel burn. The effect of a fuel load larger than that required for this mission will, however, increase induced drag over the entire flight. This is not an aspect that could be controlled in the available aircraft performance model.

8.3 Comparison of exergy maps

An exergy map providing detailed oversight of the energy use of an aircraft promises to have many uses in itself, especially if it is used during the design process with ever-improving system models. Another possible use, which may fit with the study of designs, system configurations and mission profiles, is the creation and subse-

quent comparison of two or more exergy maps. This is a topic that extends beyond the scope of this thesis, but for the purpose of initial discussion, a comparison of two mission profiles is made in this section. A secondary mission profile has been created for comparison with the profile analysed in Chapter 7 and in the preceding sections.

8.3.1 Secondary mission profile

Figure 8.5 illustrates the new mission profile compared to the original. The distance travelled, as well as start and end velocity and altitude, remain the same. Velocity and altitude above the fixed start and end points are decreased by 40% at each horizontal distance input point. This leads to slower acceleration, shallower climb and an increased flight duration from around 80 to 89.5 minutes. This comparison is made without prior presumption of improved or worsened performance.

An exergy map including the engines and performance subsystems, but not the air conditioning, was created using the same techniques and calculations discussed in Chapter 7, using the system layout depicted in Fig. 7.2.

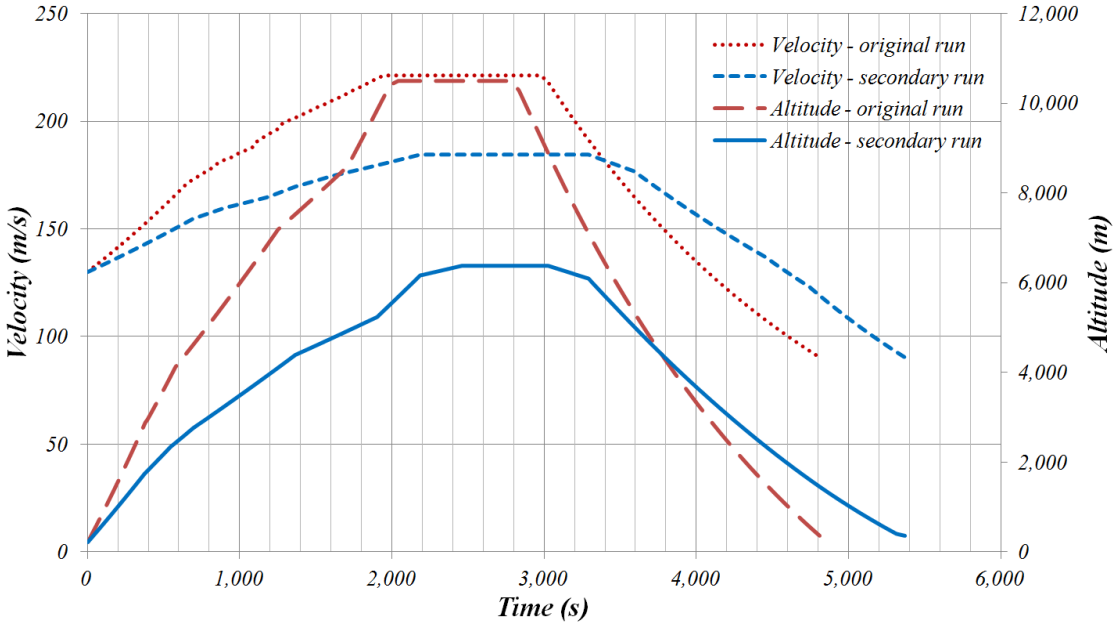

Figure 8.5: Comparison of original and secondary mission profiles

8.3.2 Results and comparison

Over the entire modified mission, the total fuel consumed was 3,425 kg, equivalent to a fuel cost of $3,339 and emissions of 10,638 kg CO_2. The breakdown for individual components is given in Table 8.5. For comparison, the original mission used 3,012 kg fuel.

Table 8.5: Engine exergy destruction costs for modified mission

Component	Direct (MJ)	Induced (MJ)	Total (MJ)	Cost (US$)	CO_2 (kg)
Inlet	0	10	10	0.22	0.19
Fan	3,703	46	3,749	77.98	46.21
LP Compressor	318	73	391	8.131	15.87
HP Compressor	3,109	108	3,217	66.91	59.51
Comb. Chamber	27,953	46	27,999	582.38	517.99
HP Turbine	1,573	31	1,604	33.36	29.67
LP Turbine	1,786	62	1,848	38.43	34.18
Core Exhaust	2,407	31	2,438	50.71	45.10
Bypass Exhaust	3,828	15	3,843	79.94	71.10
LP Shaft	455	31	486	10.10	8.99
HP Shaft	333	15	348	7.24	6.45
Engine	39,253	456	39,709	825.95	734.61
Exhaust loss	-	-	16,767	348.75	310.19

A Grassmann diagram for the engines and aircraft performance systems is given in Fig. 8.6. The previous mission's Grassmann diagram is overlaid in green for comparison. The total exergy flows for the two missions are very similar, making this type of overlay diagram usable. Although the modified mission requires more fuel in total, leading to wider arrows at the combustion chamber component fuel input, the exergy output of the combustion chamber is lower than the original mission. This is due to the reference conditions at higher altitude giving the gas flow after the combustion chamber a greater exergy value. The effect is a significantly higher exergy efficiency for the combustion chamber over the higher altitude flight.

For a closer comparison, the combustion chamber component over the entire

original and modified missions is shown in Fig. 8.7. A comparison of a portion of the climb phase (over 1,000–1,200 seconds of the mission) is given in Fig. 8.8 and of cruise (over different periods of equal duration) is given in Fig. 8.9.

The diagrams for the whole mission (Fig. 8.7) show more clearly the greater fuel exergy input and worse efficiency of the component over the modified mission. The exergy efficiency of the component would increase given colder and lower pressure mission-average reference conditions. This could, to a limited extent, be achieved by flying at higher altitude.

The climb phase comparison (Fig. 8.8) shows that the exergy flows over 200 seconds are lower in the modified mission, which is primarily due to the slower rate of climb. The exergy efficiency of the component remains significantly lower than the original mission segment. This, again, is due to the reference conditions being lower at the higher altitude.

During cruise (Fig. 8.9) at maximum altitude, the fuel input rate to the combustion chamber is similar for both missions and a similar difference in efficiencies exists. The mission segment analysed of the modified mission is later than that of the original mission in order to ensure only cruise flight is included (see Fig. 8.5).

As a further example of mission comparison, consider Fig. 8.10, containing Grassmann diagrams of the Core Exhaust component over the whole of the original and modified missions. Notably, it is shown that the total exergy emission via the exhaust gas, 'GasOut', has a very similar magnitude for both missions. This is despite a significantly lower exergy input to the component for the modified mission, which is due to the reference conditions as discussed previously. Exergy destroyed across the component control volume is primarily due to the unused expansion of the gas flow to atmospheric levels. This is greater in the original mission, again, because of reference state differences. Another significant difference can be seen at the 'RamThrust' output, where the same component in the modified mission displays a far lower output. This is due to the lower mean velocity over the flight, leading to considerably less work being done compressing the engine inlet air and, hence, a smaller ratio of net to gross thrust. This effect can also be seen at the 'BypassExhaust' components (Fig. 8.5).

8.4 Conclusions

The aim of this chapter was to consider the further use of an aircraft exergy map once it has been correctly created according to the previous chapters. An important step in the exergy map analysis is the inclusion of the effects of mass on the aircraft's exergy destruction. To consider this, mass estimates were made for the various gas turbine and air conditioning system components from the Chapter 7 case study. Although the exergy destruction due to lift generation had been touched upon before in the literature, the resulting method was found to be unsuitable for the time-variant exergy mapping process. This is because the time-variant mapping accounts exergy in gravitational potential form as being stored during climb and released upon descent; something that is not the case in the previous method. It is argued that, when analysing a finalised system over a fixed mission, the only exergy destruction due to mass is due to the additional drag it causes, the majority of which is the lift-induced drag. The proportion of drag that can therefore be assigned to the aircraft's mass can be estimated with the lift-induced drag. The work done to overcome this can then be shared proportionally among the aircraft's components according to their mass. The example calculations show that the exergy destruction due to mass will contribute significantly to lower energy subsystems, such as the air conditioning system, but is very small compared to the exergy destruction in the engine components.

A useful aspect of the exergy metric is the direct link it can provide to economic analysis. It was shown in Chapter 6 that the exergy of jet fuel can, in most cases, be considered constant. With this assumption, the monetary and CO_2 costs of the various engine and air conditioning components were calculated for comparison. The outcome is a more tangible expression of the losses associated with each component. These could feed directly into further economic analysis of the aircraft.

A problem with the lift-induced drag assignation is that it fails to take into account 'snowballing' effects that additional mass causes. If the analysis is of an aircraft still under development, an increase in component mass can lead to changes in wing size and structure, which leads to increased mass elsewhere. A larger fuel load to supply the power needed to carry the additional mass, and

the fuel to carry the additional fuel, all lead to increased total consumption that cannot be properly taken into account with this simple method.

The exergy mapping method discussed in this thesis is intended to enable the analysis of a single aircraft in order to gain greater understanding of its fuel use. This is an important and useful outcome, which could find many applications in the design and operation of aircraft. To further its use as a design tool, however, the comparison of distinct exergy maps is the next step of development. As a starting point, a second mission was mapped using the same models and calculation techniques applied to the case study in Chapter 7. This mission was modified from the first to fly at lower altitude and velocity. A number of comparisons between the two exergy maps were made to serve as examples.

The data used to produce the work in this chapter were partly the output of the analysis GUI (Chapter 4) but also required direct data manipulation using other software. For this extended exergy map analysis to become a straightforward procedure, an extension to the software tools or an additional interface would be required.

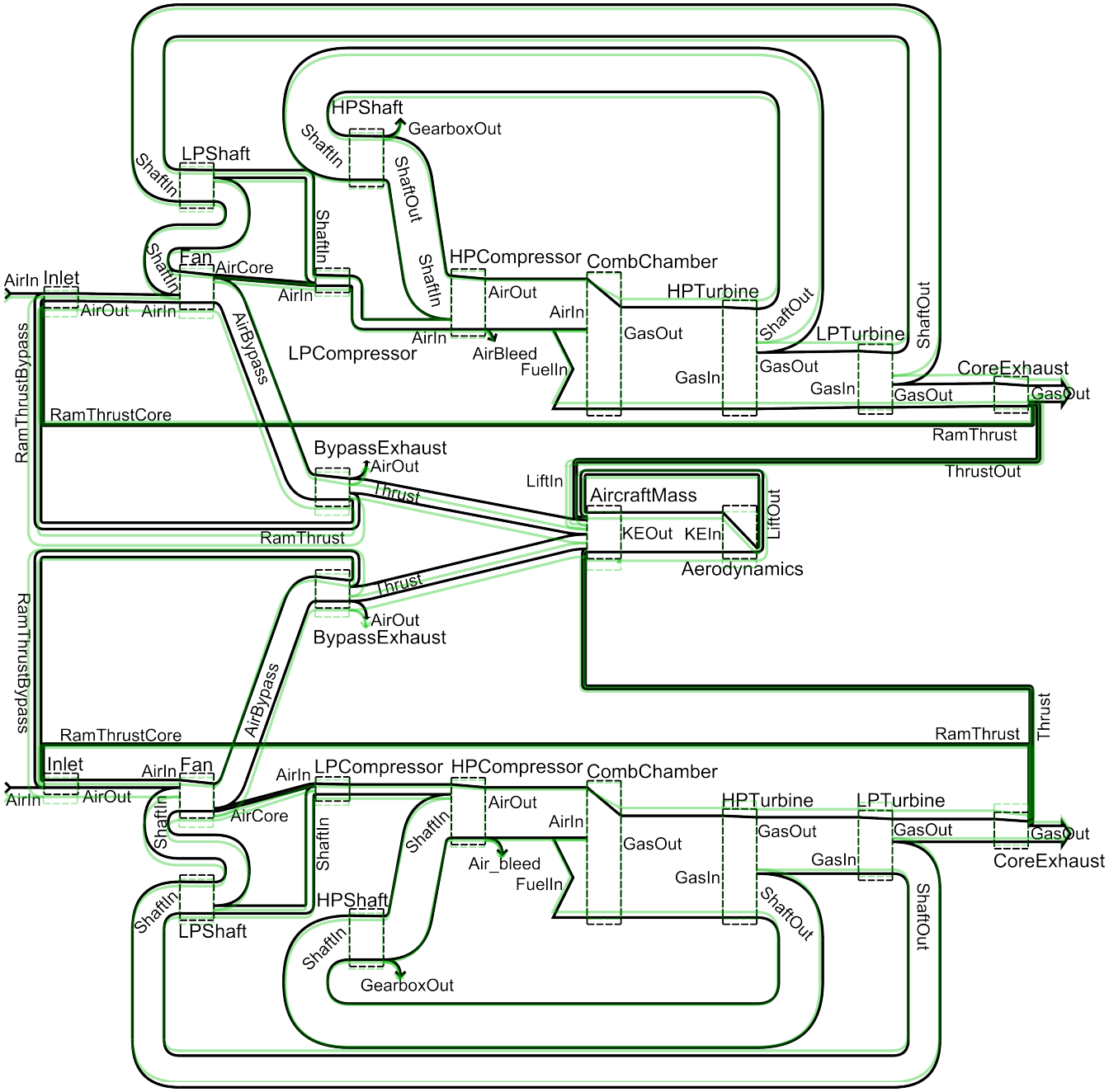

Figure 8.6: Grassmann diagram of engines and aircraft performance for modified mission. Green lines represent the original mission exergy flows for comparison. Enlarged version provided in Appendix B, Fig. B.2.

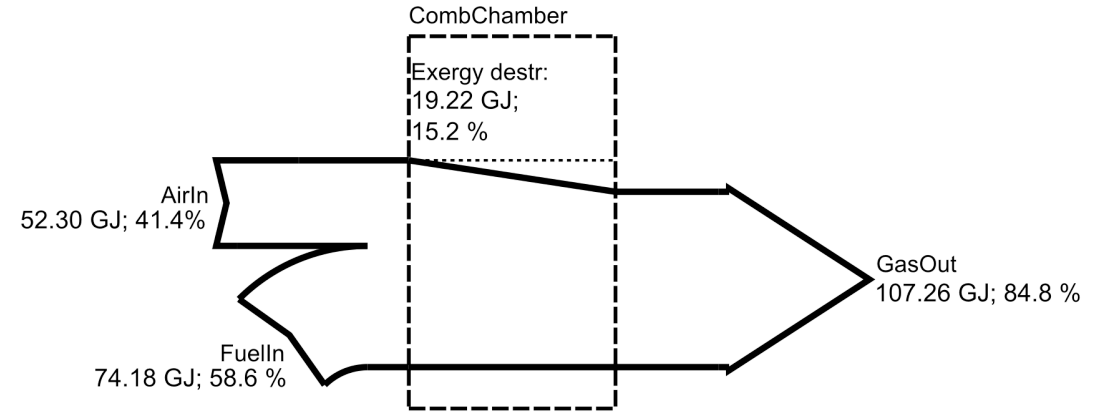

(a) Original mission

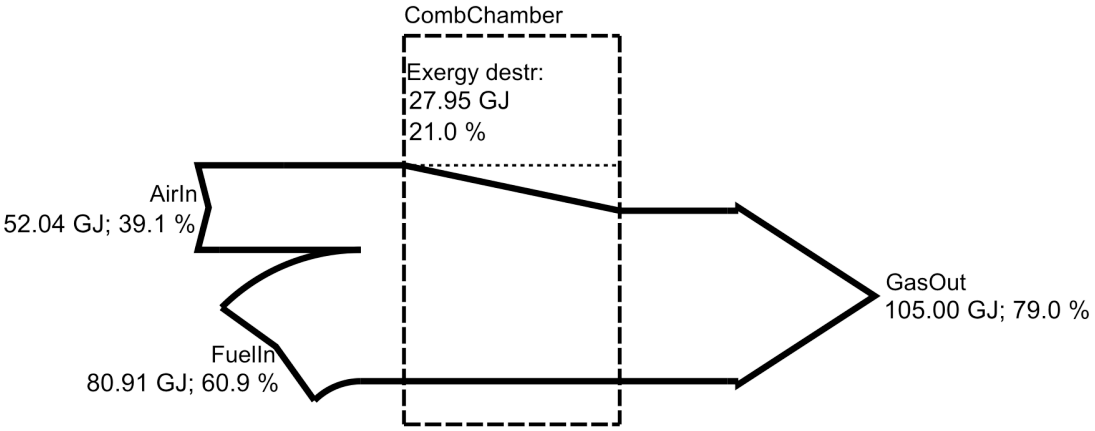

(b) Modified mission

Figure 8.7: Comparison of combustion chamber component over whole mission

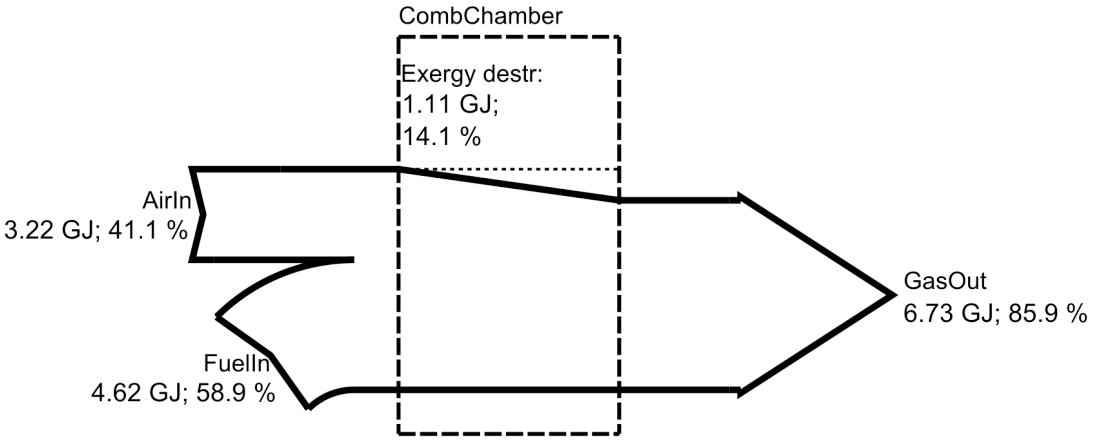

(a) Original mission: 1000–1200 seconds

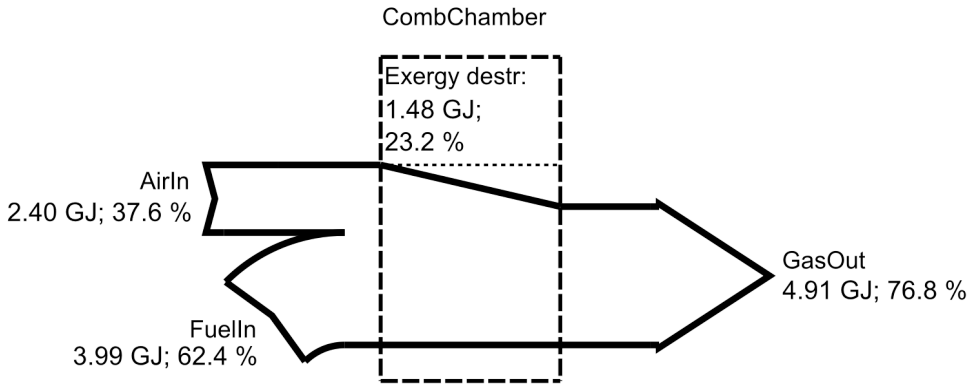

(b) Modified mission: 1000–1200 seconds

Figure 8.8: Comparison of combustion chamber component over climb

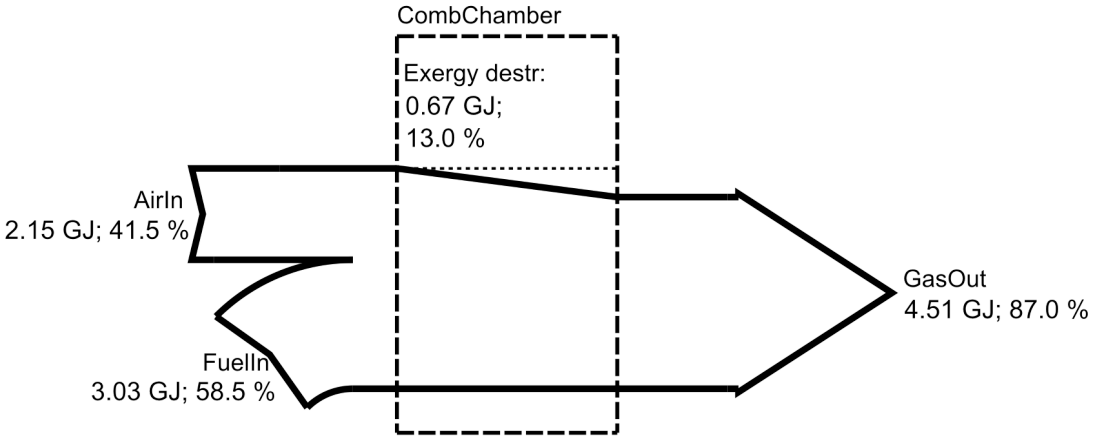

(a) Original mission: 2200–2400 seconds

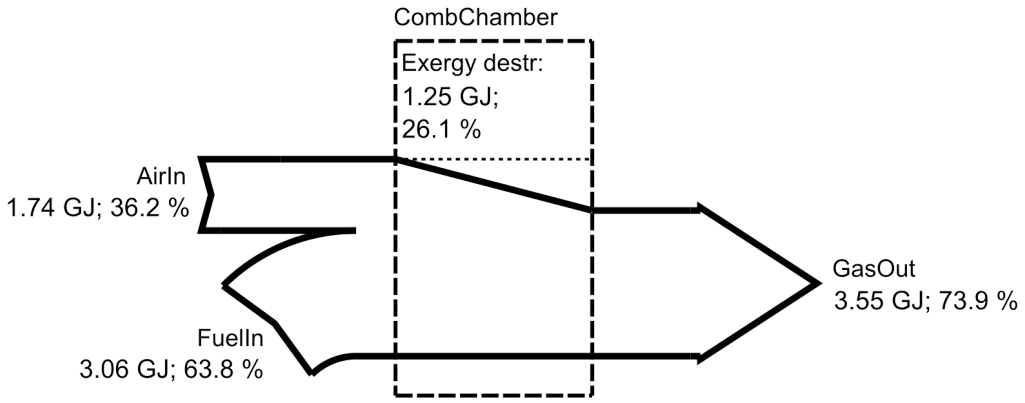

(b) Modified mission: 2500–2700 seconds

Figure 8.9: Comparison of combustion chamber component over cruise

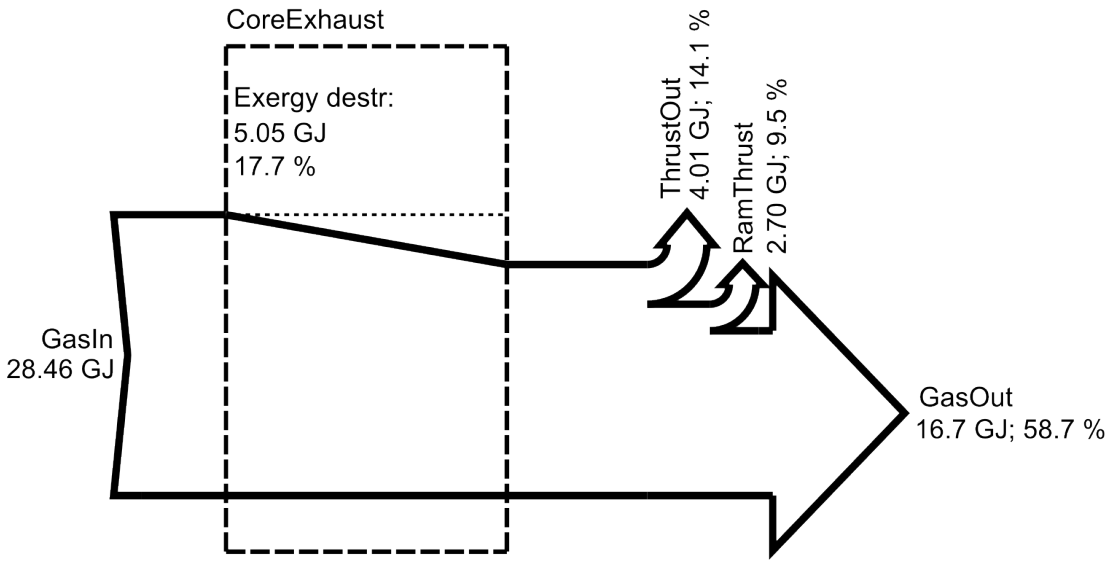

(a) Original mission

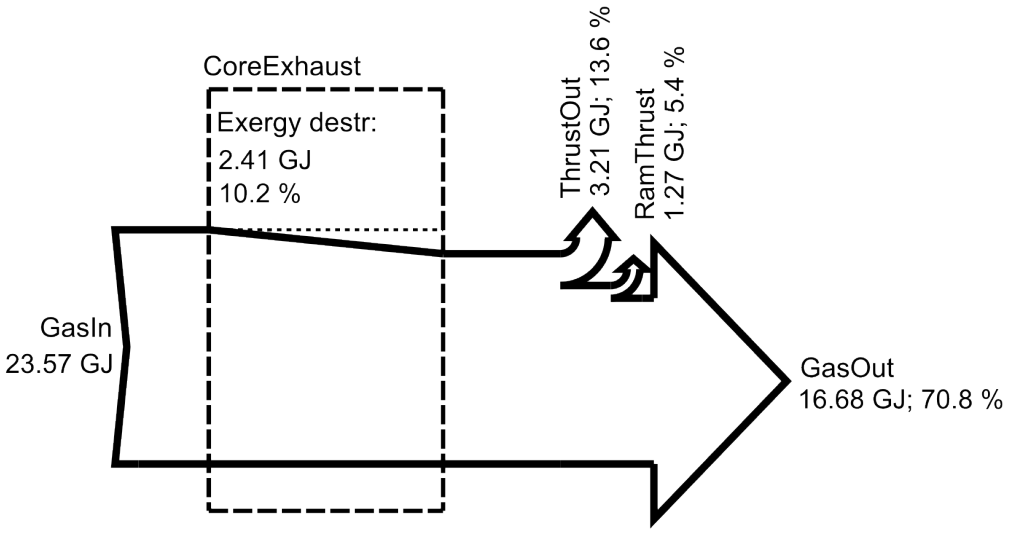

(b) Modified mission

Figure 8.10: Comparison of core exhaust component over whole mission

Chapter 9

Conclusions

The research in this thesis presents the development of a novel methodology for the detailed capture and analysis ('mapping') of the energy flows in an aircraft over a complete flight. A completed map of aircraft energy flows provides new insight into how the energy is used.

It was established that using exergy as the accounted metric instead of energy would provide clearer and more useful results. A consideration of how to apply this to a system very different to the traditional subjects of exergy analysis, such as ground-based thermal plants, was needed. Although there are a number of articles in the literature that broach the topic of exergy analysis of aircraft to some extent, these studies are always limited in scope. The difference between an exergy map and a single exergy analysis is that the exergy map is intended as a reference resource, possible to build up and improve over the course of the development of a new aircraft. The requirement is for it to be generally useful as a means of comparing and understanding a complex aircraft's energy use. It must be possible to include all the aircraft's energy-using systems within the same analysis. Since no aircraft systems operate steadily throughout a mission, especially subsystems such as the hydraulics that respond constantly to pilot inputs, a generally applicable method should not rely on continuous phases of steady-state operation. For this reason, the concept of time-variant exergy analysis is formulated, which relies on the use of exergy balances over short time steps to approximate a non-steady-state system analysis.

With the basis of the exergy mapping method established, a set of software tools was developed in order to facilitate the exergy mapping process. An external

database was designed to hold the exergy map data in a form that would be unaffected by the size and complexity of the system being mapped. Graphical user interfaces were developed to allow the data in the database to be manipulated and later analysed. A further tool was created to allow relatively quick and simple production of the Grassmann diagrams used throughout this thesis. Physical and chemical exergy calculators for ideal gas flows, useful for the most relevant and complex calculations likely to be encountered in an aircraft exergy analysis, were created.

Next, focus was placed on assessing the viability of the exergy mapping method to real systems. A hydraulic test rig was chosen as a subject of study. This is a system that fundamentally operates in a time-variant manner, as various aircraft systems such as the hydraulics do. The availability of the system to study directly provided the opportunity to test the methodology on a system that was not understood fully in advance, providing useful feedback on the validity of the method. Finally, the possibility of comparing the system to a simulation model allowed the limitations of sensor-based exergy mapping to be explored. This aspect is necessary in the discussion of whether real aircraft could be equipped with sensors in order to produce exergy maps of their flights during normal operation. An initial consideration of the system allowed an exergy map layout to be settled upon. Pressure transducers were added to the system to allow exergy flow to be calculated at various points in combination with flow meters and calculations based on piston velocity. Using the sensor data, it was possible to gain a clear view of the exergy flow behaviour with time in the system, especially on the high-pressure side in which the sensors were concentrated. With the exergy map complete, the time-variant exergy flows in the system could be evaluated during single up- and down-strokes, as well as for the whole run. The components causing the greatest exergy destruction could be clearly identified. A simulation, running with the same wave input as the rig, was adjusted so that pressure readings agreed with those of the sensors, whilst the flow values in the simulation were assumed to be more accurate. Using the simulation data, the low-pressure side of the system could be viewed in more detail and some inconsistencies of the rig data could be clarified. It was clear from even this simple example that detailed exergy mapping of systems with

sensors alone would be very costly. Currently, aircraft systems use sensors in order to ensure normal functioning. These would in most cases provide insufficient data to establish exergy control volumes around systems. A possible way of achieving live exergy mapping of a flight would be to run a detailed simulation in real-time, which is updated and kept accurate using strategically placed sensors. This topic is left as future work.

An aspect of vehicular, time-variant exergy analysis that cannot be addressed when analysing a stationary, ground-based system such as the hydraulics is the effect of a varying reference state. The exergy due to temperature and pressure is a function of both the system's internal conditions and the environmental conditions to which it is being compared. This is an important aspect of the exergy metric that contributes to its usefulness. An aircraft over a typical mission will, however, fly through a gamut of environmental conditions that will considerably affect the exergy values of the fluid flows within the aircraft. The effects of the reference environment on the physical and chemical exergies are described. The chemical exergy component of gas flows in aircraft systems may not usually be large, but the variation is considered for the sake of possible future system designs where this may be more relevant. The variation of jet fuel chemical exergy, based on a surrogate model of pure dodecane, is shown to vary minimally (up to 1 %) within the range of atmospheric temperatures an aircraft will experience. It is likely, therefore, that the exergy content of the fuel can be considered constant in most exergy mapping scenarios.

To study the effect that the varying reference conditions have on an aircraft system, a case study of a turbojet was formulated that avoids unrelated factors, such as kinetic energy due to system movement and other forms of exergy that are unaffected by the environment. A time-variant mission rising steadily from sea level to 10,000 m but with zero horizontal velocity was applied. It was shown, with the aid of this study, that using a fixed reference state, such as constant sea level conditions, will lead to distorted exergy values that will impinge on the relevance of the results. This can cause large, unphysical inefficiencies across the affected component. Static conditions directly exterior to the aircraft must be used as the reference state for exergy mapping. A final consideration was given to the effect

of a varying reference state on the value of existing exergy stocks. Although a disconnection between the cost of producing an exergy stock and its final value is caused, the practical implications of this effect are limited in normal aircraft. It is possible that there is no perfect answer to the problem of varying reference conditions, but the choice of the conditions directly exterior to the aircraft is the most generally applicable.

An aircraft case study based on an aircraft similar to an Airbus A320, was developed using three separate system models. The first, an aircraft performance model provided by Airbus, allowed the input of a mission profile and calculated flight time, velocities, thrust, altitude and fuel consumption. A turbofan model was created based on a typical A320 engine and tuned, by varying fuel flow, to provide the same thrust as the performance model output over the course of the mission. A simplified air conditioning system simulation was created as a representative subsystem. Bleed air conditions taken from the engine model and atmospheric conditions based on aircraft altitude and velocity were used as inputs to the model. The complexity of the system, as expected, did not adversely affect the function of the method or software tools. The exergy map results showed the flow of exergy clearly. However, some aspects for further consideration arise from the process of exergy mapping this system. Although the air conditioning system's exergy flows are adequately captured and viewed using the tools available, it is difficult to compare exergy flows with those of the engines visually. Normal Grassmann diagrams are inadequate for this task. One could envisage a large Grassmann diagram with different scales in different areas being used for the purpose of presentation and comparison of system magnitudes, although the time involved in producing it may be excessive. Another aspect of creating an exergy map comprising systems of such different exergy magnitudes is that the uncertainty in the engine results may lead to error as large as the whole exergy flows of the other systems. Considering the differences in order of magnitude involved means this is likely to be inevitable. This need not detract from the value of the information stored, but should be fully understood when drawing conclusions.

Exergy is passed from propulsion systems and the aerodynamics to the aircraft's mass as it accelerates and climbs, is stored and then released again upon

deceleration and descent. However, the work required to keep an aircraft aloft is significant. This must be taken into account in a full analysis. The essential connection between the induced drag and the mass of the aircraft is clarified, leading to an equation to estimate the exergy destroyed by a component's mass during flight. Only the effect of the lift-induced drag is considered, while other, smaller drag changes due to mass are neglected. The aircraft case study is used as an example, with weight estimates being used to allow mass induced exergy destruction to be calculated.

One of the major advantages of using exergy as a system-wide common currency is the direct link that exists between the exergy and the fuel value it represents. To exemplify the conversion from exergy to fuel costs, as well as equivalent CO_2 emissions, the aircraft case study is interpreted in these terms. The monetary cost of the exergy destroyed in each component is calculated, providing a clearer way of interpreting the data, which could also link into further economic analysis. The given interpretation of mass-induced exergy destruction is limited by the inability to include 'snowballing' effects in the cost of carrying additional mass. The usual procedure in aircraft design is to compare a new, complete aircraft with the potential changes to a baseline model. The possibility of comparing two exergy maps directly is discussed by producing another exergy map of the same aircraft as the previous case study over a modified flight profile. Comparison is drawn between the entire aircraft exergy use, as well as individual sections of the flight for specific components. The exergy map comparison can aid in the understanding of how the system's energy is used and how the two missions differ.

In all sections of this work, the benefits of exergy as a metric for pan-system energy use analysis are made clear. Comparison of systems carrying different energy types would often be meaningless when just using energy metrics. The value of the energy in the system would vary depending on the context, which would not always be visible. Complications in the use of exergy arise due to the variation in reference conditions, but this is not a problem that ceases to exist when using energy, only one that is more likely not to be formally addressed. Indeed, it is argued that a detailed consideration of how best to use energy as a metric for such an analysis would independently lead to the derivation of exergy

or something very similar.

9.1 Further work

In the context of the exergy map methodology, the next recommended step is the creation of a software tool that facilitates the comparison of two exergy maps directly, as well as allowing the mass and economic cost analysis undertaken in Chapter 8 to be automated. This would have immediate benefits for the practicality of exergy mapping. Further to this, significant optimisation of the existing software tools will increase their speed and, hence, usefulness significantly. Extension to the physical exergy calculator to better handle the steam component in a gas flow could be necessary when analysing more exotic systems. A more general expansion of the software tools might be a provision for maintaining a more general energy data set alongside the exergy flows. Raw thermodynamic data, such as temperature, pressure and mass flow rates for gas flows, as well as other metrics such as enthalpy and entropy, or further 2nd law metrics such as thrust potential, could be stored in a database with few additional changes to the current design. The software tools to interpret the database would require considerable extension to make use of the data. This additional information may make the final outcome more useful to the specific design groups using it and, aside from making the database larger, would not detract from its usefulness elsewhere. This may therefore benefit from further investigation.

With regard to the reference state choice, it is an inherent aspect of the exergy metric that it is influenced as much by the system's conditions as it is by the reference state. Choosing the conditions directly outside the aircraft at all times provides the most generally relevant exergy values for the aircraft systems and allows direct comparison between systems to be made. The use of different reference state schemes may still be applicable in specific circumstances. For example, when analysing a system for the purpose of low level energy harvesting, it could be more fitting to consider the cabin conditions as the reference state. This would not be possible for high energy systems, since the reference conditions should be of a body large enough to be unaffected by energy transfers from the system. Another possi-

bility for the expanded energy flow database could thus be to maintain the exergy map with more than one reference state in parallel. A fundamental limitation in the usefulness of exergy is its theoretical nature. Although it always represents the work theoretically available at each point in a system, it does not necessarily show the work available to the system itself. The most significant example of this is the thermal exergy in a gas turbine engine, which is not available to the Brayton cycle and does not contribute toward thrust. Certain system analyses must consider the thermal exergy in the engine lost. Different levels of technology for different energy types also mean the possibility of achieving the theoretically available work varies. Other work potential metrics may thus be useful in providing more pertinent results in specific cases.

The possibility of exergy mapping real flights using sensor data for the benefit of the aircraft manufacturers and operators alike may be a significant area of interest in the future. The development of a full-aircraft model that is updated and kept accurate by input from physical sensors is suggested as a line of future enquiry.

Finally, the use of the exergy map as a design tool in itself is a worthy line of further work. The method for the clear capture of exergy flows through an aircraft have been established, avoiding an exact expectation of how the results will be used. This ensures a broad applicability, but means specific design questions it might help answer are unclear. Creating an exergy map will undoubtedly require significant investment in time, particularly if the level of system detail imagined is included. The immediate uses as a means of managing and communicating the complexity of an aircraft's energy use are, by this stage, clear. However, further work on the side of application, if possible within industry, with access to real system models and accurate data would be the best position from which to investigate the specific areas and work flows in which exergy mapping will be of particular importance.

Bibliography

[1] J. H. Doty, J. A. Camberos, and D. J. Moorhouse, "Benefits of exergy-based analysis for aerospace engineering applications - part 1," *International Journal of Aerospace Engineering*, 2009.

[2] R. Gandolfi, L. F. Pellegrini, and S. Oliveira Jr., "More-electric aircraft analysis using exergy as a design comparison tool," in *48th AIAA Aerospace Sciences Meeting Including the New Horizons Forum and Aerospace Exposition*, no. 2010-809, AIAA, 2010.

[3] J. J. Lee, S. P. Lukachko, and I. A. Waitz, "Aircraft and energy use," in *Encyclopedia of Energy*, pp. 29 – 38, New York: Elsevier, 2004.

[4] A4A, "Airlines for America quarterly cost index." Website. Accessed: 11/01/2013.

[5] D. Lazarovich, "Design and integration of the power management and generation system for the dash8/400 airplane," *SAE*, vol. 981273, 1998.

[6] S. Liscouet-Hanke, S. Pufe, and J. C. Mare, "A simulation framework for aircraft power management," *Proceedings of the Institution of Mechanical Engineers, Part G: Journal of Aerospace Engineering*, vol. 222, pp. 749–756, 2008.

[7] S. Liscouet-Hanke, J. C. Mare, and S. Pufe, "Simulation framework for aircraft power system architecting," *Journal of Aircraft*, vol. 46, no. 4, pp. 1375–1380, 2009.

[8] S. Liscouet-Hanke, *A model-based methodology for integrated preliminary sizing and analysis of aircraft power system architectures*. PhD thesis, University of Toulouse, 2008.

[9] J. Bals, G. Hofer, A. Pfeiffer, and C. Schallert, "Virtual iron bird - a multidisciplinary modelling and simulation platform for new aircraft system architectures," in *DGLR Jahrestagung*, 2005.

[10] "Modelica." The Modelica Association. https://www.modelica.org.

[11] E. Sciubba and G. Wall, "A brief commented history of exergy from the beginnings to 2004," *International Journal of Thermodynamics*, vol. 10, pp. 1–26, 2007.

[12] T. J. Kotas, *The Exergy Method of Thermal Plant Analysis*. London: Butterworths, 1985.

[13] J. E. Ahern, *The Exergy Method of Energy Systems Analysis*. New York: John Wiley & Sons, 1980.

[14] M. A. Rosen, "Energy- and exergy-based comparison of coal-fired and nuclear steam power plants," *Exergy, An International Journal*, vol. 1, no. 3, pp. 180–192, 2001.

[15] M. Ameri, P. Ahmadi, and S. Khanmohammadi, "Exergy analysis of a 420 MW combined cycle power plant," *International Journal of Energy Research*, vol. 32, no. 2, pp. 175–183, 2008.

[16] J. Larminie and A. Dicks, *Fuel Cell Systems Explained*. New York: John Wiley & Sons, 2003.

[17] R. Cownden, M. Nahon, and M. A. Rosen, "Exergy analysis of a fuel cell power system for transportation applications," *Exergy, An International Journal*, vol. 1, no. 2, pp. 112–121, 2001.

[18] T. J. Leo, J. A. Durango, and E. Navarro, "Exergy analysis of PEM fuel cells for marine applications," *Energy*, vol. 35, no. 2, pp. 1164–1171, 2010.

[19] S. Song, S. Douvartzides, and P. Tsiakaras, "Exergy analysis of an ethanol fuelled proton exchange membrane (PEM) fuel cell system for automobile applications," *Journal of Power Sources*, vol. 145, no. 2, pp. 502–514, 2005.

[20] D. W. Riggins, D. J. Moorhouse, and J. A. Camberos, "Characterization of aerospace vehicles performance and mission analysis using thermodynamic availability," *Journal of Aircraft*, vol. 47, no. 3, pp. 904–916, 2010.

[21] A. Bejan and D. L. Siems, "The need for exergy analysis and thermodynamic optimization in aircraft development," *Exergy, An International Journal*, vol. 1, no. 1, pp. 14–24, 2001.

[22] I. Dincer and M. A. Rosen, *Exergy analysis of aircraft flight systems*, pp. 325–334. Amsterdam: Elsevier, 2007.

[23] D. Moorhouse, "Proposed system-level multidisciplinary analysis technique based on exergy methods: Exergy," *Journal of Aircraft*, vol. 40, no. 1, pp. 11–15, 2003.

[24] L. F. Pellegrini, R. Gandolfi, G. A. L. Araujo, and S. Oliveria Jr., "Exergy analysis as a tool for decision making in aircraft systems design," in *45th AIAA Aerospace Sciences Meeting and Exhibit*, no. 2007-1396, AIAA, 8-11 January 2007 2007.

[25] D. M. Paulus and R. A. Gaggioli, "Rational objective functions for vehicles," *Journal of Aircraft*, vol. 40, no. 1, pp. 27–34, 2003.

[26] D. M. Paulus and R. A. Gaggioli, "The exergy of lift and aircraft exergy flow diagrams," *International Journal of Thermodynamics*, vol. 6, no. 4, pp. 149–156, 2003.

[27] V. Periannan, M. R. von Spakovsky, and D. J. Moorhouse, "A study of various energy- and exergy-based optimisation metrics for the design of high performance aircraft systems," *Aeronautical Journal*, vol. 112, no. 1134, pp. 449–458, 2008.

[28] R. Gandolfi, F. P. Luiz, G. Araujo Lima da Silva, and S. Oliveira Jr., "Exergy analysis applied to a complete flight mission of a commercial aircraft," in *46th AIAA Aerospace Sciences Meeting and Exhibit*, no. 2008-153, AIAA, 2008.

[29] B. Roth, *A theoretical treatment of technical risk in modern propulsion system design.* PhD thesis, Georgia Institute of Technology, 2000.

[30] B. Roth and D. Mavris, "Method for propulsion technology impact evaluation via thermodynamic work potential," *Journal of Aircraft*, vol. 40, no. 1, pp. 56–61, 2003.

[31] R. Bryce and M. Dimitry, "A generalized model for vehicle thermodynamic loss management and technology concept evaluation," No. 2000-5562, SAE International, October 2000.

[32] B. Roth, "Aerodynamic drag loss chargeability and its implications in the vehicle design process," in *Aircraft, Technology Integration and Operations Forum*, Georgia Institute of Technology, 2001.

[33] J. M. Clarke and J. H. Herlock, "Availability and propulsion," *Journal of Mechanical Engineering Science*, vol. 17, no. 223, pp. 223–232, 1975.

[34] E. T. Turgut, T. H. Karakoc, and A. Hepbasli, "Exergetic analysis of an aircraft turbofan engine," *International Journal of Energy Research*, vol. 31, no. 14, pp. 1383–1397, 2007.

[35] C. Tona, P. A. Raviolo, L. F. Pellegrini, and S. de Oliveira Junior, "Exergy and thermoeconomic analysis of a turbofan engine during a typical commercial flight," *Energy*, vol. 35, no. 2, pp. 952–959, 2010.

[36] V. Amati, C. Bruno, D. Simone, and E. Sciubba, "Exergy analysis of hypersonic propulsion systems: Performance comparison of two different scramjet configurations at cruise conditions," *Energy*, vol. 33, no. 2, pp. 116–129, 2008.

[37] T. E. Hutchins and M. Metghalchi, "Energy and exergy analyses of the pulse detonation engine," *Journal of Engineering for Gas Turbines and Power*, vol. 125, no. 4, pp. 1075–1080, 2003.

[38] I. Perez-Grande and T. J. Leo, "Optimization of a commercial aircraft environmental control system," *Applied Thermal Engineering*, vol. 22, no. 17, pp. 1885–1904, 2002.

[39] T. J. Leo and I. Perez-Grande, "A thermoeconomic analysis of a commercial aircraft environmental control system," *Applied Thermal Engineering*, vol. 25, no. 2, pp. 309–325, 2005.

[40] R. Figliola, R. Tipton, and H. Li, "Exergy approach to decision-based design of integrated aircraft thermal systems: Exergy," *Journal of Aircraft*, vol. 40, no. 1, pp. 49–55, 2003.

[41] K. Alabi, "The use of the 2nd law as a potential design tool for aircraft air frame subsystems," *International Journal of Thermodynamics*, vol. 9, no. 4, pp. 1–14, 2006.

[42] L. Faleiro, "Summary of the European power optimised aircraft (POA) project," in *25th International Congress of the Aeronautical Sciences*, 2006.

[43] Y. A. Cengel and M. A. Boles, *Thermodynamics: An Engineering Approach, Fourth Edition*. New York: McGraw-Hill, 2002.

[44] J. Szargut, "Chemical exergies of the elements," *Applied Energy*, vol. 32, no. 4, pp. 269–286, 1989.

[45] A. Bejan, G. Tsatsaronis, and M. Moran, *Thermal Design & Optimisation*. New York: John Wiley & Sons, 1996.

[46] J. Ahrendts, "Reference states," *Energy*, vol. 5, no. 8-9, pp. 666–677, 1980.

[47] Y. Candau, "On the exergy of radiation," *Solar Energy*, vol. 75, no. 3, pp. 241–247, 2003.

[48] F. T. N. Berg, M. J. Balchin, and P. S. Keogh, "New principles for dynamic aircraft exergy mapping," *Journal of Aircraft*, vol. AIAA Early Edition, pp. 1–13, 2013.

[49] "Orbit 25/18 performance sheet." Online, 2005. Accessed: 30.01.2013.

[50] MATLAB, *version 7.10.0 (R2010a)*. Natick, Massachusetts: The MathWorks Inc., 2010.

[51] "Academic free licence 3.0." Online. Accessed: 07/02/2013.

[52] I. S. Ertesvag, "Sensitivity of chemical exergy for atmospheric gases and gaseous fuels to variations in ambient conditions," *Energy conversion & management*, vol. 2007, pp. 1983–1995, 2007.

[53] C. Cargo, *Design and Control of Hydraulic Power Take-Offs for Wave Energy Converters*. PhD thesis, University of Bath, 2013.

[54] J. Etele and M. Rosen, "The effect of reference-environment models on the accuracy of exergy analyses of aerospace engines," *SAE Technical Paper Series*, vol. 1999-01-2643, pp. 1–6, 1999.

[55] M. Rosen and I. Dincer, "Effect of varying dead-state properties on energy and exergy analysis of thermal systems," *International Journal of Thermal Sciences*, vol. 43, pp. 121–133, 2004.

[56] P. Dagaut and M. Cathonnet, "The ignition, oxidation, and combustion of kerosene: A reivew of experimental and kinetic modeling," *Progress in Energy and Combustion Science*, vol. 32, pp. 48–92, 2006.

[57] M. L. Huber, E. W. Lemmon, and T. J. Bruno, "Surrogate mixture models for the thermophysical properties of aviation fuel Jet-A," *Energy Fuels*, vol. 24, pp. 3565–3571, 2010.

[58] T. Edwards and L. Q. Maurice, "Surrogate mixtures to represent complex aviation and rocket fuels," *Journal of Propulsion and Power*, vol. 17, pp. 461–466, 2001.

[59] M. Moran, *The CRC handbook of thermal engineering*. CRC Press, 1999.

[60] "GSP version 11.1.1.4." Amsterdam, the Netherlands, National Aerospace Laboratory NLR, 2011.

[61] W. P. J. Visser, "Gas turbine engine simulation at NLR," in *CEAS Symposium on Simulation Technology*, (Delft), 1995. Accessed Online 28.02.2013: http://www.gspteam.com/downloads/documentation/gsp-documents/category/17-nlr-gas-turbine-simulation-overview-paper.

[62] L. R. Jenkinson, P. Simpkin, and D. Rhodes, *Civil Jet Aircraft Design*. London: Butterworth-Heinemann, 1999.

[63] M. Wetter, "Simulation model: Air-to-air plate heat exchanger," tech. rep., Berkeley National Laboratory, Building Technologies Department, 1998. Accessed online 15.02.2013: http://simulationresearch.lbl.gov/wetter/download/LBNL-42354.pdf.

[64] E. Torenbeek, *Synthesis of Subsonic Airplane Design*. Delft, the Netherlands: Delft University Press, 1982.

[65] F. Berg, "Vergleich und erweiterung verschiedener methoden zur massenabschaetzung enzelner komponenten im flugzeugvorentwurf," Master's thesis, University of Bath, RWTH Aachen, 2009.

[66] "Fuel price analysis 5-Apr2013." International Air Transport Association Website. Accessed: 26-Apr-2013.

Appendix A

Software tool details and instructions

This appendix gives further detail on the use of the software tools developed to enable the exergy mapping process.

A.1 General input

Figure 4.3 shows the input GUI layout with the general input tab open. The list boxes on the left show the names of the subsystems, components and interfaces in the database being edited. All the subsystems are displayed at all times, but the components and interfaces are accessed by selecting the subsystem or component they are located in.

Formatting When creating a new database, the time period over which the exergy mapping is taking place must be entered along with the size of the time step. The 'Format' button creates empty records for each interface and time point in the Data table. When an interface is added afterwards, it can be selected and the 'Prime' button can be used to add the appropriate records in the 'Data' table for the particular interface.

Vector Input The variables in the Matlab workspace are displayed here and can be selected. An interface can be selected on the left and an exergy type selected from the drop-down list. Pressing 'Go' will insert the vector from the workspace

into the datapoint associated with the selected interface. Pressing 'Queue' will add the task to the 'Batch Queue' below. The vector being inserted must be the same length as the number of time steps in the analysis. The data is added sequentially to each time point.

Batch Queue Since data insertion can be time-consuming, it can be beneficial when inserting a number of interfaces' worth of data to queue a number of tasks that can be worked through automatically. The queue list box gives the name of the vector input and the datapoint number it is to be placed in. Items are added with the 'Queue' button and removed with the 'Remove' button. The 'Save' and 'Load' buttons allow the existing queue to be saved, since these can be time-consuming to create. 'Batch Insert' starts the insertion process.

A.2 Map creation

Figure 4.4 shows the Links tab, which contains tools for the direct manipulation of the system structure in the database. The subsystem/component/interface navigation on the left remains the same as before.

Subsystems and Components The edit boxes under 'Subsystems', 'Components' and 'Interfaces' display the currently selected items. The selected item can be removed from the database with the '-' button. If a different name is entered, the '+' button can be used to create a new item, or the 'R' button can be pressed to rename the currently selected item. All changes are immediately implemented in the database.

Interfaces When an interface is selected, the links data are displayed in the table. The interfaces exergetically downstream of the selected interface are displayed with their subsystem, component, name and identifying number. To create a new link, the 'Create Link' button is pressed. This activates the list box on the right. The navigation boxes on the left can be used to select the component in which the downstream interface is located. The interfaces are displayed in the list box and a selection can be made. The 'Link' button is then pressed to create the link, which

will be displayed in the table above. The 'Delete' button can remove a selected link.

Data Points The drop-down list contains all the data points currently in the database. When an interface is selected, its associated data point will be displayed. Selecting a different data point will change the selected interface's association immediately. The list box to the right gives the names of the interfaces associated with the current data point. Pressing the '+' button will add a new data point to the database. The '-' button will remove the currently selected data point.

A.3 Calculators

Figure 4.5 shows the calculator tab with the physical exergy calculator open. Figure 4.6 shows the chemical exergy calculator, which can be accessed by minimising the physical exergy calculator. The methods used for the calculations and validation of the results are given in Subsection 4.4.4.

Variables The Matlab workspace variables are displayed here and can be selected to be used in the edit boxes below.

Physical exergy of a gas flow This interface is a calculator for the most common exergy calculation required for an aircraft exergy analysis: the physical exergy of a gas flow. The inputs to the edit boxes can either be a directly entered number or a vector of numbers in the Matlab workspace. A combination of both can be used, in which case the directly entered numbers will be considered constants. The vectors entered must otherwise be the same length. Temperatures are entered in Kelvin, pressures in Pascals and mass flow rates in kg/s. Species are entered as a cell array (e.g. {'O2','CO2','Ar'}) and mass fractions are entered as an array of numbers in the same order as the species or a cell array of workspace vector names. To simplify, the 'Air' button can be pressed to fill in standard values for air. The reference state temperatures and pressures are also required, although standard atmosphere, sea-level conditions are filled in by pressing the 'Sea Level' button. The results edit box left blank will show the result of a calculation if only

scalar values were entered in the input boxes. Otherwise, a workspace variable can be given into which the results will be placed. The variable must have the same length as the input vectors.

Chemical exergy of a gas flow As with the physical exergy calculator, the species and fractions are entered. A drop-down list allows the choice between entering molar or mass fractions. The relative humidity can also be entered as a scalar constant fraction or vector of fractions, which is used to calculate the fraction of water in the gas.

A.4 Analysis GUI

The analysis GUI, shown in Fig. 4.7, is for the viewing, interpretation and visualisation of the data entered in the aircraft exergy map database. It is intended to enable understanding the physical location of exergy destruction, the relative magnitude of exergy flows and for checking the validity of the entered data. The subsystems and the time point range of the exergy map are displayed with the 'Load' button. Entering the time step size in seconds shows the start and end times in real terms. Ticking the 'Time variance' box will permit the user to change the period over which the analysis is taking place. The correct order of magnitude in which the data in the database has been stored can be set with the 'O of M' drop-down menu.

Selecting a subsystem will display its associated components. When a component is selected, the 'Calc.' button can be used to calculate and display the exergy inputs, outputs and storage changes over the given time period. A component Grassmann diagram is drawn and displayed and the total flow values and component efficiency based on those are displayed beneath it. The 'Ext.' button will draw the same Grassmann diagram in a separate window to allow the image to be scaled or exported.

When a component is selected, its associated interfaces are displayed in the Interfaces listbox. Selecting an interface calculates and displays the separate exergy flow types over the time period in question and displays them on the right. Pressing the 'Draw' button will draw a graph of the exergy transfer at each time

point over the defined period. A colour is chosen automatically for the line and a key is added to the right to identify it. Selecting another interface and pressing 'Draw' again will add a line to the graph in another colour. The 'Clr' button will clear the graph and the 'Ext.' button will draw the graph in a separate window. The buttons below allow the display of individual exergy types for an interface, should it contain different exergy flows.

The 'Subsystem Grassmann' button will open the interface for drawing a Grassmann diagram of the currently selected subsystem over the time period specified.

A.5 Grassmann diagram generation tool

A tool was created to allow the automated drawing of a Grassmann diagram for subsystems. Although the diagrams are useful for understanding and communicating exergy flow data, their manual creation requires some skill with drawing software and a large amount of time. In order to allow the relatively quick comparison of exergy data using these diagrams, this tool was developed.

When opened, the calculations for the time period chosen in the Analysis interface are performed for every component in the selected subsystem. A GUI, shown in Fig. 4.8 opens, which allows the layout of the diagram to be established. More than one subsystem can be selected to be drawn together. Details on this interface can be found in Appendix A.

From the data available when creating a new diagram, it is not possible for an algorithm to establish a clear layout automatically. A first guess is made by the tool, which places the inputs to the subsystem on the left and the downstream components sequentially to the right. This aids the user but will only suffice in the simplest cases.

Components are placed on a grid, the spacing of which can be set with the 'Horizontal spacing' and 'Vertical spacing' edit boxes. The 'Horizontal Rank' and 'Vertical Rank' settings position the components on that grid. The 'Adjust' settings move the component incrementally to fine-tune the position.

The vertical order in which the interfaces enter and leave the component is controlled with the 'Interface vertical rank'. A drop-down list allows the selection

of the arrow style that a downstream component will have (i.e. will it proceed vertically or horizontally first, or cross diagonally). 'Vertical extend' stretches the arrow to provide more space to other arrows or components if necessary.

The established layout can require some investment in time and several attempts. Once satisfactory, the layout can be saved as a .mat file that contains all the settings for each component and interface. This is essential when working on more complex systems.

Since it is often necessary to directly compare diagrams for different time periods, these must be drawn to scale. To do this, the drawing must be placed on the same axes. By ticking the 'Hold axes' box and entering a figure number in the 'Figure window' edit box, a diagram can be drawn in an existing set of axes. To ensure proportionality, the 'Base' value of the previous diagram is entered in the new window. This is the largest exergy value in the diagram, to which the remaining diagram is scaled. Using another diagram's base value will scale the new diagram to the other. The new diagram must be moved into a clear space so that it does not intersect the previous one. The 'Diagram Vert Adjust' buttons allow all the diagram's components to be moved up or down in multiples of 10 grid units.

A.6 Exergy mapping process

This section describes the process of using the software tool to create a new exergy map.

1. Create a blank database Copy 'Blank_DB.accdb', the empty database file, and rename it suitably.

2. Open software tool and create link Run Matlab (it may be necessary to use the 32-bit version and to run as administrator for this step). In Matlab, navigate to the Exergy Tool folder and run 'Menu.m' to open the Menu GUI. Press 'New' - this will open the ODBC Data Source Administrator. Under 'User DSN' click 'Add...' and then select 'Microsoft Access Driver (*.mdb, *.accdb)' then 'Finish'. Under 'Data Source Name' type in a simple identifying name for

the database, which will be used to open it in the future from the Menu GUI. Under 'Database' click 'Select...'. Navigate to the folder with the database file and select it. Click 'OK' three times to close the windows and save the changes. In the Menu GUI, type in the identifying name of the database exactly and then click 'Data'. This will open the Data Creation GUI. After the first set-up, the database can be accessed by typing in the name in the Menu GUI without the previous steps.

3. Establish the exergy flowchart Before creating the exergy map, it is important to establish what the subsystems, components and interfaces are and what the layout of the system is. This step is non-trivial because the flow of exergy in a system is rarely intuitive. The analyst is urged to draw a flow chart with great care, since it is far simpler to enter the layout correctly first than make changes later. In complex systems, subsystems should be used to allow clear oversight to be maintained but otherwise do not serve an important function. Components should be created according to where the data is available to populate its interfaces. If greater data detail is anticipated in the future, it is simpler to create the system layout in higher detail from the start. Examples of suitable flowcharts are given for all the case studies in this thesis. Once the flowchart has been drawn, it is helpful to keep it to hand whenever editing the database and to keep note of the location of the Data Points on the diagram.

4. Enter the subsystems, components and interfaces In the 'Links' tab, enter a subsystem name without spaces and press '+'. Repeat until all subsystems are created. Click on a subsystem and enter its associated components. Select a component and enter its interfaces. Continue until all the system's interfaces are created. If an interface is for exergy storage, rather than flow, make the relevant change in the drop-down list.

5. Create and assign data points Referring to the flowchart, count the number of discrete data points that exist in the system, at which unique exergy flow data will be available. Create that number of data points by pressing the '+' button under 'Data Points' the according number of times. The drop-down list

should now display them all. Note the locations of the data points on the flowchart as desired. Select each interface in the GUI and choose the correct data point from the drop-down list. Ensure every interface is correctly assigned before continuing by checking the interfaces associated with each data point in the list box at the bottom right of the tab.

6. Create links Again referring to the flowchart, select each interface in turn, click 'Create Link' and select the downstream link from the list box to the right. Selecting a different subsystem and/or component will now display its interfaces in the right-hand list box. Once the downstream interface is chosen, click 'Link' to create the link. Proceed to the next interface. If an interface is an output to the system as a whole, it does not require a downstream link. It is worthwhile checking thoroughly that the data points and links have been entered correctly.

7. Multiple exergy maps of the same system Steps 3-6 must only be performed once for a single system. The database thus far can be copied and re-named, then connected by ODBC driver separately using steps 1 and 2. This way, different missions can be mapped for comparison without having to repeat the complex task of establishing the system layout.

8. Database formatting On the 'General' tab under 'Formatting', enter the end time, the last time point in the analysis. Also enter the size of the time steps (e.g. 0.2 for 5 Hz). Click 'Format' to allow the database's Data table to be populated with records for each time step and interface. This will take a few minutes for larger systems. The progress can be checked by viewing the database in MS Access and checking the number of records.

9. Exergy data generation The data entered in the database must be in the form of a vector the same length as the number of time points in the analysis. It is easiest to create an array in the Matlab workspace with the number of rows equal to the number of time points and the number of columns equal to the number of data points (for example using the 'zeros' command), then filling in the data for each data point in the appropriate column. Exergy data should be consistently of

the same order of magnitude for each analysis, so a choice should be made at the start. Flow interface data is held in Watts (or kW/MW), indicating the exergy flow rate at each time point. Storage interface data, the exergy stock, takes the form of Joules (or kJ/MJ) at each time point. The user can make use of the exergy calculators described in section 4.4 if calculating the exergy of gas flows.

10. Exergy data entry Using the 'Vector Input' and 'Batch Queue' tools (see section 4.4), the relevant interfaces can be selected, along with the relevant vector from the Matlab workspace. The data can then be inserted to the relevant fields in the Data table. Once the data is entered, the Analysis and Attribution GUIs can be used to view and interpret the exergy map.

Appendix B

Enlarged Grassmann diagrams

Figure B.1: Grassmann diagram of aircraft engines and performance over entire flight. Enlarged version of Fig. 7.8, Chapter 7.

Figure B.2: Grassmann diagram of aircraft engines and performance over modified flight. Original flight superimposed in green. Enlarged version of Fig. 8.6, Chapter 8.